Structure and Reactivity Studies of Stabilized Carbenoids

Ruhr-Universität Bochum

Doctoral thesis
submitted in partial fulfilment
of the requirements
of the degree of Dr. rer. nat.

submitted by
Katharina Dilchert

Bochum, 2020

Structure and Reactivity Studies of Stabilized Carbenoids

Ruhr-Universität Bochum

Doctoral thesis
submitted in partial fulfilment
of the requirements
of the degree of Dr. rer. nat.

submitted by
Katharina Dilchert

Bochum, 2020

Submission on April 2nd, 2020

At the faculty of chemistry and biochemistry of the Ruhr-University Bochum, Germany.

Examiners of the dissertation:

1st Examiner: Prof. Dr. Viktoria H. Däschlein-Gessner

2nd Examiner: Prof. Dr. Stefan M. Huber

3rd Examiner: Prof. Dr. Robert E. Mulvey

Examiners of the oral doctoral examination:

1st Examiner: Prof. Dr. Viktoria H. Däschlein-Gessner

2nd Examiner: Prof. Dr. Stefan M. Huber

3rd Examiner: Prof. Dr. Robert E. Mulvey

Date of the doctoral examination: May 29th, 2020

Date of the delivery of the doctoral certificate:

A bright future beckons. The onus is on us, through hard work, honesty and integrity, to reach for the stars.

Eine strahlende Zukunft winkt uns. Und es liegt einzig an uns, mit harter Arbeit, Aufrichtigkeit und Integrität nach den Sternen zu greifen.

Nelson Mandela, 27. April 1996

This doctoral thesis is based on the experimental work conducted within the period of time between October 2016 and March 2020 at the chair of Inorganic Chemistry II of the Ruhr-University Bochum under the supervision of Prof. Dr. Viktoria H. Däschlein-Gessner.

Acknowledgment

First and foremost, I would like to express my special thanks to my **supervisor Prof. Dr. Viktoria H. Däschlein-Gessner** for giving me the opportunity to join her group in October 2016. I am particularly thankful for your continuous support, encouragement and interest in my work. Thanks for always having an open door and ear for your group's problems.

Furthermore, I would like to thank you for the opportunity to participate in several national and international conferences as well as to go abroad to the University of Strathclyde twice during my PhD.

Thanks for always being "Santa Claus" and for all the nice group BBQs, visits to the Christmas markets and the canoe trip.

I especially thank **Prof. Dr. Robert E. Mulvey** for his warm welcome to his group at the University of Strathclyde. Thanks for all your help and the fruitful discussions during my stays in Glasgow. Thanks for making me feel at home in your group and in Glasgow. I really appreciate it and I genuinely enjoyed my time in your group.

Thanks for being my third examiner and coming all the way from Glasgow to Bochum for my viva. I feel honored having you as my third supervisor.

I am thankful to **Prof. Dr. Stefan M. Huber** for being my second supervisor and agreeing on being part of the examination board of my dissertation.

I am also thankful to the **Cluster of Excellence RESOLV** for my PhD scholarship, to the **Gesellschaft deutscher Chemiker** for travel stipends and to the **RUB Research School PLUS** for the 'Project International' grand.

I would like to express my special thanks to **Sabine Pankau** not only for her ongoing support regarding administrative issues but also for always having an open ear for personal issues as well as for being a good friend and "the heart of the chair". The chair of inorganic chemistry II would not be the same without you.

I am grateful to **Dagmar Müller** for taking care of all the issues regarding lab safety. Thanks for distracting me from my every now and then frustrating lab work and for always having time to chat for a while.

I am also thankful to **Dr. Harish Parala** for all his support regarding technical issues.

Thanks to **Dr. Bert Mallick** for all his help regarding maintenance of gloveboxes and single crystal X-ray diffraction analysis.

I would like to thank **Manuela Winter** for measuring elemental analysis.

I am also especially thankful to **Martin Gartmann** for his ongoing support regarding all NMR spectroscopic issues. Thanks for always being helpful no matter what time. Without you some of my NMR spectroscopic measurements would not have been possible.

I am grateful to **Hans Jochen Hauswald** for taking care of all NMR instruments and always making sure that the instruments run as flawless as possible.

I would like to thank **Dr. Kai-Stephan Feichtner** and **Dr. Thorsten Scherpf** for your constant support and the numerous helpful ideas which contributed to this work.

I would also like to express my special thanks to the best lab partner **Alexander Kroll**. Thanks for always cleaning the lab, doing the base and acid baths and especially cleaning NMR tubes in record time – just kidding. Thanks for being a good friend, for all the scientific and not so scientific discussions. Thanks for being calm when I was not. I really enjoyed sharing a lab with you.

Thanks to **Jana-Alina Zur** and **Michelle Schmidt** for becoming good friends and for your understanding about my lack of understanding about the chaos in the lab and glovebox sometimes. Thanks for always having an open ear and for always cheering me up. Without you my PhD would have been a lot less merry.

I am grateful to **Dr**. **Christopher Schwarz** for not letting me eat all my sweet – especially chocolate – on my own and thanks for always sharing yours with me to help me getting through sometimes long and frustrating lab days. Thanks for having an open ear for scientific and non-scientific problems.

Thanks to **Dr. Lennart T. Scharf** for always being such lovely and friendly person and for always putting your trash on my desk when we were still sitting next to each other in the office. All jokes asides. Thanks for all your help during my PhD especially regarding IT issues.

I would like to thank **Maurice Paaßen** for his help regarding my favorite organic synthesis even though you did not enjoy it much yourself. Thanks for doing it anyway.

I would like to thank **Katie McGuire** for her support while planning my first stay in Glasgow. Thanks for picking me to be your friend and hosting me for a whole week when I did not want to leave Glasgow. And of course, thanks for the unforgettable mini-golf game and not laughing at me at that time or anytime you have thought about it since.

I am also thankful to all other present and former members of the Gessner group – **Dr. Sebastion Molitor**, **Dr. Naga Babu Chatla**, **Dr. Chandrajeet Mohapatra**, **Tobias Stalder**, **Jens Tappen**, **Jens Handelmann** and **Heidar Darmandeh** - for all your help and support. Thanks for providing a nice working atmosphere - at least most of the time. Special thanks to **Henning Steinert** and **Ilja Rodstein** for organizing most of the group events.

I would also like to thank all the members of the Devi group – **Dr. Alexander Sadlo**, **Sebastian Beer**, **Lukas Mai**, **Denis Zywitzki**, **Nils Boysen**, **David Zanders**, **Jan-Lucas Wree**, **Parmish Kaur** and **Martin Wilken** - for nice “Pils and Pizza” evenings and for always helping out in case of missing glassware or chemicals.

Thanks to my bachelor, Erasmus and In-depth practical students – **Angela Großjohann**, **Elisabetta Difonzo** and **Tyler Boyd** – for your contributions to this thesis.

I would also like to thank my friends and coworkers form the University of Strathclyde for your warm welcome and for making me feel at home in your group and in Scotland.

Thanks to **Stephen Towie** for always cheering me up, for all the - most of the times - non-scientific discussion in the lab and for the countless hours we have spent hiking.

I would like to thank **Dr. Viktoria Pollard** for her warm welcome and all her help in and outside of the lab. Thanks for being adventurous enough to join for an unforgettable trip to Iceland and for letting me stay at yours when I want to come to visit.

Moreover, I am thankful to **Richard Gauld** for all his help in the lab and with single crystal X-ray diffraction analysis. Thanks for always having an open ear and time to chat. Thanks for cheering me up by buying Gregg´s donuts and for organizing for us to go to all the unforgettable Ceilidh dances.

Thanks to **Dr. Michael "Big Michael" Fairley** for being such lovely and friendly person, and for teaching me facts about the German language I – as a native speaker – did not know. Your knowledge about languages is just incredible. I especially enjoyed our hikes and your efforts to teach me Gaelic on the way passing the Gaelic road signs.

I would also like to express my thanks to **Michael "Mini Micheal" Whitelaw** for always being a though opponent during our Badminton games and never giving up on trying to beat me. I genuinely enjoyed our games.

Thanks to **Dr. Sonia Bruna-Fernandez** for always being infectiously good-humored which cheered up even the most frustrating day.

I would like to thank **Dr. Etienne V. Brouillet** for being the charming French guy he is. For merciless beating me at squash but letting me win at badminton. Thanks for the unforgettable hikes and for "torturing" me with my first two Munros hike.

I would like to express my thanks to **Pasquale Mastropierro** for cheering up every day by being your always happy and good-humored self.

I am grateful to **Dr. Ross McLellan** for his support with all the administrative issues upon arrival and all his support with my DOSY NMR spectroscopic studies. And for beating me every single time at squash.

I would like to thank **Callum Yeardly** for supplying me and Big Michael with little treats to make sure we keep up with your speed during our hikes.

Thanks to **Scott Brown** for always being up to a bit of fun so the time in the lab never got boring.

Furthermore, I would like thank **Craig Irving** for all his help regarding DOSY NMR spectroscopic measurements and all his time he has spent answering my questions.

I would also like to thank **Isabel Scott** and **Angela Anderson** for all their support regarding administrative issues while and before my stays at the University of Strathclyde.

Furthermore, I would like to thank all other past and present members of the Mulvey, O´Hara, Robertson and Hevia group at Strathclyde University. Thanks to **Dr. Charles O´Hara**, **Dr. Stuart Robertson** and **Dr. Eva Hevia** for your support and the fruitful discussion during my time in Glasgow. Thanks to **Leonie Bole**, **Dr. Marina Uzelac**, **Dr. Samantha Orr**, **Dr. Florian Mulks** and **Alessandra Logallo**.

Moreover, I am grateful to **Dr. Christoph Schran**, **Dr. Christian Schneider** and **Dr. Raimund Koerver** for being my friends for nearly ten years and for sharing all the ups and downs during a PhD regardless of where you or I have been during these years.

I am thankful to **Juliane Koop** for proof-reading this thesis without understanding a single word of the scientific part of this thesis and for being such an amazing friend over the years. I am honored to have a friend like you.

I would like to express my sincere thanks to my family and especially my parents, **Frank** and **Angelika Dilchert** for their unique support and unlimited patience to listen to endless descriptions and complains about my work without having the slightest idea of what I am actually doing in the lab.

My special thanks goes to my twinsister and best friend **Janine Dilchert** for always having my back and an open ear. Thanks for your constant support even though being over 450 km away.

Last but not least, I want to express my special thanks to **Mark Lipok** for his unlimited patience, understanding and willingness to support me in the last over ten years. Thanks for being understanding when I went abroad and supporting me despite being over 1200 km away. Thank you for bearing all my nagging and my moods without being annoyed at all – at least most of the times

Content

List of Abbreviations

12-C-4	*12-crown-4*
14-C-4	*14-crown-4*
18-C6	*18-crown-6*
Å	*Angstrom*
adam	*Adamantane*
approx.	*Approximately*
BINAP	*2,2-bis(diphenylphosphino)-1,1-binaphthyl*
Bu	*Butyl*
CAAC	*Cyclic(alkyl)(amino)carbene*
CCM	*Constant current mode*
CHM	*Constant height mode*
CS	*Compact spheres*
CSA	*Camphor sulfonic acid*
Cy	*Cyclohexyl*
dba	*Dibenzylideneacetone*
DCM	*Dichloromethane*
DOSY	*Diffusion ordered spectroscopy*
D_{rel}	*Relative diffusivity*
DSE	*Dissipated spheres and ellipsoids*
e^-	*Electron*
ECC	*External calibration curves*
ED	*Expanded discs*
ELSD	*Evaporative light scattering detector*
eq.	*Equivalent*
er	*Enatiomeric ratio*
Et	*Ethyl*
Et_2O	*Diethylether*
EWG	*Electron-withdrawing group*
h	*Hour*
Hal	*Halogene*

HPLC	*High performance liquid chromatography*
HSAB	*Hard and soft acids and bases*
Hz	*Hertz*
ICC	*Internal calibration curve*
IGLO	*Individual gauge for localized orbitals*
IMes	*1,3-dimesitylimidazol-2-ylidene*
IPr	*1,3-bis(2,6-diisopropylphenyl)-1,3-dihydro-2H-imidazol-2-ylidene*
I_t	*Tunneling current*
K	*Kelvin*
M	*Molar*
MeLi	*Methyllithium*
mg	*Milligram*
min.	*Minute*
mL	*Milliliter*
ML	*Monolayer*
MW	*Molecular weight*
NaHMDS	*Sodium bis(trimethylsilyl)amide*
NFSI	*N-fluorobenzenesulfonimide*
NHC	*N-heterocyclic Carbenes*
NMR	*Nuclear magnetic resonance*
p	*Pico*
Ph	*Phenyl*
pm	*Picometer*
PMDETA	*N,N,N',N'',N''-pentamethyldiethylenetriamine*
PSGE	*Pulsed-field gradient spin-echo*
s	*Second*
STM	*Scanning tunneling microscope*
THF	*Tetrahydrofuran*
TMEDA	*N,N,N',N'-tetramethylethane-1,2-diamine*
TMP	*2,2,6,6,-tetramethylpiperidine*
TMS	*Tetramethylsilane*
Tol	*Toluene*

UHV	*Ultra high vacuum*
VT	*Variable temperature*
δ	*Chemical shift*

Introduction

The History of Carbenoid Chemistry

The urge to find, investigate and understand new and unusual phenomena in science is ubiquitous and one of these unusual and fascinating findings are carbenoids. Carbenoid chemistry dates back to the report of Simmons and Smith on the selective cyclopropanation of (*Z*)-2-butene **3** with diiodomethane **1** and a zinc-copper couple *via* a carbenoid intermediate **2** to the respective cyclopropane **4** in 1958 (Scheme 1).[1]

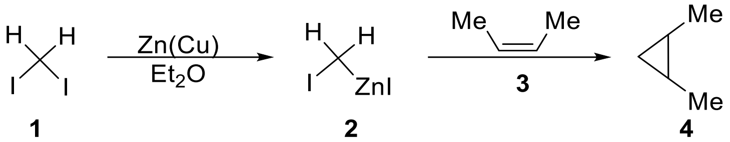

Scheme 1. Cyclopropanation reaction according to Simmons and Smith.

In 1962, Closs and Moss tried to find a synthetic route to diphenylcarbene and observed a distinctive difference in stereoselectivity based on their reaction protocol. The reaction of diphenyldibromomethane **5** with methyllithium (MeLi) resulted in the formation of an intermediate species which reacted stereoselectively with (*Z*)-2-butene **3** to the respective *cis*-cyclopropane **9**. Contrary, a product mixture of *cis*- and *trans*- **9** was obtained *via* the photolytic generation of carbene **7** starting from the corresponding diazomethane compound **8** (Scheme 2).[2]

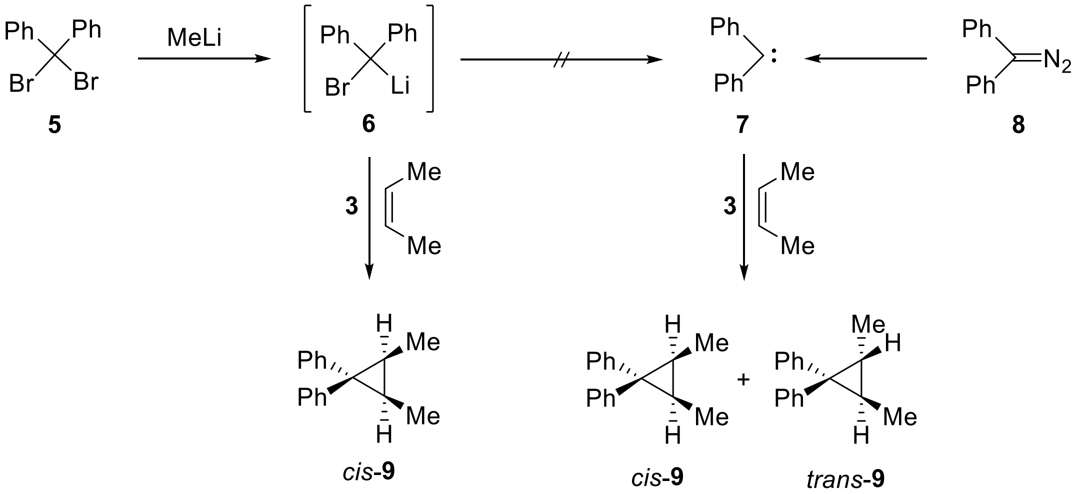

Scheme 2. Comparison of the stereoselectivity of a cyclopropanation reaction *via* a carbenoid and carbene route.

Due to these stereoselectivity differences observed with these two species a distinction became necessary. Consequently, Closs and Moss coined the term carbenoid for compounds ‘which exhibit reactions qualitatively similar to those of free carbenes without necessarily being free divalent species’.[3] In comparison to carbenes – which have gained dramatic research interest in the last decades due to their potential in a wide range of applications – carbenoids have only been frequently used in organic syntheses, mostly in cyclopropanation and homologation reactions.[4]

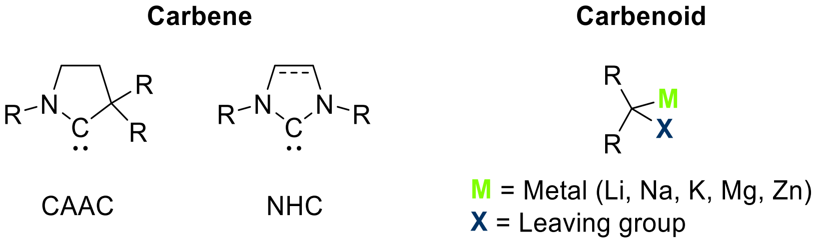

Figure 1. Comparison of carbenes and carbenoids.

Carbenes were long thought to be highly reactive reaction intermediates due to their electronic configuration bearing an electron sextet. This changed when carbenes became ‘bottle-able’ with the first stable carbene by Betrand,[5] the synthesis of *N*-heterocyclic carbenes (NHC) in 1991 by Arduengo[6] and most recently with the discovery of cyclic(alkyl)(amino)carbenes (CAAC) in 2005 (Figure 1).[7] Thanks to the change in reactivity of carbenes this class of compound is now able to be applied in diverse directions, e.g. ligands in transition metal chemistry for example as anticancer drugs[8] or in catalysis,[9] as catalysts in organocatalysis,[10] for activation of small molecules[11], such as CO,[12] H_2,[13] NH_3[13] and P_4[14] or for the stabilization of highly reactive compounds.[11a] The stabilization of carbenes has been the key factor for their broad applicability. A similar development of carbenoid chemistry is desirable creating carbenoids that are as stable as possible but as reactive as necessary since the limited application is mainly due to their poor thermal stability and high reactivity. The carbene-like behavior of carbenoids arose the question about their structure and remarkable electrophilicity – despite their carbanionic nature.

Properties of Carbenoids

Ambiphilicity

In general, the carbenoid character was found in systems bearing a metalated carbon atom with an additional leaving group X (Figure 1) resulting in the general constitution $R_2C(X)M$ (M = Zn, s-block metal). The concomitant presence of an electron-withdrawing and an electron-donating substituent at the same carbon atom results in one of the most fascinating characteristic properties of carbenoids – their ambiphilic character. The extreme ionization of the polar bonds leads to the liberation of a carbanion (**10**$_N$) and a cabocation (**10**$_E$) from **10** (Scheme 3). Generally, carbenoids react as nucleophiles at low temperatures while the electrophilic character becomes more dominant at higher temperatures.[15] Since this thesis mainly deals with the stability and reactivity of alkali metal carbenoids, it will focus on the respective s-block carbenoids in the following. Even though there are great advances in the field of stable magnesium and zinc carbenoids.[16]

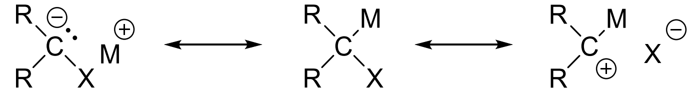

10$_N$ nucleophilic character **10** **10**$_E$ electrophilic character

Scheme 3. Schematic represenation of the ambiphilic nature of M/X carbenoids**.**

The first evidence of the anionic nature of carbenoids was supplied by the reaction of trifluorovinyllithium with carbon dioxide and subsequent protonation resulting in the formation of 2,3,3-trifluoro-2-propenoic acid.[17] The electrophilic character of carbenoids were proven in C-H activation reaction or in 1,2-alkyl/aryl migration reactions in *β*-aryl-substituted vinylic halides, the so-called Fritsch-Buttenberg-Wiechell rearrangement (Scheme 4).[18] Usually, zinc carbenoids are less nucleophilic and predominantly feature a stronger electrophilic behavior,[18a] while lithium and magnesium carbenoids mostly react as carbanions due to their excellent nucleophilicity.[19] The nucleophilicity of this class of compounds is mainly influenced by the metal and the character of the carbon-metal-bond.

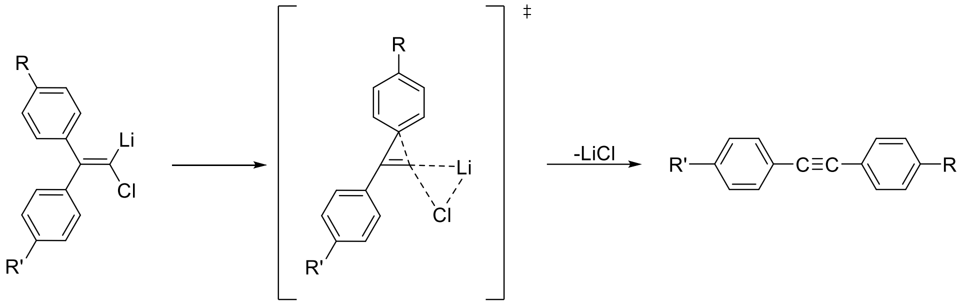

Scheme 4. Fritsch-Buttenberg-Wiechell rearrangement in β-aryl-substituted vinylic carbenoids.

Thermal Stability

The above-mentioned thermal lability of carbenoids is due to the ‘uncontrolled’ α-elimination of the metal salt and the concomitant liberation of an extremely reactive free carbene which limited early structure and reactivity investigations.[20] Thanks to results from X-ray crystallographic,[21] NMR spectroscopic[22] and computational studies[23] the instability of carbenoids can be explained by their unique hybridization in comparison to the protonated precursor. The C–X bond in carbenoids features a higher p-character in comparison to the protonated species resulting in their profound tendency to eliminate X^- and MX, respectively.

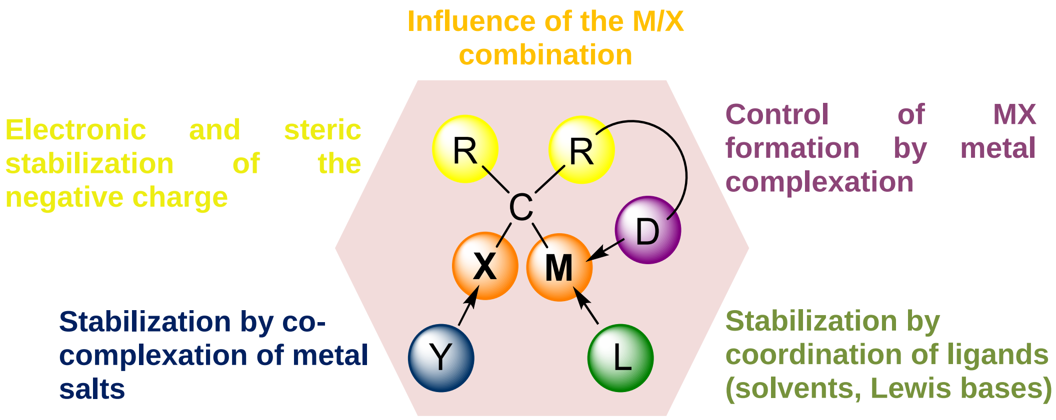

Figure 2. Factors influencing the thermal stability of carbenoids.

The thermal stability of a metal carbenoid and thus its carbenoid character can be influenced by a variety of factors (Figure 2): a) the M/X combination, b) the substitution pattern, c) the solvent as well as the presence of additional metal salts or donor bases.[20, 24] However, it is difficult to compare stabilities of different carbenoids since they are only comparable under the very same conditions. There are many known examples reporting on different stabilities for the same carbenoid.[25] The complexity of these species is due to the fact that the carbenoid stability depends on many parameters. This fact makes it extremely challenging but also highly desirable to control the reactivity and stability of carbenoids to broaden the scope of applications. This control could help to find alternatives to synthetic procedures requiring expensive transition metals and/or highly reactive or toxic reagents, mostly aryl-fuctionalized species, namely diazo or ylide compounds.

M/X Combination

In general, an increased stability from lithium to magnesium to zinc is observed. This is due to the decrease in bond polarity of the M–C bond in this series. This observation is in agreement with the stability of simple metal organyls which has been proven among others by Boche using metalated oxazoles.[23] While the ZnCl-oxazole **12-Zn** derivative could be isolated at –30 °C all attempts to prepare the corresponding lithiated species **12-Li** were unsuccessful resulting in the (Z)-2-isocyanollithium enolate **13-Li** because of a ring opening reaction (Scheme 5) which proceeded even at –78 °C. Computational studies revealed a higher p-character of the C–O bond in **12-Li** compared to **12-Zn** resulting in a more pronounced carbenoid character as well as a lower stability of the lithiated oxazole.

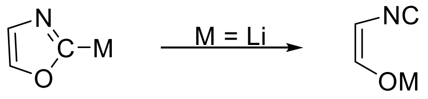

M = Li; **12-Li**
M =ZnCl; **12-Zn**

13-Li

Scheme 5. Lithiated and zincated oxazoles.

Due to the increased polarity of the metal–carbon bond from lithium to the heavier congeners, simple alkali metal organyls become less stable and more reactive. Surprisingly, alkali metal carbenoids show an inverse stability trend when going down the group of periodic table compared to simple alkali metal organyl compounds. Presumably, the higher stability is due to the lower Lewis acidity of the heavier alkali metals and the higher polarization of the M–C interaction. This results in a decreased polarization of the C–Cl bond and a hampered MX elimination.[26]

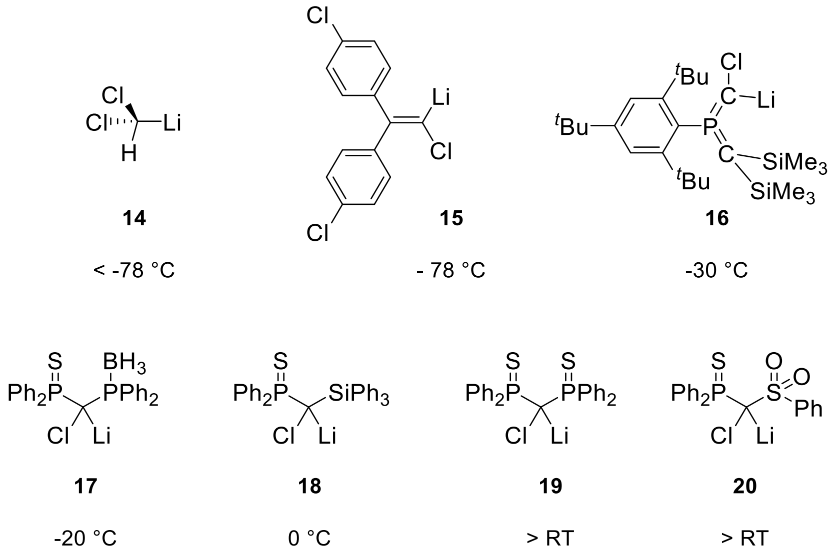

Figure 3. Isolated Li/Cl carbenoids and their decomposition temperature.

Gessner reported on an increased stability of the normally reactive compounds by simply changing from lithium to sodium or potassium. The sodium and potassium carbenoids **18-Na** and **18-K** were stable at room temperature, this allowed the isolation and the first structure elucidation of sodium and potassium carbenoids.[26] Not only the nature of the metal influences the stability and reactivity of carbenoids, but also the leaving group X. The leaving groups which result in the most pronounced carbenoid character are in general halogens (Hal) and ethers. Li/Hal carbenoids are the most reactive carbenoids and often have to be handled at temperature as low as –78 °C. These fundamental results date back to the 1960s when Köbrich studied simple carbenoid systems such as $LiCH_2Cl$ und $LiCH_2Br$.[27] A variety of experiments also proved that Li/Hal carbenoids are much more reactive than Li/OR carbenoids. In 2000, theoretical calculation suggest a decreasing carbenoid character in the series of $LiCH_2F > LiCH_2Cl > LiCH_2Br > LiCH_2I$.[28] The most reactive and least stable carbenoids, according to these series, are Li/F carbenoids and thus, they are still considered ‘the beast’ in carbenoid chemistry.[20] The simple carbenoid CF_3Li is quite elusive and decomposes under LiF elimination at temperatures below –100 °C. In 2014, Mitzel and coworkers[29] were able to isolate the carbenoid C_2F_5Li **21**, even though violent decomposition for the synthesis of **21** from $C_2F_5Cl/{}^nBuLi$ mixtures were reported before.[30] The carbenoid **21** was found to be stable in solution below –60 °C. The solid state structure (Figure 4) revealed a dimeric structure with the lithium atoms being coordinated by two ether molecules and one fluorine atom. The increased stability in comparison to the elusive CF_3Li is explained by the better stabilization of the carbene F_2C**:** in comparison to $F_3C(F)C$**:** and thus, the less favored formation of the later.[29] Furthermore, the carbenoid character for simple carbenoids of the general constitution $LiCH_2X$

is more pronounced with groups of the second row of the periodic table (X = NH_2, OH, F) than for third row elements (X = PH, SH, Cl). This trend was attributed to the decreasing electronegativity and the increasing anion-stabilizing ability due to negative hyperconjugation und polarization effects when going to the heavier congeners. Noteworthy, α-lithiated amines do not possess a carbenoid character[31] with one exception: aziridines.

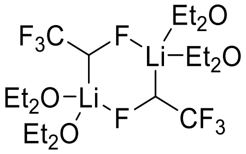

21

Figure 4. Dimeric structure of C_2F_5Li in the solid state.

The strain in the three-membered ring causes them to perform α-elimination reactions.[32] Moreover, α-lithiated arylthioethers, such as $LiC(SAr)_3$[33] or $PhSCH_2Li$,[34] were found to exhibit a carbenoid like behavior.[35] Although, most lithiated thioethers show an analogous reaction behavior to simple organolithium species. Recently, sulfoxides were added to the group of species that might exhibit a carbenoid character.[36]

The Substitution Pattern

Besides the M/X combination, the substitution pattern of a carbenoid is also a crucial factor in determining its stability. The first isolated and structurally characterized Li/Cl carbenoid **15** was reported by Boche and coworkers in 1993 (Figure 3).[21b, 21c] The increased thermal stability in comparison to the simple CH_2MX (M = alkali metal, X = halogen) carbenoids is due to the change of hybridization in the vinylic system **15** from sp^3 to sp^2 resulting in a higher s-character of the C–M bond leading to an improved stabilization of the negative charge and a higher stability of the respective carbenoid. Carbenoid **15** was found to be stable up to –60 °C. Only two years later, Niecke *et al.* succeeded in synthesizing the methylene(phosphoranylidene) carbenoid **16** which was the most stable Li/Cl carbenoid for a long time being stable up to – 10 °C. The fact that the carbenoid center is part of a delocalized electron framework expanding over three atoms might be the reason for the enhanced kinetic stability of this species.[37] The right choice of substituents even allows the isolation of room temperature stable carbenoid systems which was impressively demonstrated by Le Floch and coworkers in 2007 by the isolation of the Li/Cl carbenoid **19** (Figure 3). The strong stabilization of the lithium cation provided by the coordination of the two sulfur atoms as well as the ether molecules hamper the LiCl elimination and thus, results in an increased stability. Additionally, theoretical calculations suggest the lone pair of the central lithiated carbon atom being located in a pure p-orbital and thus, being efficiently stabilized by negative hyperconjugation into the phosphorus antibonding orbitals. Consequently, the Li/Cl carbenoid **19** bears a rather strong C–Cl bond due to the high carbon s-character in this bond.[38] Until now, a number of room temperature stable Li/Cl carbenoids have been isolated by Gessner,[19a, 39] and Mezailles.[40] Applying the same principles, Chivers and coworkers reported on a stable bis(thiophosphoryl) Li/I carbenoid.[41] In general, the use of electron-withdrawing groups is beneficial since they stabilize the carbenoid and consequently, decrease the chance of MX elimination. This can be shown nicely by comparing the simple systems $LiCHBr_2$ and $LiCBr_3$. Tribromomethyllithium is more stable than dibromomethyllithium and can even be synthesized by reacting dibromomethyllithium and bromoform.[27a] Besides applying electron-withdrawing substituents to stabilize the carbenoid carbon center, the absence or existence of possible decomposition pathways can also determine the carbenoid thermal stability. This phenomenon can be seen by comparing the decomposition temperature of **17** and **19**. The presence of the BH_3 group in **17** paves the way to intramolecular B–H activation and thus, results in a significant decrease of stabilization in comparison to the symmetric bis(thiophosphoryl) system **19** (Figure 3).[38, 40a]

The Presence of Additional Donor Bases or Metal Salts

The most common decomposition pathway of carbenoids is the α-elimination and it can be significantly hampered by the complexation of the metal by donor bases or metal salts. This stabilization can occur intra- or intermolecularly by donor-functionalized substituents or by coordinating solvents or additional Lewis bases, respectively. Generally, the complexation of the metal by donor bases leads to a decrease in the Lewis acidity of the metal, an increase of its solubility, and a disruption of the M–X interaction. This disruption significantly hinders the α-elimination of the metal salt and thus, results in an increased thermal stability.[20] In this regard, Gessner *et al.* were able to show that the presence of crown ether indeed increases the thermal stability of Li/Cl carbenoid **18** and its K/Cl congener. The solid state structure of both carbenoids shows a separated ion pair and thus, a full disruption of the M–X interaction (Figure 5).[26, 42] In case of the Li/Cl carbenoid the thermal stability in tetrahydrofuran (THF) increased from 0 °C in the absence of 14-crown-4 (14-C-4) to 20 °C in the presence of 14-C-4. The same trend was observed for the K/Cl carbenoid, without 18-crown-6 (18-C-6) the VT-NMR spectroscopic studies reveal a decomposition of the system at 30 °C and with the additional

Lewis base the carbenoid remained stable up to 40 °C. However, the influence of the additional Lewis base is more pronounced in case of the Li/Cl compound than in case of the heavier congener.[42] An influence of the solvent to the thermal stability of carbenoids was already observed by Köbrich and coworkers in their seminal studies on simple carbenoids. Carbenoids featured a higher stability in THF than in diethylether (Et_2O). They determined critical ratios of Et_2O/THF in which the carbenoid was still stable and able to perform selective conversion.[24, 25b, 27c, 43] In this course, the so-called 'Trapp mixture' (THF/Et_2O/petrol ether = 4/4/1) was suggested as the ideal solvent mixture for the preparation of carbenoids due to its low viscosity and the still present favorable influence of the coordinating solvent THF.[24]

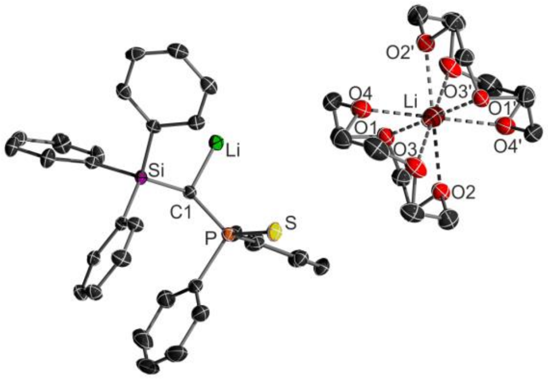

Figure 5. Molecular structure of the Li/Cl carbenoid **18** • (12-C-4)$_2$.

Another strategy to increase the stability of carbenoids is the use of strong and often multidentate *N*- or *O*-donor ligands, such as *N,N,N′,N′*-tetramethylethane-1,2-diamine (TMEDA) and *N,N,N′,N″,N″*-pentamethyldiethylenetriamine (PMDETA). Additionally, this is also beneficial for the isolation of carbenoids. This concept was for example employed in the case of **15 (**Figure 3**)**. With the help of TMEDA, it was possible to isolate and structurally characterize **15**. The presence of additional donor ligands can also effect the stereochemistry of transformations, e.g. in the lithiation and subsequent deuteration of *m*-trifluoromethylstyrene oxide. The presence of TMEDA in the reaction mixture resulted in a change of the enantiomeric ratio (er) from 85:15 to 96:4.[44] Another approach to influence the carbenoid stability is the coordination of the nucleofugal group by metal salts. Salt effects in *α*-elimination reactions have been observed already in the 1960s. The yield as well as the product ratio in cyclopropanation reaction was found to depend on the halide ion present in solution.[45] Later, salt effects were also found in metal halide carbenoids by Villieras *et al.* observing a higher yield of $LiCH_2Br$ in the presence of an additional equivalent of LiBr.[46] The work groups of

Matteson[25c, 47] and Pace[48] highlighted the benefit on carbenoid formation of using MeLi•LiBr as a mixed metalating reagent (Scheme 6).

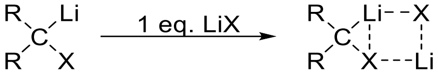

Scheme 6. Stabilization of Li/X carbenoids by Li halide complexation.

The additional metal salt MX is thought to co-aggregate the carbenoid resulting in a weakened or disrupted M–X interaction within the carbenoid and thus, in a stabilization of the carbenoid by hampering α-elimination of the metal salt[46] which is a typical and characteristic feature of carbenoids and the reason for carbenoid thermolability. As shown, carbenoid stability is influenced by a variety of factors making it difficult to predict carbenoid stability and reactivity under certain reaction conditions, but also, allowing to adjust, fine-tune and control their stability and reactivity.

Preparation of Carbenoids

Due to the thermal sensitivity of carbenoids their generation is typically performed at low temperatures and often no isolation of these sensitive compounds is attempted, instead they are directly used *in-situ* after their generation. As mentioned above, the choice of the right reaction conditions (temperature, solvent, additional donor bases or metal salts) is crucial for the successful carbenoid synthesis. Usually, the last step of the carbenoid synthesis is the introduction of either the metal or the leaving group. The later requires a germinal-dimetalated precursor, thus, metalation is the commonly used approach to carbenoid synthesis. There are three synthetic routes for carbenoid formation (Figure 6): a) direct metalation of the protonated precursor, b) halogen/metal exchange and c) mild oxidation of a twice metalated precursor.[20] The right synthetic approach for carbenoid generation is dependent on the halogen atom used. Especially in case of bromine and iodine starting materials the halogen/metal exchange is widely used for the generation of lithium carbenoids.[2-3, 15, 24, 27a, 46-47, 49] However, only a few halogen/magnesium exchange reactions are known.[49a, 50] One commonly used method in case of the generation and use of halomethyllithium carbenoids is the so-called ‘Barbier method’. During his work on organomagnesium chemistry, Barbier discovered a one-step reaction including the carbenoid generation directly in the presence of the electrophile. These reaction conditions guarantee the immediate reaction of the reactive carbenoid species, mostly halomethyllithium, with the substrate.[51] Following this reaction protocol, carbenoids have been successfully employed in organic synthesis.[48, 49d, 52] Even though, the applicability of the Barbier conditions are limited in case of a faster reaction of the alkyl lithium reagent with the substrate than the formation of the carbenoid.[53]

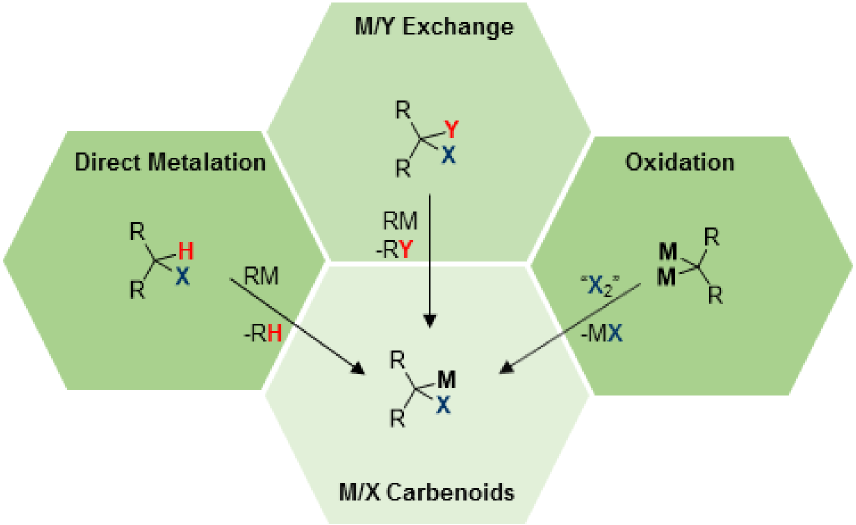

Figure 6. Synthetic routes for the preparation of M/X carbenoids.

Direct metalation of a protonated haloprecursor is also a common way to synthesize carbenoids in case of electron-withdrawing groups (EWG) as substituents.[19b, 26, 42, 54] Another possibility for the lithium carbenoid synthesis is the mild oxidation of a double lithiated precursor as demonstrated by Le Floch using hexachloroethane as an oxidation reagent resulting in the formation of the Li/Cl carbenoid **19** (Figure 3).[38] The analogous Li/I carbenoid could be successfully obtained using iodine as the oxidation reagent.[41] However, this synthetic approach for carbenoid synthesis is limited by the small number of methandiides as readily accessible precursors.[19a, 39] Additional to these synthetic approaches, a number of other strategies for carbenoid generation has been reported. They are limited to a small number of substrates and not generally applicable, among them is the preparation of enantiomerically pure chloromethyllithium *via* tin/lithium exchange[25d] or sulfoxide/metal exchange reactions. This was first only reported for magnesium carbenoids[55] but was later transferred to lithium compounds.[56]

Structures and Characterization of Carbenoids

NMR Spectroscopy

Due to the already mentioned thermal lability of carbenoids the first experimental investigations were mainly limited to *in-situ* solution NMR spectroscopic studies at low temperatures. Here, the group of Seebach is to mention which performed detailed studies on different lithium carbenoids.[22, 57] These studies on a variety of lithium carbenoids revealed a distinct deshielding of the carbenoid carbon atom in the ^{13}C NMR spectrum with a down-field shift – up to $\Delta\delta_C$ = 280 ppm in case of iodoform – in comparison to the protonated congeners (Table 1). The deshielding of the carbenoid carbon atom increases in the series Cl < Br < I and also with an increasing number of halogen atoms bound to the carbenoid carbon atom (entries 1-3, Table 1).[57c] The same is valid for the number of oxygen substituents at the carbenoid carbon atom (entries 9-10). The NMR spectroscopic results observed for Li/OR carbenoids are in agreement with the ones for Li/Hal carbenoids, although, the down-field shift is not as pronounced emphasizing the more pronounced carbenoid character of Li/Hal carbenoids.[58] This observation is in contrast to the typical high-field shift for simple organolithium compounds[22, 59] but agrees with the NMR spectroscopic studies of free carbenes. Therefore, the shift is less pronounced in zinc or magnesium carbenoids. Especially, in zinc systems no distinctive down-field shift is observable (see entries 13 and 14, Table 1). Boche *et al*. were able to confirm the experimentally observed down-field shift with the help of IGLO (individual gauge for localized orbitals) calculations with which it is possible to localize the molecular orbitals of compounds. Usually, the carbenoid carbon atoms bears a partial negative charge which would result in a shielding instead of a deshielding. However, the theoretical calculations were able to explain the experimental results by a polarization of the C–X bond as a result of the metalation which results in the deshielding. Carbenoids were found to have a higher $\sigma_{C\text{-}Li}$- and a lower $\sigma^*_{C\text{-}X}$-orbital. The higher the $\sigma_{C\text{-}Li}$- and the lower the $\sigma^*_{C\text{-}X}$-orbital the greater is the deshielding.[58] Although, the deshielding of the carbenoid carbon atom in ^{13}C NMR spectroscopy is indicative for its carbenoid character, it is no exclusion criterion since the NMR shifts can change dramatically depending on the complexation of the metal or the substitution pattern.[22]

Table 1. Comparison of the ^{13}C NMR chemical shifts of a variety of metal carbenoids compared to the protonated analogues.

	Carbenoid	**δ_{13C} [ppm]**	**$\Delta\delta_{13C}$ M/H [ppm]**
1[22]	$LiCH_2Cl$	57.9	32.3
2[60]	$LiCHCl_2$	105.5	50.0
3[60]	$LiCCl_3$	145.9	65.9
4[57c]	$LiCHI_2$	≈ 131	278
5[58]	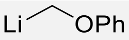	74.5	19.7
6[58]	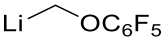	92.2	29.9
7[61]	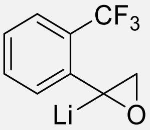	≈ 83.3	≈31.3
8[58]	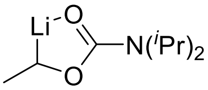	67.3	7.0
9[58]	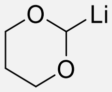	134.8	40.0
10[58]	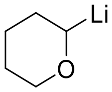	95.7	26.2
11[26]	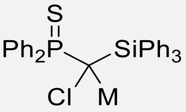	M = Li: 37.6 M = Na: 42.9 M = K: 42.6	M = Li: -4.7 M = Na: 0.6 M = K: 0.3
12[62]	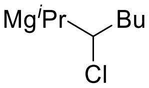	68.8	24.8
13[63]	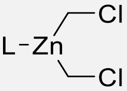	L = DME: 29.6 L = Bipy: 32.9	L = DME: 4.0 L = Bipy: 7.3
14[64]	$XZnCH_2I$	X = $(BuO)_2P(O)O$: -23.7 RO: ≈ -27.0	X = $(BuO)_2P(O)O$: -0.1 RO: ≈ -3.4

The disruption of the carbon metal bond by coordinating donor bases, namely PMDETA or crown ether, results in a minimization of the ^{13}C NMR spectroscopic shift.[58] Another parameter found to be indicative for the carbenoid character is the $^{1}J_{13C\text{-}6Li}$ coupling constant. One characteristic feature of carbenoids is the almost constant $^{1}J_{13C\text{-}6Li}$ coupling constant of 16.3 – 17.0 Hz due to the higher s-character of the carbenoid carbon atom in comparison to simple organolithium species usually featuring a coupling constant of 8 – 10 Hz. These values are valid for halogen, cyclopropyl as well as vinylic carbenoids. It was found to be independent of the number or nature of the halogen.[22] Generally, the respective $J_{13C\text{-}13C}$ and $J_{13C\text{-}1H}$ coupling constants in carbenoids were found to decrease due to the higher p-character of the respective bonds (Figure 7).[57a-c, 65]

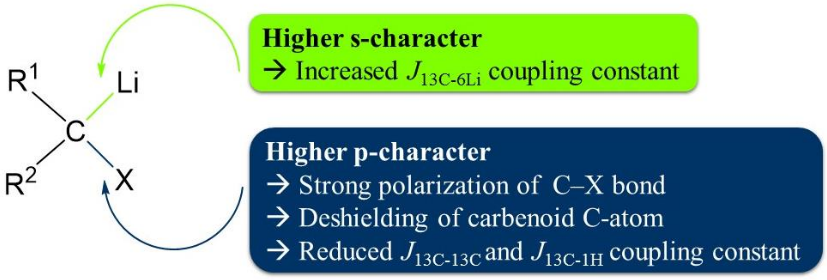

Figure 7. NMR spectroscopic characteristica of Li/X carbenoids.

Analogous observations were not found for zinc or magnesium carbenoids due to the higher covalent character and thus, the higher p-character in the metal-carbon bond. The ^{13}C NMR spectra of these compounds often show a high-field shift compared to the protonated precursor.[66]

Computational Studies

To further elucidate the structure and stabilities of carbenoids theoretical calculation were performed on simple carbenoid species with the general constitution MCH_2X (M = Li, Na and X = CH_3, NH_2, OH, F, SiH_3, SH and Cl). However, these calculations neither consider the solvation by solvent molecules nor dimeric structures. The seminal studies by Schleyer and coworkers revealed a preference of a bridged structure such as **I (**Figure 8) bearing contacts between the lithium and both the carbon atom and the leaving group. This conformation is especially favored by compounds exhibiting nucleofugal groups from the first row since they are better stabilized by lithium bridging. Sodium flourine carbenoids show a smaller tendency for the bridged conformation than their lithium analogs due to the favorable Li–F interactions.[67]

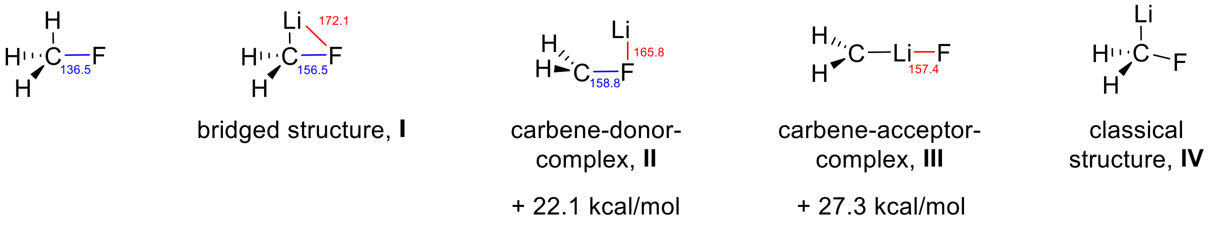

bridged structure, **I**

carbene-donor-complex, **II**
+ 22.1 kcal/mol

carbene-acceptor-complex, **III**
+ 27.3 kcal/mol

classical structure, **IV**

Figure 8. Results of the quantum chemical calculation on the different structural isomeres of $LiCH_2F$ with selected bond lengths in pm.[68]

The bridged structure **I** was found to be preferable to the classical structure **IV**, the carbene-donor-complex **II** and the carbene-acceptor-complex **III**. The classical structure **IV** was not observed for lithium fluorine carbenoids due to the strong Li–F interaction. The same trends were found to be valid for $LiCH_2OH$ and $LiCH_2NH_2$ bearing energetically favorable Li–O and Li–N coordination, respectively. Later, theoretical studies revealed the existence of aggregates analogous to simple organolithium compounds.[69] In case of $LiCH_2F$, a dimeric structure (VI, Figure 9) bearing a weaker Li^1F^1 contact ($\Delta d = 26.6$ pm) and also an elongated C^1F^1 bound ($\Delta d = 7.1$ pm) compared to the monomeric structure it was found to be more stable by 56.2 kcal/mol.[70] Noteworthy, also the enthalpy of formation of the free carbene H_2C: was found to be lower by 21.9 kcal/mol starting from the dimer compared to the monomer.

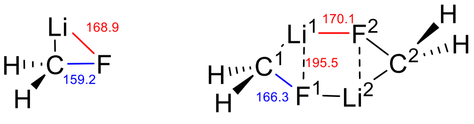

V

VI
-56.2 kcal/mol

Figure 9. Results of the quantum chemical calculations on the aggregation of $LiCH_2F$ with selected bond lengths in pm.

One characteristic feature for carbenoids is the elongation of the C–X bond. In case of $LiCH_2F$ the C–F bond is elongated by $\Delta d = 20$ pm to 156.5 pm in comparison to the respective bond in fluoromethane (136.5 pm).[68] A smaller elongation was found in $LiCH_2NH_2$ with a difference in bond length of only $\Delta d = 11.4$ pm compared to the protonated congener.[71] An exception to this rule is the $LiCH_2SH$ system, showing a shortening of the C–S bond in comparison to the protonated precursor.[20, 33-34] Consequently, the elongation of the C–X bond is not an exclusion criteria for the carbenoid nature of compounds since no carbenoid like reactivity was found for $LiCH_2NH_2$ systems, with the exceptions of aziridines,[32, 72] but for thioethers. Furthermore, carbenoids bearing no C–X bond elongation but a carbenoid reactivity were isolated.[73]

Additionally, to gain structural information, DFT calculation were performed to elucidate the electronic structure of carbenoids. The C–M bond bears a higher s-character resulting in a higher p-character of the C–X bond compared to the carbenoid precursor. This trend was at first only demonstrated for lithium carbenoids,[28] was then also found to be valid for zinc[28] and magnesium[74] species. Worth mentioning, the room temperature stable carbenoid **17** (Figure 3) was found to be an exception to this rule since the respective C–Cl bond does not bear a significantly higher p-character.[38]

X-ray Diffraction Analysis

As predicted by theoretical calculation and analogously to simple organolithium compounds a variety of structural motifs (monomer, dimer, tetramer and oligomer) were found for carbenoids by means of X-ray diffraction analysis. The structural motifs depend on the degree of hybridization of the carbenoid carbon atom, steric and/or electronic effects of the substituents, additional donor functionalities within the molecule and the coordination of additional Lewis bases. Harder *et al.* reported on the first successful X-ray diffraction analysis of the lithium carbenoid **22** in 1989 (Figure 10).[75]

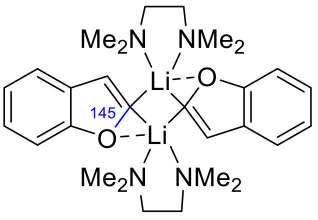

22

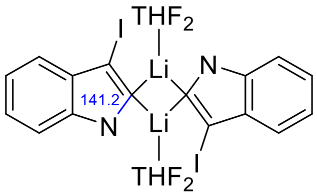

23

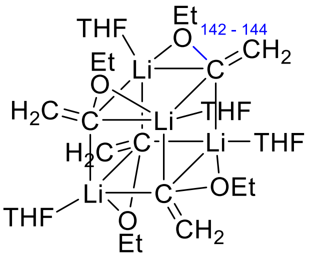

24

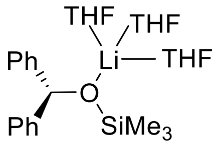

25

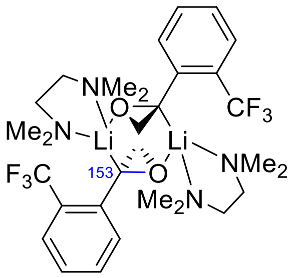

26

Figure 10. Isolated and structurally characterized α-lithiated ethers and amines.

Based on the X-ray diffraction data the lithiated ether exhibits a long C–O bond of 145 pm and a dimeric structure with the benzofuryl rings being bridged by the two lithium atoms which are each additionally coordinated by one TMEDA molecule. A similar structure was found for the 2-bromo-substituted congener.[76] Both species are stable at room temperature and unfortunately, show no Li/OR elimination tendency indicating only a weak carbenoid character.[20] The α-lithiated amine **23** also shows a slight elongation of the C–N bond and a deshielding of the anionic ^{13}C NMR signal which is in accordance with observations of species of the general type $LiCR^1R^2(NR_2)$. So far, no carbenoid like reactivity was reported for these α-lithiated amines,[31a-c, 77] contrary to their ether analogs. Consequently, they are only classified as simple carbanions and not carbenoids.[18b] For the α-ethoxyvinyllithium compound **24** elongated C–O bonds (142-144 pm) and a distinctive deshielding of the carbenoid carbon atom was observed. In the solid state the carbenoid forms a lithium bridged tetramer.[78] The silylether **25** characterized by Boche *et al.* in 1993 was the first carbenoid exhibiting a carbene-donor motif (Figure 8, **II**). Even though, no direct C–Li contact was observed the carbenoid nature was confirmed by the downfield shift of the ^{13}C NMR spectroscopic signal of the carbenoid carbon as well as the strong elongation of the C–O bond to 148.8 pm.[79] The comparison with the average bond lengths of a variety of differently hybridized $C_{sp2/3}$ $OSiMe_3$-groups indicates a sp^3- rather than a sp^2-hybridization in compound **25**.[66] Further carbenoid representatives are lithiated epoxides which have long been considered short-lived intermediates. The strain in the three-membered ring results in a pronounced carbenoid character and high reactivity. Carpriati and Stalke reported on the oxiranyllithium **26** bearing a dimeric structure in the solid state and a long C–O bond of 153 pm.[61] Li/Cl carbenoids were isolated and structurally characterized after the first Li/OR carbenoids owing to their thermal lability and high reactivity. In 1993, Boche and coworkers were able to fully characterize the vinylic Li/Cl carbenoid **15** (Figure 3) by means of X-ray diffraction analysis. As expected for carbenoids, compound **15** bears a long C–Cl bond of 185.5 pm ($\Delta d = 12.4$ pm). No Li–C–Cl interaction was observed due to the coordination of the Li atom by both TMEDA and THF.[21b, 21c] The first Li/Cl carbenoid **14** (Figure 3) bearing a tetrahedral carbon atom was isolated in 1996.[25a] Similar to **15**, the Li atom in **14** is also coordinated by additional donor bases, in this case three pyridine molecules. As characteristic for carbenoids, this compound shows an elongation of the C–Cl bonds by $\Delta d = 10$ pm to 183.3 and 185.7 pm, respectively. The sum of angles around the carbenoid carbon atom is relatively small (308°) in comparison to the expected 328° for an ideal tetrahedral geometry. This suggests a higher p-character in both the C–H and C–Cl bond and thus, a higher s-character in the respective C–Li bond. The first room temperature stable Li/Cl carbenoid **19 (**Figure 3**)** does not exhibit the characteristic C–Cl bond elongation.[38] However, the carbenoid character was proven by the reactivity of **19** towards $[Pd(PPh_3)_4]$ yielding a carbene complex (Scheme 18).[19c] Recently, the group of Gessner succeeded in isolating a number of room temperature stabile carbenoids thanks to the introduction of a variety of stabilizing substituents. The compounds **18**· (12-crown-4)$_2$[26] (12-C-4) and **20**[39a] (Figure 3) do not exhibit a Li/Cl contact and almost no lengthening of the C–Cl bond in the solid state (Δd = 2 pm and Δd = 0.5 pm). Besides Li/Cl carbenoids, only a limited number of other Li/Hal carbenoids has been isolated to date. In case of Li/I carbenoids only the analogous Li/I species of compound **19** (Figure 3) which also shows no C–I bond elongation. However, it is temperature labile due to the proximity of the lithium and iodide atom found in the solid state which results in an facile Li/I elimination.[41] The first structurally characterized Li/Br and Li/F carbenoids are the analogs of species **16 (**Figure 3**)**. The Li/Br congener shows a distinctive C–Br bond lengthening from 187.7 to 196.7 pm (Δd = 9 pm).[80] The first alkyl Li/Br system, the analogous compound to **19**, was published by Gessner *et al.* bearing no lengthening of the C–Br bond.[81] Only recently, the first sp^3-hybridized Li/F carbenoid F_3CCF_2Li was structurally characterized. The carbenoid crystallizes as a dimer and bears a distinctive C–F elongation by Δd = 6.6 pm to 141.6 pm characteristic for carbenoids. In 2016 and 2017, the group of Gessner reported on the first isolated and structurally characterized Na/Cl and K/Cl[26] as well as Na/Br and K/Br carbenoids,[81] respectively. The first being the Na and K congeners of **18** and the later being analogous species of **19 (**Figure 3**)**. Compound **18-Na** crystallizes as a monomer with three coordinating THF molecules, while **18-K** forms a dimeric structure with each potassium being coordinated by the chloro and thiosphosporyl substituents as well as one THF ligand and one silicon-bound phenyl group by η^6-coordination (Figure 11). In both cases no C–M contact is observed and the structural motif can be described as a carbene-donor-complex (Figure 8, **II**). Both congeners exhibit a lengthening of the respective C–Cl bond form 178.8 pm to 184.5 pm (**18-Na**) and 182.4 pm (**18-K**).[26]

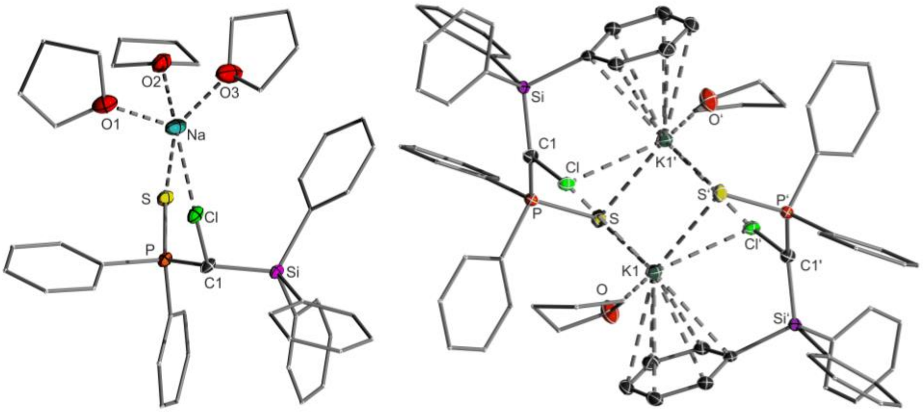

Figure 11. Molecular structure of **18-Na** (left) and **18-K** (right). Hydrogen atoms are omitted for clarity.

In case of the M/Br carbenoids, the solid state structure of both carbenoids reveals a lengthening of the C-Br bond from 196.4 pm to 197.3 pm (Na/Br) and 196.7 pm (K/Br), respectively, which is in contrast to the Li/Cl congener. Analogously to the above-mentioned Na/Cl **18-Na** and K/Cl **18-K** carbenoids the respective bromine carbenoids show similar solid state structures. The Na/Br carbenoid **19-Na** crystallizes as a monomer with the Na atom being coordinated by both sulfur atoms and three additional THF ligands. The K/Br compound forms a dimeric structure in which the potassium is coordinated by both sulfur atoms of the thiophosphoryl moiety, the chloro substituent as well as two THF molecules. Worth mentioning, the structural motifs observed in M/Hal carbenoids do not compare with the variety observed in Li/OR carbenoid chemistry. So far, no M/Hal carbenoid exhibing the bridged structural motif (Figure 8, **I**) which was predicted by computational studies and observed in case of Li/OR carbenoids (Figure 10) was isolated. In case of Li/Cl carbenoids, most compounds exhibit either the classical structural motif bearing a C–Li interaction, e.g. carbenoids **14-16** or a coordination of the lithium atom by only external solvent molecules or intramolecular substituents featuring a donor group. A sufficient coordination of the metal ion is crucial to hamper or even prevent MX elimination. In most cases, the expected C–X bond elongation was observed in the solid state. However, the degree of bond lengthening is not a measure for the carbenoid stability since compound **19-I** does not feature any lengthened C–I bond but is nonetheless less stable than the respective chloro congener **19**.

Reactivity of Carbenoids

Application in Organic Synthesis

Until now, most reactions using carbenoids are performed at low temperatures due to the possible α-elimination of the corresponding metal salt. Especially reaction protocols with Li/X carbenoids require temperatures as low as –78 °C. First reactivity studies focused mostly on lithium carbenoids owing to their higher reactivity compared to the heavier congeners. Due to their ambiphilic nature carbenoids can either react as nucleophiles or electrophiles. The use of carbenoids in cyclopropanation reactions proved their electrophilic character[1-2] but also their nucleophilic nature was early confirmed by the reaction of the vinylic Li/F carbenoid **27** with CO_2 at –105 °C with subsequent acidic workup yielding the corresponding carbonic acid **28**.[27b] The presence of the β-fluorosubstituents results in a stabilization of the Li/F carbenoid **29** and thus, allowing a selective reaction to the carbonic acid **30** at only –40 °C (Scheme 7).[17] Further typical reactions demonstration the nucleophilic nature of carbenoids are the conversion with carbonyl compounds[46, 82] and alkylhalides.[83]

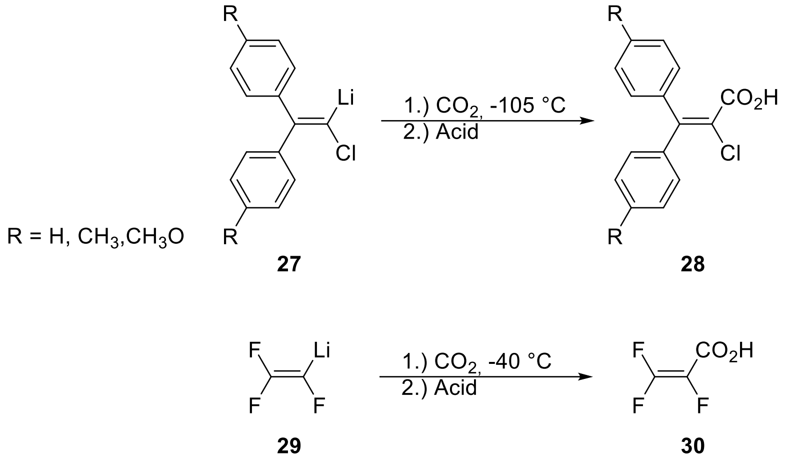

Scheme 7. Reaction of Li/Hal carbenoids with CO_2.[17, 27b]

However, the electrophilic character of carbenoids is by far more interesting and fascinating since it distinguishes carbenoids from simple metal organyls. Since the pioneering work of Simmons and Smith[1] the cyclopropanation of olefins is the most common application of carbenoids to date. Noteworthy, mostly zinc carbenoids are employed owing to their more pronounced covalent character resulting in a higher selectivity compared to the lithium congeners. Further studies of cyclopropanation reactions enabled diastereo- and enantioselective reaction protocols.[84] Theoretical calculations were performed to shed light on the mechanism of this reaction (Scheme 8).

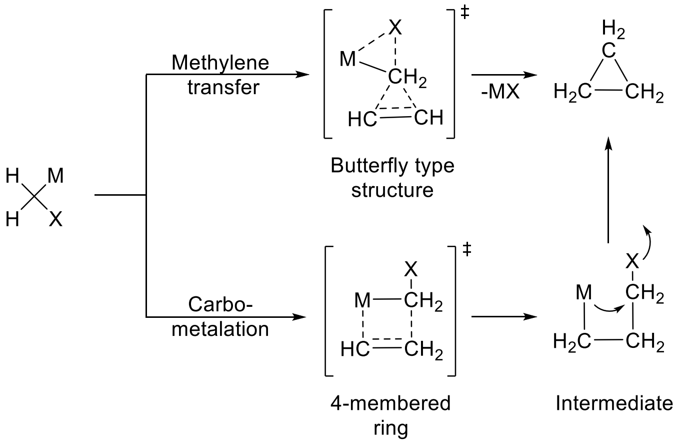

Scheme 8. Possible reaction mechanism of cyclopropanation reaction.

In case of lithiated dichloromethane the intermediates of the two possible reaction pathways – methylene transfer and carbometalation – were found to be similar in energy. On the contrary, the intermediates of the corresponding zinc system showed a high preference for the methylene transfer.[85]

Further investigations on a variety of carbenoids also considered the influence of aggregation and solvation on the mechanism. Under these conditions the concerted pathway of the methylene transfer is favored compared to the stepwise mechanism of the carbometalation.[86] Boche *et al.*[28] examined the influence of the halogen on the formation of cyclopropane rings showing that there is no significant halogen influence since the energy gain of the Li–X bond formation compensates the higher required energy of the C–X bond breaking. However, there is an influence of the leaving group since both theoretical as well as experimental studies showed that Li/OR carbenoids are not suitable for cyclopropanation reactions.[87] Cyclopropanation reactions are not the only class of reactions showing the electrophilic nature of carbenoids. Köbrich and coworkers were able to proof the electrophilicity of these compounds investigating 1,2-aryl- and alkyl rearrangement. The most popular and oldest representative of this class of reactions is the Fritsch-Buttenberg-Wichell-rearrangement of β-aryl-substituted vinylic carbenoids yielding alkynes (Scheme 4).[88] Upon warming, the vinylic carbenoid reacts to the corresponding diarylalkyne. The stereoselectivity of this reaction suggested the presence of the metal and halogen in the transition state since it would not have been observed *via* the free vinylidene. The postulated mechanism includes the replacement of the chlorine substituent by the aryl moiety trans to it resulting in the observed product.[27b] Another reaction that can take place upon warming is the eliminative dimerization which is well known for carbenes.[89] However, it is really challenging to proof this kind of reaction for carbenoids experimentally.[90] In 1966, Köbrich and coworkers succeeded in proofing that carbenoids undergo eliminative dimerization reactions in which course the carbenoid reacts with itself as a nucleophile as well as an electrophile. Dichloromethyllithium **31** reacts to 1,2-dichloromethane **33**. Nevertheless, it was not possible to verify the existence of the intermediate species **32** owing to the fast α-elimination of LiCl (Scheme 9).[25b] In case of less reactive vinylic copper and zinc carbenoids it is possible to isolate the intermediate.[91]

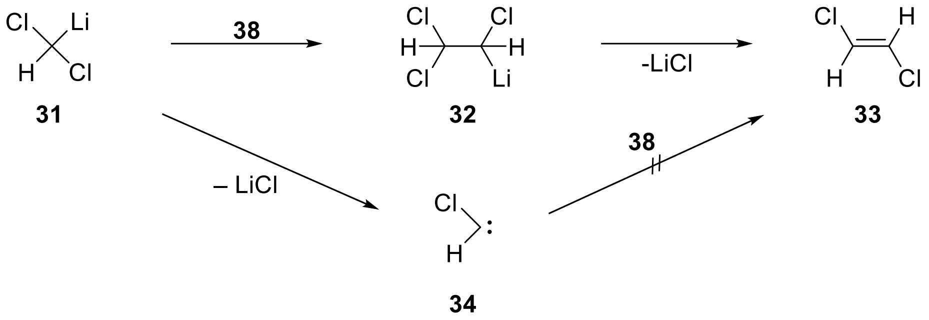

Scheme 9. Eliminative dimerizatoin of $CHCl_2Li$ **31**.

Chivers[41] and Gessner[81] observed dimerization in case of the stabilized M/X carbenoids **18** and **19-I** (Figure 3) resulting in a cyclic dimer bearing an unsaturated six-membered $S_2C_2P_2$ ring. Chivers postulated the product **37** to be derived from the union of two carbenes **35** without the incorporation of LiI. First an intermolecular nucleophilic attack of the sulfur atom of the carbene **35** at the electron-deficient carbene carbon center takes place resulting in the C–S bond formation. Concomitantly, the S–P bond is formed to afford a five-membered ring. Finally, the sulfur atom of the five-membered ring of the intermediate **36-Carb** intramolecularly attacks the exocyclic carbene center forming the six-membered ring in **37** (Scheme 10). On the contrary, Gessner *et al.* showed that this cyclization proceeds *via* a thioketone intermediate **36-Thio** instead of the free carbene **35**. After the elimination of the metal salt, the thioketone intermediate **36-Thio** is formed *via* a sulfur transfer from the phosphorous atom to the central carbon atom (Scheme 10). This assumption was proven by trapping the thioketone intermediate **36-Thio** with MeLi or PhLi.[54b]

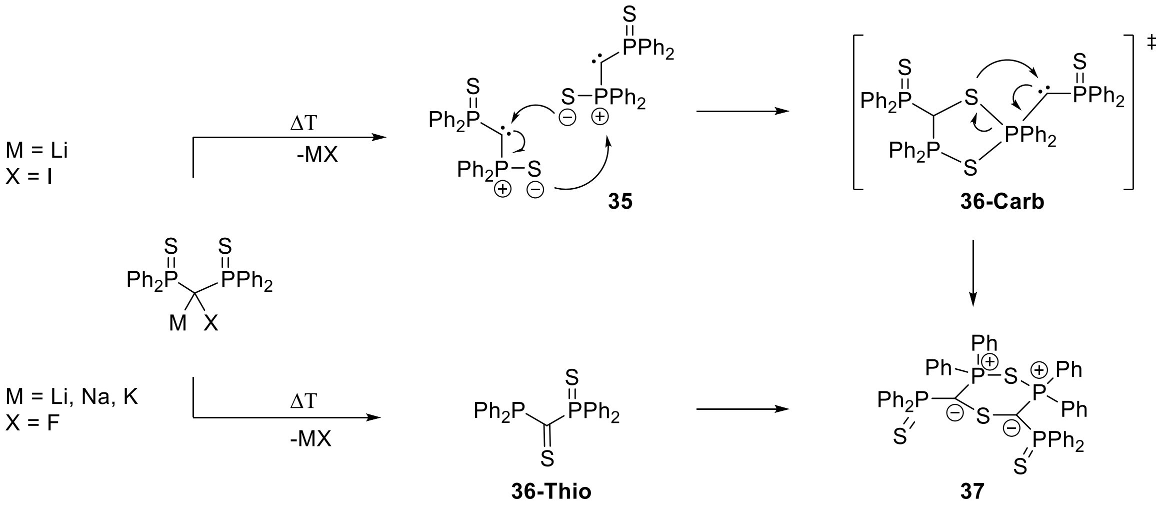

Scheme 10. **P**ostulated mechanism of carbenoid dimerization of M/X carbenoids.

Besides dimerization reactions carbenoids can undergo insertion reaction with concomitant α-elimination. Goldstein and Dolbier became interested in these reactions and the question if the carbenoid or the free carbene formed by α-elimination undergo these C–H(D) insertions reactions (Scheme 11, left). They found that the product mixture **39** and **40** depends on the nature of the halogen. Consequently, the halogen has to be involved in the intermediate state in some way leading to the conclusion that the carbenoid itself and not the carbene undergo insertion reactions.[92] In this regard, Kirmse and Wächterhäuser investigated the product mixture of insertion reactions of M/I (M = Li, Na, K, Mg, Zn, Cu) carbenoids and carbenes – derived from the respective diazo compound – in neoalkyl like compounds. They reported on a metal dependence of the insertion reactions. In case of lithium, sodium and magnesium the main products are cyclopropane **42** and **43**, contrary, using zinc and copper results in a 1,2-alkyl shifts and consequently, olefins **44** and **45** as products (Scheme 11, right). [93]

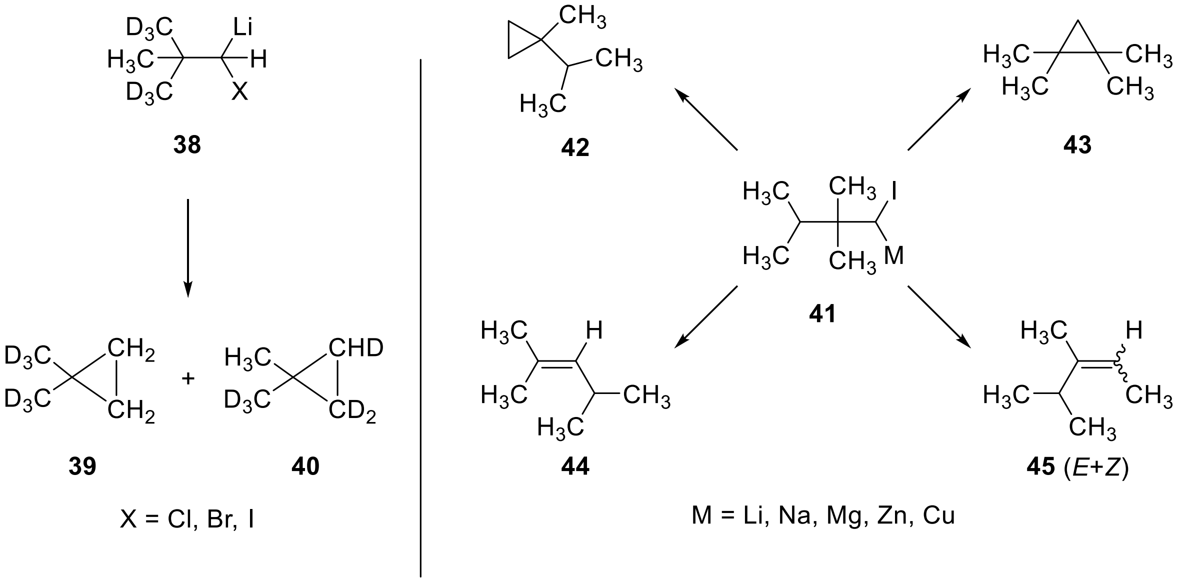

Scheme 11. Left: C–H(D) insertion reactions starting from Li/X carbenoids. Right: Product dependence on the metal atom in insertion reactions starting from I/M carbenoids.

Another type of insertion reaction carbenoids are used for are homologation reaction. These reactions are a fundamental tool to elongate a given fragment *via* the formal insertion of a CH_2 moiety. Homologation reaction can proceed *via* two different approaches: a) the insertion of a nucleophilic methylene unit and b) the addition of an electrophilic CH_2 fragment. Due to their intrinsic ambiphilicity carbenoids are predestined to perform homologations *via* both routes. As mentioned before (cf. p.3), the metal as well as the temperature determine the reactivity profile of carbenoids.[15, 94] Consequently, electrophiles, such as carbonyl type compounds,[48, 52d, 52f, 95] boron,[52g, 56b, 96] zirconium,[53] germanium, silicon[97] and tin[49c] containing molecules, are predominately homologated by lithium and magnesium carbenoids featuring a nucleophilic character. On the contrary, in zinc carbenoids the electrophilic character predominates.[98]

Reactivity Towards Main Group Element Compounds

One of the earliest examples of homologation reaction of boron compounds was reported by Köbrich *et al.* in 1967.[99] The reaction of triphenylborane with vinylic Li/Cl carbenoids resulted in the homologated product **48** proceeding *via* the ate-complex **47** (Scheme 12).

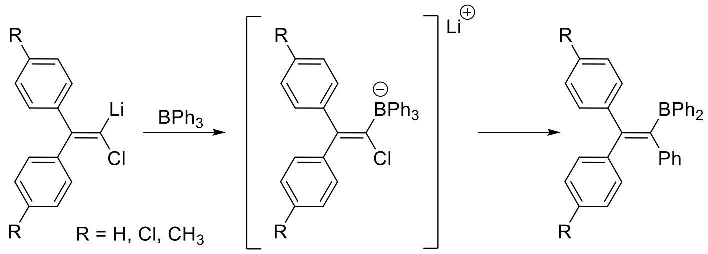

46 **47** **48**

Scheme 12. Homologation of triphenylborane using Li/Cl carbenoids.

Only recently it was discovered that this transformation can also be performed using boronates, diboranes and silylboranes.[100] Amongst others the work groups of Aggarwal discovered that the lithiation-borylation reaction can be used for stereoselective transformations and iterative protocols for building up long alkyl chains. An impressive example of the iterative lithiation-borylation-protodeboronation is shown in (Scheme 13). The coupling of smaller building blocks such as **49** and **50** allows the synthesis of hydroxyphthioceranic acid **51**. Carbenoids not only undergo homologation reactions with boranes but also insertion reactions into the B–H bond of simple BH_3 Lewis base adducts. This was first observed by Mezailles, So and coworkers.[40a]

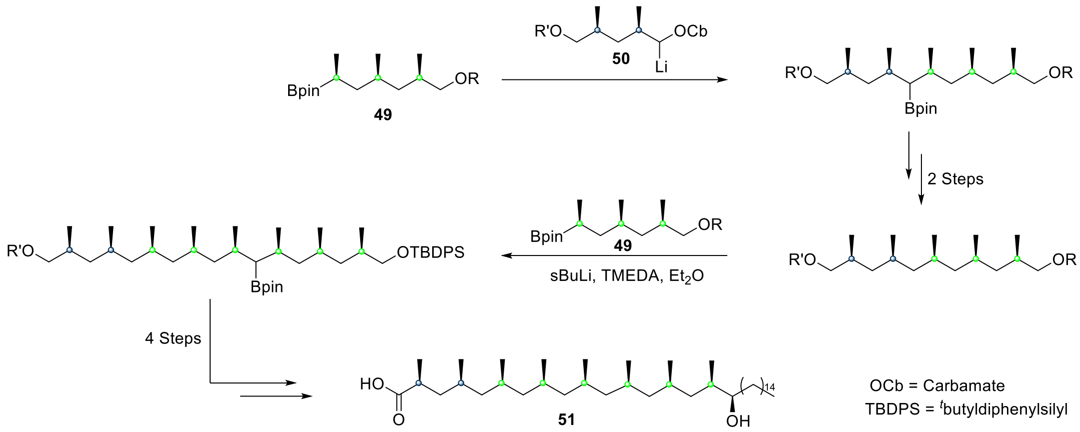

Scheme 13. Synthesis of hydroyphthioceranic acid *via* lithiation-borylation-protodeboronation.

Upon warming to room temperature the phosphino-borane functionalized Li/Cl carbenoid **17** inserts intramolecularly into the B–H bond with concomitant elimination of LiCl yielding the borane **52** bearing a dimeric structure and coordination *via* the thiosphoryl moiety.[40a] Gessner reported on an intermolecular B–H bond activation using the silyl substituted carbenoid **18**, however, the reaction of BH_3·THF and **18** did not yield a similar borane but the borate **53** which formed with concomitant reduction of the former carbenoid **18** (Scheme 14).[54a]

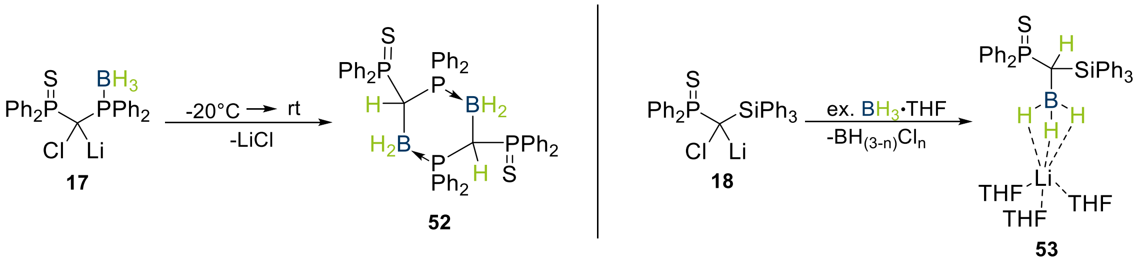

Scheme 14. B–H activation using Li/Cl carbenoids.

Two years later in 2015, Mezailles *et al.* reported on the reaction of carbenoid **54** with BH_3•SMe_2 resulting in the B–H bond activation product **55**. This was further used in CO_2 reduction selectively delivering methanol derivatives as products. This reaction impressively demonstrates the potential of carbenoids in catalytic reactions (Scheme 15).[40b]

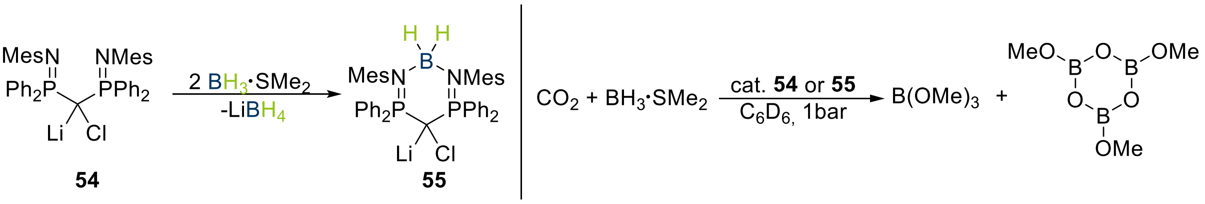

Scheme 15. Left: B–H bond activation using carbenoid **54**. Right: Its application in catalytic CO_2 reduction.

Analogous P–H bond activations were not observed when reacting electronically stabilized carbenoids with secondary phosphines. Instead the work group of Gessner discovered the selective formation of the respective diphosphines. This kind of carbenoid-mediated dehydrocoupling was unprecedented. The reaction protocol was found to tolerate a number of functionalized aryl substituted phosphines including electron rich and poor ones. But the steric demand of the aryl groups effects the efficiency of the conversion since the tolyl substituted phosphine was still sufficiently coupled while the mesityl substituent prevents the coupling to the diphosphane. Contrary to aryl substituted phosphines, no selective dehydrocoupling was observed in case of alkyl substituted ones suggesting that electronic effects and the P–H polarity might influence the reaction mechanism (Scheme 16).[19b]

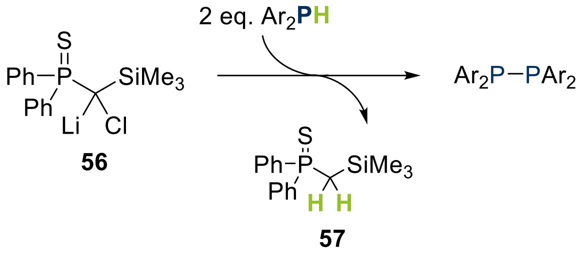

Ar = i.a. p-Tol, p-Me$_2$NC$_6$H$_4$, p-Me$_2$OC$_6$H$_4$, 4-ClC$_6$H$_5$, 3,5-Cl$_2$C$_6$H$_4$

Scheme 16. Carbenoid mediated dehydrocoupling of secondary phosphines.

Reactivity of Carbenoids Towards Transition Metal Compounds

Even though carbenoids exhibit a carbene-like reactivity their use in the formation of carbene complexes is rather scare owing to the fact that carbenoids do not necessarily react to the carbene species with transition metal compounds. The reaction of a variety of carbenoids – non-stabilized and stabilized ones – with diphenyl zircocenes **58** proceeds *via* insertion of the carbenoid **59** into the Zr–C bond of **58** and subsequent protic work up yield the respective C–C bond formation product **60** (Scheme 17). This reaction was found to be more selective using Zr instead of other transition metals, such as titanium, vanadium, cobalt or nickel.[101]

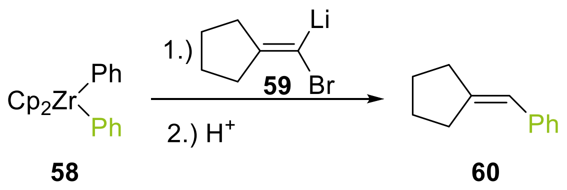

Scheme 17. Reaction of lithium carbenoids with organo zircocenes.

The reaction protocol was also extended to zirconacycles resulting in ring expansion reactions.[53, 102] The use of carbenoids as carbene transfer reagents for the synthesis of carbene complexes was demonstrated by the reaction of the Li/Cl carbenoid **61** with CpWI(CO)$_3$ yielding the carbene complex **63** and thus offering an alternative to the employment of the diazo compound (Scheme 18).[103] In 2007, Milstein reported on the reaction of [Zn(CH$_2$I)$_2$] with [(PPh$_3$)$_3$RuCl] resulting in the carbene complex **64** (Scheme 18). Using [Zn(CHPhCl)$_2$] as a carbeniod allows the synthesis of the famous Grubbs catalyst.[104]

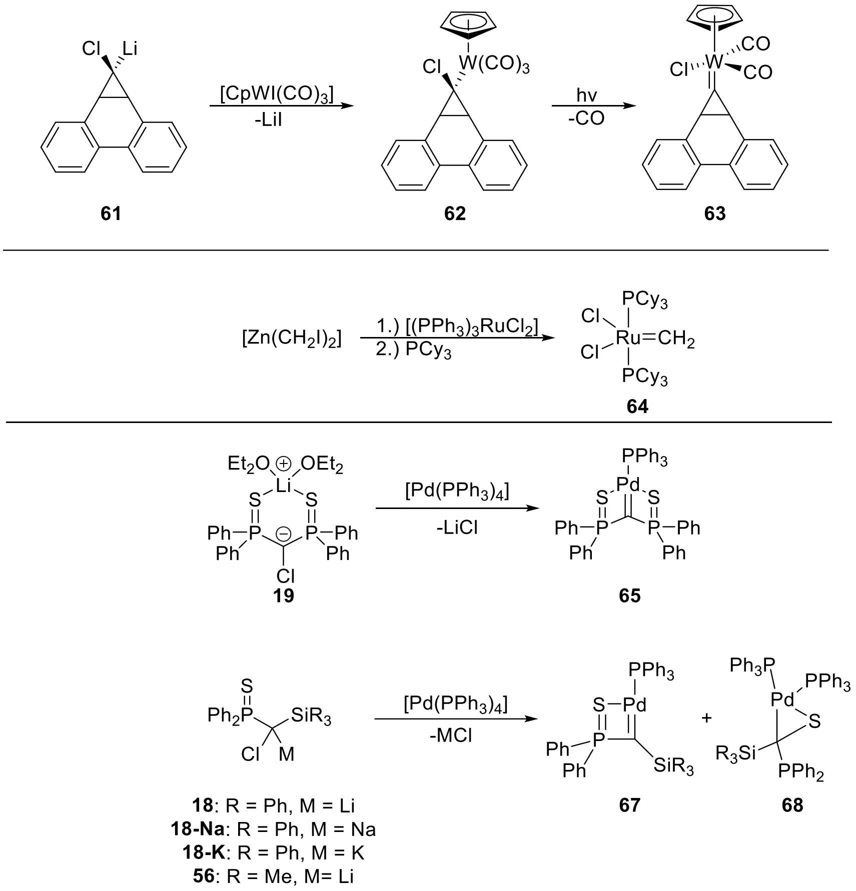

Scheme 18. Synthesis of transition metal carbene complexes starting from carbenoids as carbene transfer reagents.

Note, the palladium carbene complex **65** was obtained by Le Floch *et al.* starting from the stabilized Li/Cl carbeniod **19** and reacting it with [Pd(PPh$_3$)$_4$] (Scheme 18). Its formation is remarkable since the synthesis of nucleophilic carbene complexes bearing late transition metals is limited *via* alternative approaches.[38] The change from one thiophosphoryl moiety in **19** to a silyl substituent in **18** showed the limitations of the apparently straight-forward carbene transfer. The higher reactivity of the silyl substituted carbenoid **18** did not yield the desired product **67** selectively but a mixture with the thioketone complex **68**. The selectivity of this carbene transfer reaction seems to be a good measure for the stability of the employed carbenoid. The $SiMe_3$ substituted carbenoid **56** formed the thioketone complex while the more stabilizing $SiPh_3$ substituent gave 50 % conversion to **67**. Moreover, changing from lithium to the heavier alkali metals (**18-Na** and **18-K**) results in more stable carbenoids and consequently, in selective formation of **67** (Scheme 18). The results shown in Scheme 18 demonstrate that manipulation of the carbenoid stability might be a valuable tool to control the carbene transfer reactions of carbenoids and thus, help to further explore the scope of this reactivity.[19c]

Aim

Carbenoids are temperature labile compounds whose stability and reactivity is influenced by a number of factors, namely the substitution pattern, the M/X combination, the presence of additional donor bases or metal salts and the nature of the solvent. Adjustment of these parameters allows to control and fine-tune the reactivity and stability of these compounds. The choice of the substitution pattern has a fundamental impact on the carbenoid stability. Especially the use of EWGs as well as a change of hybridization at the carbenoid carbon center from sp^3 to sp^2 increase the stability.

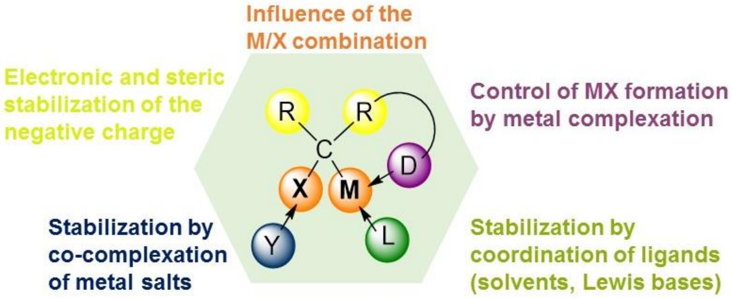

Figure 12. Factors influencing the thermal stability of carbenoids.

The variation of the nucleofugal group X and the metal M also influences the thermal lability crucially. In general, the stability of carbenoids increases in the series of F < Cl < Br < I and Li < Na < K. The decomposition of the carbenoid *via* α-elimination can be controlled/hampered by the introduction of donor functions either intramoleculary as part of the substitution pattern or intermoleculary with the help of additional Lewis bases, metal salts or coordinating solvents.

The aim of this thesis is to especially investigate the influence of the nature of the solvent on the carbenoid stability as well as its aggregation and solvation behavior in solution in dependence of the temperature and the solvent. In this regard, a number of stabilized M/X carbenoids (M = Li, Na, K and X = F, Cl) should be studied with respect to their stability in solution in coordinating and non-coordinating solvents as well as their solvation/aggregation in different solvents at different temperatures. Furthermore, the impact of metal salts on the structure formation and stability should be examined. To this end, carbenoids **83-M** and **84-M** should be synthesized (Scheme 19). These carbenoids were chosen due to the importance of sulfoximine-substituted carbenoids in synthesis and their expected high stability. Moreover, the stereoinformation of the sulfoximine group could also be used as spectrocscopic probe.

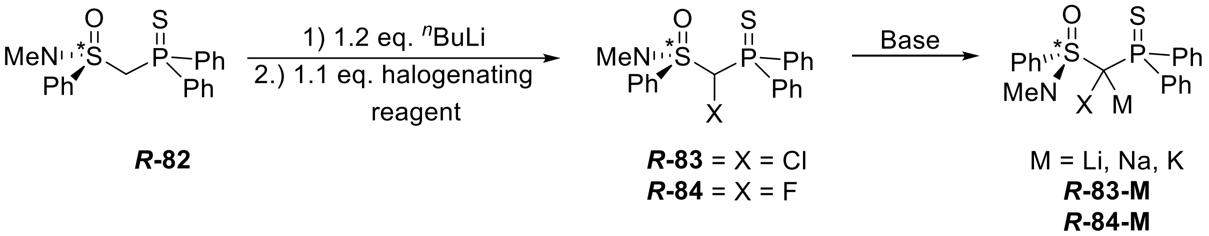

Scheme 19. Synthetic route to the chiral carbenoids *R*-**83**-M and R-**84**-**M**.

These studies will help to further understand the influence of the solvent on the carbenoid stability to be able to control their reactivity with the right choice of reaction conditions. Reactivity and stability control of these extremely labile species is highly desirable to broaden their scope of applications.

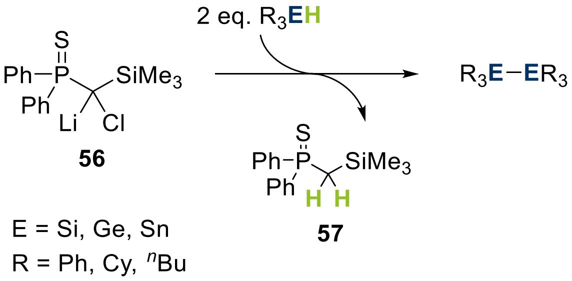

Scheme 20. Reactivity studies of carbenoid **56** towards different main group element hydride species.

Especially their potential in applications in main group element chemistry has only been scarcely investigated. Only a few examples of the reactivity of stabilized carbenoids towards element-hydrogen or element-element bonds are known, even though their ambiphilic nature predestine them for the use in activation of these bonds.[105] Other systems being able to react as nucleophiles and electrophiles have been shown to be highly suitable in bond activation reactions.[106] Most studies using carbenoids in bond activation reactions focused on boranes. Activation of B–H,[54a] B–C,[99b] B–B[100b, 107] and B–Si[100b, 107a] bonds have been reported to date. Only recently, our group was able to report on an until then unprecedented reaction behavior of carbenoids. Surprisingly, when examine the reactivity of stabilized carbenoids towards P–H bonds no bond activation is observed. Contrary, stabilized Li/Cl carbenoids were found to perform selective dehydrocoupling of aryl substituted secondary phosphines.[19b] This reaction pattern is remarkable and thus, this thesis also focuses on further elucidating the carbenoid reactivity towards a variety of E–H (E = Si, Ge, Sn) (Scheme 20) and E–E' (E = P and E' = B) bonds. Based on the difference in reactivity of stabilized carbenoids towards B–H and P–H bonds it is assumed that the change of the hydridic nature of the E–H bond might be the reason for this change in reactivity. Thus, the carbenoid reactivity towards group 14 hydrides as well as towards P–B bonds will be examined.

Results & Discussion

Carbenoid Mediated Formation and Activation of Element-Element and Element-Hydrogen Bonds

Although insertion/homologation reactions of carbenoids are well known for a variety of E–X bonds, the carbenoid mediated formation of main-group element bonds was first reported by Gessner *et al.* in 2014.[19b] This reactivity was unprecedented for carbenoids. Thiophosphoryl-, silyl- and sulfonyl substituted carbenoids were found to be suitable for dehydrocoupling of aryl substituted secondary phosphines. The anion-stabilizing character of the thiophosphoryl as well as the low lying $\sigma^*_{PS/SiR}$- orbitals result in stabilization of the carbenoid due to electrostatic interactions and negative hyperconjugation. Therefore, the carbenoid stability is sufficient for the selective reaction while still keeping its ambiphilic nature. Reaction of the stabilized Li/Cl carbenoid **56** with secondary phosphines results in dehydrocoupling of the phosphines with concomitant protonation of the carbenoid. Noteworthy, only stabilized carbenoids are able to selectively conduct this reaction. The use of labile carbenoids results in the formation of complex reaction mixtures. In this regard, further investigations were conducted to expand the scope of this reaction. Contrary to secondary phosphines BH_3 Lewis base adducts undergo B–H addition to the carbenoid carbon atom suggesting an influence of the E–H bond polarity on the reactivity. In this regard, further substrates, namely group 14 element hydrides, were tested.

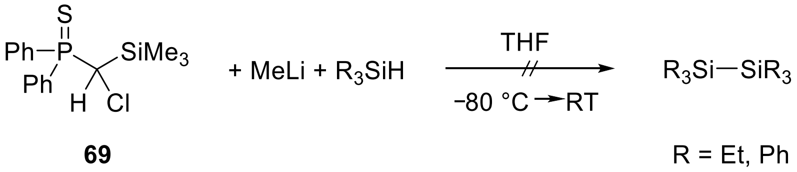

Scheme 21. Reaction of **69** with MeLi and silanes.

First, the reactivity of carbenoid **56** towards silanes was tested (Scheme 21). Therefore, the chlorinated precursor **69** was treated with MeLi in THF at low temperatures and subsequently, added to the respective silane. The reaction solution was analyzed by ^1H, $^{31}P\{^1H\}$ and ^{29}Si NMR spectroscopy. Unfortunately, neither the reaction with Et_3SiH nor Ph_3SiH yielded a selective reaction product. NMR spectroscopic data revealed the presence of the chlorinated precursor **69** along with the twice protonated precursor **57**. However, no evidence was found for either the formation of the corresponding disilanes or cyclic silanes. One possible explanation for these results is the higher polarity of the Si–H bond in comparison to the P–H bond. Therefore, less hydridic germanium hydrides were tested (Scheme 22). The reaction of **56** with 2 eq. triphenylgermanium hydride at low temperatures resulted in a greenish-grey solution after slowly warming to room temperature. As evidenced by $^{31}P\{^1H\}$ NMR spectroscopy the protonated precursor **57** was formed in roughly 67 % yield. After drying and washing of the white residue at –10 °C the corresponding digermane **70** was obtained in moderate yields of 51 %. Compound **70** was characterized by ^1H and $^{13}C\{^1H\}$ NMR spectroscopy and the obtained data are in accordance with previously reported ones in literature.[108]

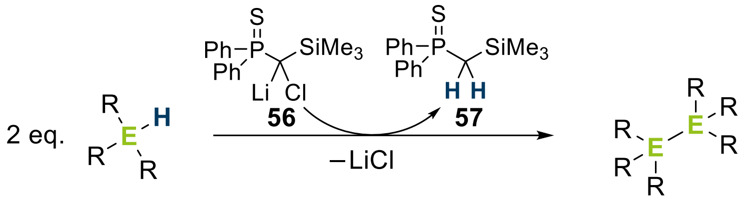

E = Ge, Sn
R = Ph,^{n}Bu, Cy

70: E = Ge, R = Ph (51 %)
71: E = Sn, R = Ph (31 %)
72: E = Sn, R = Cy (17 %)
73: E = Sn, R = Bu (38 %)

Scheme 22. Carbenoid-mediated dehydrocoupling of group 14 element hydrides.

Slow evaporation of a saturated DCM solution of **70** gave access to crystals suitable for single crystal X-ray diffraction analysis. The digermane **70** crystallizes in the trigonal space group $P\overline{3}$ with one sixth and one third of a molecule in the asymmetric unit. The molecular structure of **70** was already reported in three different modifications. This modification is, however, unknown so far.[109] Unfortunately, the solid state structure is heavily disordered and thus, the quality of the data is quite low. After successful dehydrocoupling of triphenylgermanium hydride, alkyl substituted congeners were tested. However, no evidence was found for selective dehydrocoupling of $^nBu_3GeH$ by NMR spectroscopy. Based on ^1H NMR data approx. 80 % of the precursor $^nBu_3GeH$ is still unreacted, the $^{31}P\{^1H\}$ NMR spectrum of the reaction solution shows a number of different signals suggesting unselective reaction and decomposition of carbenoid **56**. This result is in accordance with earlier findings regarding secondary phosphines which also showed no selective dehydrocoupling in case of alkyl substituents. Then the reactivity of carbenoid **56** towards stannanes, first aryl substituted ones, was examined. Applying the same reaction protocol to Ph_3SnH results in full conversion of the stannane to **71** according to $^{119}Sn\{^1H\}$ NMR spectroscopy data of the reaction solution after warming to RT. However, separation of **71** from the twice protonated precursor **57** was difficult, hence, the distannane **71** was only isolated in low yields of 31 % as a white solid. The obtained NMR spectroscopic data are in agreement with literature.[110] Furthermore, the nature of **71** was unambiguously confirmed by single crystal X-ray diffraction analysis (Figure 13, left). Single crystals were obtained by slow diffusion of hexane into the reaction mixture at RT. Even though the molecular structure of **71** has already been published before the obtained compound crystallizes in a different crystal system, namely the trigonal space group $P\bar{3}$, with one disordered molecule and one sixth of a molecule in the unit cell. The Sn–Sn bond lengths in both molecules of 2.7468(13) and 2.7763(10) Å were found to be slightly different. The former is slightly shorter in comparison to the reported Sn–Sn distances.[111]

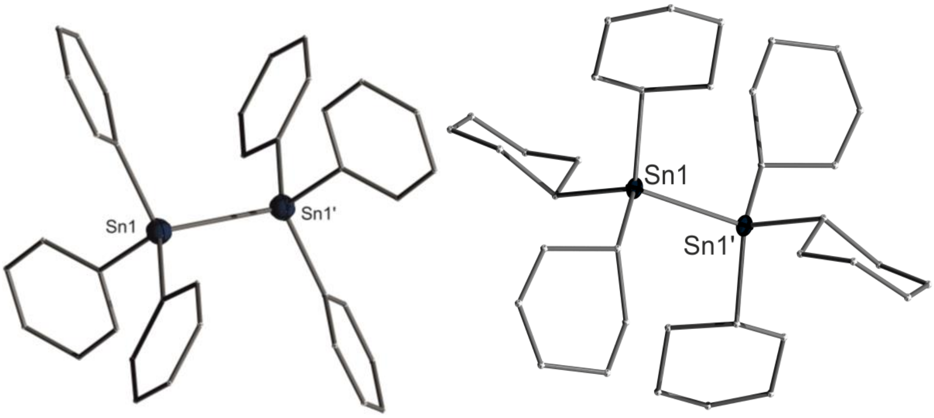

Figure 13. Left: Molecular structure of **71**. Displacement ellipsoids drawn at the 30 % probability level. All hydrogen atoms have been omitted for clarity. Selected bond length [Å]: Sn–Sn' 2.7763(10). Right: Molecular structure of **72**. Displacement ellipsoids drawn at the 50 % probability level. All hydrogen atoms have been omitted for clarity. Selected bond length [Å]: Sn–Sn' 2.8038(6).

Table 2. Crystallographic data and structure refinement of **71** and **72**.

Parameter	Compound 71	Compound 72
Emperical formula	$C_{36}H_{30}Sn_2$	$C_{36}H_{66}Sn_2$
Formula weight	699.98 g/mol	736.26 g/mol
Temperature	99.9(3) K	100(2) K
Wavelength	1.54178 Å	0.71073 Å
Crystal system	Trigonal	Trigonal
Space group	$P\bar{3}$	$R\bar{3}$
Unit cell dimensions	a = 17.3977(5) Å b = 17.3977(5) Å c = 8.5675(4) Å α= 90° β= 90° γ = 120°	a = 9.7273(3) Å b = 9.7273(3) Å c = 32.5028(8) Å α= 90° β= 90° γ = 120°
Volume	2245.78(16) $Å^3$	2663.41(18) $Å^3$
Formula unit per cell	3	3
Density (calculated)	1.553 Mg/m^3	1.377 Mg/m^3
Absorption coefficient	13.419 mm^{-1}	1.428 mm^{-1}

F(000)	1038	1146
Crystal size	0.156 x 0.110 x 0.092 mm^3	0.594 x 0.427 x 0.241 mm^3
Θ range for data collection	5.084 to 69.990°	3.484 to 30.880°
Index ranges	$-21 \leq h \leq 21$, $-21 \leq k \leq 20$, $-8 \leq l \leq 10$	$12 \leq h \leq 13$, $-13 \leq k \leq 13$, $-46 \leq l \leq 45$
Reflections collected	15837	13522
Independent reflections	2856 [*R*(int) = 0.0411]	1659 [*R*(int) = 0.0595]
Refinement method	Full-matrix least-squares on F^2	Full-matrix least-squares on F^2
Data / restraints / parameters	2856 / 440 / 264	1659 / 204 / 108
Goodness-of-fit on F^2	1.092	1.102
Final R indices [I>2σ(I)]	$R1 = 0.0347$, $wR2 = 0.0874$	$R1 = 0.0362$, $wR2 = 0.0892$
R indices (all data)	$R1 = 0.0372$, $wR2 = 0.0901$	$R1 = 0.0377$, $wR2 = 0.0901$
Largest diff. peak and hole	1.053 and -0.663 e.Å^{-3}	1.157 and -1.221 e.Å^{-3}

After successful coupling of aryl substituted stannanes aliphatic ones were tested. Surprisingly, both Cy_3SnH as well as $^nBu_3SnH$ could be coupled using carbenoid **56**. In both cases the reaction resulted in full conversion of the tin hydride to the respective distannanes **72** and **73** (Scheme 22) as evidenced by $^{119}Sn\{^1H\}$ NMR spectroscopic studies of the reaction solution. However, analogously to **71** the separation of the coupled products from **57** was found to be problematic. Consequently, **72** and **73** were only isolated in low yields of 17 and 38 %, respectively. In case of **73** the recorded NMR spectroscopic data were in agreement with literature.[112] Compound **72** was fully characterized by ^1H, $^{13}C\{^1H\}$ and $^{119}Sn\{^1H\}$ NMR spectroscopy. The $^{119}Sn\{^1H\}$ NMR spectrum shows one singlet at –70.2 ppm which was assigned to **72**. Single crystals suitable for X-ray diffraction[1] were obtained by slow evaporation of a solution of **72** in C_6D_6 at room temperature. The distannane **72** crystallizes in the trigonal space group $R\overline{3}$ (Figure 13, right) and has been reported by Toupance.[113] All cyclohexylrings were found to be disordered. The Sn1–Sn1' bond length is 2.8038(6) Å and thus in good agreement with the one in **71** (2.7763(10) Å).

To test the limits of this reaction protocol also the secondary stannane Ph_2SnH_2 was reacted with **56** and resulted in a mixture of a number of cyclic and acyclic oligostannanes. The six-membered ring $Ph_{12}Sn_6$ **74** was found to be the main product by $^{119}Sn\{^1H\}$ NMR spectroscopy giving rise to a signal at -207.7 ppm. It was isolated in 31 % yield as a yellow solid and its nature was unambiguously confirmed by X-ray crystallography with crystals obtained by slow evaporation of a saturated DCM solution at RT. The compound crystallizes in the monoclinic space $P2_1/c$ with two half molecules in the asymmetric unit. The structural parameters differ slightly from the previously reported ones due to crystallization in a different space group.[114]

---

[1] Structure refinement was performed by Dr. B. Mallick.

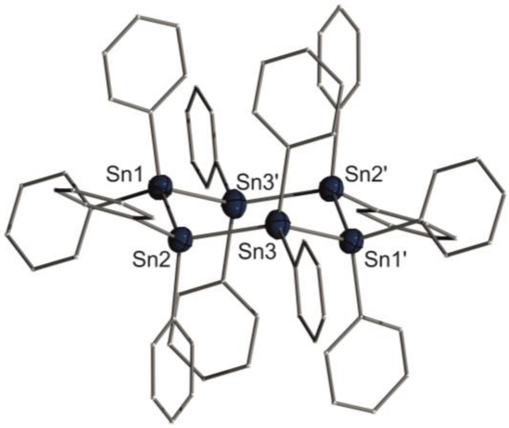

Figure 14. Molecular structure of **74**. Displacement ellipsoids drawn at the 50 % probability level. All hydrogen atoms have been omitted for clarity. Selected bond length [Å] and angles [°]: Sn-Sn 2.7674(10) – 2.783(9), Sn–Sn–Sn 107.52(3) – 118.58(3).

Encouraged by the successful homo-dehydrocoupling of a number of group 14 element hydrides hetero-dehydrocoupling was attempted using the same reaction protocol (Scheme 23) adding both hydride species simultaneously. Unfortunately, the reaction of one equivalent of the secondary phosphine (*p*-Tol)$_2$PH and Ph$_3$SnH, respectively, and one equivalent of **56** only resulted in the formation of the respective homo-dehydrocoupled distannane and a number of phosphorous containing species, amongst others the diphosphane, unreacted (*p*-Tol)$_2$PH, the chlorinated precursor **69** and the twice protonated precursor **57** but not in the heterocoupled compound Ph$_3$Sn–P(*p*-Tol)$_2$ based on ^{31}P{^{1}H} and ^{119}Sn{^{1}H} NMR spectroscopic data. Since hetereocoupling of stannanes with phosphines was not successful the possibility of carbenoid mediated deydrocoupling of two different stannanes was tested. However, the reaction of **56** with one eq. of ^{n}Bu$_3$SnH and Ph$_3$SnH, respectively, yielded only **71** and **73** alongside with **57**. No evidence for the formation of ^{n}Bu$_3$Sn–SnPh$_3$ was found in the ^{119}Sn{^{1}H} NMR spectra of the reaction solution.

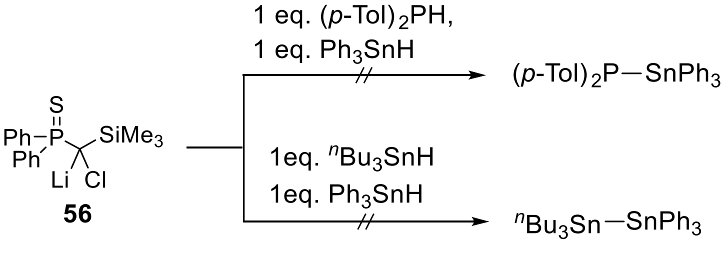

Scheme 23. Attempted carbenoid-mediated hetero-deyhrocoupling using secondary phosphines and stannanes.

In general, species with E–E and E–E' bonds are accessible *via* a number of different routes, including catalytic conversion by transition metal complexes[115] as well as main group element species[116] or stoichiometric approaches,[116b, 117] e.g. salt metathesis or reductive coupling. In case of secondary phosphine also dehydrocoupling using NHCs has been reported.[118] The same approach gives access to **71**, however, these pathways require elevated temperatures and long reaction times.[110] The alkyl substituted tin hydride $^{n}Bu_3SnH$ as well as the aryl substituted derivate Ph_3SnH can be coupled by heating a neat solution under low pressure.[112] Compound **72** can be synthesized *via* the reaction of Cy_3SnNEt_2 and the respective hydride species.[119] The carbenoid-mediated dehydrocoupling of tin hydrides seems to be a promising alternative without any need of elevated temperatures or long reaction times. To exclude the possibility of the chlorinated precursor **69** being the active species in the dehydrocouping, compound **69** was reacted with $^{n}Bu_3SnH$ in THF. No reaction was observed in this case confirming that **56** is the active species.

These results show that carbenoid mediated dehydrocoupling of E–H compounds (E = Sn, Ge) is applicable to more main group element hydride species than just secondary phosphines. All reactions seem to proceed *via* a similar mechanism since the twice protonated carbenoid precursor **57** is observed as a side product in all cases. The successful coupling of heavier group 14 element hydrides suggests that also substrates with a more hydridic E–H bond than in phosphines can be coupled by carbenoids. However, previous studies of boranes are in contrast to that finding since they only undergo B–H activation (see above). Boranes formally add to the carbenoid carbon atom under the same conditions applied for the dehydrocoupling. So far only BH_3 Lewis base adducts have been tested with stabilized Li/Cl carbenoids, so the use of the more hydridic HBpin and HBcat was attempted. Unfortunately, NMR spectroscopic studies revealed an unselective reaction pathway with the formation of a variety of products, amongst others the chlorinated precursor **69** and the twice protonated compound **57**. The failed dehydrocoupling of boranes might be due to their highly electrophilic nature, thus favoring borate formation instead of hydride transfer. The formation of borates in carbenoid chemistry has already been reported, e.g. as being the first step in B–H bond activation reactions of BH_3 with carbenoids (see above).[54a] This allows to draw conclusions about a possible mechanism of the carbenoid mediated dehydrocoupling. The dehydrocoupling seems to proceed *via* protonation/hydride transfer instead of a nucleophilic attack at the group 14 element hydride species. This observation is in agreement with findings of the carbenoid mediated dehydrocoupling of secondary phosphines which presumably proceeds *via* a similar mechanism. Here, experimental results as well as theoretical calculations suggest deprotonation of the respective secondary phosphine to be the initial step. Trapping the intermediate of the reaction of **56** and (p-Tol)$_2$PH with an excess of Ph_2PCl resulted in the formation of the mixed product $Ph_2P–P(p\text{-}Tol)_2$ suggesting the presence of the lithiated species $(p\text{-}Tol)_2PLi$. Furthermore, the deprotonation of the phosphane was energetically favored compared to alternative routes.[19b, 66] Consequently, the assumption that the carbenoid mediated dehydrocoupling of the tetreles proceeds *via* protonation as the initial step seems reasonable.

To test the assumption that the borate formation prevents efficient coupling of boranes the reactivity of carbenoid **56** towards the phosphinoborane $Ph_2P\text{-}Bcat$ **75,** which was synthesized starting form catBCl[120] and Ph_2PSiMe_3, was tested.[121] In this case borate formation should be favored as the first step resulting in either an α-diborylated compound alongside with the coupled diphosphane Ph_4P_2 or formal addition of the P–B bond to the carbenoid center analogously to simple BH_3 Lewis base adducts.

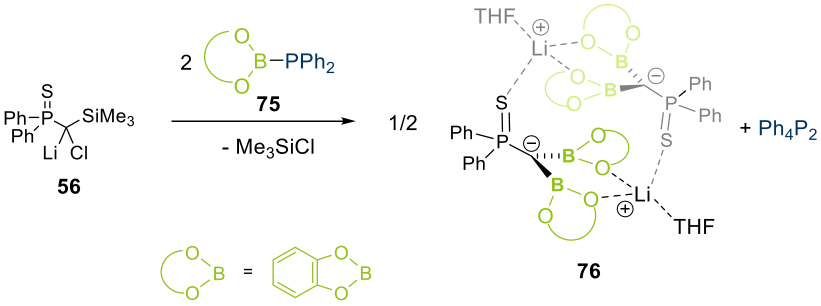

Scheme 24. Diborylation of **56** with **75** and concomitant formation of Ph_4P_2.

Low temperature reaction of **56** with **75** and subsequently warming to room temperature slowly overnight resulted in the discoloration of the former yellow reaction solution (Scheme 24). Analyzing the reaction solution by $^{31}P\{^1H\}$ NMR spectroscopy revealed the formation of the disphosphine Ph_4P_2 as evidenced by a singlet at $\delta_P = 15.3$ ppm and indicated the formation of the α-diborylated silane. However, further NMR spectroscopic studies of the reaction solution showed the formation $ClSiMe_3$ giving rise to a singlet at $\delta_H = 0.41$ ppm and at 30.8 ppm in the ^{29}Si NMR spectrum. With the help of single crystal XRD analysis[2] the nature of the borylated compound could be elucidated. Single crystals of the lithiated diborylated species **76** were obtained by slow diffusion of pentane into a saturated solution of **76** in THF (Figure 15). Compound **76** crystallizes in the triclinic space group $P\bar{1}$with half a molecule in the asymmetric unit. It exhibits a centrosymmetric dimeric structure with the Li atom being coordinated by the sulfur atom of the thiosphoryl moiety, one oxygen atom of each catechol unit and one additional THF molecule.

---

[2] Structure refinement was performed by Dr. T. Scherpf.

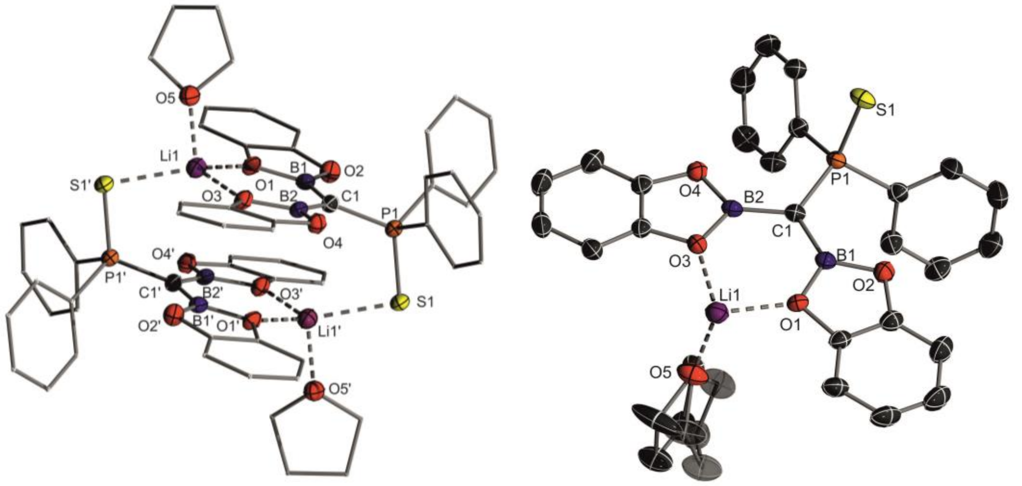

Figure 15. Left: Dimeric molecular structure of **76**. Right: Section of the molecular structure of **76** only showing one molecule of **76**. Displacement ellipsoids drawn at the 50 % probability level. All hydrogen atoms have been omitted for clarity. Selected bond lengths [Å] and angles [°]:S1–P1 2.0025(7), P1–C1 1.7453(17), B1–C1 1.505(3), B2–C1 1.497(3), P1–C1–B1 118.02(13), P1–C1–B2 121.15(13), B1–C1–B2 120.45(15).

Table 3. Crystallographic data and structure refinement of **74** and **76**.

Parameter	**Compound 74**	**Compound 76**
Emperical formula	$C_{146}H_{120}Sn_{12}$	$C_{29}H_{26}B_2LiO_5PS$
Formula weight	3298.69 g/mol	546.09 g/mol
Temperature	100(2) K	99.9(2) K
Wavelength	1.54184 Å	1.54184 Å
Crystal system	Monoclinic	Triclinic
Space group	$P2_1/c$	$P\bar{1}$
Unit cell dimensions	a = 21.9497(6) Å	a = 10.8271(12) Å
	b = 13.6699(4) Å	b = 12.1201(18) Å
	c = 21.0706(5) Å	c = 12.8106(16) Å
	α= 90°	α = 113.378(13)°
	β= 94.056(2)°	β = 109.434(11)°
	γ = 90°	γ = 96.460(11)°
Volume	6306.4(3) Å^3	1395.9(3) Å^3
Formula unit per cell	2	2
Density (calculated)	1.737 Mg/m^3	1.299 Mg/m^3
Absorption coefficient	18.914 mm^{-1}	1.874 mm^{-1}
F(000)	3192	568
Crystal size	0.111 x 0.062 x 0.049 mm^3	0.181 x 0.112 x 0.021 mm^3
Θ range for data collection	3.812 to 77.598°	4.130 to 66.994°
Index ranges	$-27 \leq h \leq 27$, $-17 \leq k \leq 16$, $-26 \leq l \leq 26$	$-10 \leq h \leq 12$, $-14 \leq k \leq 14$, $-15 \leq l \leq 10$
Reflections collected	64075	9328
Independent reflections	13059 [*R*(int) = 0.1133]	4968 [*R*(int) = 0.0244]

Refinement method	Full-matrix least-squares on F^2	Full-matrix least-squares on F^2
Data / restraints / parameters	13059 / 0 / 703	4968 / 104 / 389
Goodness-of-fit on F^2	1.017	1.033
Final R indices [I>2σ(I)]	$R1 = 0.0833$, $wR2 = 0.2312$	$R1 = 0.0402$, $wR2 = 0.1018$
R indices (all data)	$R1 = 0.0989$, $wR2 = 0.2510$	$R1 = 0.0467$, $wR2 = 0.1064$
Largest diff. peak and hole	5.266 and -0.747 e.Å^{-3}	0.737 and -0.345 e.Å^{-3}

The central carbon atom formally bearing a negative charge exhibits a planar coordination sphere with a sum of angles of 359.6(1)° indicating a delocalization of the negative charge through the whole B–C–B unit. This assumption is confirmed by the relatively short B–C bonds of 1.505(3) and 1.497(3) Å in comparison to the respective bonds in the neutral tetraborylethane $(Bcat_2CH)_2$ which exhibit bond lengths of 1.551(5) and 1.559(5) Å.[122] No comparable structure bearing an α-carbanionic bis(boronate) has been isolated and structurally characterized. Consequently, no comparison between the structural parameters of **76** and a negatively charged compound can be made. Comparing the P–C bond lengths of **57** (1.823(2) Å) and **76** (1.7453(17) Å) reveals a shortened one in **76**. The P–C bond distance is comparable with the one in **18**·(12-crown-4)$_2$ (1.7515(2) Å) in which the central carbon atom as well bears a negative charge. The electrostatic attraction between the carbanionic carbon atom and the phosphorous atom results in the observed shortening of the P–C bond.

The formation of Ph_4P_2 from the reaction of **56** with catB–PPh$_2$ and the molecular structure of **76** might give the impression that the reaction proceeds *via* a similar reaction mechanism as the dehydrocoupling of phosphines and group 14 element hydrides in which the Bcat moiety is treated analogously to the hydrogen atoms of the secondary phosphines. However, the difference of the eliminated compound, which has been LiCl in case of the secondary phosphines and Me_3SiCl in the borylation reaction, might hint at a change in the mechanism which could be caused by the increased tendency of the formation of a stable borate intermediate as well as the presence of additional oxygen donors within the catecholato unit. This results in a stronger coordination of the Li atom to the borate intermediate and thus prevents its elimination as LiCl. Since this strong coordination of the lithium atom is not possible in case of BH_3 Lewis base adducts, which are only able to form weak B–H···Li interactions, LiCl elimination and B–H bond activation take place. Based on the above considerations a mechanism for the formation of **76** was proposed (Scheme 25), however, further research is needed to proof this mechanism experimentally. The intial step is the borate formation (**Int1**) *via* the reaction of **56** with catB–PPh$_2$ with the lithium ion being coordinated by the thiophosphoryl unit and one oxygen atom of the catechelolato moiety. This is followed by the elimination of $ClPPh_2$ and thus the formation of the boryl stabilized anion **Int2**. The intermediate **Int2** then reacts with a second equivalent of catB–PPh_2 to form the borate intermediate **Int3**. The final step is the reaction of **Int3** with the previously formed $ClPPh_2$ to yield the twice borylated species **76** with concomitant elimination of Ph_4P_2 and $ClSiMe_3$.

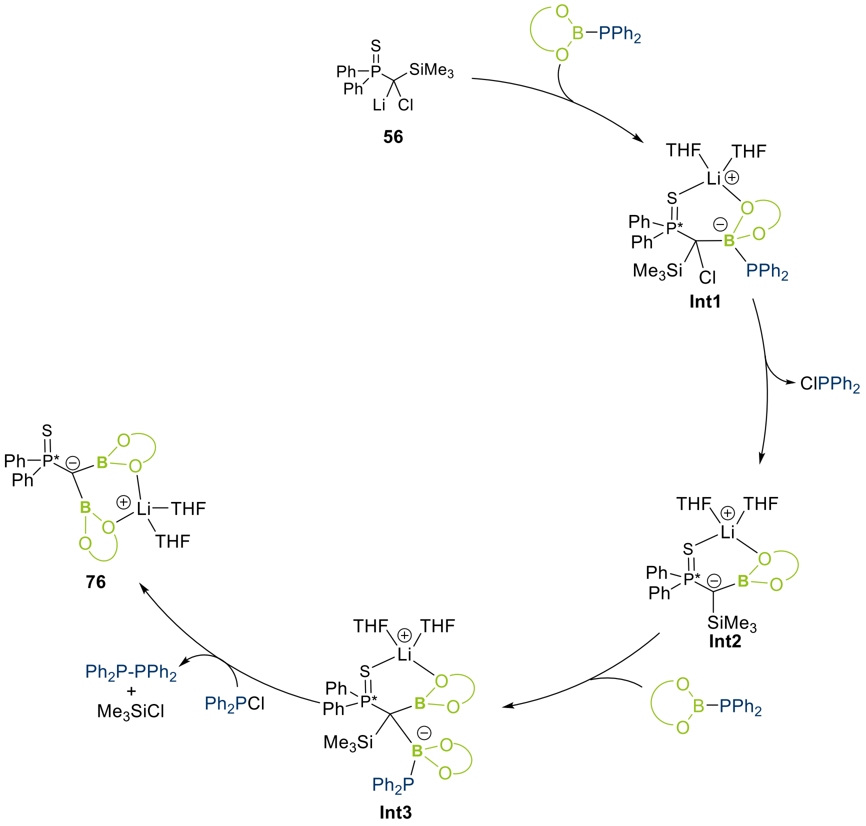

Scheme 25. Proposed mechanism of the formation of **76** starting from **56** and catB–PPh_2.

In general, diborylated compounds are used as difunctional precursors for a number of applications in organic synthesis. Over the years, especially the groups of Endo, Shibata, Morken, Meek and Matteson have reported on notable contributions to the use of 1,1-diborylated compounds in e.g. Suzuki couplings,[123] deborylation-alkylation/ functionalization[124] and boron-Wittig type reactions[125] yielding vinyl boronates. In some of these protocols *α*-boryl-anions are used, however, they have so far only been generated and used *in-situ*.

Conclusion

The scope of the carbenoid mediated dehydrocoupling was extended from secondary phopshines to group 14 element hydride species (Scheme 22). In contrast to silanes which could not be coupled selectively the reaction of the carbenoid **56** with the less hydridic Ph_3GeH yield the respective digermane and the protonated precursor **57**. The nature of the digermane **70** was successfully confirmed by NMR spectroscopy and X-ray diffraction analysis. Analogously to the observations in case of secondary phosphines no alkyl substituted germanium hydride species could be coupled with the help of carbenoid **56**. Besides germanium hydrides it was also possible to selectively dehydrocouple a variety of tin hydrides. Besides the aryl substituted Ph_3SnH, also the alkyl substituted species $^nBu_3SnH$ and Cy_3SnH yield in full conversion to the respective distannane based on NMR spectroscopic data. The nature of Ph_6Sn_2 **71** and Cy_6Sn_2 **72** were also confirmed by X-ray diffraction analysis. The use of the secondary stannane Ph_2SnH_2 resulted in the formation of a mixture of cyclic and acyclic products, with the six-membered ring $Ph_{12}Sn_6$ **74** being the main product. Unfortunately, selective hetero-dehydrocoupling of the two different stannanes $^nBu_3SnH$ and Ph_3SnH was not successful and only yielded the respective homocoupled products. The same holds true for the attempted heterocoupling of one equivalent of the secondary phosphine $(p\text{-Tol})_2PH$ and Ph_3SnH, respectively, yielding no heterocoupled product. The successful coupling of group 14 element hydrides supports the assumption that the carbenoid mediated dehydrocoupling can be further extended to other main group element hydride species bearing a more hydridic E–H bond than secondary phosphines. However, in case of HBpin and HBcat no selective conversion to the diborane was observed which might be due to the highly electrophilic nature of boranes favoring borate formation compared to hydride transfer. The assumption that borate formation prevents the successful carbenoid mediated dehydrocoupling is supported by the reaction of Ph_2PBcat resulting in the formation of the diborylated compound **75** (Figure 15) and Ph_4P_2. A preliminary mechanism for the formation of **75** was presented (Scheme 25) which needs to be proven by further experiments.

Synthesis, Characterization and Application of Chiral Carbenoids

Based on the successful carbenoid mediated dedydrocoupling of secondary phosphines and a number of group 14 element hydrides the possibility of stereoselective dehydrocoupling became appealing. The chiral carbenoids (Figure 16) were designed to have a sufficient stabilization which is required for the successful dehydrocoupling since non-stabilized carbenoids have found to be unsuitable for this application due to the more favored carbene formation compared to stabilized carbenoids.[19b] Moreover, the presence of a heteroatom, such as phosphorous, allows the facil and straightforward detection and monitoring of reactions and decomposition studies by $^{31}P\{^1H\}$ NMR spectroscopy.

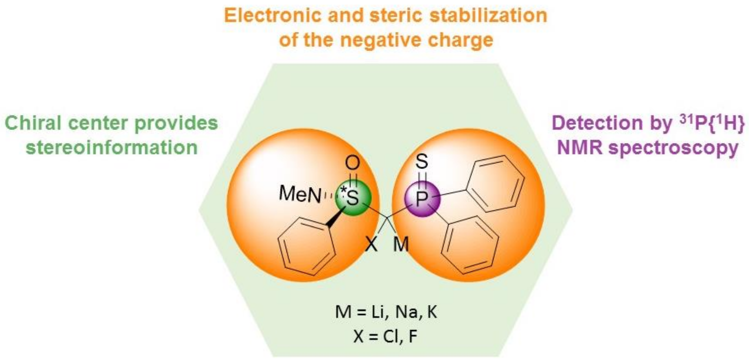

Figure 16. Structural advantages of chiral carbenoids **83-M** and **84-M**.

Synthesis and Characterization

The chiral carbenoids **83-M** and **84-M** were synthesized according to Scheme 26. The methyl phenyl sulfoxide **78** was prepared according to literature[126] by oxidizing thioanisole **77** with the help of sodium periodate. The product **78** was obtained as a slightly yellow liquid in 80 % yield. Compound **78** was then reacted with sodium azide and the racemic methyl phenyl sulfoximine *rac*-**79** was obtained as a colorless oil in 63 % yield.[127] Racemic resolution of the methyl phenyl sulfoximine *rac*-**79** was carried out with enantiomerically pure (*S*)-camphor sulfonic acid (CSA). The enantiomerically pure compound *S*-**80** was obtained in 76 % yield and the purity was proven by ^1H NMR spectroscopic data.[128] The camphor salt *S*-**80** was then treated with formaldehyde in formic acid. The corresponding *N*-methylated sulfoximine *S*-**81** was obtained as a colorless liquid in 78 % yield.

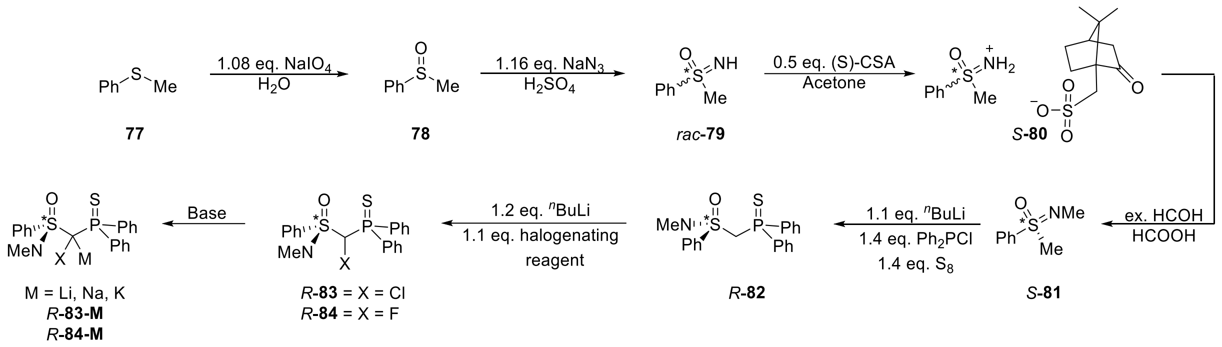

Scheme 26. Synthetic route to the chiral carbenoids *R*-**83-M** and *R*-**84-M**.

Reaction of *S*-**81** with ^{n}BuLi followed by the addition of chlorodiphenylphosphine and elemental sulfur yielded the coupled product *R*-**82** as an off-white solid in 57 % yield.[129] The enantiomeric purity of the species *R*-**82** was confirmed by HPLC using a chiral column with hexane and isopropanol in the ratio 85:15 as an eluent. The HPLC chromatogram (Figure 17) confirmed that compound *R*-**82** was prepared enatiomerically pure.

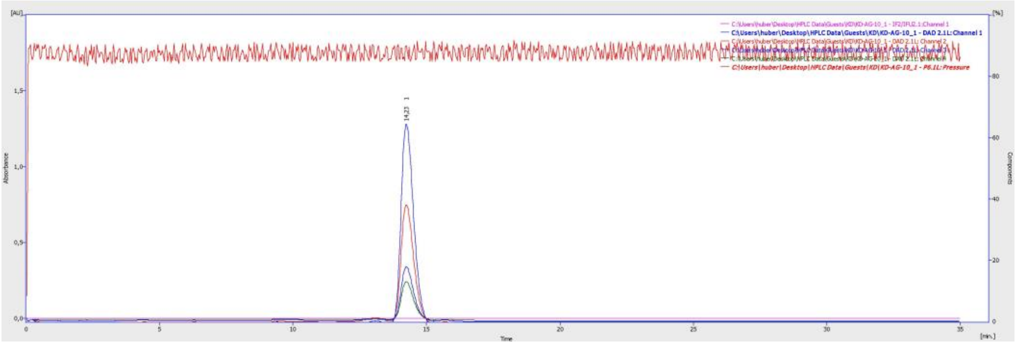

Figure 17. HPLC chromatogramm of *R*-**82**.

The chlorination of *R*-**82** was achieved by lithiation with ^{n}BuLi and subsequent reaction with C_2Cl_6 giving product *R*-**83** as a highly viscous oil in 54 % yield. The compound *R*-**83** was fully characterized by NMR spectroscopy, elemental analysis and single crystal X-ray diffraction analysis. The NMR spectra show two sets of signals in a ratio of 60:40 due to the presence of diastereomeric species. The ^{1}H NMR spectrum shows two singlets at $\delta_H = 2.87$ and $\delta_H = 2.97$ ppm caused by the nitrogen bound methyl group and also two doublets for the H atom bound to the central carbon atom at $\delta_H = 5.79$ and 5.88 ppm bearing slightly different coupling constants of $^2J_{HP} = 4.54$ and 4.90 Hz, respectively. Compound *R*-**83** shows two singlets in the ^{31}P{^{1}H} NMR spectra at $\delta_P = 45.1$ and $\delta_P = 46.5$ ppm. The bridging carbon atoms of the diastereomeres give rise to two doublets in the ^{13}C{^{1}H} NMR spectrum at $\delta_C = 69.1$ and 75.7 ppm with a coupling constant of $^1J_{CP} = 32.4$ and 36.0 Hz, respectively. Crystals suitable for single crystal X-ray diffraction analysis of the *S*, *S*-conformer crystallized from an oily racemic mixture at room temperature.[3] The compound *S*, *S*-**83** crystalizes in the monoclinic space group *P*2₁ with two molecules in the asymmetric unit (Figure 18). The chlorinated compound exhibits a P1–C1 and a S1–C1 bond distance of 1.8588(13) Å and 1.8643(14) Å, respectively. These bond lengths are in good agreement with the ones observed in the twice protonated precursor (P1–C1: 1.8363(18) and S1–C1: 1.824(2) Å).[129]

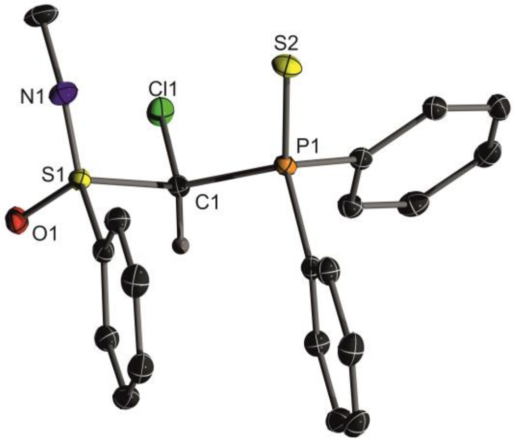

Figure 18. Molecular structure of *S*, *S*-**83**. Displacement ellipsoids drawn at the 50 % probability level. All hydrogen atoms except the one at the C1 atom have been omitted for clarity. Selected bond lengths [Å] and angles [°]: P1–C1 1.8588(13), S1–C1 1.8643(14), Cl1–C1 1.7739(13), S1–C1–Cl1 104.85(7), P1–C1–S1 118.13(7), P1–C1–Cl1 110.40(7).

Parameter	**Compound *S*, *S*-83**
Emperical formula	$C_{20}H_{19}ClNOPS_2$
Formula weight	419.90 g/mol
Temperature	100(2) K
Wavelength	0.71073 Å
Crystal system	Monoclinic
Space group	*P*2₁
Unit cell dimensions	a = 9.3549(5) Å b = 9.4299(5) Å c = 10.8508(6) Å α= 90° β= 92.165(2)° γ = 90°
Volume	956.53(9) Å^3
Formula unit per cell	2
Density (calculated)	1.458 Mg/m^3
Absorption coefficient	0.511 mm^{-1}

---

[3] Crystals were obtained by Dr. K.-S. Feichtner and X-ray diffraction analysis was performed by Prof. Dr. V. H. Däschlein-Gessner

F(000)	436
Crystal size	0.30 x 0.25 x 0.24 mm^3
Θ range for data collection	3.812 to 77.598°
Index ranges	$-11 \leq h \leq 11$, $-11 \leq k \leq 11$, $-13 \leq l \leq 13$
Reflections collected	17758
Independent reflections	3907 [*R*(int) = 0.0188]
Refinement method	Full-matrix least-squares on F^2
Data / restraints / parameters	3907 / 1 / 236
Goodness-of-fit on F^2	1.031
Final *R* indices [$I>2\sigma(I)$]	*R*1 = 0.0179, w*R*2 = 0.0521
R indices (all data)	*R*1 = 0.0181, w*R*2 = 0.0523
Largest diff. peak and hole	0.295 and -0.136 e.$Å^{-3}$

The chiral Li/Cl carbenoid *R*-**83-Li** is accessible by reacting the chlorinated precursor *R*-**83** with MeLi in THF at low temperatures. Subsequent removal of the solvent yields the carbenoid *R*-**83-Li** as a yellow solid in 85 % yield. Compound *R*-**83-Li** was fully characterized by NMR spectroscopy at low temperatures owing to its potential thermal lability. The absence of any signal for a bridging H-atom in the ^{1}H NMR spectrum confirms the complete and successful formation of the carbenoid *R*-**83-Li**. The $^{31}P\{^1H\}$ NMR spectra shows one singlet at $\delta_P = 42.2$ ppm in d_8-THF. Surprisingly, the $^{13}C\{^1H\}$ NMR spectra does not show the characteristic downfield shift of the carbenoid carbon atom which is normally observed for carbenoids. The respective carbon atom gives rise to a doublet at $\delta_C = 49.2$ ppm with a coupling constant of $^1J_{CP} = 83.1$ Hz. The higher coupling constant in *R*-**83-Li** indicates the higher s-character of the C–P bond in *R*-**83-Li** in comparison to the protonated precursor *R*-**83** owing to the change of hybridization from sp^3 in *R*-**83** to sp^2 in *R*-**83-Li**.

Moreover, the structure of the chiral Li/Cl carbenoid *rac*-**83-Li** was elucidated with the help of single crystal X-ray diffraction analysis. Due to the fact that racemic species tend to crystallize more easily than enantiomerically pure ones suitable crystals were obtained from a concentrated racemic reaction solution at –30 °C in THF. The product *rac*-**83-Li** crystallizes in the monoclinic system *P*21/c.

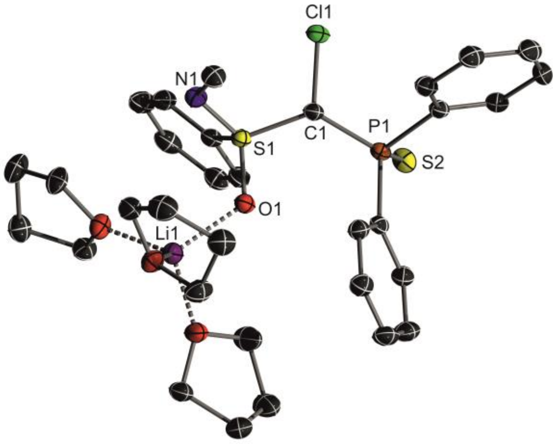

Figure 19. Molecular structure of *rac*-**83-Li**. Displacement ellipsoids are shown at the 50 % probability level. Hydrogen atoms have been omitted for clarity. Selected bond lengths [Å] and angles [°]:P1–C1 1.7586(15), S1–C1 1.6933(15), Cl1–C1 1.7734(14), O1–Li 1.935(3), S1–C1–Cl1 111.29(8), P1–C1–S1 126.80(8), P1–C1–Cl1 111.59(8).

The molecular structure reveals a monomeric structure with the Li atom being coordinated by the O1 atom of the sulfoximine moiety and three additional THF solvent molecules. This structure is in agreement with other molecular structures of M/X carbenoids which bear a coordination of the lithium atom only by external solvent molecules or intramolecular substituents featuring donor functionalities.[26, 38] This coordination results in no contact between the carbenoid carbon atom C1 and the Li atom as well as the chlorine and the lithium atom. Consequently, the arrangement can be classified as a carbene-donor complex (Figure 8, II). Comparison of the C1–Cl1 bond lengths of *S*, *S*-**83** (1.7739(13) Å) with the one of carbenoid *rac*-**83-Li** (1.7734(14)Å) reveals almost no change which can be explained by the missing contact between the lithium atom and the central carbon atom as well as the chlorine atom, respectively (Table 4). This is in accordance with other Li carbenoids bearing no such contact and thus no elongation of the respective C–Cl bond.[26, 39a] The P1–C1 (1.7586(15) Å) and S1–C1 (1.6933(15) Å) bonds in *rac*-**83-Li** are shortened compared to the protonated species *S*, *S*-**83** (P1–C1 1.8588(13) Å and S1–C1 1.8643(14) Å) due to electrostatic effects. The P1–C1–S1 angle of 126.80(8)° in *rac*-**83-Li** is enlarged. The sum of angles around the central carbon atom C1 is 349.68°.

The corresponding Na/Cl carbenoid ***R*-83-Na** can be synthesized by the reaction of the chlorinated species ***R*-83** with an excess of NaH in THF at 0 °C. The product ***R*-83-Na** was obtained as a yellowish solid in 91 % yield. NMR spectroscopic characterization was carried out at room temperature without showing any decomposition of the carbenoid ***R*-83-Na** which is in accordance with the increased thermal stability of the higher congeners in comparison to the Li/Cl carbenoid.[26] Full deprotonation of the precursor ***R*-83** was confirmed by the disappearance of the doublet caused by the hydrogen atom at the bridging carbon atom in the ^{1}H NMR spectrum. The carbenoid *R*-**83-Na** is characterized by a singlet at δ_{P} = 43.1 ppm in the ^{31}P{^{1}H} spectrum. The ^{13}C chemical shift of the Na/Cl carbenoid is comparable to its lithium analog. The central carbon atom is also not showing the typical downfield shift of carbenoids in the ^{13}C{^{1}H} NMR spectrum. The respective doublet can be seen at δ_{C} = 50.4 ppm. As expected, the coupling constant $^{1}J_{CP}$ is 88.75 Hz and thus larger than in the non-metalated compound *R*-**83**.

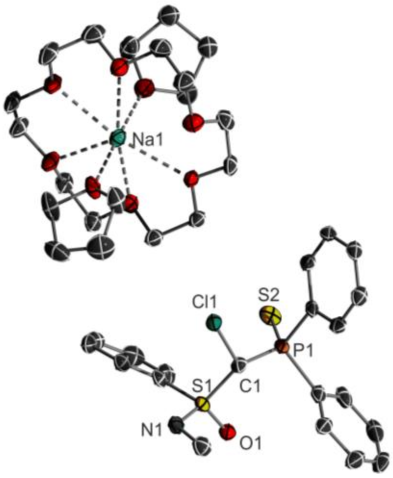

Figure 20. Molecular structure of **83-Na•**[18-C-6]. Displacement ellipsoids drawn at the 50 % probability level. Hydrogen atoms have been omitted for clarity. Selected bond lengths [Å] and angles [°]: P1–C1 1.764(3), S1–C1 1.701(3), Cl1–C1 1.780(3), S1–C1–Cl1 112.11(16), P1–C1–S1 121.16(17), P1–C1–Cl1 114.87(16).

The chiral carbenoid *rac*-**83-Na** was also characterized by X-ray diffraction analysis. However, crystallization was only achieved by addition of an additional donor molecule, in this case 18-C-6, to a saturated racemic solution in THF at –30 °C. The Na/Cl carbenoid *rac*-**83-Na** crystallizes as a monomer in the triclinic space group $P\bar{1}$ (Figure 20). Due to the presence of the crown ether the Na atom does not exhibit any contact to either the chlorine or the central carbenoid carbon atom. The sodium atom is coordinated by one molecule of 18-C-6 and two THF molecules. Consequently, the C1–Cl1 (1.780(3) Å) bond does not show any change in length compared to the protonated precursor *R*-**83** (1.7739(13) Å) and is comparable to the one in the Li congener (1.7734(14) Å) (Table 4). The sum of angles around the central carbon atom C1 is 348.14 ° and thus it does not bear a planar coordination geometry. Analogous to the Li/Cl carbenoid *rac*-**83-Li** the P1–C1 (1.764(3) Å) and S1–C1 (1.701(3) Å) bonds are significantly shortened in comparison to *S*, *S*-**83** (1.8588(13) and 1.8643(14) Å).

Table 4. Selected bond lengths and angles of *S*, *S*-**83**, *rac*-**83-Li**, *rac*-**83-Na** and *rac*-**83-K**.

Bond length [Å]	*S, S*-**83**	*rac*-**83-Li**	*rac*-**83-Na**	*rac*-**83-K**
P1–C1	1.8588(13)	1.7586(15)	1.764(3)	1.759(5)
Cl1–C1	1.7739(13)	1.7734(14)	1.780(3)	1.780(6)
S1–C1	1.8643(14)	1.6933(15)	1.701(3)	1.705(5)
O1–Li		1.935(3)		
S1–N1	1.5000(13)	1.5233(13)	1.526(3)	1.526(5)
S1–O1	1.4554(10)	1.4742(10)	1.465(2)	1.462(5)
P1–S2	1.9403(5)	1.9699(5)	1.9783(11)	1.9700(19)

Angle [°]				
S1–C1–Cl1	104.85(7)	111.29(8)	112.11(16)	112.8(3)
S1–C1–P1	118.13(7)	126.80(8)	121.16(17)	121.7(3)
Cl1–C1–P1	110.40(7)	111.59(8)	114.87(16)	115.1(3)

The potassium analog *R*-**83-K** can be obtained in a similar manner as *R*-**83-Na** using KH instead of NaH. The K/Cl carbenoid was obtained as a yellow solid in 88 % yield which can be handled and fully characterized by NMR spectroscopy at room temperature. The successful synthesis of the chiral K/Cl carbenoid was evidenced by the appearance of a singlet in the ^{31}P{^{1}H} NMR at δ_P = 44.1 ppm. Similar to the lighter congeners the K/Cl carbenoid also shows no downfield shift in the ^{13}C{^{1}H} NMR spectrum. The doublet for the central carbon atom arises at δ_C = 49.8 ppm ($^{1}J_{CP}$ = 86.3 Hz) with a coupling constant in the same range as found for the Li and Na analogues. The molecular structure of *rac*-**83-K** was elucidated with the help of single crystal X-ray diffraction analysis. Suitable crystals were obtained from a concentrated solution of 2 eq. of 14-C-4 and *rac*-**83-K** in THF at –30 °C. The chiral carbenoid crystallizes as a monomer in the triclinic space group $P\bar{1}$. The molecular structure (Figure 21) shows a coordination of the K1 atom by two crown ether molecules and thus bearing no coordination by the sulfoximine moiety of the carbenoid as evidenced in case of *rac*-**83-Li**.

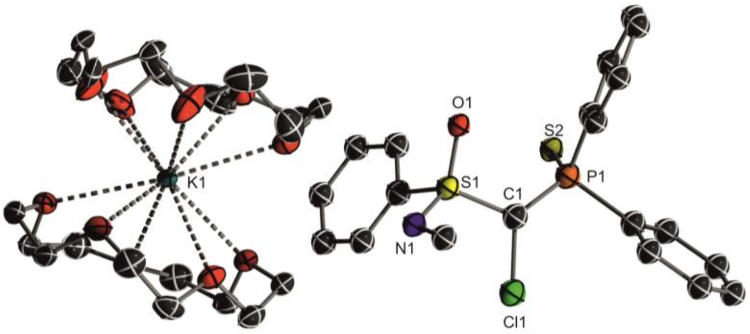

Figure 21. Molecular structure of *rac*-**83-K**•2[14-C-4]. Displacement ellipsoids drawn at the 50 % probability level. Hydrogen atoms have been omitted for clarity. Selected bond lengths [Å] and angles [°]: P1–C1 1.759(5), S1–C1 1.705(5), Cl1–C1 1.780(6), S1–C1–Cl1 112.8(3), P1–C1–S1 121.7(3), P1–C1–Cl1 115.1(3).

The bond lengths of *rac*-**83-K** are comparable with the ones of *rac*-**83-Li** and *rac*-**83-Na** (Table 4). Consequently, it does not bear an elongated C–Cl bond due to the disruption of the K···C···Cl contact by the coordination of two 14-C-4 crown ether molecules. The P1–C1–S1 backbone of the carbenoid is also contracted due to electrostatic interactions.

Table 5. Crystallographic data and structure refinement of *rac*-**83-Li,** *rac*-**83-Na** and *rac*- **83-K**.

Parameter	**Compound *rac*-83-Li**	**Compound *rac*-83-Na**	**Compound *rac*-83-K**
Emperical formula	$C_{32}H_{42}ClLiNO_4PS_2$	$C_{80}H_{116}Cl_2N_2Na_2O_{18}P_2S_4$	$C_{40}H_{58}ClKNO_{11}PS_2$
Formula weight	642.14 g/mol	1700.80 g/mol	898.51 g/mol
Temperature	100(2) K	100(2) K	100(2) K
Wavelength	1.54184 Å	1.54184 Å	1.54184 Å
Crystal system	Monoclinic	Triclinic	Triclinic
Space group	$P2_1/c$	$P\bar{1}$	$P\bar{1}$
Unit cell dimensions	a = 8.9364(4) Å	a = 9.2135(3) Å	a = 9.1916(3) Å
	b = 19.994(3) Å	b = 20.4163(6) Å	b = 20.6188(8) Å
	c = 18.1879(14) Å	c = 23.8781(8) Å	c = 23.3493(5) Å
	α = 90°	α = 75.754(3)°	α = 89.975(2)°
	β= 97.652(6)°	β = 80.345(3)°	β = 84.739(2)°
	γ = 90°	γ = 87.399(3)°	γ = 89.983(3)°
Volume	3220.8(5) $Å^3$	4291.7(2) $Å^3$	4406.5(2) $Å^3$
Formula unit per cell	4	2	4
Density (calculated)	1.324 Mg/m^3	1.316 Mg/m^3	1.354 Mg/m^3
Absorption coefficient	3.025 mm^{-1}	2.586 mm^{-1}	3.323 mm^{-1}
F(000)	1360	1808	1904
Crystal size	0.409 x 0.164 x 0.116 mm^3	0.129 x 0.059 x 0.059 mm^3	0.295 x 0.036 x 0.017 mm^3
Θ range for data collection	3.301 to 72.483°	3.290 to 67.080°	2.865 to 67.499°

Index ranges	-11 ≤ h ≤ 11, -21 ≤ k ≤ 24, -22 ≤ l ≤ 21	-11 ≤ h ≤ 9, -24 ≤ k ≤ 20, -28 ≤ l ≤ 28	-10 ≤ h ≤ 11, -24 ≤ k ≤ 24, -26 ≤ l ≤ 27
Reflections collected	25932	29548	79386
Independent reflections	6357 [*R*(int) = 0.0302]	15283 [*R*(int) = 0.0564]	15421 [*R*(int) = 0.1498]
Refinement method	Full-matrix least-squares on F^2	Full-matrix least-squares on F^2	Full-matrix least-squares on F^2
Data / restraints / parameters	6357 / 0 / 505	15283 / 0 / 996	15421 / 0 / 1049
Goodness-of-fit on F^2	1.028	1.018	1.040
Final *R* indices [I>2σ(I)]	*R*1 = 0.0343, w*R*2 = 0.0895	*R*1 = 0.0517, w*R*2 = 0.1273	*R*1 = 0.0799, w*R*2 = 0.2051
R indices (all data)	*R*1 = 0.0379, w*R*2 = 0.0928	*R*1 = 0.0796, w*R*2 = 0.1425	*R*1 = 0.0855, w*R*2 = 0.2103
Largest diff. peak and hole	0.513 and -0.367 e.Å^{-3}	1.562 and -0.601 e.Å^{-3}	1.422 and -1.312 e.Å^{-3}

After having synthesized and successfully characterized the respective Li, Na and K chlorine carbenoids the synthesis of the most probably more reactive and thermally labile M/F carbenoids was attempted. Therefore, the twice protonated compound *S*-**82** was treated with ^{n}BuLi and *N*-Fluorobenzenesulfonimide (NFSI) at low temperatures yielding the product as a sticky colorless oil in 31 % yield. The fluorinated compound *S*-**84** was fully characterized by means of NMR spectroscopy and elemental analysis. Analogous to compound *R*-**83** the NMR spectra of *S*-**84** exhibit two sets of signals due to the presence of diastereomeric species. The product is characterized by two doublets in the ^{31}P{^{1}H} NMR spectrum at δ_{P} = 36.1 and 36.9 ppm in d$_{8}$-THF with coupling constants of $^{2}J_{P\text{-}F}$ = 55.8 and 55.7 Hz, respectively, and two doublets at δ_{F} = -177.1 and -175.6 ppm in the ^{19}F{^{1}H} NMR spectrum. The purity of *S*-**84** was confirmed by elemental analysis.

The Li/F carbenoid was synthesized in THF by reacting *S*-**84** with 1 eq. MeLi solution in Et$_{2}$O in THF at –50 °C to ensure selective formation and exclude decomposition of the Li/F carbenoid. The product *S*-**84-Li** was obtained as a yellow solid in 86 % yield and NMR spectroscopically characterized at –30 °C to prevent decomposition. Due to the change of hybridization from sp^{3} to sp^{2} of the central carbon atom only one set of signals is observed in the NMR spectra. The absence of the signals of the hydrogen atom at the bridging carbon atom in the ^{1}H NMR spectrum confirms the successful formation of *S*-**84-Li**. The compound gives rise to a doublet in the ^{31}P{^{1}H} NMR spectrum at δ_{P} = 33.4 ppm ($^{2}J_{PF}$ = 43.8 Hz) and one in the ^{19}F{^{1}H} NMR spectrum at δ_{F} = -210.4 ppm ($^{2}J_{FP}$ = 44 Hz). Unfortunately, the signal of the bridging carbon atom is not detectable in the ^{13}C{^{1}H} NMR spectrum. Despite numerous attempts no crystals suitable for single crystal X-ray diffraction analysis could be obtained neither of the enantiomerically pure *S*-**84-Li** nor of a racemic mixture.

The sodium congener was obtained by the reaction of *S*-**84** with an excess of NaH in THF at 0 °C. The carbenoid *S*-**84-Na** was obtained as a yellow solid in 87 % yield and characterized by means of NMR spectroscopy at –30 °C in d_8-THF. As expected the compound shows a doublet in the $^{31}P\{^1H\}$ and $^{19}F\{^1H\}$ NMR spectrum at $\delta_P = 33.6$ ($^2J_{PF}$ = 42.5 Hz) and δ_F = -207.7 ppm ($^2J_{FP}$ = 43.1 Hz), respectively. Unfortunately, the signal of the bridging carbon atom is not detectable in the respective NMR spectrum and as in case of *rac*-**84-Li** no crystals for X-ray diffraction analysis were obtained.

The reaction of *S*-**84** with an excess of KH in THF at 0 °C gives access to *S*-**84-K** in 92 % yield. The light yellow solid was dissolved in cold d_8-THF and characterized by means of NMR spectroscopy at –30 °C. The $^{31}P\{^1H\}$ spectra reveals a doublet at δ_P = 34.4 ppm while the $^{19}F\{^1H\}$ NMR spectrum shows two doublets at δ_F = -210.4 ppm ($^2J_{FP}$ = 44.9 and 45.0 Hz). The splitting of the $^{19}F\{^1H\}$ NMR signal of *S*-**84-K** suggests a different structure in solution compared to the lighter congeners. Unfortunately, it was not possible to fully elucidate the structure of the K/F carbenoid causing the unexpected splitting. The characteristic downfield shift in the $^{13}C\{^1H\}$ NMR spectrum of the central carbon atom (δ_C = 111.6 ppm, $^1J_{CP}$ = 53.9 Hz; $^1J_{CF}$ = 190.3 Hz) by 41.9 and 35.3 ppm, respectively, compared to the two diastereomers of *R*-**83**, stresses the higher carbenoid character of M/F carbenoid compared to M/Cl ones.[26] Despite several attempts so far no single crystals suitable for X-ray diffraction analysis could be obtained.

Summarizing, a number of chiral M/X carbenoids (M = Li, Na, K and X = Cl, F) could be obtained and fully characterized by means of NMR spectroscopy. The M/Cl carbenoids do not show a downfield shift in the $^{13}C\{^1H\}$ NMR spectrum as found to be characteristic for carbenoids. However, compounds bearing no typical downfield shift of the central carbon atom were found to exhibit carbenoid character, so that the downfield shift is indicative but no exclusion criteria for the carbenoid nature of a compound.[20] The absence of the deshielding of the carbenoid carbon atom might be explained by the disruption of the carbon metal bond in solution as seen in case of the molecular structure of the Li/Cl carbenoid bearing no carbon lithium contact even without the presence of additional donor bases, such crown ethers.[58] In case of the chiral carbenoids **83-M** (M = Li, Na, K) the molecular structure was elucidated by

X-ray diffraction analysis. The obtained arrangements can be classified as carbene-donor complexes (Figure 8, **II**) since no contact between the respective alkali metal, the central carbon atom as well as the nucleofugal group was observed in any case. In case of the Li/Cl carbenoid the molecular structure (Figure 19) was elucidated without the presence of additional donor molecules, contrary, crystallization of the respective Na and K congeners (Figure 20 and Figure 21) was only achieved in presence of crown ether.

The respective M/F (M = Li, Na, K) carbenoids ***S*-84-M** were also fully characterized by means of NMR spectroscopy and contrary to their chlorine congeners the K/F carbenoid shows the characteristic down field shift of the carbenoid carbon atom in the $^{13}C\{^1H\}$ NMR spectra highlighting the higher carbenoid character of flourine carbenoids compared to chlorine ones. Unfortunately, the respective M/F carbenoids could not be characterized by means of single crystal X-ray diffraction analysis so far, despite several attempts to grow suitable crystals.

Diffusion Ordered Spectroscopy of Chiral Carbenoids

Diffusion ordered spectroscopy – A short introduction

Besides the well-known and mostly used NMR tools - chemical shifts δ and spin-spin coupling constants *J* - the diffusion constant is far less known. Even though NMR spectroscopic self-diffusion measurements date back to the pioneering discovery of spin echoes in 1950.[130] Hahn reported on the dependence of the spin echo on several effects, amongst others the diffusional effect on the echo amplitudes in an inhomogeneous magnetic field. In the mid-sixties the basic spin echo experiment was considerably improved to the pulsed-field gradient spin-echo (PSGE) method. However, only recently chemists have started to use PGSE NMR diffusion methods as well as the two dimensional variant, diffusion ordered spectroscopy (DOSY),[131] due to continuous hard- and software improvements. These improvements allow straightforward recording of diffusion type experiments. In DOSY NMR studies the diffusion coefficients of individual signals in a spectrum can be determined and consequently, they can be used to distinguish between the signals of different compounds in a mixture. Thus, DOSY NMR spectroscopy can be used for a) the estimation of molecular volumes and the detection of poly-nuclear and oligomeric species, b) recognition of interactions between polar ligands and solvents or anions and solvents, c) direct proof of the existence of strong/weak ion pairing,[131] d) separation of complex mixtures, e.g. pharmaceuticals and dietary supplements.[132] The 2D method DOSY disperses the signals according to their diffusion coefficient in one dimension and thus provides a virtual separation of the components of the mixture. The diffusion coefficients of species, however, depend on the nature of the solvent, the coordination of the species,[133] their shape and size.[134]

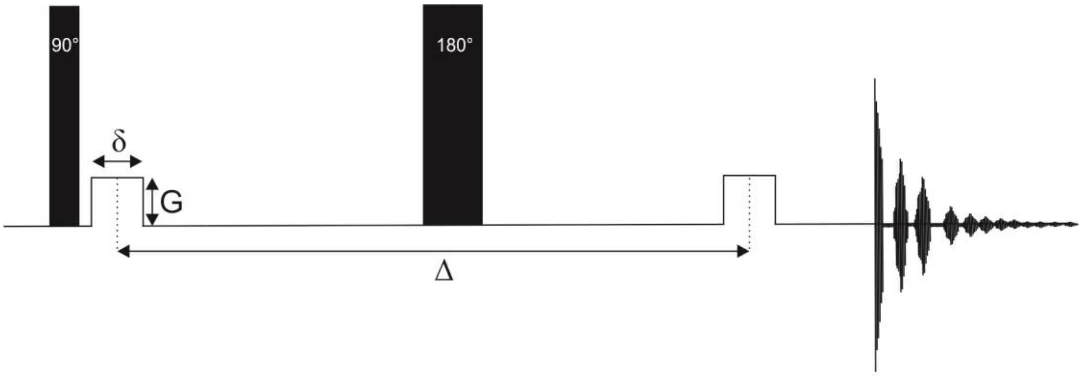

Figure 22. Typical pulse sequence for the PGSE experiment.

How does DOSY work? To answer this question understanding of the simple PGSE NMR diffusion methods is required. A typical PGSE experiment consists of a spin-echo sequence – a 90° pulse followed by a 180° pulse (black bars in Figure 22) – and two pulsed field gradients (white bars in Figure 22) which are separated by a waiting time Δ. The first gradient defocuses and the second one refocuses the magnetization. However, the molecules diffuse from their original position during the delay Δ, thus, resulting in a different effective magnetic field experienced by the spins during both gradients (Figure 23). The difference in the effective magnetic field results in incomplete refocusing of the spins leading to a decrease of the intensity of the NMR signals. With an increased intensity and duration of the gradient pulse the spatial selectivity increases and the intensity of the NMR signals decreases.

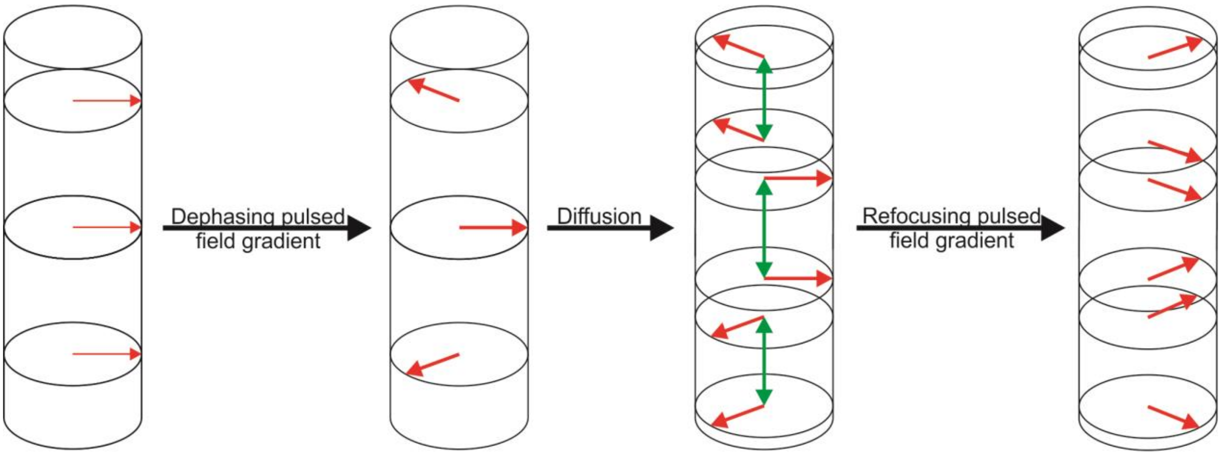

Figure 23. Effect of diffusion combined with magnetic field gradient pulses. The physical movement of nuclei reduces the effectiveness of the refocusing pulse reducing the resulting signal strength.

In case of DOSY NMR studies the pulse sequence is repeated many times and data sets are collected incrementing the gradient strength G (Figure 24). From this data set the diffusion coefficient D can be obtained according to $\mathrm{Ln}\left(\frac{\mathrm{I}}{\mathrm{I}_0}\right) = \gamma_X \delta^2 \mathrm{G}^2 \left(\Delta - \frac{\delta}{3}\right) \mathrm{D}$ with γ_X = gyromagnetic ratio of the X nucleus, δ = length of the gradient pulse, G = gradient strength and Δ = delay between the midpoints of the gradients.[131] The above descripted spin-echo sequence can be modified by splitting the one 180° pulse into two 90° to increase the signal-to-noice ratio.[131]

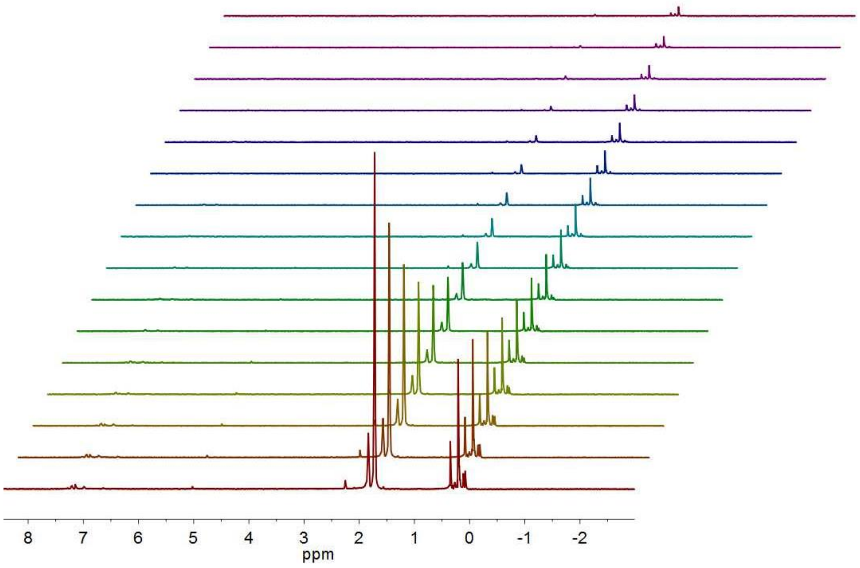

Figure 24. Exemplary diffusion spectrum illustrating the decreased signal intensity with incrementing gradient strength.

Different empirical methods for correlating the obtained diffusion coefficient D to the molecular weight (MW) of the respective species are reported. Besides the Stokes-Einstein equation and its modifications which are convenient to estimate the molecular size of particles that are much larger than the solvent the empirically derived power law is often used to determine the MW of compounds. The MW correlates to the diffusion coefficient D according to $\mathrm{D} = \mathrm{KMW}^{\alpha}$ with K being a molecule dependent constant and α a coefficient that depends significantly on the shape of the compound.[134] This power law was thought to be limited to a specific class of compounds, such as polymers, globular proteins,[135] oligosaccharides,[136] polyethyleneoxides[137] and denaturated peptides[138] in different solvents. Later, the appropriateness of the power law for the determination of the MW of small molecules by using internal reference molecules, such as tetramethylsilane (TMS) or water to obtain an internal calibration curve (ICC) was proven.[139] With the help of ICCs the accuracy for MW determination of small molecules has been considerably increased. Applying ICCs Mulvey *et* *al.* were able to characterize 2,2,6,6,-tetramethylpiperidine (TMP)[140] and diisopropylamide[141] turbo-Grignard reagents in THF solution. However, the ICC approach exhibits some disadvantages. First, the ICC is only based on a few – mostly three – reference molecules bearing only a small MW distribution and second, the ICC is only applicable for one NMR sample. Moreover, the internal reference substances have to fulfill a number of requirements: a) inertness to the analyte in solution, b) no overlapping of the NMR signals with other species, c) no coordinating ability towards the analyte, d) sufficient solubility and e) small MW distribution.[139b] Sometimes the choice of the right internal reference is challenging. Besides that several other sources of error have to be taken into account, such as diversities in temperature, fluctuation, convection, viscosity and concentration effects and also NMR device specific constants like gradient strength and pulse duration. Consequently, DOSY NMR spectra are only comparable under the exact same conditions. One way to reduce the influence of viscosity and temperature is to use an internal standard providing more reliable diffusion coefficients[142] by determining the so-called relative diffusivity D_{rel} which is defined as $D_{rel} = D_x/D_{ref}$ in which D_x and D_{ref} are the diffusion coefficient of the analyte and the reference, respectively.[134] The group of Stalke further developed this approach by using relative diffusion coefficients with fixed diffusion values. They found that the logarithmic diffusion values have an approximately linear connection and are independent of the gradient and magnetic field strength, the gradient pulse duration, the gyromagnetic ratio and also changes in viscosity or temperature. This realization led them to the following equation $\log D_{x,norm} = logD_{ref,fix} - \log D_{ref} + logD_x$ where $\log D_{ref,fix}$ corresponds to the fixed value of the reference, $\log D_{ref}$ to the measured diffusion coefficient of the reference, $\log D_x$ to the diffusion coefficient of the analyte and $\log D_{x,norm}$ to the relative diffusion value of the analyte x normalized to the reference. The approach was found to yield excellent results for the normalized diffusion coefficient for a number of model compounds independent of the NMR device. In the same paper Stalke and coworkers have reported on the external calibration curves for the accurate MW determination of small molecules with the help of DOSY NMR. The use of 28 model compounds in independent NMR samples gave access to external calibration curves (ECC). However, the results were not accurate enough especially for very low and high MWs. To further improve the precision they considered the shape and compactness features. Based on their results three different types of compounds (Figure 25) were defined a) compact spheres (CS), b) dissipated spheres and ellipsoids (DSE) and c) expanded discs (ED).

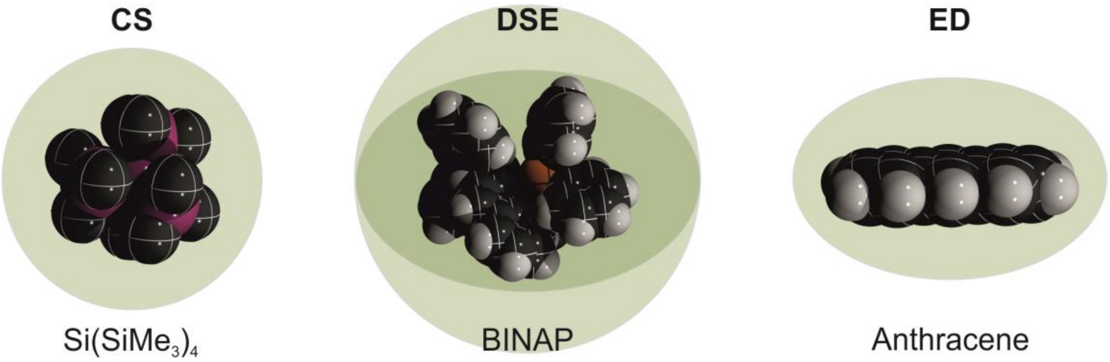

Figure 25. Example molecules for the three different categories based on their diffusion behavior.

Examples for these categories are adamantane (adam) or $Si(SiMe_3)_4$ for CS since they have the same radius in all dimension with a high density space. Tetramethoxypropane or 2,2-bis(diphenylphosphino)-1,1-binaphthyl (BINAP) for DSE being either spherical like or less compact compounds (e.g. bearing dative bonds) compared to CS or ellipsoidal molecules and anthracene or tetraphenylnaphthalene for ED. Noteworthy, most small molecules diffuse like DSE, even small aromatic compound such as toluene, indene or naphthalene with MW < 160 g/mol. With increasing MW the two dimensional geometry starts to play a role that is the case at a MW of roughly 178 g/mol. By this method it is possible to determine the MW of the tested species with an error of only 9 %. The advantage of the ECC approach is that the diffusion coefficients are normalized and consequently, the ECC can be used independent of the NMR device and only one internal reference has to be used. Moreover, the MW determination by ECC is also valid over a wide range of temperates.[134]

Indepent on what approach is used, with the help of DOSY NMR the solution structure of a wide range of s-block organometallic compounds, e.g. alkali-metal cyclopentadienides,[143] turbo-Grignards[141, 144] as well as common lithium bases such as ^{n}BuLi[145] or $Li(HMDS)_2$[146] were elucidated. However, comparable studies of carbenoids have not been reported so far.

DOSY NMR Studies of Chiral Carbenoids

As described before carbenoids are very reactive and temperature labile species. There are several ways to stabilize these reactive species. One way to do so is the right choice of solvent. However, so far not much is known on the influence of the solvents on the solvation and aggregation behavior of carbenoids in solution. To gain knowledge about the solvation/aggregation of carbenoids is highly desirable to understand the effects of solvents on their stability and reactivity which can be used for an advanced reactivity control. The main goal will be to establish a tool box for the fine-tuning between reactivity and stability. The control of reactivity will be used to synthesize carbenoids that are as stable as possible but as reactive as necessary to develop new and selective applications. In order to obtain systematic information on the structure-reactivity/stability relationship of carbenoids the chiral carbenoids *rac*-**83-M** and *rac*-**84-M** were investigated by means of DOSY NMR studies in a coordinating and a non-/ weakly coordinating solvent to gain insights into the influence of the nature of the solvent on the solution structure of carbenoids. THF was chosen as the coordinating solvent while toluene (Tol) as the non-coordinating one. Moreover, the influence of the temperature on the solvation/aggregation behavior of the chiral carbenoids was investigated by performing variable temperature (VT) DOSY NMR studies at –30 °C, –20 °C and 27 °C, respectively. For the evaluation of the VT DOSY NMR studies the ECC approach investigated by Stalke and coworkers was used.[134] As the internal standard TMS was used in THF and adamantane in toluene. All carbenoids were treated like DSE like structures during evaluation of the obtained data. Furthermore, the calculated masses of the coordinating solvents are based on the protonated species since the atomic radius of deuterium compared to hydrogen is almost similar. Depending on the correlation between the atomic volume and the diffusion coefficient deuterated and protonated species diffuse approximately the same despite the slight difference in weight.

The carbenoids *rac*-**83-M** have been prepared as described in the previous chapter. The dried carbenoids were dissolved in cooled deuterated NMR solvent and transferred into a J. Young NMR tube by a syringe. In case of TMS the standard was added after transferring the carbenoid under inert gas atmosphere. The adamantane was added to the J. Young NMR tube before the transfer of the carbenoids and then the J. Young NMR tube was evacuated and flushed with argon three times.

Figure 26 shows an exemplary DOSY NMR spectrum obtained using carbenoid *rac*-**83-Li** in THF with TMS as standard at 27 °C. The signals inside of the green frame belong to the carbenoid, the ones in the blue one belong to THF and the one inside the purple one is the internal standard TMS. For the calculation of the MW of the carbenoids in solution Stalke´s ECCs approach as well as his ECC-MW estimation software were applied.[143] For *rac*-**83-Li** a calculated weight of 464 g/mol was found which deviates from the mass of *rac*-**83-Li** plus one coordinated THF molecule by 8% (Table 6).

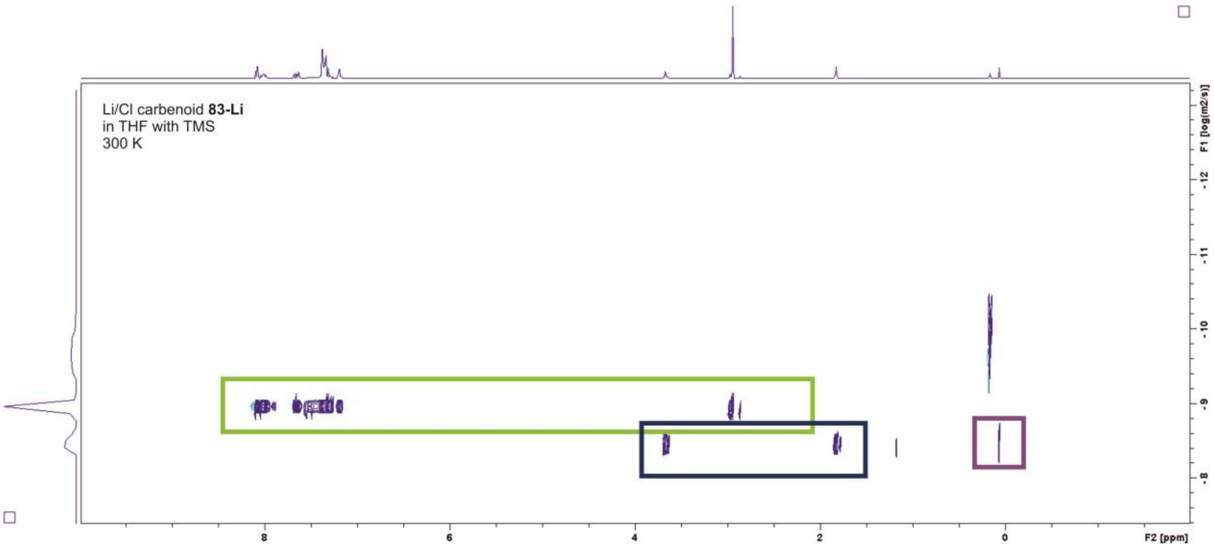

Figure 26. 2D DOSY NMR spectrum of *rac*-**83-Li** in d_8-THF with TMS as internal standard measured at 27 °C. The signals in the green frame belong to *rac*-**83-Li**, the ones in the blue frame to THF and the one in the purple frame to TMS.

The VT DOSY measurement at –20 °C in THF gave a MW of 554 g/mol which is distinctively higher than the one obtained at 27 °C and the actual mass of *rac*-**83-Li** (425.85 g/mol). So it is reasonable to assume a coordination of the solvent THF to the carbenoid. Comparison of the calculated mass with the masses of the carbenoids plus a changing number of THF molecules yields the best fit for the mass of one molecule of *rac*-**83-Li** and two THF molecules (570.07 g/mol) with only a very small deviation of 3 %. Lowering the temperature even further to –30 °C the calculated mass is even higher (600 g/mol) which is in between the masses of *rac*-**83-Li** plus two and three THF molecules. Thus, it is reasonable to assume an 1 : 1 equilibrium of these two species with a fast exchange of the coordinated THF molecules with non-coordinated ones from the surroundings. Due to this fast exchange of THF solvent molecules the coordinated THF molecules can not be seen as separate signal in the DOSY NMR spectra. The obtained diffuision coefficient for THF is consequently an average signal for free and coordinated THF molecules. The average mass of *rac*-**83-Li** plus two and three THF molecules coordinated is 606.13 g/mol which is in very good agreement with the obtained MW from the DOSY NMR studies with a deviation of only 1 %. Noteworthy, this result matches the molecular structure of *rac*-**83-Li** obtained in THF at –30 °C exhibiting three coordinated THF solvent molecules (Figure 19).

Table 6. ^{1}H DOSY NMR data for *rac*-**83-M** in d$_8$-THF with TMS as standard, the actual and calculated masses, their deviation and the respective solution structure.

	Temp [°C]	D_{ref} [m^2s^{-1}]	$logD_{ref}$	Ø D_{carb} [m^2s^{-1}]	Ø $logD_{carb}$	MW_{DOSY} [g/mol]	MW_{calc} [g/mol]	Species	Error [%]
rac-**83-Li**	27	2.14E-9	-8.67	8.98E-10	-9.05	464	497.96	Monomer + 1 THF	-8
rac-**83-Na**	27	2.33E-9	-8.63	9.42E-10	-9.03	471	477.96	Monomer + 0/1 THF	-2
rac-**83-K**	27	2.17E-9	-8.66	8.25E-10	-9.09	521	530.12	Monomer + 1THF	-2
rac-**83-Li**	–10	1.28E-9	-8.89	4.69E-10	-9.33	554	570.07	Monomer +2 THF	-3
rac-**83-Na**	–10	1.44E-9	-8.84	5.07E-10	-9.30	595	586.12	Monomer +2 THF	+2
rac-**83-K**	–10	1.24E-9	-8.91	4.54E-10	-9.34	555	566.18	Monomer + 1/2 THF	-2
rac-**83-Li**	–30	8.75E-10	-9.06	3.07E-10	-9.51	600	606.13	Monomer +2/3 THF	-1
rac-**83-Na**	–30	1.01E-9	-8.99	3.84E-10	-9.41	683	658.23	Monomer + 3THF	+4
rac-**83-K**	–30	9.16E-10	-9.04	3.11E-10	-9.51	633	638.29	Monomer + 2/3 THF	-1

Changing the solvent from THF to non-/ or weakly coordinating toluene and using adamantane as an internal standard gave a molecular mass of 904 g/mol at 27 °C and thus a significantly higher mass than the actual MW of the monomeric compound *rac*-**83-Li** (425.85 g/mol) (Figure 27).

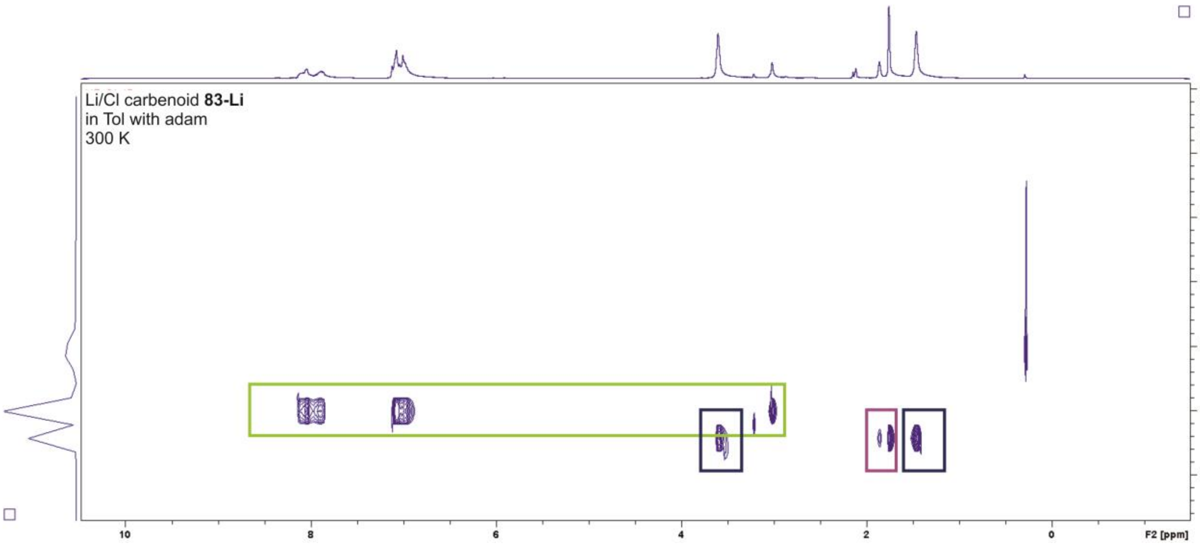

Figure 27. 2D DOSY NMR spectrum of *rac*-**83-Li** in d$_8$-Tol with adamantane as internal standard recorded at 27 °C. The signals in the green frame belong to *rac*-**83-Li**, the ones in the blue frames to THF and the one in the purple frame to adamantane.

This result indicates a dimeric structure in solution in toluene (Table 7). However, the MW of the dimer is only 851.7 g/mol. Consequently, solvent molecules have to be coordinated to the dimer. Note, due to the synthesis of *rac*-**83-Li** in THF and the inability to remove the THF completely *in vacuo* also the DOSY samples measured in toluene still contain a small amount of THF. Owing to the fact that THF has a stronger tendency to coordinate to the carbenoid in solution, the masses for comparison were calculated with THF instead of toluene as the coordinated solvent. Another indication of THF being the coordinated solvent is the higher mass calculated for THF (183 g/mol at 27 °C, 140 g/mol at –10 °C and 148 g/mol at –30 °C, actual mass of THF: 72 g/mol) based on its diffusion coefficient which can be explained by a coordination to the carbenoid. For *rac*-**83-Li** the best match was obtained for a dimer with one THF molecule coordinated (923.81 g/mol) with a difference of 2 %. Lowering the temperature to –20 °C results in an increased number of coordinated THF molecules analogously to THF. At –20 °C another equilibrium is present with the dimer being coordinated by two and three THF molecules. The same is true for the structure at –30 °C. These results indicate a solvent and temperature dependent solvation and aggregation behavior of the chiral carbenoid *rac*-**83-Li**. To proof this assumption analogous studies were performed with *rac*-**83-Na** and *rac*-**83-K** using the same parameters.

Table 7. ^{1}H DOSY NMR data for *rac*-**83-M** in d$_8$-Tol with adamantane as standard, the actual and calculated masses, their deviation and the respective solution structure.

	Temp [°C]	D_{ref} [m^2s^{-1}]	Ø $logD_{ref}$	Ø D_{carb} [m^2s^{-1}]	Ø $logD_{carb}$	MW_{DOSY} [g/mol]	MW_{calc} [g/mol]	Species	Error [%]
rac-**83-Li**	27	1.69E-9	-8.77	5.63E-10	-9.25	904	887.76	Dimer + 0/1 THF	+ 2
rac-**83-Na**	27	1.80E-9	-8.75	4.72E-10	-9.33	1330	1316.46	Dimer + 6 THF	+ 1
							1325.70	Trimer	+ 2
rac-**83-K**	27	1.71E-9	-8.77	5.01E-10	-9.31	1135	1132.35	Dimer + 3 THF	+ 1
rac-**83-Li**	–10	8.62E-10	-9.06	2.63E-10	-9.58	1051	1031.98	Dimer + 2/3 THF	+ 2
rac-**83-Na**	–10	9.14E-10	-9.04	2.43E-10	-9.62	1312	1316.46	Dimer + 6 THF	- 1
							1325.70	Trimer	
rac-**83-K**	–10	9.51E-9	-9.02	2.97E-10	-9.53	1012	1060.24	Dimer + 2 THF	- 5
rac-**83-Li**	–30	5.36E-10	-9.27	1.67E-10	-9.78	1025	1031.98	Dimer + 2/3	- 1
rac-**83-Na**	–30	5.52E-10	-9.26	1.55E-10	-9.81	1195	1172.24	Dimer + 4 THF	+ 2
rac-**83-K**	–30	4.70E-10	-9.33	1.29E-10	-9.89	1252	1251.46	Dimer + 6 THF	+ 1

In THF the same trend was observed regardless of the alkali metal present. The lower the temperature the more THF molecule are coordinated to the carbenoid (Table 6). The results in toluene are somewhat more complex than the ones obtained in THF. In all cases a dimeric structure was obtained, however, in some cases, *rac*-**84-Na** at –20 °C and 27 °C, the obtained masses fit to both a dimer with six THF molecules coordinated as well as a trimeric structure with no solvent molecules attached. The oligomeric structure of compounds *rac*-**83-M** in toluene can be explained by their presumably lower stability in non- or weakly coordinating environment. An increased stability is achieved by the aggregation to a dimer or trimer.

In general, the studied chiral carbenoids *rac*-**83-M** exhibit a solvent and temperature dependent solvation and aggregation behavior (Table 6, Table 7). In THF they bear a monomeric structure while in toluene mostly dimeric (or trimeric) structures were observed. To test if these trends are also valid for carbenoids featuring another nucleofugal group the carbenoids *rac*-**84-M** were studied by VT DOSY NMR spectroscopy.

Similar to their chlorinated analogs the fluorinated species *rac*-**84-M** form a monomeric structure in THF in all cases and at all temperatures. Furthermore, the trend of an increasing number of coordinated THF molecules while decreasing the temperature is also valid for *rac*-**84-M**. The Li/F carbenoid *rac*-**84-Li** for examples is coordinated by two THF molecules at 27 °C and exhibits an equilibrium of two and three coordinated solvent molecules –30 °C (Table 8).

Table 8. ^{1}H DOSY NMR data for *rac*-**84-M** in d$_8$-THF with TMS as standard, the actual and calculated masses, their deviation and the respective solution structure.

	Temp [°C]	D_{ref} [m^{2}s^{-1}]	logD_{ref}	Ø D_{carb} [m^{2}s^{-1}]	Ø logD_{carb}	MW_{DOSY} [g/mol]	MW_{calc} [g/mol]	Species	Error [%]
rac-**84-Li**	27	2.30E-9	-8.64	8.44E-10	-9.07	554	553.62	Monomer + 2 THF	+ 1
rac-**84-Na**	27	2.57E-9	-8.59	8.93E-10	-9.05	611	605.73	Monomer + 2/3 THF	+ 1
rac-**84-K**	27	2.38E-9	-8.62	8.44E-10	-9.07	590	585.78	Monomer + 2 THF	+ 1
rac-**84-Li**	–10	1.25E-10	-8.90	4.84E-10	-9.34	550	553.62	Monomer + 2 THF	-1
rac-**84-Na**	–10	1.37E-9	-8.86	4.78E-10	9.32	606	605.73	Monomer + 2/3 THF	+ 1
rac-**84-K**	–10	1.26E-9	-8.90	4.44E-10	-9.35	592	585.78	Monomer + 2 THF	+ 2
rac-**84-Li**	–30	8.57E-10	-9.07	3.04E-10	-9.52	588	589.68	Monomer + 2/3 THF	- 1
rac-**84-Na**	–30	8.61E-10	-9.07	3.19E-10	-9.50	545	533:62	Monomer + 1/2 THF	+ 3
rac-**84-K**	–30	8.59E-10	-9.07	2.98E-10	-9.53	612	621.84	Monomer + 2/3 THF	- 2

Analogously the same species is a dimer in toluene (Table 9). However, due to its thermal lability it was not possible to record a DOSY NMR spectrum at 27 °C without decomposition of the sample. Even though according to literature the higher congeners should be thermally more stable than the Li analog, it was not possible to prepare the respective sodium and potassium species *rac*-**84-Na** and *rac*-**84-K** in toluene. Consequently, no DOSY data could be obtained.

Table 9. ^{1}H DOSY NMR data for *rac*-**84-Li** in d_8-Tol with adamantane as standard, the actual and calculated masses, their deviation and the respective solution structure.

	Temp [°C]	D_{ref} [m^2s^{-1}]	Ø $logD_{ref}$	Ø D_{carb} [m^2s^{-1}]	Ø $logD_{carb}$	MW_{DOSY} [g/mol]	MW_{calc} [g/mol]	Species	Error [%]
rac-**83-Li**	–10	8.67E-10	-9.05	2.88E-10	-9.55	991	999.08	Dimer + 2/3 THF	-1
rac-**83-Li**	–30	5.19E-10	-9.26	1.55E-10	-9.81	1193	1179.35	Dimer + 5 THF	+ 2

Summing up, by performing DOSY NMR studies of a variety of chiral carbenoids, important insight into the solution structure of carbenoids in different solvent environments in dependence of the temperature were obtained. So far, no comparable studies have been performed. The aggregation of the examined carbenoid species only depends on the solvent in case of THF but not on the temperature since they featured a monomeric structure in THF at all temperatures. Contrary, a temperature dependency was observed in case of the solvation behavior. The number of coordinated THF molecules increased with decreasing temperature. This trend holds true for the chlorine and fluorine carbenoids *rac*-**83-M** and *rac*-**84-M** independent of the alkali metal used. Unfortunately, no such clear trends were observed in the non- or weakly coordinating solvent toluene which is well in line with the weaker coordination ability of toluene compared to THF. In most cases a dimeric structure was observed and in some cases (*rac*-**83-Na**, –20 °C and 27 °C) a trimer might be present which cannot clearly be distinguished from a dimer with six coordinating THF molecules due to a similar MW (trimer: 1325.7 g/mol, dimer + 6 THF: 1316.46 g/mol). Nonetheless, based on the performed diffusion experiments a significant difference in the solution structure of the chiral carbenoids *rac*-**83-M** and *rac*-**84-M** could be proven and thus a strong influence of the solvent on the solvation/aggregation of carbenoids. These results are helpful to further understand and fine-tune the reactivity and stability of carbenoids.

Stability Studies of Chiral Carbenoids

The decomposition of the heavier congeners of *rac*-**84**-**M** in toluene even at –30 °C are in stark contrast to the reported increasing stability when going down the periodic table from lithium to potassium. These observations sparked our interest to investigate the thermal stability of these compounds systematically. Therefore VT $^{31}P\{^{1}H\}$ NMR spectroscopic studies in THF and toluene were performed. The sample preparation was performed analogously to the VT DOSY studies only without adding the internal standard. The samples were inserted into the already cooled NMR instrument to prevent decomposition even before the start of the measurements. During the course of the measurements a ^{1}H and a $^{31}P\{^{1}H\}$ NMR spectrum were recorded at –30 °C, respectively, and then the sample was kept at that temperature for 1h. After that time another ^{1}H and $^{31}P\{^{1}H\}$ NMR spectrum were recorded. Subsequently, the NMR instrument was automatically warmed up to –20 °C and the sample was kept at that temperature for 1h and then the NMR spectra were recorded. This process was repeated with incrementing the temperature by steps of 10 °C until the temperature of 50 °C was reached. Due to the more facile detection of decomposition by $^{31}P\{^{1}H\}$ NMR spectra those were used to determine the decomposition temperatures of the respective carbenoids in solution (Table 10, Figure 28). First, the chlorinated carbenoids *rac*-**83**-**M** were studied. In case of *rac*-**83**-**Li** in THF no decomposition was observed in the $^{31}P\{^{1}H\}$ NMR spectra even at temperatures as high as 50 °C. The observed stability is quite unusual for a Li/Cl carbenoid since they are – according to previous observations and studies – thermally labile and reactive species.[20, 26-27, 39b] Based on former results of our group[26] an even higher stability for the heavier congeners of *rac*-**83**-**M** was expected. Surprisingly, the obtained NMR spectroscopic data for *rac*-**83**-**Na** did not validate this assumption. For the Na congener the respective NMR spectrum recorded at 50 °C showed an additional signal at 55.2 ppm indicating beginning decomposition at that temperature (Figure 28, middle). The carbenoid *rac*-**83**-**K** was found to be only stable up to 40 °C and thus being the least stable one of the three examined carbenoids. The decomposition yield a number of different decomposition products and thus does not result in the selective formation of one decomposition product (see Figure 28, right).

Table 10. Decomposition temperatures of chiral carbenoids *rac*-**83-M** obtained by VT NMR spectroscopy.

Carbenoid	Decomposition Temp. in THF [°C]	Decomposition Temp. in Tol [°C]
rac-**83-Li**	> 50	–10
rac-**83-Na**	50	50
rac-**83-K**	40	50

These results are in stark contrast to findings by Gessner *et al.*[26] which showed an increased stability going from lithium to potassium in case of thiosphosphoryl and silyl substituted carbenoids. This observation is in contrast to the general trend in the periodic table of the heavier analogs bearing a higher reactivity. The increased stability of the Na and K carbenoids compared to the Li one is explained by the higher polarity of the M–C bond which may results in a weaker polarization of the C–Cl bond and the lower Lewis acidity of the heavier metals (cf. M/X Combination). The reversed observation in case of the chiral carbenoids might be explained by the change in substitution pattern from a silyl group to the sulfoximine group bearing an oxygen donor functionality. The strong coordination of the Li atom by the sulfoximine group and additional THF molecules can prevent α-elimination of the LiCl salt and thus results in an increased stability compared to sodium and potassium exhibiting a less pronounced propensity to be coordinated by oxygen donor molecules according to the HSAB theory. Changing the solvent from the coordinating solvent THF to the non-coordinating one toluene might results in a reversed trend since the stabilizing coordination of the Li atom by oxygen atoms of the solvent is missing in toluene.

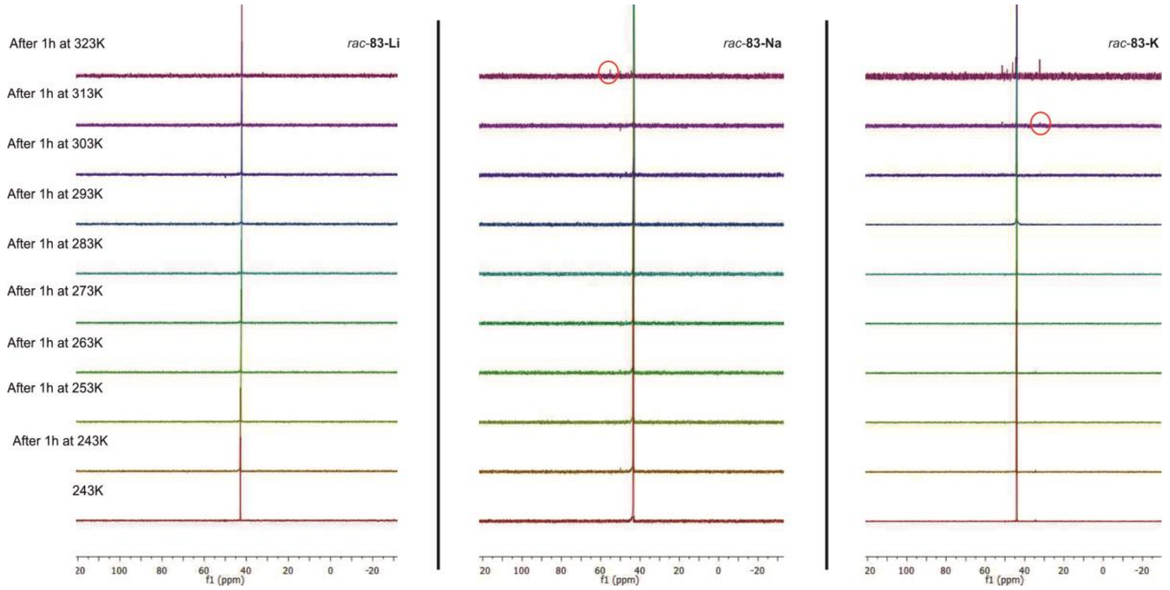

Figure 28. VT NMR spectra of *rac*-**83-M** in THF.

This assumption was confirmed by recording analogous NMR studies of the carbenoids *rac*-**83-M** in toluene. And indeed the Li/Cl carbenoid *rac*-**83-Li** was found to be significantly more labile than in THF already decomposing at –10 °C. In contrast, the sodium and potassium analogues showed an increased stability in toluene compared to THF being stable up to 50 °C. The determined decomposition temperatures in toluene are in agreement with the early results and the higher stability of the heavier homologs can be explained by the same reasons (see above). The chlorine carbenoids *rac*-**83-M** show a clear solvent dependent stability with *rac*-**83-Li** exhibiting the strongest dependence on the solvent environment on its thermal stability and the Na congeners showing the smallest one with no change in its decomposition temperature.

To verify this solvent dependent stability the respective flourine carbenoids *rac*-**84-M** were studied as well. The Li/F carbenoid *rac*-**84-Li** exhibits a thermal stability up to 50 °C and is only slightly more labile than the Li/Cl carbenoid *rac*-**83-Li**. Note, that Li/F carbenoids are in general the most reactive carbenoids and still considered ‘the beast’ in carbenoid chemistry.[20] Thus, the determined decomposition temperature of 50 °C is remarkable for a Li/F carbenoid.

To the best of my knowledge, compound *rac*-**84-Li** is the most stable and the first room temperature stable Li/F carbenoid to date. Its high thermal stability stresses the outstanding stabilizing effects of the sulfoximine and thiophosphoryl moiety by both their electron withdrawing properties as well as their donor functionalities. For comparison the Li/F analog of the bis(thiophosphoryl) system **19** (Figure 3) is only stable up to 0 °C and the respective Li/F carbenoid of **18** (Figure 3) even decomposes at –70 °C. Consequently, the introduction of the sulfoximine group is the key factor for this remarkable stability of *rac*-**84-Li** and this underlines the influence of the substitution pattern on the carbenoid stability and the great potential of carbenoids owing to their high tunability.

Examining the respective Na/F species *rac*-**84-Na** in THF reveals a slightly lower thermal stability compared to the Li/F carbenoid of 40 °C. This is in agreement with the stabilities observed in case of the M/Cl species *rac*-**83-M**. Also the carbenoid *rac*-**84-K** follows this trend showing decomposition at 30 °C. Consequently, the following conclusion can be drawn. In case of the examined chiral carbenoids *rac*-**83-M** and *rac*-**84-M** a decreasing thermal stability in THF is observed when going down the periodic table from lithium to potassium. The VT NMR studies of *rac*-**84-Li** in toluene (Figure 29, left) reveal a decreased thermal stability up to only 20 °C compared to 50 °C in THF. In case of *rac*-**84-Na** no VT NMR experiments could be performed due to immediate decomposition of the sample in toluene even when the NMR solvent was cooled to temperatures as low as –80 °C. $^{31}P\{^{1}H\}$ NMR data reveal the presence of the protonated precursor in solution. A similar observation has been made with *rac*-**84-K**. However, after several attempts and slightly changing the sample preparation VT ^{31}P{^{1}H} NMR spectroscopic studies could be performed with the K/F carbenoid. However, the synthesis of *rac*-**84-K** was not reproducible and hence no DOSY NMR spectra could be recorded (see above). Surprisingly, the NMR spectroscopic data suggest a thermal stability of *rac*-**84-K** up to 50 °C (Figure 29, right) which is in stark contrast to the observed decomposition in several attempts to prepare the sample in toluene.

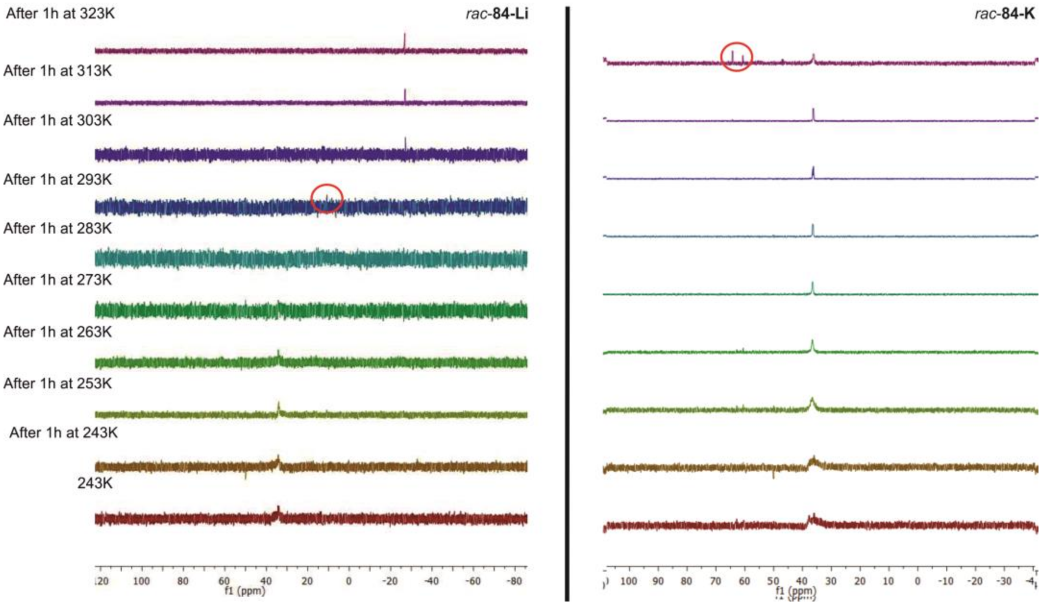

Figure 29. VT NMR spectra of *rac*-**84-Li** (left) and *rac*-**84-K** (right) in toluene.

Only taking the decomposition temperatures of *rac*-**84-Li** and *rac*-**84-K** into account a reversed stability compared to THF is observed. The fluorinated carbenoids show - analogously to their chlorinated congeners - an increasing stability going from Li to K. The lower thermal stability of the Li/F carbenoids is explained by the missing coordination of the Li atom in solution and thus facile LiF salt elimination. The increased stability of the K/F species might be due to the favored propensity of K to coordinate to the π-system of arenes in this case toluene or the phenyl groups of the carbenoid itselfs resulting in a decreased tendency of α-elimination.

With the help of VT ^{31}P{^{1}H} NMR spectroscopic studies the decomposition temperatures of a series of chiral chlorine and fluorine carbenoids *rac*-**83-M** and *rac*-**84-M** in THF and toluene could be obtained. These results allow to gain insights into the influence of the solvent on the thermal stability of carbenoids. Contrary to previous results the Li congeners in both cases *rac*-**83-M** and *rac*-**84-M** exhibit the highest thermal stability in THF compared to the heavier metal species. The increased stability of the Li/Cl and Li/F carbenoids is due to the coordination of the Li atom by both the oxygen atom of the sulfoximine and the coordinating solvent THF as seen in the solid state structure of *rac*-**83-Li**. The strong coordination of the lithium atom hampers the salt elimination and thus results in a higher stability compared to its heavier analogs. Based on the HSAB theory the hard donor oxygen binds stronger to the smaller Li ion than the softer Na and K ions which explains the decreasing stability. The respective bond dissociation energy for Li–O bond (340.5±6.3 kJ/mol) is significantly higher than the ones for the respective sodium (274.4±4 kJ/mol) and potassium (271.5±12.5 kJ7mol) oxygen bonds. Also the Li–O bond is stronger than the Li–S bond (312±7.5 kJ/mol)[147] which explains the higher stability of the Li carbenoids compared to the thiophosphoryl- and silylsubstituted Li/Cl carbenoid **18** (Figure 3) which is only able to form weaker lithium sulfur interactions.

However, changing the solvent environment to a non-coordinating solvent like toluene results in significantly changed trends of stability. Here, the potassium species *rac*-**83-K** and *rac*-**84-K** are more stable than their lighter homologs owing to the increased propensity of potassium to bind to π-systems of arenes presumably resulting in a coordination of the K ion by toluene or the phenyl groups of the carbenoid. These results impressivly demonstrate the importance of systematic studies on carbenoids and the different factors influencing their stability and reactivity.

Table 11. Decomposition temperatures of chiral carbenoids *rac*-**84-M** obtained by VT NMR spectroscopy.

Carbenoid	Decomposition Temp. in THF [°C]	Decomposition Temp. in Tol [°C]
rac-**84-Li**	50	20
rac-**84-Na**	40	
rac-**84-K**	30	50

By changing the solvent the reactivity and stability of carbenoids can be inverted. This great tunability is a blessing and a curse at the same time. On the one hand the reactivity control is the key to apply these highly reactive species in a variety of applications since carbenoids can be fine-tuned to be stable enough for selective conversions while still being reactive enough. On the other hand the strong dependence of the carbenoid stability and reactivity on many different factors makes it extremely difficult to predict their properties and to compare their stability. A good example is *rac*-**84-Li** which is - to the best of my knowledge – the most stable Li/F carbenoid to date. In this case the increased stability can be attributed to the sulfoximine substituent since the Li/F carbenoid bearing two thiophosphoryl moieties decomposes at around

0 °C in THF.[54b] Consequently, the introduction of the sulfoximine group results in a by 50 °C enhanced stability. Compared to the Ph_3Si substituted carbenoid the stability is even increased by over 120 °C since the silyl substituted Li/F carbenoid decomposes already at -70 °C.

Conclusion

The first chiral carbenoids **83-M** and **84-M** could be successfully isolated and characterized by NMR spectroscopy and in case of *rac*-**83-M** also by means of single crystal X-ray diffraction analysis. Furthermore, VT DOSY NMR spectroscopic studies have been performed to elucidate the solution structure of these species in dependence of the nature of the solvent. A monomeric structure for all chiral carbenoids regardless of the nucleofugal group and the alkali metal was found in the coordinating solvent THF. Depending on the temperature a varying number of THF molecules coordinate to the carbenoid. The lower the temperature the more THF molecules coordinate to the carbenoid species. In case of *rac*-**83-Li** the solution structure (monomer with two to three THF molecules) is in very good agreement with the solid state structure which exhibits a monomeric structure with three THF molecules being coordinated to the Li atom. The trends observed in toluene are not as clear and straightforward. In most cases a dimeric structure was obtained, however, due to similar masses of the dimer with six THF molecules coordinated and a trimer in two cases (*rac*-**83**-**Na** at 27 °C and –10 °C) it was not possible to distinguish between these two species in solution. With the help of VT DOSY NMR spectroscopic studies a solvent as well as temperature depending solvation and aggregation behavior of the examined carbenoids were found. The influence of the solvent was further studied with respect to its influence on the thermal stability of *rac*-**83**-**M** and *rac*-**84-M**. VT NMR spectroscopy revealed a solvent dependent stability. In THF the respective lithium carbenoids *rac*-**83-Li** and *rac*-**84-Li** are the most stable ones (Table 11). The decomposition temperature decreases when going from Li to Na and K. However, in toluene a contrary trend was observed. The lithium carbenoids are least stable and the potassium ones are the most stable ones. VT NMR spectroscopy confirmed that the Li/F carbenoid *rac*-**84-Li** is the first room temperature stable Li/F carbenoid and is by 50 °C more stable than the previously most stable bis(thiophosphoryl) system (Li/F analog of **19**, Figure 3).

Carbenoid Deposition and STM Analysis

Scanning Tunneling Microscopy – Short introduction

The scanning tunneling microscope (STM) is a powerful technique to identify the surface topography of conductive samples. STM was invented by G. Bining and H. Rohrer in the 1980s.[148] With the help of STM topographic images it is possible to resolve monatomic steps, surface reconstructions and atomic resolution of a material. STM can be performed under a broad range of conditions, e.g. *in vacuo*, in atmosphere, in reactive gases, in corrosive solution and even at cryogenic temperatures.[149] This variability makes STM a versatile tool to investigate chemical bonding[150] and adsorption,[151] cluster formation[152] and thin film growth.[153]

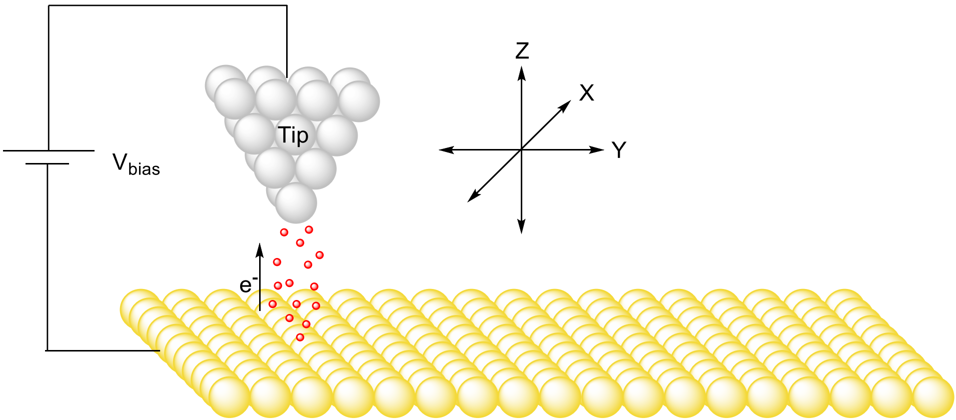

Figure 30. Schematic illustration of the working principle of a STM.

STM is based on the tunneling effect between a tip which ideally ends in just one atom and the conductive sample surface. Imagine two conductive electrodes which are separated by an isolator that acts as a barrier preventing a flow of electrons. In case the barrier gets small enough electrons can pass through the barrier due to the quantum tunneling effect. The barrier in STM is a vacuum gap with the size of few nanometers.

The tip is connected to a piezoelectric element, so-called piezos, which can be moved with a very high precision in three perpendicular directions X, Y and Z. These piezos are important to maintaining the tip-sample distance owing to their contraction or expansion in dependence of the applied voltage. Applying a voltage V_{bias} between the tip and the sample causes electrons (e^-) to tunnel between the surface and the tip if the distance between them is small enough (4-7 Å) a tunneling current (I_t) flow from the tip to the surface or vice versa. By moving the tip over the sample information about the surface topology can be gained since the tunneling current is highly distance depending.[149] There are two different modes that are commonly used for imaging (a) constant height mode (CHM) and (b) constant current mode (CCM).

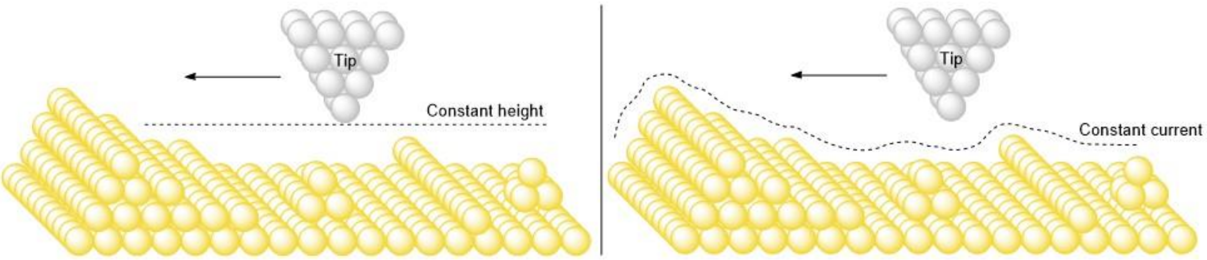

Figure 31. Left: Constant height mode. Right: Constant current mode

In CHM (Figure 31, left) the tip screens the sample surface at a fixed height. Based on the current strength of the tunneling current conclusions can be drawn about the height profile of the sample. The closer the tip is to the surface the higher is the tunneling current. One advantage of this mode is the high scan rate (up to 10 kHz). However, this mode entails the risk of a crash between the tip and the surface. Applying the CCM (Figure 31, right) the current is kept constant while the height of the tip can be adjusted. Based on the position of the tip the, sample topography can be acquired very accurately. The resolution of this mode is high enough to reveal the atomic and electronic structure of the surface.

Deposition of a stabilized Na/Br carbenoid

After having studied the solution structure of carbenoids we became interested in the behavior of stabilized carbenoids on different surfaces. It is known in literature that metal salts present in solution can stabilize carbenoids due to the disruption of the M/X interaction and thus decrease the tendency of α-elimination (Scheme 6).[46] Thus, the question arose if there are stabilizing interactions between the carbenoid and a salt/metal surface? Furthermore, we wondered if the nature of the surface has an influence on the stability of the carbenoid. To answer these questions the deposition of a thermally stable carbenoid on different surfaces, i.e. Ag(111) and NaBr surface was attempted. Therefore, the carbenoid has to fulfill a number of requirements. First, the presence of sodium as the metal and bromine as the nucleofugal group is advantageous to enable interaction with the sodium and bromine atoms on the surface. Second, the carbenoid has to be thermally stable to guarantee the deposition on the surface without previous decomposition under the deposition conditions. The bis(thiophosphoryl) substituted Na/Br carbenoid **85**•3THF (Figure 32) was chosen for this project due to its high thermal stability and the presence of both sodium and bromine.

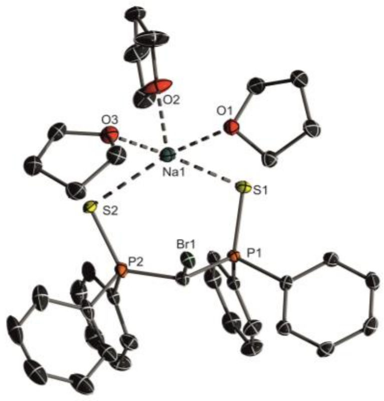

Figure 32. Molecular structure of **85**•3THF. Displacement ellipsoids are shown at the 50 % probability level. Hydrogen atoms have been omitted for clarity.

The stabilized carbenoid **85**•3THF was obtained as a yellow solid by the reaction of the protonated precursor **86** with sodium bis(trimethylsilyl)amide (NaHMDS) at RT in THF. The ^{1}H NMR spectroscopic data reveal the presence of THF even after drying the compound in high vacuum and at slightly elevated temperatures. This indicates that the THF is coordinating to the Na atom of the carbenoid **85**. Note, the compound used for further studies is consequently not pure **85** and THF is still present.

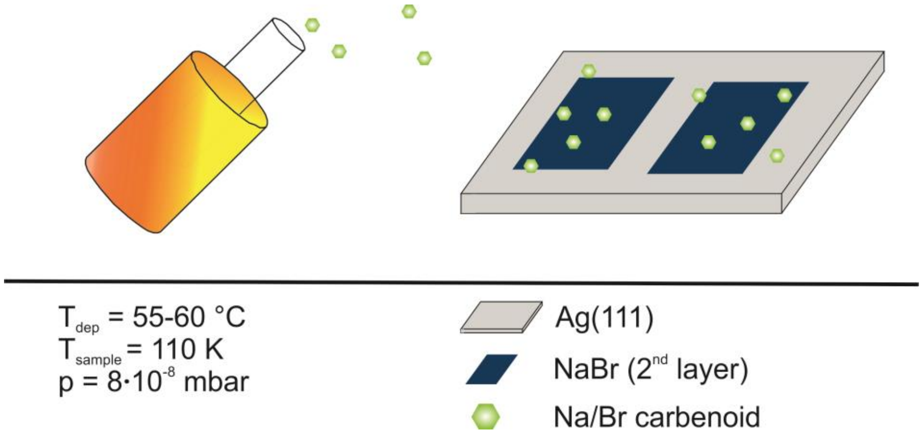

Figure 33. Schematic illustration of the deposition of the Na/Br carbenoid **85**•3THF on a NaBr layer.

STM studies were conducted by Dr. Abhijit Bera in the group of Prof. Dr. K Morgenstern. For STM studies, the powder sample was degassed in UHV at 45-50 °C for 48 hours to remove excessive THF from the solid. Thereby, it was not possible to remove the residual coordinating THF even after long degassing time at slightly elevated temperatures. After degassing, the compound was sublimed at 60 °C to deposit on different surfaces for STM studies. The residual compound **85**•3THF was analyzed by NMR spectroscopy after procedure to determine the degree of decomposition during the deposition. Based on the $^{31}P\{^1H\}$ NMR spectrum in average 94 % of the sample were still intact. Consequently, it can be excluded that the sample completely decomposed in the molecular unit during the deposition due to the elevated temperature.

STM measurements are performed by variable temperature STM with a base pressure of $1.5 \cdot 10^{-10}$ mbar. All images are taken in constant current mode at 120-130 K. A clean Ag(111) surface is obtained by repeated cycle of Ar^+ sputtering and annealing. To check the cleanliness of the Ag(111) surface and straight step edges the sample was checked by STM at RT (Figure 34, left). For NaBr layer formation, NaBr powder is evaporated from an electron bombardment, heated Mo crucible with a rate of 0.02 ML/min. onto the Ag(111) surface held at RT (Figure 33). To deposit the carbenoid **85**•3THF on Ag(111) and NaBr surface, the substrate is cooled to 110 K and deposited for 30 s.

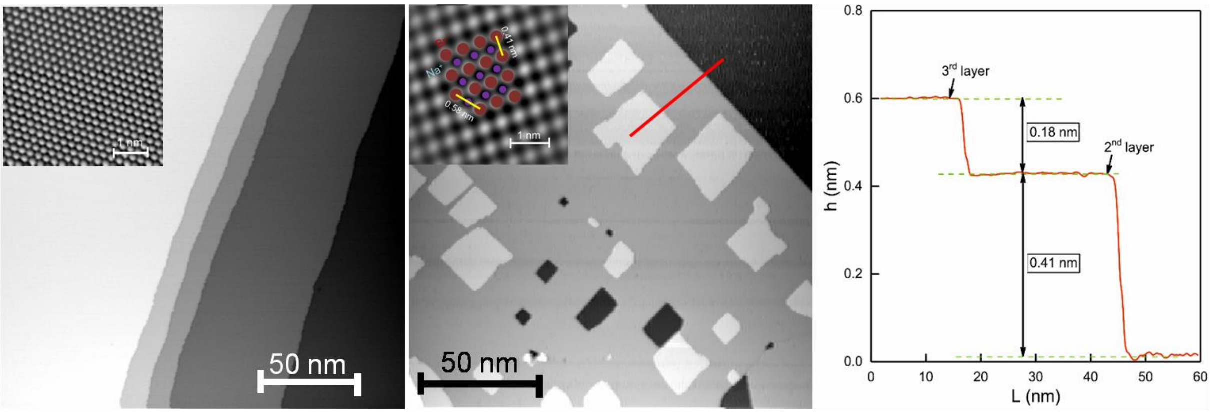

Figure 34. Left: STM image of clean Ag(111) with atomic resolution (inset). Middle: 2nd and 3rd layer of NaBr on Ag(111) with atomic resolution (inset). Right: line profile of NaBr layers (V_{bias} = 2.1 V, I_t = 170 pA, T=120±1 K).

After deposition of NaBr on Ag(111) surface the surface was imaged by STM at RT. The obtained images show that NaBr island formation is started with second layer and then consequently third layer on Ag(111). These islands show a quadratic lattice with a distance between the protrusions of (410 ± 6) pm and (415 ± 8) pm in the two perpendicular directions in atomic resolution images (Figure 34, middle (inset)). Here bromine is imaged as protrusions and sodium imaged as depression by a metallic STM tip.

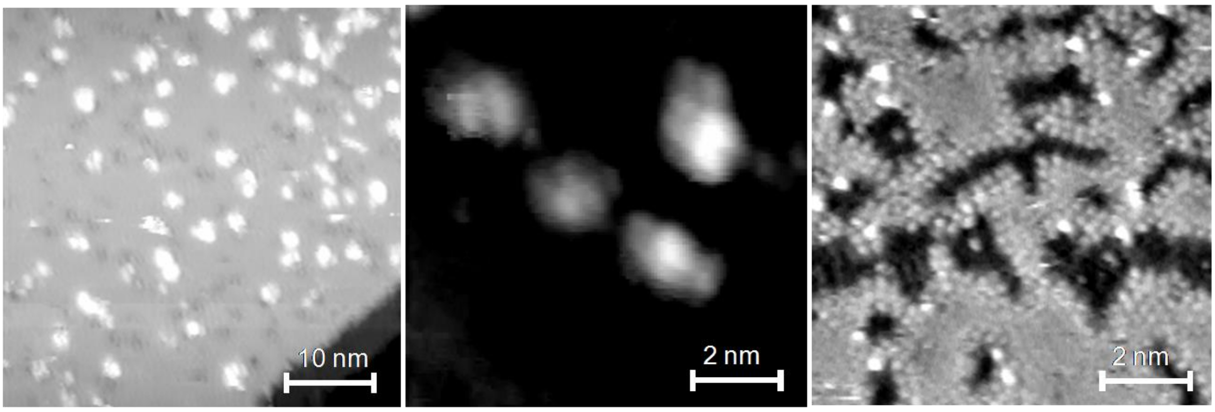

Figure 35. Left: STM image of compound **85**•3THF on Ag(111). Middle: Enlarged section of the top layer. Right: Enlarged section of the bottom layer (V_{bias} = 2.1 V, I_t = 170 pA, T=120±1 K).

After characterization of the NaBr layer carbenoid **85**•3THF was deposited on both Ag(111) and NaBr surface to compare the behavior of the Na/Br carbenoid. In the STM images well separated randomly distributed compounds (top layer[4]) with additional aggregates of small molecules (bottom layer[4]) were observed on both surfaces (Figure 35). The aggregates might come from the free THF solvents which deposited on the surface during deposition. To confirm this assumption, pure THF was deposited on Ag(111) applying the same deposition conditions. The obtained images of pure THF were compared with the aggregates of small molecules. It was found that THF forms a (2×2) superstructure on Ag(111) with intermolecular spacing of 0.6 nm (Figure 36, left). When comparing pure THF with the bottom layer of deposited carbenoid **85**•3THF it is noticeable that the shape and size nicely match (Figure 36, middle and right). The distance between two molecules was found to be 0.6 nm in both cases. Therefore, it can be assumed that the bottom layer observed during the deposition of compound **85**•3THF is formed by THF molecules.

---

[4] As per definition, the observed arrangement are not considered as layers, but are referred to as such for simplicity.

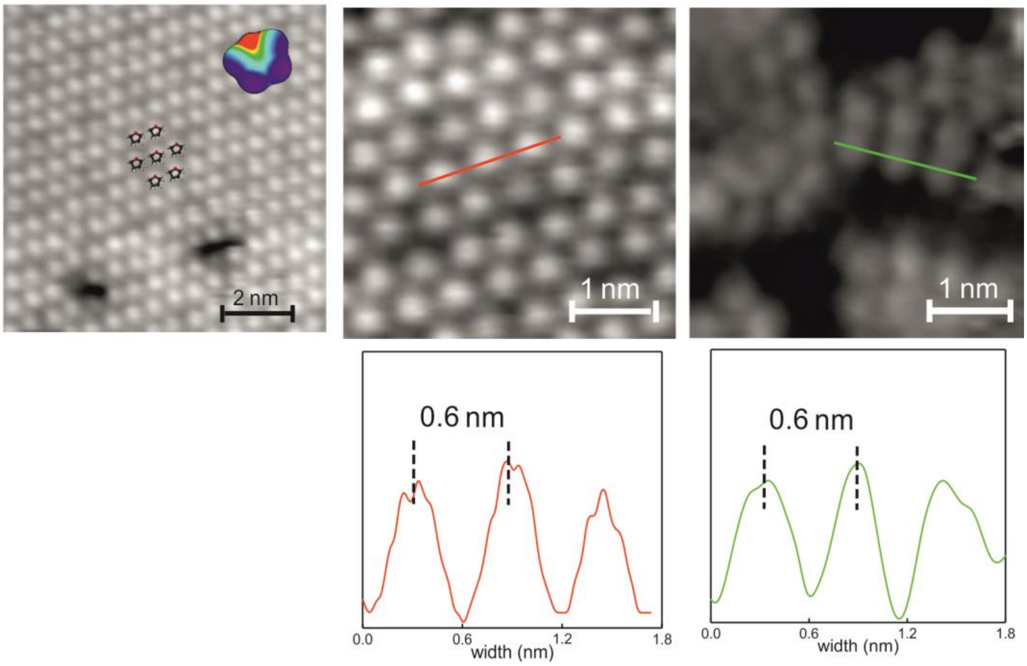

Figure 36. Left: STM image of pure THF showing a (2x2) superstructure on Ag(111), electrostatic surface potential map of THF fitted to the molecules (inset) (V_b = 2.5 V, I_t =260 pA). Middle: STM image of THF on Ag(111) and corresponding line profile (red line). Right: STM image of the bottom layer of the deposition of **85**•3THF on Ag(111) and corresponding line profile (green).

Besides the layer of THF some places were found where isolated compounds are present without much residual THF molecules. Figure 37 (left) shows an STM image depicting three compounds distributed on Ag(111). The shape of the compounds on the surface seems to fit to the solid state structure of **85**•3THF and it appears that the coordinating THF molecules are still present (Figure 37, middle).

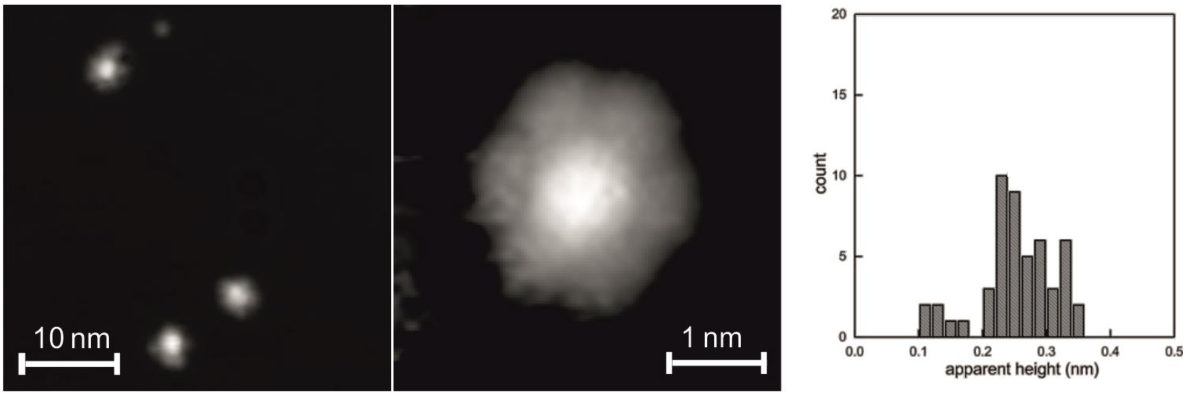

Figure 37. Left: STM image of carbenoid **85**•3THF deposited on Ag(111) surface (V_b = 2.1 V, I_t = 60 pA, T = 120 ±1 K). Middle: enlarged section of the left STM image. Right: Histogram of the distribution of height profile of carbenoid **85**•3THF on Ag(111).

When examining the shape of the deposited compounds on the surface it is notable that they are slightly different which could be explained by different orientations of the carbenoid **85**•3THF on the surface. To proof this assumption the apparent height of 50 separate compounds by drawing line scan across the compound was measured. After plotting the histogram (Figure 37, right), the distributions was found to be broad varying from 0.1-0.35 nm. The broad distribution suggests a rondom distribution of the carbenoid **85**•3THF on Ag(111) surface without any preferred orientations. Concluding, no favored interaction between the carbenoid and the Ag(111) surface is observed.

To investigate possible difference in orientation of the carbenoid on different surfaces a NaBr layer on top of Ag(111) was introduced. Deposition of the carbenoid **85**•3THF on a NaBr surface and subsequent analysis with means of STM in constant current mode gave access to the images shown in Figure 38. The left picture shows three compounds in close proximity. Further enlarging one molecule exhibits a similar shape as observed on Ag(111). In general, the outlines of the compound on the surface seem a bit more uniform on NaBr than on Ag(111). This hints at a preferred orientation on the salt surface compared to the Ag(111) surface.

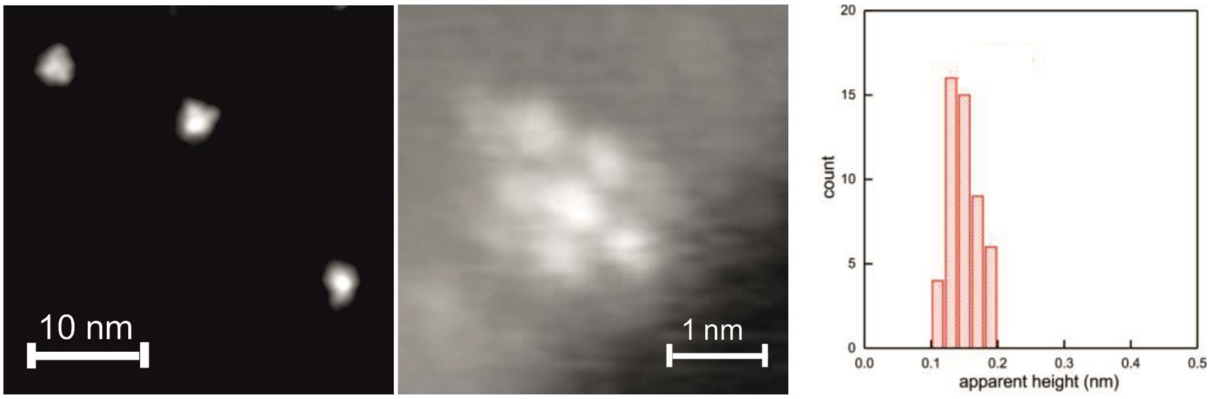

Figure 38. Left: STM image of carbenoid **85•3THF** deposited on NaBr surface (V_b = 2.1 V, I_t = 60 pA, T = 120 ±1 K). Middle: enlarged section of the left STM image. Right: Histogram of the distribution of height profile of carbenoid **85•3THF** on NaBr.

In the height profile histogram a significantly narrower height distribution is observed on the NaBr surface. After examining the images and height profile histogram it is very clear that, carbenoid **85**•3THF has a preferred orientation on the NaBr surface. A coordination of the Na and Br atoms of carbenoid **85**•3THF with the NaBr salt surface is assumed and thus a preferable deposition on the NaBr in a specific orientation.

To avoid the presence of THF during the deposition of carbenoid **85**•3THF the synthesis in a non-coordinating solvent was attempted. Toluene was chosen for this purpose. However, the carbenoid is found to be significantly more thermally labile than in THF. Even conducting the reaction at temperatures below –80 °C did not lead to successful isolation of compound **85** in toluene. Low temperature NMR spectroscopic studies proved the decomposition of the Na/Br carbenoid. This stresses the importance of coordinating solvents on the thermal stability of **85**. Consequently, the presence of THF during the deposition can, unfortunately, not be avoided due to its stabilizing effect. For comparison the protonated precursor **86** was deposited on Ag(111) due to its expected similar shape on the surface and not having THF coordinated (Figure 39, left).

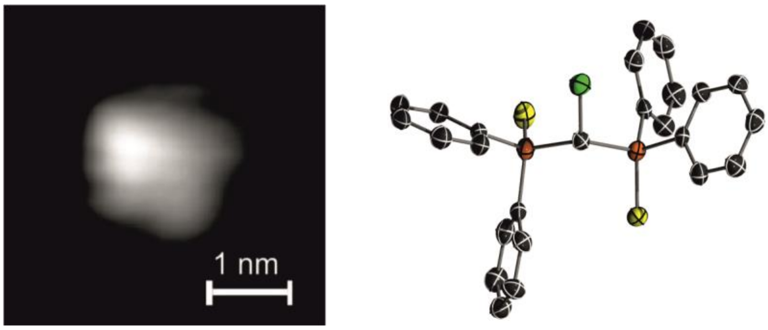

Figure 39. Left: STM image of the protonated precursor **86** on Ag(111) (V_b = 2.1 V, I_t =60 pA, T = 120±1 K). Right: Solid state structure of **86-Cl.**

The shape of the precursor molecule **86** on the Ag(111) surface differs from the one found for the Na/Br carbenoid **85•3THF**. Unfortunately, no solid state structure of **86** is known. Thus, for comparison of the shape of the deposited molecule the solid state structure of the respective chlorine congener **86-Cl** was used (Figure 39, right). The outlines of the protrusion and the solid state structure of **86-Cl** seem to fit and they differ from the shape found for the carbenoid **85**•3THF. Therefore, it can be assumed that THF molecules are still coordinated to the carbenoid on the surface.

Conclusion

In cooperation with the group of Prof. Dr. K. Morgenstern the deposition of a Na/Br carbenoid **85**•3THF was realized on Ag(111) and NaBr surface. The carbenoid was chosen since it exhibits a sufficient stability under the deposition conditions and to feature sodium as the metal and bromine as the halogen to be able to form salt interactions with the NaBr surface. $^{31}P\{^{1}H\}$ NMR spectroscopy was performed after the deposition of the residual carbenoid **85**•3THF and showed that the compound was in average 94 % intact. Due to the high sublimation temperature of the Na/Br carbenoid even in UHV it was not possible to use softer reaction conditions than 60 °C. Consequently, the reaction parameters were chosen to guarantee sufficient compound deposition and to avoid decomposition of species **85**•3THF. The deposition of the Na/Br carbenoid **85**•3THF on Ag(111) and analysis by means of STM revealed the presence of two layers. The bottom layer was found to be THF which is still present in the sample due to the synthesis of **85**•3THF in THF and the inability to completely remove it *in vacuo*. Changing the reaction conditions to toluene as the solvent, unfortunately, resulted in decomposition of the carbenoid even at low temperatures. The shape of the deposited compounds suggests the presence of THF which is coordinated to the carbenoid. In general, the shape of the deposited compounds on the NaBr surface seems to be a bit more uniform suggesting a preferred orientation of the carbenoid on the surface due to interactions between the salt surface and the Na/Br carbenoid. Determination of the height distribution for **85**•3THF on both Ag(111) and NaBr surface showed that the height is more homogenous on the salt surface. This result supports the assumption of a preferred orientation on the NaBr surface. However, further investigations are needed to clearly proof and understand the influence of the salt surface on the orientation of the carbenoid and its possible influences on the carbenoid reactivity and stability.

Palladium Catalyzed Cross- Coupling

Pd-catalyzed C–C Cross-Coupling Reactins – A short introduction

Cross-coupling reactions are a one of the most efficient protocols for the formation of C–C bonds. This type of reactions ranks among the most useful and versatile methods in organic synthesis both in academic laboratories as well as in industry.[154] The most used transition metal in this regard is Pd, its use dates back to the early 1970's[155] and the first report on the use of Pd black in the Heck reaction[156] as well as the first use of supported Pd metal by Julia *et al.*[157] The seminal discovery of the dramatic activity enhancement in case of using metal complexes with sterically demanding and strongly σ-donating ligands was a milestone in the field of Pd-catalyzed C–C bond coupling and revolutionized the field of synthetic organic chemistry. The applications are widespread in the field of organic synthesis, material science as well as in the pharmaceutical, agrochemical and fine chemical industry.[154, 158]

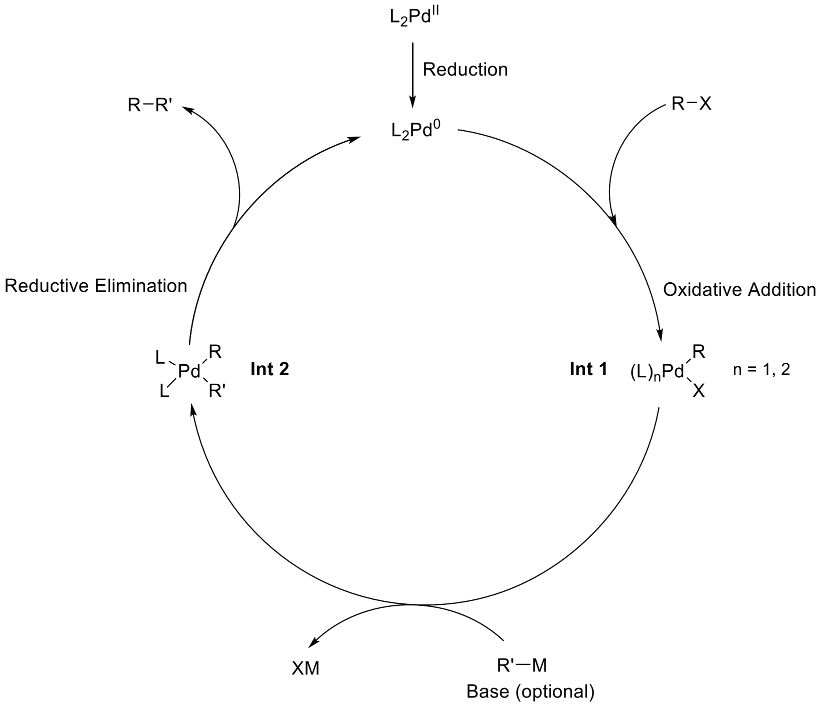

Scheme 27. General catalytic cycle for cross-coupling reactions.

The success led to the attribution of the Nobel prize in chemistry to Heck, Negishi and Suzuki in 2010.[159] In all these reactions a transition metal catalyst is required to guarantee a synthetically useful rate. Even though a variety of metals would be able to catalyze the different steps of these reactions, without doubt Pd is the most commonly used one. These coupling reactions have become the standard measure for evaluating the reactivity of novel Pd complexes as potential catalysts.[154]. In case of palladium catalyzed cross-coupling reactions, the mechanism (Scheme 27) is well understood. When starting from a Pd(II) precatalyst, the species has to be reduced to Pd(0) in the first step to enter the catalytic cycle. This step is followed by the oxidative addition of the arylhalide to the Pd center resulting in the L_nPdRX (n = 1, 2) intermediate **Int.1**. The next step is the transmetalation of the first intermediate with an organometallic compound R'M yielding the second reaction intermediate L_2PdRR' **Int.2**. The final step is the reductive elimination leading to the coupling product R–R' and the catalytic active Pd(0) species.[154] Depending on the type of reaction, the used organometallic partner RM varies. Organotin species in case of Stille coupling,[160] organoboron for Suzuki-Miyaura coupling reaction,[161] organozinc compounds in Negishi coupling[162] and organomagnesium compounds for Kumada coupling reactions.[163] Although, a wide variety of organometallic reagents can be used for the Pd catalyzed cross-coupling and some of these organometallic reagents, especially organoboron and organotin, are synthesized *via* the corresponding lithium reagents the direct use of organolithium reagents in C–C cross-couplings has not been realized. Their use is problematic due to their high reactivity and the often required high temperatures.[164] Moreover, efficient catalytic coupling is not achieved due to lithium-halogen exchange and homocoupling. In 2013, Feringa reported on a practical approach to perform an efficient and highly selective direct Pd catalyzed cross-coupling reaction using organolithium reagents at mild reaction conditions (Scheme 28).[165] The reaction has a broad scope and readily proceeds with alkyl-, aryl- and heteroaryllithium reagents.

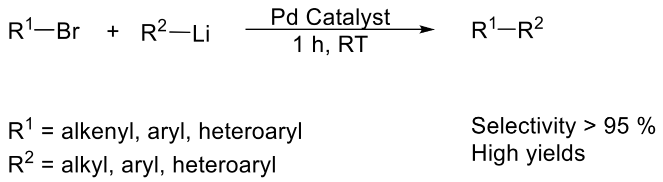

Scheme 28. Cross-coupling using organolithium compounds.

To achieve a high selectivity, the fast lithium-bromide exchange has to be prevented to enable fast oxidative addition and the subsequent reductive elimination. The key to sufficiently suppress the undesired lithium-bromide exchange is the control of the reactivity and aggregation of the respective organolithium compound. This can be achieved by the right choice of solvent, in this case toluene, to avoid ethereal compounds enhancing halogen-metal exchange. Additionally, the organolithium reagent was highly diluted and added very slowly over 3h to avoid an excess of the reagent in solution.

Palladium Catalyzed Cross-Coupling of Carbenoids and Aryl Halides

Inspired by the interesting work of Feringa the palladium catalyzed coupling of carbenoids was attempted using a modified Pd catalyst bearing a new class of electron rich phosphine ligands, the ylide-substituted phosphines (YPhos), developed in our group.[166] The negatively charged carbon atom in the immediate vicinity of the phosphorous centers results in extremely strong donor properties even surpassing the donor ability of NHCs such as IMes or IPr. The novel YPhos ligands have been proven to be highly active in Buchwald-Hartwig aminations[167] and α-arylation of alkyl ketones with aryl chlorides[168] at mild conditions. Variation of the YPhos ligand in the C–N coupling of alkylamines hampered β-hydride elimination, keYPhos (**L1**) yielded a substantial percentage of enamine whereas trYPhos (**L2**) and joYPhos (**L3**) (Scheme 29) resulted in a selective conversion. These results indicated a great potential in palladium catalysis therefore we attempted the coupling of organolithium compounds and aryl chlorides.

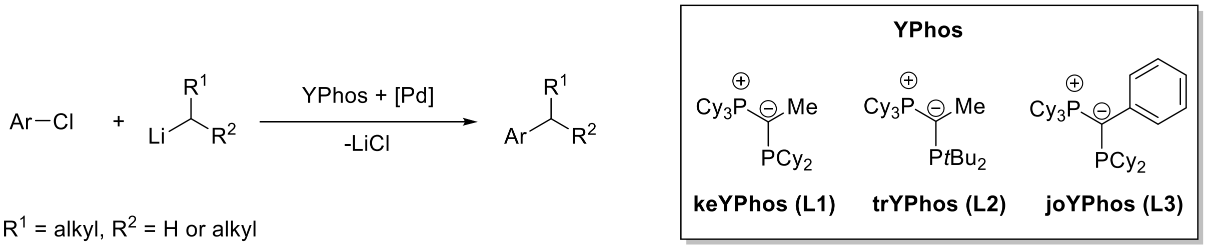

Scheme 29. General equation of the Pd catalyzed cross-coupling of primary and secondary alkyl lithium reagents with aryl halides using YPhos ligands.

To test the general suitability of the YPhos ligands in Pd catalyzed cross-coupling reactions using lithium reagents the coupling of common organolithium species instead of carbenoids with aryl halides was attempted. For the test reactions 1 mol% of ligand **L1** were mixed with the equivalent amount of $Pd_2(dba)_3$ (dba = dibenzylideneacetone) as the palladium source to catalyze the cross coupling reaction of ^{n}BuLi as the organolithium reagent and 4-bromotoluene and 4-chlorotoluene, respectively. The reaction was performed under similar conditions as described by Feringa *et al.*, such as room temperature and slow addition of a highly diluted solution of the organolithium reagent to a toluene solution of the Pd catalyst and the arylhalide. Removal of the solvent yielded a colorless liquid which was analyzed by NMR spectroscopy. The ^{1}H NMR spectrum confirms the successful cross-coupling with a yield of roughly 90 % of the desired product 1-butyl-4-methyltoluene and only small amounts of unreacted 4-bromotoluene and the homocoupled product. Also in case of chlorohalide a high selectivity of the desired cross-coupled product of over 80 % was observed and only the homocoupled species was observed as a side product. Encouraged by these first promising results the more challenging combination of 4-chlorotoluene and the secondary alkyl lithium reagent ^{sec}BuLi was attempted. Based on the ^{1}H NMR spectroscopic data roughly 50 % of the aryl chloride and ^{sec}BuLi have been successfully cross-coupled. Both unreacted 4-chlorotoluene as well as the homocoupled product were observed. Reaction of the most reactive ^{t}BuLi with 4-chlorotoluene resulted in a product mixture. Surprisingly, not the expected product but the isomerization product 4-(1-methylpropyl)toluene as well as the homocoupled product were identified. To increase the selectivity of this conversion the reaction was performed at 0 °C, however, no reaction was observed under these conditions. The test reactions which were performed at RT showed that keYPhos is a suitable ligand to perform Pd cross coupling reactions of alkyl lithium reagents and aryl halides. The next step was to test the applicability of this system for the Pd catalyzed cross-coupling of carbenoids and aryl halides (Scheme 30).

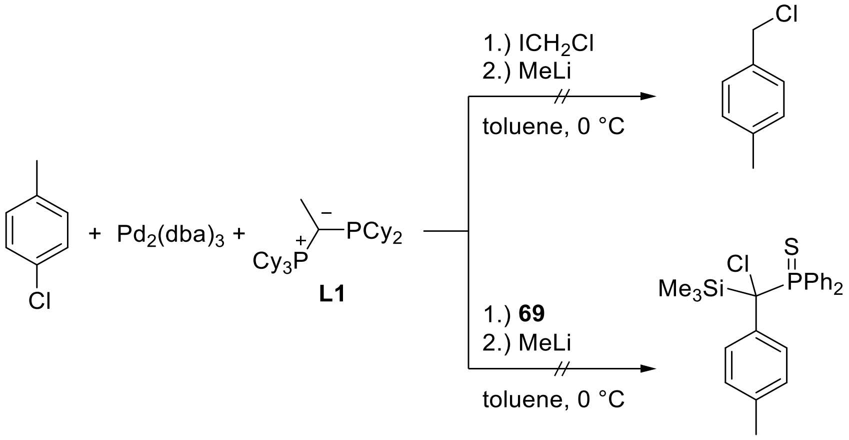

Scheme 30. Attempted Pd catalyzed coupling of carbenoids and aryl halides.

The performance of the reaction had to be changed due to the thermal lability of the used carbenoids. The carbenoids are not room temperature stable thus the preformed carbenoid could not be added slowly *via* a syringe pump. The palladium source and **L1** were stirred in toluene at RT for 30 min. to guarantee complete formation of the Pd catalyst, subsequently 4-chlorotoluene was added and the mixture was stirred. After 10 min. the carbenoid precursor, ICH_2Cl or **69** (Scheme 21), was added, respectively and the reaction solution was cooled to 0 °C or –80 °C. Diluted MeLi solution (0.36 M) was added slowly *via* a syringe pump. After complete addition the solution was stirred for 10 min. at 0 °C and then quenched. After work up an orange-yellow semi-solid compound was obtained. In case of the $LiCH_2Cl$ analysis by ^{1}H NMR revealed almost no reaction. In case of the stabilized carbenoid **56** no selective reaction was observed. Based on the ^{31}P{^{1}H} NMR spectrum a variety of phosphorous containing species were obtained. The ^{1}H NMR data showed the presence of several signals most probably belonging to protons bound to a bridging C atom. Further attempts were made by changing the reaction protocol. It was also tried to add the already formed carbenoid **56** in toluene at –80 °C to a toluene solution containing the Pd catalyst as well as the aryl halide. The reaction mixture was then allowed to warm up to room temperature slowly. After aqueous work up and purification by column chromatography the chlorinated precursor **69** as well as twice protonated species **57** amongst others were obtained. Unfortunately, variation of the reaction protocol in that way that the carbenoid **56** was cooled to –80 °C in toluene and then the Pd catalyst as well as the aryl halide were slowly added did not result in a selective reaction. No evidence for the successful cross-coupling of the carbenoid **56** with 4-chlorotoluene was observed by NMR spectroscopy. In none case a selective and successful cross-coupling reaction of carbenoids and aryl halides was observed. Performance of this reaction at low temperatures is necessary due to the thermal lability of the carbenoids. But the change to lower temperatures even prevents the Feringa type coupling under the optimized conditions. Moreover, a number of further changes of the reaction proctocol could lead to unwanted side reactions and thus prevent the successful cross-coupling of carbenoids: a) the carbenoid has to form *in situ*, b) is not added as slow as in case of Feringa´s conditions or c) the substrate and catalysts are added slowly to the carbenoid consequently an excess of the lithium carbenoid is present. To avoid excess of organolithium species is one of the most important requirements in the direct cross-coupling of alkyl lithium reagents. A promising approach could be the use of a room temperature stable carbenoid which can be added as slow as required. However, room temperature stable Li/Cl carbenoids are very bulky. There steric demand might prevent sufficient coupling.

Due to the ineptitude of this approach using carbenoids as the organolithium species for Pd catalyzed cross-coupling, the topic was continued by Dr. Thorsten Scherpf focusing on common primary and secondary organolithium reagents.

Conclusion

The transfer of the Feringa type direct Pd catalyzed cross-coupling of organolithium reagents with aryl halides to carbenoids was attempted. However, no catalytic conversion was observed when reacting carbenoids, both stabilized and unstabilized ones, and aryl halides with a palladium catalyst. However, the exact reaction conditions used by Feringa were not suitable for carbenoids due to their thermal lability hence they cannot be added at RT very slowly. Adjusting the reaction conditions to avoid the decomposition of carbenoids did, unfortunately, not result in cross-coupling of the carbenoid and the aryl halide. This might be due to a number of reasons a) the lower reaction temperature which also prevents sufficient coupling under Feringa conditions b) the carbenoid has to be formed *in situ* what might lead to unwanted side reactions or c) an excess of carbenoid in solution since the catalyst and the substrate are added to a solution of the carbenoid. The use of room temperature stable carbenoids could be an alternative avoiding the necessity of changing the reaction conditions. However, thermally stable Li/Cl carbenoids are really bulky thus their steric demand might prevent catalytic cross-coupling.

Conclusion & Outlook

The aim of this thesis was the synthesis of a variety of stable chiral carbenoids and the investigation of their stability and solution structure in dependence of the temperature and nature of the solvent. The obtained information is useful to control the reactivity and stability of carbenoids which is highly desirable to broaden the scope of applications. Besides the solution structure of carbenoids also the structure on different surfaces, namely Ag(111) and NaBr was studied by means of STM to gain insights into the interaction of carbenoids with metal salts. Furthermore, this thesis focused on the application of carbenoids in main group element dehydrocoupling reactions and Pd catalytic cross-coupling reactions.

Carbenoid Mediated Formation and Activation of Element-Element and Element-Hydrogen Bonds

Recently, our group reported on the dehydrocoupling of aryl substituted secondary phosphines using stabilized carbenoids.[19b] The scope of this thesis was to transfer this protocol to a variety of main group element hydride species and to examine its potential in main group element element bond formation. Here, a special focus was set on group 14 element hydrides. First, silanes, namely Et_3SiH and Ph_3SiH, were reactied with the stabilized carbenoid **56**, however, no selective dehydrocoupling was observed. One possible explanation for these results is the higher polarity of the Si–H bond in comparison to the P–H bond.

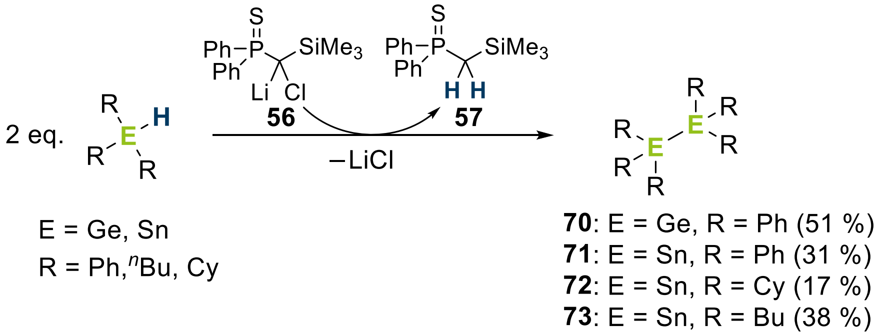

Figure 40. Carbenoid-mediated dehydrocoupling of group 14 element hydrides.

In contrast, Ph_3GeH could be coupled selectively yielding the hexaphenyldigermane and the twice protonated precursor **57** (Figure 40). The nature of the digermane **70** was unambigously confirmed by NMR spectroscoy and X-ray diffraction analysis. Besides, germanium hydrides also stannanes were successfully coupled. To our delight, not only aryl stubstituted tin hydrides as in case of secondary phopshines could be coupled but also alkyl substituted ones. Based on $^{119}Sn\{^1H\}$ NMR spectroscopy full conversion to the respective distannanes was achieved for Ph_3SnH, Cy_3SnH and $^nBu_3SnH$. In case of **71** and **72** the nature of the coupled products was also confirmed by single crystal X-ray diffraction analysis (Figure 41). To test the limits of this reaction protocol, also the reactivity of the Li/Cl carbenoid **56** towards the secondary stannanes Ph_2SnH_2 was tested, yielding the six-membered ring $Ph_{12}Sn_6$ **74** as the main product along with a number of cyclic and acyclic products.

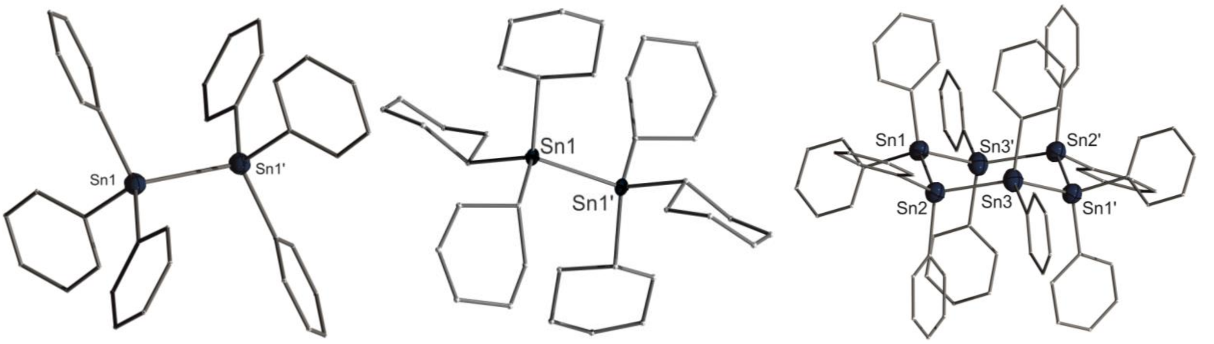

Figure 41. Solid state structure of **71** (left), **72** (middle) and **74** (right).

Despite the successful carbenoid mediated homodehydrocoupling no selective heterocoupling of two different stannanes or stannanes and secondary phosphines, respectively, was observed. Previous results suggested the carbenoid mediated dehydrocoupling being limited to P–H bonds but the successful coupling of the more hydridic germanium and tin hydrides supported the assumption that this reactivitiy is more generally applicable and can be extended to other main group element hydride species. However, when reacting borane hydride species, such as HBpin and HBcat, under the same reaction condition no similar reaction behavior was observed. An explanation might be the favored borate formation due to the highly electrophilic nature of boron. The successful coupling of group 14 element hydrides with concomitant formation of the twice protonated precursor **57** suggests a similar reaction mechanism for both the dehydrocoupling of secondary phosphines and the group 14 element hydrides with the deprotonation of the hydride species being the initial step.[19b]

The assumption that borate formation prevents the successful coupling of boron hydrides is supported by the reaction of the Li/Cl carbenoid **56** and catB–PPh_2 resulting in the formation of the diborylated compound **75** and Ph_4P_2 (Figure 42). A preliminary mechanismus was presented, however, further research is necessary to proof it experimentally. So far, no α-diborylated carbanion has been characterized by means of single crystal X-ray diffraction analysis.

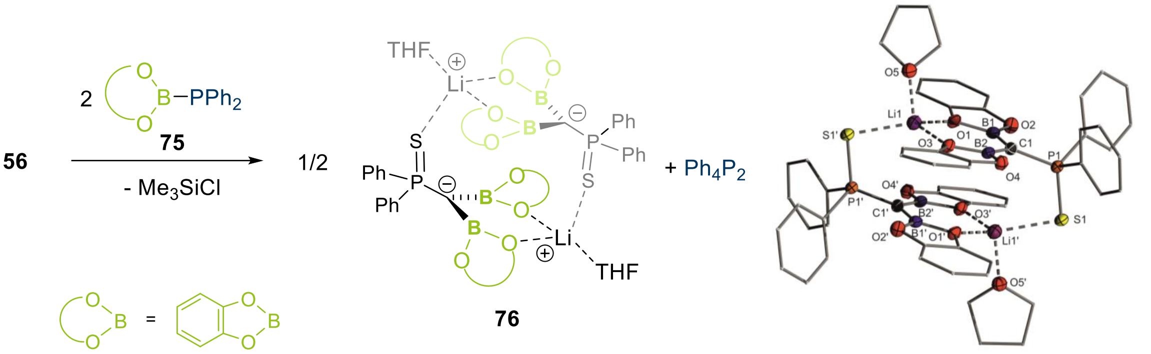

Figure 42. Left: Diborylation of **56** with **75** and concomittant formation of the diphopshine Ph$_4$P$_2$. Right: Dimeric molecular structure of **76**.

Synthesis, Characterization and Application of Chiral Carbenoids

The first isolated and structurally characterized chiral carbenoids **83-M** and **84-M** (M = Li, Na, K) were prepared *via* a multistep synthesis.[126-128, 129] NMR spectroscopic studies confirmed the successful formation of the respective carbenoids *R*-**83-M**. In all cases no characteristic down-field shift of the central carbenoid atom is observed in the ^{13}C{^{1}H} NMR spectrum. This down-field shift is indicative for the carbenoid character of compounds but no exclusion criteria.

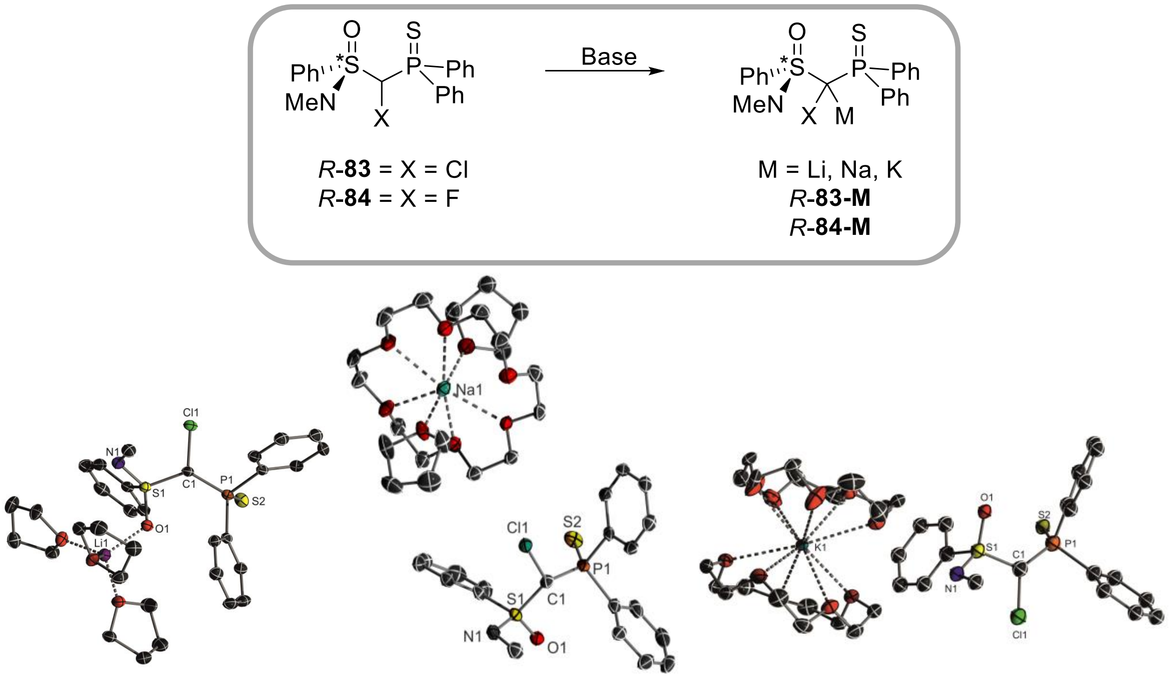

Figure 43. Top: Last step of the synthesis of *R*-**83-M** and *R*-**84-M**. Bottom, left: Molecular structure of *rac*-**83-Li**. Middle: Molecular structure of *rac*-**83-Na**•[18-C-6][2THF]. Right: Molecular structure of *rac*-**83-K**•2[14-C-4].

The solid state structures of *rac*-**83-M** reveal no contact between the metal and the carbenoid carbon atom in all cases (Figure 43). In case of *rac*-**83-Li**, the Li atom is coordinated by the oxygen atom of the sulfoximine moiety and three additional THF solvent molecules. For the heavier congeners *rac*-**83-Na** and *rac*-**83-K** crystallization was only achieved in the presence 18-C-6 in case of *rac*-**83-Na** and 14-C-4 in case of *rac*-**83-K**. The Na atom of *rac*-**83-Na** is coordinated by one crown ether molecule and two THF molecules, while the K atom in *rac*-**83-K** is coordinated by two 14-C-4 crown ether molecules. Due to the missing contact of the metal and the cabenoid carbon atom and the chlorine molecule, respectively, no elongation of the respective C–Cl bond is observed.

The M/F analogs *S*-**84-M** have been isolated and fully characterized by NMR spectroscopy. Only in case of *S*-**84-K** the signal of the carbenoid carbon atom could be detected in the respective NMR spectrum. Contrary to its chlorine analogs it features a distinctive downfield shift in comparison to the protonated precursor *R*-**82**. This finding stresses the more pronounced carbenoid character of flourine carbenoids in comparison to chlorine ones.

Stability and reactivity control is very important in carbenoid chemistry to allow the use of these normally highly reactive carbenoids in a broader field of applications. By performing VT DOSY NMR spectroscopic studies of the chiral carbenoids *rac*-**83-M** and *rac*-**84-M** valuable insights into the solution structure in dependence of the nature of the solvent and the temperature of these carbenoids were obtained. THF was choosen as coordinating, toluene as non-/ weakly coordinating solvent. A clear trend was found for the carbenoids *rac*-**83-M** in THF. Regardless of the alkali metal and the temperature a monomer was found to be present which is coordinated by a varying number of THF solvent molecules (Table 12). The lower the termperature is the higher is the number of coordinated THF molecules.

Table 12. Overview of solution structures of carbenoids *rac*-**83-M** obtained by VT DOSY NMR spectroscopy.

Temperature [°C]	Carbenoid	Structure in THF	Structure in Tol
–30 C	*rac*-**83-K**	Monomer+2/3THF	Dimer + 6 THF
	rac-**83-Na**	Monomer+3THF	Dimer+4 THF
	rac-**83-Li**	Monomer+2/3THF	Dimer+2/3 THF
–20 °C	*rac*-**83-K**	Monomer+1/2THF	Dimer+1/2 THF
	rac-**83-Na**	Monomer+2THF	Dimer+6 THF / Trimer

	rac-**83-Li**	Monomer+2THF	Dimer+2/3 THF
27 °C	*rac*-**83-K**	Monomer+1THF	Dimer+3 THF
	rac-**83-Na**	Monomer+0/1THF	Dimer+6 THF / Trimer
	rac-**83-Li**	Monomer	Dimer+1 THF

The DOSY NMR data in toluene do not show such a clear trend as observed in THF. Contrary to the findings in THF, an oligomeric structure is observed. In most cases a dimeric structure was found in case of *rac*-**83-Na** at –20 °C and 27 °C it is not possible to distinguish clearly between a dimer with six coordinating THF molecules and a trimer with no solvent molecules coordinated due to similar molecular weights. To validate these results, also the chiral M/F carbenoids *rac*-**84-M** were studied by VT DOSY NMR spectroscopy. In THF the same solvation and aggregation behavior as observed for *rac*-**83-M** was found. All carbenoids *rac*-**84-M** form a monomeric structure with an increasing number of THF molecules coordinated when lowering the temperature. However, when changing the solvent from THF to toluene immediate decomposition even at –80 °C of the heavier congeners *rac*-**84-Na** and *rac*-**84-K** were observed, even though previous results suggested an increased stability from Li to Na and K.[26] In summary, with the help of VT DOSY NMR studies valuable insights into the aggregation and solvation behaviour of carbenoids in solution in dependence of the nature of the solvent and the temperature were gained

VT ^{31}P{^{1}H} NMR spectroscopic studies were peformed to examine the influence of the solvent on the carbenoid stability. These studies revealed a solvent dependent stability of the chiral carbenoids *rac*-**83-M** and *rac*-**84-M**. In THF all carbenoids showed an increased stabilty going from K to Na to Li and thus, a contrary trend to previous studies of thiosphoryl and silyl substituted carbenoids.[26] The reversed stabiltiy in case of the examined chiral carbenoids might be explained by the change of the substitution pattern from a silyl to a sulfoximine moiety bearing an oxygen donor functionality. The stronger coordination of Li by the oxygen of the sulfoximine group compared to Na and K more efficiently prevents α-elimination of the LiCl salt and thus results in an increased stability compared to sodium and potassium. Changing the solvent from the coordinating solvent THF to the non-coordinating toluene resulted in a reversed trend since the stabilizing coordination of the Li atom by oxygen atoms of the solvent is missing in toluene and the softer alkali metal bind stronger to toluene (Figure 44).

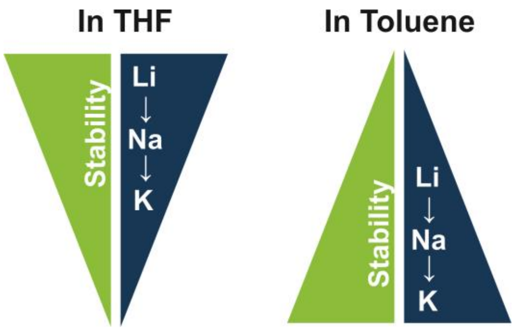

Figure 44. Illustration of the stability in dependence of the solvent and the alkali metal for *rac*-**83-M** and *rac*-**84-M**.

Noteworthy, compound *rac*-**84-Li** was found to be remarkable stable for a Li/F carbenoid which are considered 'the beast' in carbenoid chemistry. But *rac*-**84-Li** was found to be stable up to 50 °C and thus is, to the best of my knowledge, the most stable and also the first room temperature stable Li/F carbenoid. This result stresses the outstanding stabilizing effect of the sulfoximine and thiosphoryl group through both their electron withdrawing properties as well as their donor functionalities. Other Li/F carbenoids, such as **18-F** and **19-F** decompose at significantly lower temperatures (Figure 45).

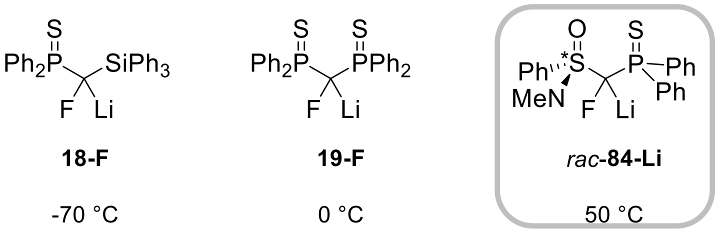

Figure 45. Isolated Li/F carbenoids and their decomposition temperature.

These results demonstrate the importance of systematic studies of the reactivity and stability of carbenoids. If understood and studied thoroughfully carbenoids feature a great potential in a wide range of synthetic applications due to their high tunability. By further exploring the impact of all potential factors, such as the substitution pattern, nature of the solvent and presence of additional donor molecues, influencing the carbenoid stability and reactivity it might be possible to synthesize carbenoids which are as reactive as required but as stable as possible.
Here, thereotical calculation on the solution structure of the chiral carbenoids can help to proof the experiementally obtained aggregation and solvation behavior and give further insight into the influence of the solvent on the solution structure as well as on the thermal stability.

Having successfully synthesized the stable chiral carbenoids **83-M** and **84-M** the suitability of these species in stereoselective deyhdrocoupling of secondary phosphines (Figure 46) or other main group element hydride species can be studied. The successful use of carbenoids in dehydrocoupling reactions require a sufficient stability since for labile carbenoids the carbene formation is favoured compared to the deprotonation of the secondary phosphine. Based on the results of the VT $^{31}P\{^{1}H\}$ NMR studies the Li/Cl carbenoid **83-Li** should be sufficiently stable to perform carbenoid mediated dehydrocoupling.

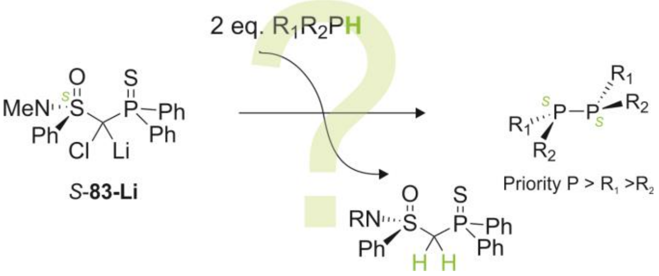

Figure 46. Hypothetical stereoselective dehydrocoupling of secondary phosphines using *S*-**83-Li**.

Carbenoid Deposition and STM Analysis

After having studied the solution structure of carbenoids in dependence of the nature of the solvent and the temperature the surface structure of carbenoids in dependence of the nature of the surface was studied in coorperation with the group of Prof. Dr. K. Morgenstern the Na/Br carbenoid **85**•3THF was deposited on Ag(111) as well as NaBr and analyzed by means of STM for the first time. The carbenoid **85**•3THF (Figure 47) was chosen because it bears sodium as the metal and bromine as the leaving group and is thus thought to be able to form interactions with the NaBr surface.

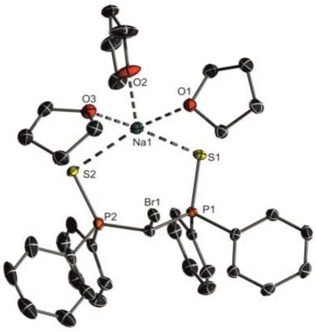

Figure 47. Molecular structure of **85**•3THF.

Due to the high sublimation temperature of **85**•3THF even in UHV the deposition of the carbenoid was performed at 60 °C. $^{31}P\{^{1}H\}$ NMR spectroscopic studies of the residual sample after the deposition confirmed that 94 % of the sample were still intact. The STM analysis of **85**•3THF on Ag(111) revealed the presence of two different layers. Further experiments identified the bottom layer as THF molecules due to residual THF being present from the synthesis of the sample and the top layer as the actual carbenoid **85**•3THF. However, avoiding THF during the synthesis by changing the solvent to toluene was not possible due to the significantly decreased thermal stability of **85** in toluene.

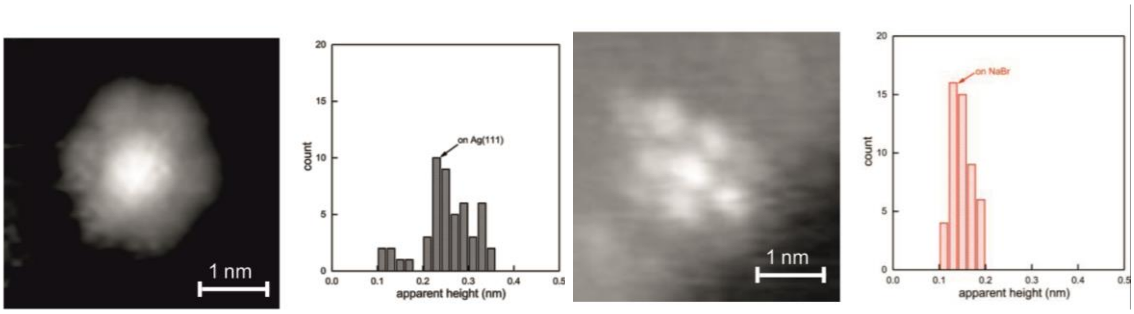

Figure 48. Left: STM image of carbenoid **85**•3THF deposited on Ag(111) surface (V_b = 2.1 V, I_t = 60 pA, T = 120 ±1 K). Second left: Histogram of the distribution of height profile of carbenoid **85**•3THF on Ag(111). Second right: STM image of carbenoid **85**•3THF deposited on NaBr surface (V_b = 2.1 V, I_t = 60 pA, T = 120 ±1 K). Right: Histogram of the distribution of height profile of carbenoid **85**•3THF on NaBr.

STM studies suggested that the THF molecules are still coordinated to the carbenoid on both surfaces. However, the shape of **85**•3THF was found to be more uniform on NaBr surface compared to Ag(111). This assumption was proven by the determination of the height distribution of the deposited species on both surfaces. The height distribution is more homogenous on NaBr which suggests a preferred orientation of the carbenoid **85**•3THF on the salt surface (Figure 48). This preferred orientation can be explained by interaction of the sodium and bromine atoms of the carbenoid with the NaBr surface. This interaction cannot be formed on the Ag(111) surface.

Consequently, it was proven that the presence of salt interactions also have an influence on the surface structure of carbenoids and might also increase their stability on such kind of surfaces compared to metal surfaces. The actual impact of these interactions on the thermal stability has to be examined in future studies.

Palladium Catalyzed Cross-Coupling of Carbenoids and Aryl Halides

Besides gaining information about the solution and the surface structure of carbenoids another focus of this thesis was to discover new application of carbenoids. Besides their use in dehydrocoupling of main group element hydride species and bond activation of element–element bonds their suitablitiy in direct palladium catalyzed cross-coupling reactions with aryl halides was targeted. This work was inspired by the recent report of Feringa on direct Pd catalyzed cross-coupling reactions using organolithium reagents and aryl halides.[165] For this purpose we tested the applicability of the YPhos ligands developed in our group recently.

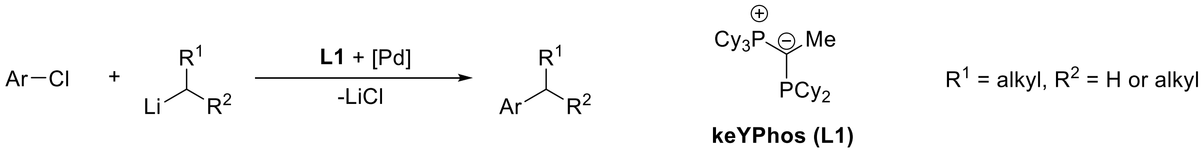

Figure 49. General equation of the Pd catalyzed cross-coupling of primary and secondary alkyl lithium reagents with aryl halides using YPhos ligands.

The test reactions using simple organolithium reagents and bromo- and chlorotoluene proved the suitablility of YPhos ligands in this regard (Figure 49). Unfortunately, a transfer of the reaction protocol to Li/Cl carbenoids were not successful due to a number of reasons. First, the insufficient thermal stability of the used carbenoids did not allow slow addition of a room temperature solution which is required to prevent Li/Hal exchange. Second, lowering the reaction temperature to prevent the carbenoid decomposition prevented the Pd catalyzed cross-coupling reaction even under the optimized conditions of Feringa. Third, changing the reaction conditions resulted in an excess of carbenoid in solution which prevented a selective reaction.

Future research could focus on the use of thermally more stable carbenoids which would allow the transfer of the optimized reaction condition reported by Feringa. However, it has to be considered that termally stable Li/Cl carbenoids bear very bulky substituents to sterically stabilize the in general very labile and reactive species. The steric bulk of the substituents might prevent successful coupling.

Zusammenfassung & Ausblick

Das Ziel der vorliegenden Arbeit war die Synthese von chiralen Carbenoiden und die Untersuchung ihrer Stabilität sowie ihrer Struktur in Lösung in Abhängigkeit der Temperatur und der Art des Lösungsmittels. Die erhaltenen Informationen sind wertvoll im Hinblick auf die Reaktivitäts- und Stabilitätskontrolle von Carbenoiden, die essentiell sind, um das Spektrum ihrer Anwendungen zu erweitern. Neben der Struktur in Lösung von Carbenoiden sollte auch die Struktur dieser Verbindungen auf unterschiedlichen Oberflächen, wie Ag(111) und NaBr, mit Hilfe von STM untersucht werden, um Einblicke in die Wechselwirkungen von Carbenoiden und Metalsalzen zu erhalten. Darüber hinaus befasste sich diese Arbeit auch mit der Anwendung von Carbenoiden in Dehydrokupplungen von Hauptgruppenelement-Verbindungen und in Pd kalalysierten Kreuzkupplungen.

Carbenoid vermittelte Bildung und Aktivierung von Element–Element- und Element–Wasserstoffbindungen

Jüngst berichtete unsere Arbeitsgruppe über die Dehydrokupplung von arylsubstituierten sekundären Phosphanen unter Verwendung von stabilisierten Carbenoiden.[19b] Das Ziel dieser Arbeit war es, diese Anwendung von Carbenoiden auf eine Vielzahl von Hauptgruppenelementhydriden zu übertragen und ihr Potenzial in der Aktivierung von Hauptgruppenelement-Element-Bindungen zu untersuchen. Hierbei wurde der Fokus auf Gruppe 14 Elementhydride gelegt. Zuerst wurde die Reaktivität von Silanen, nämlich Et_3SiH und Ph_3SiH, mit dem stabilisierten Carbenoid **56** untersucht, jedoch konnte keine selektive Dehydrokupplung beobachtet werden. Dies könnte auf die höhere Bindungspolarität der Si–H Bindung im Vergleich zur P–H Bindung zurückzuführen sein.

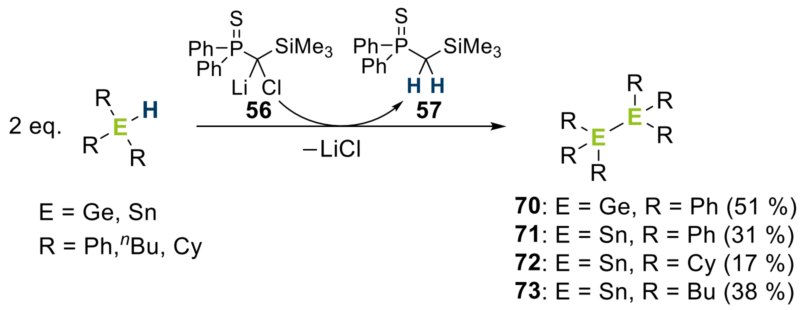

Abbildung 1. Carbenoid vermittelte Dehydrokupplung von Gruppe 14 Elementhydriden.

Im Gegensatz dazu konnte Ph_3GeH selektiv zum Hexaphenyldigerman und dem zweifach protonierten Präkusor **57** umgesetzt werden (Abbildung 1). Das Digerman **70** konnte mit Hilfe von NMR-Spektroskopie und Röntgenstrukturanalyse zweifelsfrei nachgewiesen werden. Neben Germaniumhydriden konnten auch Stannane erfolgreich gekuppelt werden. Im Fall von Zinnhydriden konnten nicht nur, wie im Fall von sekundären Phosphanen, aryl-, sondern auch alkylsubstituierte Verbindungen gekuppelt werden. Basierend auf $^{119}Sn\{^{1}H\}$-NMR-Spektroskopiedaten konnten eine vollständige Umsetzung zum jeweiligen Distannan für Ph_3SnH, Cy_3SnH and $^{n}Bu_3SnH$ erreicht werden. Die Strukutur der Verbindungen **71** und **72** konnten durch Einkristallstrukturanalyse bestätigt werden (Abbildung 2). Um die Grenzen dieser Reaktion zu testen, wurde die Reaktivität des Li/Cl Carbenoids **56** mit dem sekundären Stannan Ph_2SnH_2 untersucht. Als Hauptprodukt wurde der Sechsring $Ph_{12}Sn_6$ **74** neben einer Vielzahl von weiteren zyklischen und nicht zyklischen Zinnverbindugen erhalten.

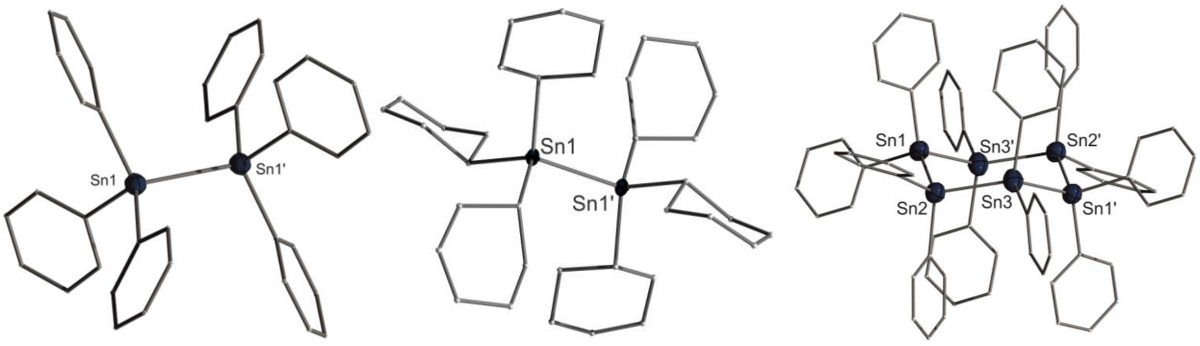

Abbildung 2. Molekülstrukturen von **71** (links), **72** (Mitte) und **74** (rechts) im Festkörper.

Trotz der erfolgreichen Carbenoid vermittelten Homodehydrokupplung konnte keine selektive Heterokupplung zweier unterschiedlicher Zinnhydride oder eines Stannans mit einem sekundären Phosphan beobachtet werden. Frühere Arbeiten deuteten daraufhin, dass die Dehydrokupplung mittels Carbenoiden auf P–H Bindungen limitiert sei, jedoch beweist die erfolgreiche Kupplung der hydridischeren Germanium- und Zinnhydride, dass diese Reaktivität eine breite Anwendung haben und diese auf weitere Hauptgruppenelementhydride ausgeweitet werden könnte. Jedoch konnte kein vergleichbares Reaktionsverhalten mit Borhydriden wie beispielsweise HBpin oder HBcat unter den gleichen Bedingungen beobachtet werden. Eine mögliche Erklärung hierfür könnte die bevorzugte Boratbildung auf Grund der sehr elektrophilen Natur von Bor sein. Die im Gegensatz dazu erfolgreiche Kupplung von Gruppe 14 Elementhydriden unter Bildung der zweifach protonierten Ausgangsverbingung **57** deutet auf einen ähnlichen Mechanismus wie bei der Dehydrokupplung von sekundären Phosphanen hin, bei dem zuerst die Hydridspezies deprotoniert wird.[19b] Die Hypothese, dass die

Boratbildung eine erfolgreiche Kupplung von Borhydriden verhindert, wurde durch die Reaktion des Li/Cl Carbenoids **56** und catB–PPh$_2$, welche in der Bildung der diborylierten Verbindung **75** und Ph$_4$P$_2$ resultierte, bestärkt (Abbildung 3). Es wurde ein vorläufiger Mechnanismus für die Bildung von **75** presentiert, jedoch bedarf es weiterer Untersuchungen, um diesen experimentell zu belegen. Bislang konnte noch kein α-boryliertes Carbanion mittels Röntgenstrukturanalyse charakterisiert werden.

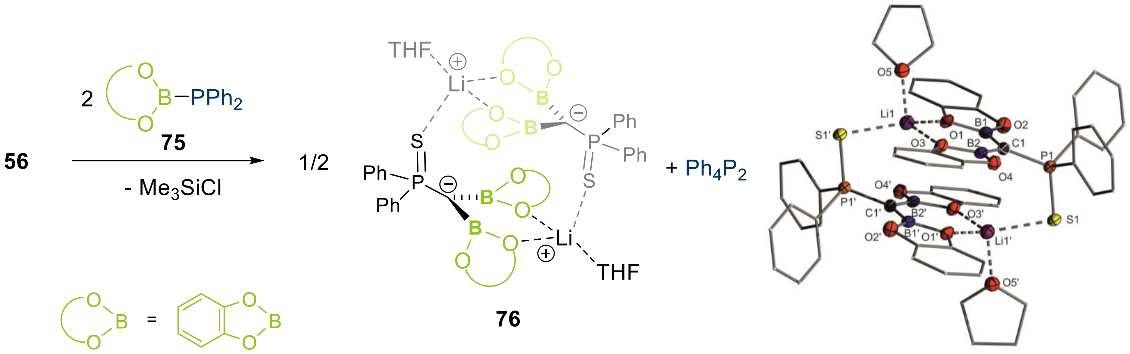

Abbildung 3. Links: Diborylierung von **56** mit **75** und der gleichzeitigen Bildung des Diphosphans Ph$_4$P$_2$. Rechts: Dimere Molekülstruktur von **76** im Festkörper.

Synthese, Charakterisierung und Anwendung von chiralen Carbenoiden

Die ersten isolierten und strukturell charakterisierten chiralen Carbenoide **83-M** und **84-M** (M = Li, Na und K) konnten über eine mehrstufige Synthese erhalten werden. [126-128, 129] NMR-spektroskopische Untersuchungen bestätigten die erfolgreiche Bildung der Carbenoide *R*-**83-M**. In allen Fällen konnte keine charakteristische Tieffeldverschiebung des zentralen carbenoiden Kohlenstoffatom im ^{13}C{^{1}H}-NMR-Spektrum beobachtet werden. Die Tieffeldverschiebung deutet auf einen carbenoiden Charakter von Verbindungen hin, ist jedoch für diesen nicht zwingend erfoderlich.

Die Molekülstrukturen von *rac*-**83-M** zeigen, dass kein Kontakt zwischen dem jeweiligen Metal und dem carbenoiden Kohlenstoffatom vorliegt (Abbildung 4). Im Fall von *rac*-**83-Li** ist das Lithiumatom vom Sauerstoffatom der Sulfoximinegruppe und drei zusätzlichen THF Lösungsmittelmolekülen koordiniert. Die Na und K Analoga konnten nur durch den Zusatz von Kronenethern, 18-C-6 im Fall *rac*-**83-Na** und 14-C-4 im Fall von *rac*-**83-K**, kristallisiert werden. Das Natriumatom in *rac*-**83-Na** wird von einem Kronethermolekül und zwei THF Molekülen, wohingegen das Kaliumatom in *rac*-**83-K** von zwei 14-C-4 Kronenethermolekülen koordiniert wird. Auf Grund des fehlenden Kontakts zwischen dem jeweiligen Metal und dem carbenoiden Kohlenstoffatom sowie dem Chloratom, ist keine Verlängerung der C–Cl Bindungen zu beobachten.

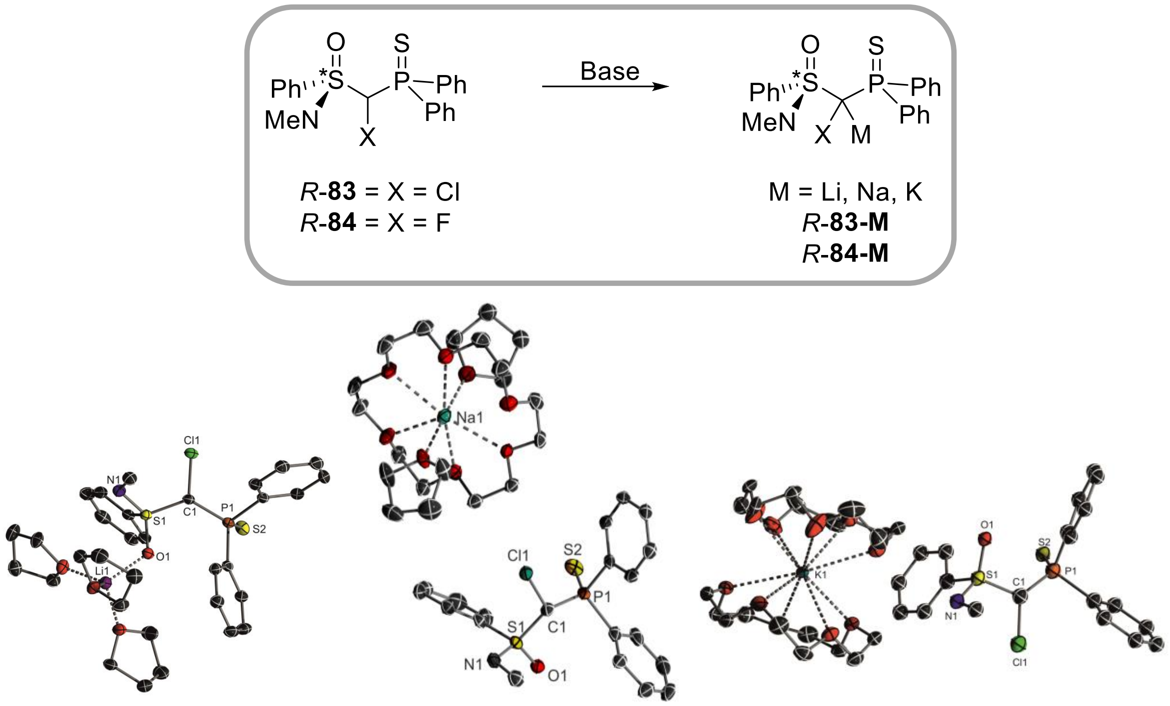

Abbildung 4. Oben: Letzter Syntheseschritt von *R*-**83-M** and *R*-**84-M**. Unten, links: Molekülstruktur von *rac*-**83-Li** im Festkörper. Mitte: Molekülstruktur von *rac*-**83-Na**•[18-C-6][2THF] im Festkörper. Rechts: Molekülstuktur von *rac*-**83-K**•2[14-C-4] im Festkörper.

Die analogen M/F Carbenoide *S*-**84-M** wurden erfolgreich isoliert und vollständig NMR-spektroskopisch charakterisiert. Das ^{13}C-NMR-Signal des zentralen carbenoiden Kohlenstoffatoms konnte nur für *S*-**84-K** detektiert werden. Im Gegensatz zu den Chloranalogen weist es eine deutliche Tieffeldverschiebung im Vergleich zu der protonierten Ausgangsverbindung *R*-**82** auf, was den stärkeren carbenoiden Charakter von Fluor-vergleichen mit Chlorcarbenoiden verdeutlicht.

Stabilitäts- und Reaktivitätskontrolle ist in der Carbenoidchemie von elemtarer Bedeutung, um das Anwendungsgebiet dieser normalerweise hochreaktiven Verbindungen zu erweitern. Mit Hilfe von VT-DOSY-NMR-spektroskopischen Untersuchungen der chiralen Carbenoide *rac*-**83-M** und *rac*-**84-M** wurden wertvolle Informationen über ihre Struktur in Lösung in Abhängigkeit des Lösungsmittels und der Temperatur erhalten. Hierbei wurde THF als das koordinierende und Toluol als das nicht-koordinierende Lösungsmittel gewählt. In THF konnte ein eindeutiger Trend für die Carbenoide *rac*-**83-M** beobachtet werden. Unabhänging vom Alkalimetal und der Temperatur konnte immer eine monomere Struktur, die von einer variierenden Anzahl von THF Lösungsmittelmolekülen koordiniert ist, nachgewiesen werden

(Tabelle 1). Je niedriger die Temperatur ist, desto höher ist die Zahl der koordinierenden THF Moleküle.

Tabelle 1. Übersicht der durch VT-DOSY-NMR-Spektroskopie erhaltenen Strukturen in Lösung der Carbenoide *rac*-**83-M**.

Temperatur [°C]	Carbenoid	Struktur in THF	Struktur in Tol
–30 C	*rac*-**83-K**	Monomer+2/3THF	Dimer + 6 THF
	rac-**83-Na**	Monomer+3THF	Dimer+4 THF
	rac-**83-Li**	Monomer+2/3THF	Dimer+2/3 THF
–20 °C	*rac*-**83-K**	Monomer+1/2THF	Dimer+1/2 THF
	rac-**83-Na**	Monomer+2THF	Dimer+6 THF / Trimer
	rac-**83-Li**	Monomer+2THF	Dimer+2/3 THF
27 °C	*rac*-**83-K**	Monomer+1THF	Dimer+3 THF
	rac-**83-Na**	Monomer+0/1THF	Dimer+6 THF / Trimer
	rac-**83-Li**	Monomer	Dimer+1 THF

Die VT-DOSY-NMR-spektroskopischen Daten in Toluol zeigen leider keinen so eindeutigen Trend, wie er in THF zu beobachten ist. Im Gegensatz zur monomeren Struktur in THF, ist eine oligomere Struktur der Carbenoide in Toluol zu beobachten. In den meisten Fällen handelt es sich hierbei um eine dimere Struktur, im Fall von *rac*-**83-Na** bei –20 °C und 27 °C kann allerdings nicht mit Sicherheit zwischen einem Dimer mit sechs koordinierten THF Molekülen und einem Trimer ohne zusätzlich koordinierte Lösungsmittelmoleküle unterschieden werden, da beide eine sehr ähnliche molekulare Masse besitzen. Um diese Ergebnisse zu bestätigen, wurden auch die jeweiligen M/F Carbenoide *rac*-**84-M** mittels VT-DOSY-NMR-Spektroskopie analysiert. In THF wurde ein analoges Solvatations- und Aggregationsverhalten zu *rac*-**83-M** beobachtet. Alle Carbenoide *rac*-**84-M** weisen in THF eine monomere Struktur mit einer steigenden Anzahl von koordinierenden THF Molekülen bei abnehmender Temperatur auf. Jedoch wurde beim Wechsel des Lösungsmittels zu Toluol eine sofortige Zersetzung der entsprechenden Natrium- und Kaliumverbindungen *rac*-**84-Na** und *rac*-**84-K**, sogar bei –80 °C, beobachtet, obwohl frühere Ergebnisse auf eine zunehmende Stabilität von Li zu Na und K hindeuten.[26] Zusammenfassend konnten mit Hilfe von VT-DOSY-NMR-spektroskopischen Untersuchungen wertvolle Informationen über das Aggregations- und Solvatationsverhalten von Carbenoiden in Lösung in Abhängigkeit des Lösungsmittels und der Temperatur erhalten werden.

VT-^{31}P{^{1}H}-NMR-spektroskopische Untersuchungen wurden geführt, um den Einfluss des Lösungsmittels auf die Stabilität der Carbenoide zu untersuchen. Diese Untersuchungen zeigten eine große Abhängigkeit der Stabilität der chiralen Carbenoide *rac*-**83-M** und *rac*-**84-M** vom Lösungsmittel. In THF weisen alle Carbenoiden eine steigende Stabilität von K zu Na und Li auf und damit einen gegensätzlichen Trend zu früheren Untersuchungen von thiophosphoryl- und silylsubstituierten Carbenoiden.[26] Die gegensätzliche Stabiliät der untersuchten chiralen Carbenoide kann durch den Austausch der Silyl- durch die Sulfoximingruppe, welche über einen Sauerstoffdonor verfügt, erklärt werden. Die verglichen mit Natrium und Kalium stärkere Koordination des Lithiums durch das Sauerstoffatom der Sulfoximingruppe verhindert die α-Eliminierung des LiCl Salzes besser und resultiert in einer höheren Stabilität im Vergleich zu Natrium und Kalium. Der Wechsel vom koordinierenden Lösungsmittel THF zum nicht-koordinierenden Toluol resultierte in einem entgegengesetzten Trend, da die stabilisierende Koordination des Lithiumatoms durch die Sauerstoffatome des Lösungsmittels in Toluol nicht mehr vorhanden ist und die weicheren Alkalimetalle stärker an Toluol binden (Abbildung 5).

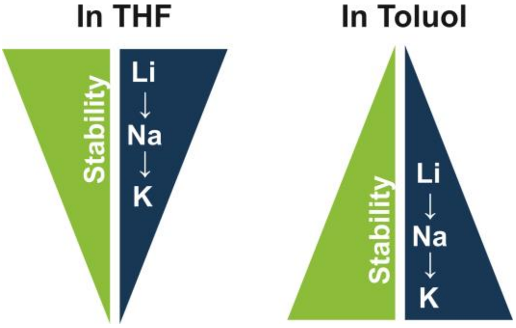

Abbildung 5. Darstellung der Stabiltät in Abhängigkeit des Lösungsmittels und der Alkalimetalle für *rac*-**83-M** und *rac*-**84-M**.

Bemerkenswert ist, dass die Verbindung *rac*-**84-Li** für ein Li/F Carbenoid, welche immer noch als „das Biest" in der Carbenoidchemie angesehen werden, außergewöhnlich stabil ist. Dennoch ist *rac*-**84-Li** bis zu einer Temperatur von bis zu 50 °C stabil, damit ist es, nach meinem Kenntnisstand, nicht nur das stabilste, sondern auch das erste bei Raumtemperatur stabile Li/F Carbenoid. Dieses Ergebnis hebt den ausgezeichneten stabilisierenden Einfluss der Sulfoximinund der Thiophosphorylgruppe sowohl durch ihre elektronenziehenden Eigenschaften als auch durch die Donorfunktionalitäten hervor. Andere Li/F Carbenoiden, wie beispielsweise **18-F** und **19-F**, zersetzen sich bereits bei deutlich niedrigeren Temperaturen.

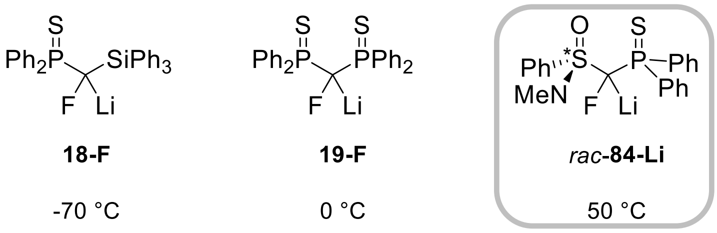
18-F -70 °C

19-F 0 °C

rac-**84-Li** 50 °C

Abbildung 6. Isolierte Li/F Carbenoide und ihre Zersetzungstemperaturen.

Diese Ergebnisse verdeutlichen die Wichtigkeit von systematischen Studien der Reaktivität und Stabilität von Carbenoiden. Wenn diese genau verstanden und gründlich untersucht werden, haben Carbenoide ein sehr großes Potential in einem breiten Spektrum von synthetischen Anwendung auf Grund ihrer hohen Anpassungsfähigkeit. Durch weitere Untersuchungen des Einflusses aller Faktoren, wie z.B. der Substituenten, des Lösungsmittels und der Präsens von zusätzlichen Donormolekülen, die die Stabilität und Reaktivität von Carbenoiden beinflussen, könnte es möglich sein, Carbenoide zu synthetisieren, die reaktiv genug, aber dennoch so stabil wie möglich sind. Hierbei können auch theoretische Untersuchungen der Struktur in Lösung der chiralen Carbenoide helfen, das experimentell bestimmte Aggregations- und Solvatationsverhalten zu bestätigen und weitere Informationen über den Einfluss des Lösungsmittels auf die Struktur in Lösung und die thermische Stabilität zu gewinnen.

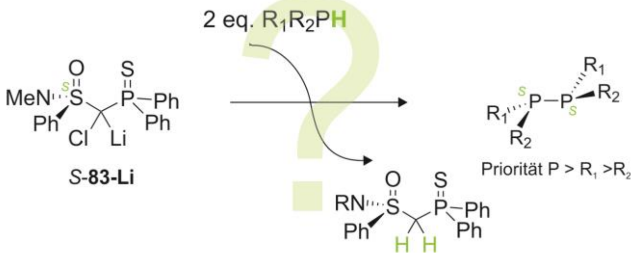

S-**83-Li**

Abbildung 7. Hypothetische stereoselektive Dehydrokupplung von sekundären Phosphanen mit *S*-**83-Li**.

Nach der erfolgreichen Synthese der stabilien chiralen Carbenoide **83-M** und **84-M** kann deren Eignung in der stereoselektiven Dehydrokupplung von sekundären Phosphanen oder anderen Hauptgruppenelementhydriden untersucht werden. Die erfolgreiche Anwendung von Carbenoiden in Dehydrokupplungen erfordert eine ausreichende Stabilität, da für labile Carbenoide die Carbenebildung im Vergleich zur Deprotonierung des sekundären Phosphans bevorzugt ist. Basierend auf den VT-$^{31}P\{^1H\}$-NMR-spektroskopischen Untersuchungen des Li/Cl Carbenoids **83-Li** sollte dieses eine ausreichende thermische Stabilität aufweisen, um für die Carbenoid vermittelten Dehydrokupplung geeignet zu sein.

Abscheidung und STM Analyse eines Carbenoids

Nach der Untersuchung der Carbenoidstruktur in Lösung in Abhängigkeit der Lösungsmitteleigenschaften wurde die Oberflächenstruktur von Carbenoiden in Abhängigkeit der Oberflächeneigenschaften in Kooperation mit der Arbeitsgruppe von Prof. Dr. K. Morgenstern untersucht. Hierzu wurde das Na/Br Carbenoid **85**•3THF sowohl auf Ag(111) als auch auf NaBr abgeschieden und anschließend zum ersten Mal mit Hilfe von STM analysiert. Das Carbenoid **85**•3THF (Abbildung 8) wurde ausgewählt, da es Natrium als Metal und Brom als Abgangsgruppe aufweist und dementsprechend in der Lage sein sollte, mit der NaBr Oberfläche wechselzuwirken.

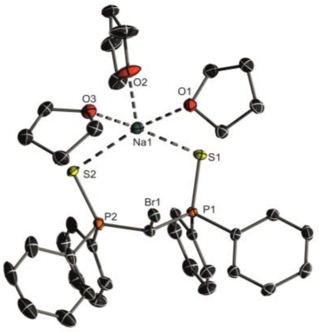

Abbildung 8. Molekülstruktur von **85**•3THF im Festkörper.

Auf Grund der hohen Sublimationstemperatur von **85**•3THF sogar im UHV wurde die Abscheidung des Carbenoids bei 60 °C durchgeführt. $^{31}P\{^1H\}$-NMR-spektroskopische Untersuchungen der zurückgebliebenen Probe von der Abscheidung bestätigten, dass 94 % der Probe noch intakt waren. Die STM Analyse von **85**•3THF auf Ag(111) offenbarte das Vorhandensein von zwei Schichten. Weitere Experimente bewiesen, dass es sich bei der unteren Schicht um THF Moleküle, die auf Grund der Synthese der Probe in THF noch vorhanden waren, handelt und die obere Schicht vom Carbenoind **85**•3THF gebildet wird. Es war jedoch nicht möglich, THF während der Synthese zu vermeiden und diese in Toluol durchzuführen, da die thermische Stabilität von **85** in Toluol stark abnimmt. STM Untersuchungen legten nahe, dass die THF Moleküle auf beiden Oberflächen immer noch an das Carbenoid koordiniert sind (Abbildung 9). Jedoch scheint die Form der Moleküle von **85**•3THF auf der NaBr Oberfläche homogener zu sein. Diese Vermutung konnte durch die Bestimmung der Höhenverteilung der abgeschiedenen Spezies auf beiden Oberflächen belegt werden (Abbildung 9). Die Höhenverteilung ist auf NaBr homogener und deutet somit auf eine präferierte Orientierung des Carbenoids **85**•3THF auf der Salzoberfläche hin. Diese bevorzugte Orientierung kann durch Wechselwirkungen des Natrium- und Bromatoms des Carbenoids mit der NaBr Oberfläche erklärt werden. Diese Wechselwirkungen können auf der Ag(111) Oberfläche nicht ausgebildet werden.

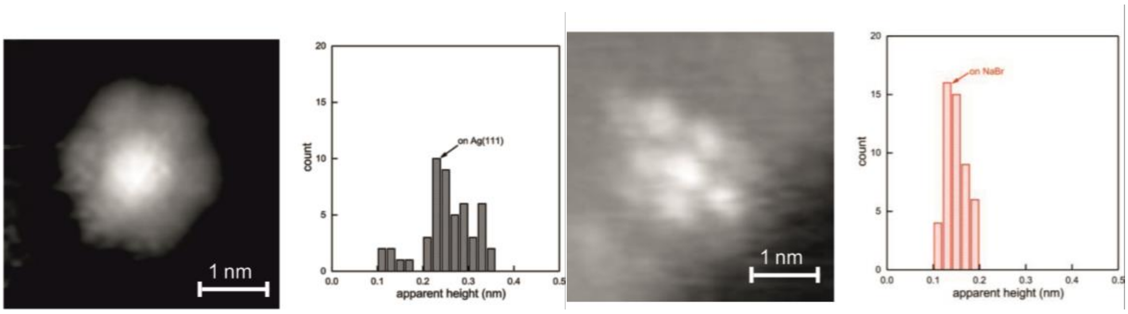

Abbildung 9. Links: STM Bild des Carbenoids **85**•3THF abgeschieden auf einer Ag(111) Oberfläche (V_b = 2.1 V, I_t = 60 pA, T = 120 ±1 K). Zweites von links: Histogramm der Höhenprofilverteilung des Carbenoids **85**•3THF auf Ag(111). Zweites von rechts: STM Bild des Carbenoids **85**•3THF abgeschieden auf einer NaBr Oberfläche (V_b = 2.1 V, I_t = 60 pA, T = 120 ±1 K). Rechts: Histogramm der Höhenprofilverteilung des Carbenoid **85**•3THF auf NaBr.

Folglich konnte bewiesen werden, dass das Vorhandensein von Wechselwirkungen einen Einfluss auf die Oberflächenstruktur von Carbenoiden hat und dass diese Wechselwirkungen eventuell auch ihre Stabilität auf salzartigen Oberflächen im Vergleich zu Metalloberflächen erhöhen könnten. Der tatsächliche Einfluss dieser Wechselwirkungen auf die thermische Stabilität muss in zukünftigen Studien untersucht werden.

Palladium-katalysierte Kreuzkupplung von Carbenoiden und Arylhalogeniden

Neben dem Erkenntnisgewinn über die Struktur von Carbenoiden in Lösung und auf Oberflächen befasste sich diese Arbeit außerdem damit, neue Anwendungen von Carbenoiden zu erschließen. Zusätzlich zu ihrem Einsatz in Dehydrokupplungen von Hauptgruppenelementhydriden und Bindungsaktivierung von Element–Elementbindungen wurde ihre Verwendung in direkten Palladium-katalysierten Kreuzkupplungsreaktionen mit Arylhalogeniden untersucht. Dieses Projekt wurde durch die Ergebnisse von Feringa über die direkte Palladium-katalyisierte Kreukupplung von Organolithiumverbindungen und

Arylhalogeniden inspiriert.[165] Zu diesem Zweck wurden die Eingnung von YPhos Liganden, die kürzlich in unserer Arbeitsgruppe entwickelt wurden, getestet.

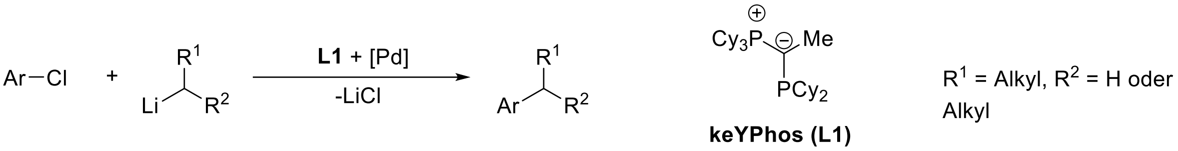

Abbildung 10. Allgemeines Reaktionsschema der Pd-katalysierten Kreuzkupplung von primären und sekundären Alkyllithiumverbindungen mit Arylhalogeniden unter Verwendung von YPhos Liganden.

Um die Eignung der YPhos Liganden in dieser Reaktion zu testen, wurden einfache Organolithiumverbindungen mit Brom- und Chlortoluol reagiert (Abbildung 10). Leider war eine genaue Übertragung der Reaktionsbedingungen bei der Verwendung von Li/Cl Carbenoiden auf Grund einer Vielzahl von Gründen nicht möglich. Erstens erlaubte die unzureichende thermische Stabilität der verwendeten Carbenoide keine langsame Zugabe der Lösung bei Raumtemperatur, was zur Vermeidung eines Li/Hal Austauschs jedoch erforderlich gewesen wäre. Zweitens wurde durch das Herabsetzen der Reaktionstemperatur, was jedoch nötig war, um eine Zersetzung der Carbenoide zu verhindern, die Pd-katalysierte Kreuzkupplung sogar unter den sonst optimierten Reaktionsbedingungen von Feringa unterdrückt. Drittens resultierte die Anpassung der Reaktionsbedingungen in einem Überschuss des Carbenoids in Lösung, was einen selektiven Reaktionsverlauf verhinderte.

Zukünftige Untersuchungen könnten sich auf die Verwendung von thermisch stabileren Li/Cl Carbenoiden konzentrieren, die eine exakte Übertragung der Reaktionsbedingungen von Feringa erlauben. Jedoch muss hierbei bedacht werden, dass thermisch stabile Li/Cl Carbenoiden sterisch sehr anspruchsvolle Substituenten besitzen, um die im Allgemeinen sehr labilen und reaktiven Spezies sterisch zu stabilisieren. Der sterische Anspruch der Substituenten könnte jedoch eine Kupplung verhindern.

Experimental Section

General Procedure and Analytical Methods

Reaction conditions: All experiments were carried out under a dry, oxygen-free argon (99.999 %) atmosphere using standard Schlenk and glovebox techniques if not stated otherwise.

Solvents: The used solvents (diethylether, ^{n}pentane, ^{n}hexane, THF, DCM, and toluene) were purified *via* a MBraun solvent purification system (SPS 800) and stored under argon atmosphere over molecular sieves 3 Å or 4 Å, respectively.

Reagents: All used reagents were used as commercial products without further purification except $^nBu_3SnH$ which was freshly distilled prior to use. Solutions of alkyl lithiums were titrated against diphenylacetic acid before use. Used water was distilled. All reagents were commercial products of Sigma-Aldrich GmbH, Acros, ABCR, Heraeus, Alfa Aesar, Thermo Fisher Scientific Inc. or Rockwood Lithium. The deuterated solvents for NMR spectroscopy (C_6D_6, $CDCl_3$, d_8-Tol, d_8-THF) were commercial products of Euroisotop, Sigma-Aldrich or Deutero GmbH and were degassed before use and stored under argon atmosphere over molecular sieves 3 Å or 4 Å, respectively.

Column Chromatography: For column chromatography silica gel 60M purchased from Machery-Nagel was used. The solvent mixtures are given as volume fractions (v/v). Pre-coated TLC sheets (ALUGRAM ALOX N/UV$_{254}$) with fluorescence indicator purchased from Machery-Nagel were used. The detection was done by means of UV light (λ = 254 nm).

Automated Column Chromatography: For automated Column Chromatography a Reveleris X2 Flash Instrument by Büchi was used. Solid loaders with a screw cap and Flash catridges (FlashPure Silica) by Büchi were used. The detection was done by means of integrated UV detection (λ_1 = 254 nm, λ_2 = 265 nm, λ_3 = 280 nm) and ELSD.

HPLC: For the determination of the *ee* an analytical Knauer Azura HPLC system equipped with a Dr. Maisch Reprosil Chiral-NR 8µm, 250•4.6 mm was used. A mixture of hexane and isopropanol (85:15) were used with a flow rate of 1.5 mL/min.

NMR Spectroscopy: Insturments used for NMR spectroscopic studies are Avance DPX 250 (250.13 Hz), Avance III 400 (400.3 Hz) and Avance 600 (600.13 Hz). If not otherwise stated the temperature was 25 °C. Lock (internal standard): ^{1}H NMR: C_6D_6 (δ = 7.16 ppm), $CDCl_3$ (δ = 7.26 ppm), d_8-THF (δ = 3.58 ppm); ^{13}C NMR: C_6D_6 (δ = 128.06 ppm), $CDCl_3$ (δ = 77.16 ppm), d_8-THF (δ = 25.31 ppm); ^{31}P NMR: external standard: 85% H_3PO_4; all ^{13}C and ^{31}P NMR spectra were recorded ^{1}H broadband decoupled ($\{^1H\}$) Signals in ^{13}C and ^{31}P NMR spectra are singlets if not stated otherwise.

The chemical shift in ppm refers to the δ scale. Spin spin coupling constants (J) are given in Hertz (Hz) ($^nJ_{XY}$: coupling of nucleus X with nucleus Y, distance of n bonds). To describe multiplicities and signal shapes, the following abbreviations are used: s = singlet, d = doublet, t = triplet, dd = doublet of doublets, ddd = doublet of doublet of doublets, sept = septet, br = broad. The assignment of signals was done *via* HSQC, HMBC, APT and COSY NMR spectra.

DOSY measurements were recorded on an AV 400 MHz spectrometer operating at 400.13 MHz **(83-M)** and on an Avance 600 MHz spectrometer operating at 600.13 Hz **(84-M)**. A double stimulated echo sequence (dstebpg3s) was used and the pulse gradients (g) were incremented from 2 to 95% of the maximum gradient strength in a linear ramp. The Stejskal-Tanner diffusion delay (d20) was set to 0.2 s and the eddy-current delay (d21) to 5 ms. After Fourier transformation and baseline correction, the diffusion dimension was processed with the Topspin 3.6.1 software (BrukerBiospin). Diffusion coefficients were calculated by exponential fits with the T1/T2 software of Topspin. Tetramethylsilane and adamantane have been used as references in DOSY measurements in THF and toluene, respectively. The molecular masses were calculated by the ECC-MW estimation software by Stalke *et al*.[143]

Elemental analysis: An Elementar vario MICRO-cube (*Elementar*) was used. The analytical data of compounds are given as ratios of the respective elements in percent.

Single crystal X-ray diffraction analysis: Single crystal X-ray diffraction analysis was performed using an Oxford Synergy (Cu-mircosource, HyPix detector). The program CysAlisPro (Agilent Technologies, Version 1.171.36.24) was used for data collection, unit cell assignment and absorption correction. Structure refinement was performed with the help of SHELXL14.

Synthesis

The following compounds have been synthesized according to literature:

- (p-Tol)$_2$PH[19b]
- catBCl[169]
- Ph$_3$SiCl[121]
- Compound **56**[19b, 54a]
- Compound **78**[126]
- Compound **79**[127]
- Compound **80**[128]
- Compound **81**[129]
- Compound **82**[129]
- Compound **85**[66]
- Compound **86**[66]

Synthesis of 70

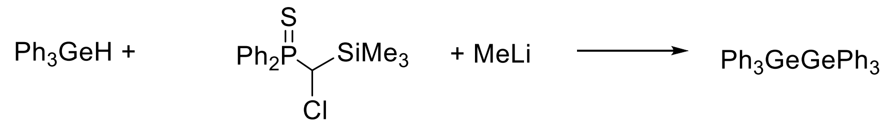

69 **70**

351.03 g/mol 338.51g/mol 21.98 g/mol 607.90 g/mol

100 mg (0.295mmol) of **69** were dissolved in 2 mL THF and cooled down to –80 °C. 0.133 mL (2.21 M in Et$_2$O) MeLi were added slowly to **69** which resulted in a yellow solution. The reaction mixture was stirred at low temperatures for 45 min. 179.95 mg (0.592 mmol) of triphenylgermaniumhydrid were dissolved in 2 mL THF and cooled down to –80 °C. The yellow solution of was added slowly to triphenylgermaniumhydride. The reaction mixture was warmed up to RT slowly over the weekend. The green/gray reaction solution was filtered at –10 °C and the white residue was washed with pentane (3 x 1 mL) at –10 °C. The white residue was dried. The product was obtained in 51% (90.6 mg, 0.149 mmol) yield.

Crystals suitable for X-ray diffraction analysis were obtained from a concentrated solution of **70** in DCM at RT.

^{1}H NMR (400.33Hz, $CDCl_3$): δ_H = 7.25 – 7.36 (m, 30H)
^{13}C{^{1}H} NMR (100.67 Hz, $CDCl_3$): δ_C= 128.4 (s, C_{Ph}), 128.9 (s, C_{para}), 135.7 (s, C_{Ph}), 137.5 (s, C_{ipso})

Other physical data match those reported in literature.[108]

Synthesis of 71

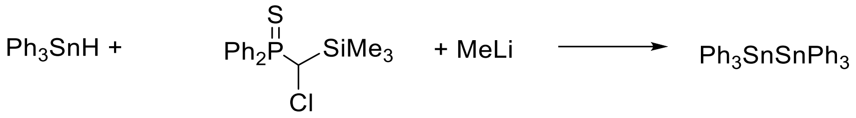

69 **71**

351.03 g/mol 338.51g/mol 21.98 g/mol 700.06 g/mol

28.91 mg of **69** (0.0854 mmol) were dissolved in 1 mL THF and cooled down to –80 °C. 0.54 mL (0.157 M in Et_2O) MeLi were added slowly. The yellow reaction mixture was stirred for one hour at –80 °C. In a second schlenk flask 30 mg of triphenyltinhydride (0.0854 mmol) were dissolved in 1 mL THF and cooled down to –80 °C. The reaction mixture of was added slowly *via* cannula to the solution of triphenyltinhydride. The reaction solution was warmed to RT slowly overnight resulting in a yellow solution. The reaction solution was filtered by cannula and the solvent was removed *in vacuo*. The white residue was washed with pentane and subsequently dried. The product **71** was obtained as a white solid in 31% yield (125mg, 0.179 mmmol). Spectroscopic data are in accordance with literature reports. [118]

Suitable crystals for X-ray diffraction analysis were obtained by slow diffusion of hexane into the concentrated reaction solution.

^{1}H NMR (400.33Hz, C_6D_6): δ_H = 7.08 – 7.10 (m, 18H), 7.60 – 7.74 (m, 12H)
^{119}Sn{^{1}H} NMR (149.26 Hz, C_6D_6): δ_{Sn} = -142.1 (s)

Other physical data match those reported in literature.[110]

Synthesis of 72

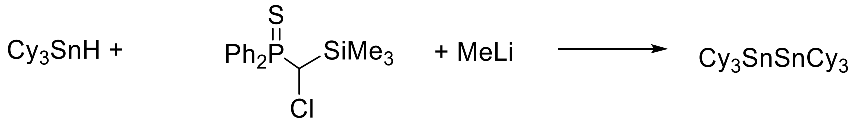

69 **72**

351.03 g/mol 338.51g/mol 21.98 g/mol 736.34 g/mol

100 mg (0.296 mmol) of **69** were dissolved in 3 mL THF and cooled down to –80 °C. 0.133 mL (2.21 M in Et_2O, 0.296 mmol) MeLi were added slowly and the yellow reaction mixture was stirred for 30 min. at low temperatures. 218.46 mg (0.592 mmol) of tricylcohexyltinhydride were dissolved in 1 mL THF and cooled down to –80 °C. The yellow reaction mixture was added *via* cannula to tricyclohexyltinhydride resulting in a cloudy yellow solution. The reaction solution was warmed up to RT slowly overnight. The cloudy solution was filtered at –30 °C and the white residue was washed with 3 x 1 mL of pentane. The white solid was dried *in vacuo*. The product was obtained in 16 % yield as a white solid (35.2 mg, 0.048 mmol).

Crystals suitable for X-ray diffraction analysis were obtained by slow evaporation of a saturated solution of **72** in C_6D_6 at room temperature

^{1}H NMR (400.33Hz, C_6D_6): δ_H = 1.37 – 1.42 (m, 18H), 1.62 – 1.94 (m, 38H), 2.13 – 2.15 (m, 10H)
^{13}C{^{1}H} NMR (100.67 Hz, C_6D_6): δ_C = 27.9 (s, C_{para}); 28.7 (s, C_{ipso}), 30.4 (s, C_{ortho}), 34.6 (s, C_{meta})
^{119}Sn{^{1}H} NMR (149.27 Hz, C_6D_6): δ_{Sn} = -70.2 (s)

Synthesis of 73

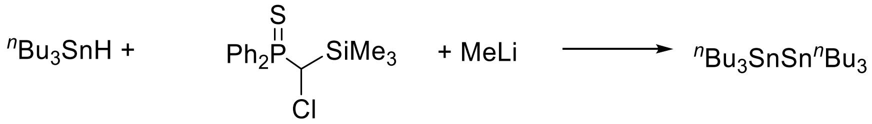

69 **73**

291.04 g/mol 338.51g/mol 21.98 g/mol 580.12 g/mol

100 mg (0.295 mmol) of **69** were dissolved in 3 mL THF and cooled down to –80 °C. 0.19 mL (0.295 mmol, 1.15M in Et_2O) MeLi was added dropwise to **69**. The resulting yellow reaction solution was stirred at for one hour at low temperatures. In a second schlenk flask 171.73 mg

(0.590 mmol) of tri-^{n}butyltinhydride were dissolved in 2 mL THF and cooled down to –80 °C. The reaction mixture was added slowly *via* cannula to tri-^{n}butyltinhydride. The reaction solution was warmed to RT slowly overnight. The green reaction solution was filtered by cannula. The solvent was removed *in vacuo* and the residue was extracted with 5 x 2 mL pentane. The filtrate was dried and the product was obtained as a colorless liquid in 38% yield (128.3 mg, 0.221 mmol).

^{1}H NMR (400.33Hz, C_6D_6): $\delta_H = 0.98$ (t, 3H), 1.14 – 1.18 (m, 2H), 1.38 – 1.47 (sext, 2H), 1.64 – 1.71 (m, 2H)
^{119}Sn{^{1}H} NMR (149.27 Hz, C_6D_6): $\delta_{Sn} = -83.7$ (s, $^1J_{119Sn\text{-}117Sn} = 1279.6$ Hz)

Other physical data match those reported in literature.[112]

Synthesis of 75

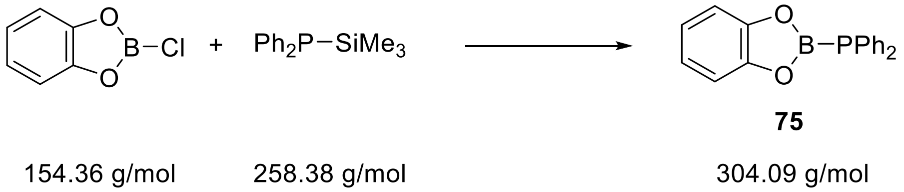

75

The synthesis of Ph_2PBcat was performed analogously to the synthesis of Ph_2PBpin.[120]

2.67 g (0.010 mmol) of Ph_2PSiMe_3 and 1.82 g (0.012 mmol) of catBCl were dissolved in 20 mL DCM and cooled to 0 °C, respectively. The solution of Ph_2PSiMe_3 was added to the solution of catBCl. The clear reaction mixture was warmed to RT slowly overnight. The solvent was removed *in vacuo* ($1•10^{-1}$ mbar) to yield a white solid which was dissolved in 7 mL of toluene and filtered *via* cannula and subsequently, layered with 30 mL of hexane and stored at –30 °C. The supernatant solution was filtered off and the white residue was dried *in vacuo.* The product was obtained as a white solid (930 mg, 30 %).

^{1}H NMR (400.33Hz, $CDCl_3$): δ_H = 7.26 – 7.28 (m, 2H), 7.42 – 7.44 (m, 2H), 7.54 – 7.55 (m, 6H), 7.75 – 7.79 (m, 4H)
^{31}P{^{1}H} NMR (162.1 MHz, $CDCl_3$): $\delta_P = -66.7$ (br)
^{11}B{^{1}H} NMR (128.4MHz, $CDCl_3$): $\delta_B = 37.4$ (br)

Synthesis of *R*-83

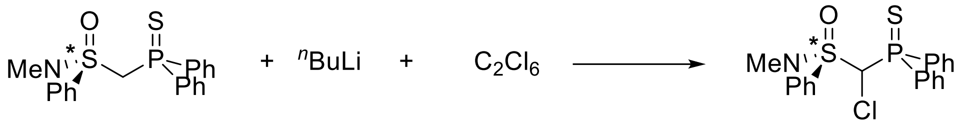

R-**82** *R*-**83**

385.48 g/mol 64.06 g/mol 236.74 g/mol 419.92 g/mol

901 mg (2.337 mmol) of *R*-**82** were dissolved in 50 mL THF and cooled to –80 °C. 1.64 mL (1.71 M in Hex, 2.805 mmol) *ⁿ*BuLi were added dropwise. The yellow solution was stirred between –80 °C and –30° C for 1 h. 719.24 mg of hexachloroethane were dissolved in 50 mL THF. The yellow reaction mixture was transferred to hexachloroethane *via* temperature gradient and warmed to RT slowly overnight. 25 mL of H_2O were added and the phases were separated. The aqueous phase was extracted with 25 mL of Et_2O three times. The combined organic phases were dried over Na_2SO_4. After filtration the solvent was removed *in vacuo*. The crude product was purified by column chromatography (THF/Hex 1:2.5, r_f = 0.4).The product was obtained as a white solid in 54 % yield (525 mg, 1.25 mmol).

Crystals suitable for X-ray diffraction analysis were obtained by crystallization of the *S,S*-conformer from a racemic oil at RT.

^{1}H NMR (400.33Hz, $CDCl_3$): δ_H = 2.77 + 2.88 (s + s, 3H; NCH_3), 5.71 + 5.78 (d + d, 1H, $^2J_{HP}$ = 4.49 Hz + 4.81 Hz; C*H*Cl), 7.29-7.35 (m, 4H; C$H_{Ph,meta/para/ortho}$), 7.37-7.51 (m, 5H, C*H*), 7.73-7.93 (m, 6H; C$H_{Ph,ortho/meta/para}$)

^{13}C{^{1}H} {^{31}P} NMR (100.67 Hz, $CDCl_3$): δ_c = 29.6 (s, N*C*H_3), 31.0 (s, N*C*H_3), 69.2 (s, *C*Cl) 75.9 (s, *C*Cl), 128.5 (s, P$C_{Ph, para}$) 128.5 (s, P$C_{Ph, para}$), 128.6 (bs, P$C_{Ph, para}$), 129.0 (s, $S_{Ph. meta}$), 129.2 (s, $S_{Ph. meta}$), 130.3 (s, P$C_{Ph, ipso}$), 130.6 (s, P$C_{Ph, para}$), 130.6 (s, P$C_{Ph, para}$), 130.9 (s, S$C_{Ph, ortho}$), 131.6 (s, P$C_{Ph, para}$), 132.1 (s, P$C_{Ph, ortho/meta}$), 132.1 (s, P$C_{Ph, ortho/meta}$), 132.2 (s, P$C_{Ph, ortho/meta}$), 132.2 (s, P$C_{Ph, ortho/meta}$), 132.2 (s, P$C_{Ph, ortho/meta}$), 132.3 (s, P$C_{Ph, ortho/meta}$), 132.4 (s, P$C_{Ph, ortho/meta}$), 132.5 (s, P$C_{Ph, ortho/meta}$), 133.5 (s, S$C_{Ph, para}$), 134.0 (s, S$C_{Ph, para}$), 135.6 (s, S$C_{Ph, ipso}$), 139.0 (s, S$C_{Ph, ipso}$)

^{31}P{^{1}H} NMR (162.1 MHz, $CDCl_3$): δ_P = 45.1 (s), 46.5 (s)

Elemental analysis for $C_{20}H_{19}ClNOPS_2$

	C [%]	H [%]	N [%]	S [%]
calculated	57.21	4.56	3.34	15.27
measured	57.32	4.55	3.28	15.30

Synthesis of *R*-83-Li

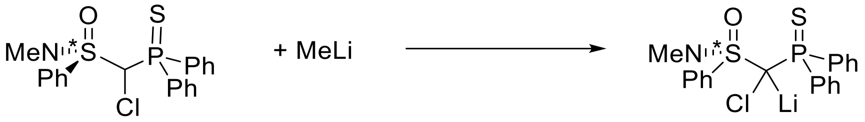

R-**83** *R*-**83-Li**

385.48 g/mol 21.98 g/mol 425.85 g/mol

47 mg (0.112 mmol) of *R*-**83** were dissolved in 3 mL of THF and cooled to 0 °C. 0.67 mL (0.112 mmol, 0.16M in Et_2O) MeLi were cooled to 0 °C and added slowly. The resulting yellow solution was stirred for 1 h at 0 °C. The solvent was removed and the product was obtained as a yellow solid in 85 % yield (40.5 mg, 0.092 mmol). NMR spectroscopic characterization was performed at –30 °C.

Single crystals suitable for X-ray diffraction analysis were obtained from a concentrated THF solution at -30 °C.

^{1}H NMR (400.33 MHz, d_8-THF): δ_H = 2.85 (s, 3H; NCH_3), 7.08-7.28 (m, 9H; $SCH_{Ph,meta,para}$ + $PCH_{Ph,meta,para}$), 7.54-7.59 (m, 2H; $PCH_{Ph,ortho}$), 7.89-7.95 (m, 2H; $PCH_{Ph,ortho}$), 7.98-8.00 (d, 2H; $SCH_{Ph,ortho}$)
^{13}C{^{1}H} NMR (100.67 MHz, d_8-THF):δ_C = 29.8 (s, NCH_3), 49.2 (d, $^1J_{P\text{-}C}$ = 83.1 Hz, CCl), 127.8 – 128.1 (d+d, $^3J_{P\text{-}C}$ = 11.9Hz; $PC_{Ph,meta}$); 128.0 (s, $SC_{Ph,\ meta}$); 129.0 ($SC_{Ph,\ ortho}$); 130.0 (d, $^4J_{CP}$ = 2.5 Hz; $C_{Ph,para}$); 130.2 (d, $^4J_{CP}$ = 4.4 Hz; $PC_{Ph,para}$); 130.2 (s, $_2J_{CP}$ = 10.3 Hz; $SC_{Ph,para}$); 133.1 (d, $_2J_{CP}$ = 9.8 Hz; $PC_{Ph,ortho}$); 133.2 (d, $_2J_{CP}$ = 10.1 Hz; $PC_{Ph,ortho}$); 139.1 + 140.7 (d + d, $^1J_{CP}$ = 88.8 Hz + 96.2 Hz; $PC_{Ph,ipso}$); 145.8 (s, $SC_{Ph,ipso}$)
^{31}P{^{1}H} NMR (162.1 MHz, d_8-THF): δ_P = 42.2 (s)

Synthesis of *R*-83-Na

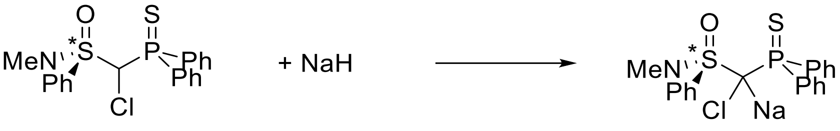

R-**83** *R*-**83-Na**

419.93 g/mol 23.99 g/mol 441.92 g/mol

25.5 mg (0.0607mmol) of *R*-**83** were dissolved in 1 mL of THF and cooled to 0 °C. Subsequently, the solution was added to 4.4 mg (0.1821 mmol) of NaH. The reaction solution was stirred for 1 h at 0 °C and was filtered subsequently. The solvent was removed *in vacuo*. The product was obtained as a yellow solid in 91 % yield (24.41 mg, 0.55 mmol).

Suitable crystals for X-ray diffraction analysis were obtained by slow diffusion of pentane into a solution of 1eq. of 18-C-6 and *rac*-**83-Na** in THF at -30 °C.

^{1}**H NMR** (400.3 MHz, d_8-THF): δ_H = 2.84 (s, 3H; NCH_3), 7.13-7.31 (m, 9H; SC$H_{\mathrm{Ph,meta,para}}$ + PC$H_{\mathrm{Ph,meta,para}}$), 7.85-7.89 (m, 2H; PC$H_{\mathrm{Ph,ortho}}$), 7.98-8.10 (m, 4H; PC$H_{\mathrm{Ph,ortho}}$ + SC$H_{\mathrm{Ph,ortho}}$)
^{13}**C{^{1}H} NMR** (100.7 MHz, d_8-THF): δ_C = 30.2 (NCH$_3$), 50.4 (d, $^{1}J_{\mathrm{CP}}$ = 88.5 Hz; CCl), 127.7 + 127.9 (d + d, $^{3}J_{\mathrm{CP}}$ = 12.1 Hz; P$C_{\mathrm{Ph,meta}}$), 128.1 (S$C_{\mathrm{Ph,meta}}$), 128.4 (S$C_{\mathrm{Ph,ortho}}$), 129.8 (S$C_{\mathrm{Ph,para}}$), 130.0 (d, $^{4}J_{\mathrm{CP}}$ = 2.2 Hz; P$C_{\mathrm{Ph,para}}$), 130.2 (d, $^{4}J_{\mathrm{CP}}$ = 2.9 Hz; P$C_{\mathrm{Ph,para}}$), 133.3 (d, $_{2}J_{\mathrm{CP}}$ = 10.3 Hz; P$C_{\mathrm{Ph,ortho}}$), 139.2 + 140.5 (d + d, $^{1}J_{\mathrm{CP}}$ = 87.9 Hz + 95.6 Hz; P$C_{\mathrm{Ph,ipso}}$), 147.3 (s, S$C_{\mathrm{Ph,ipso}}$)
^{31}**P{^{1}H} NMR** (162.1 MHz, d_8-THF): δ_P = 43.1

Synthesis of *R*-83-K

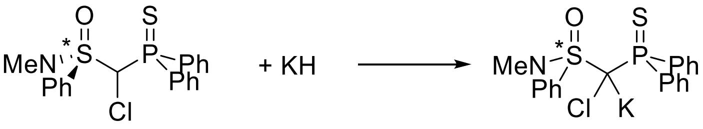

R-**83** *R*-**83-K**

419.93 g/mol 40.11 g/mol 458.03 g/mol

22.2 mg (0.0528 mmol) of *R*-**83** were dissolved in 1 mL of THF and cooled to 0 °C. Subsequently, the solution was added to 6.4 mg (0.16 mmol) KH and stirred at 0 °C for 1 h.

The reaction solution was filtered and the solvent was removed *in vacuo*. The product was obtained as a yellow solid in 88 % yield (21.3 mg, 0.046 mmol).

Crystals suitable for X-ray diffraction analysis were obtained from a saturated solution of *rac*-**83-K** and 2 eq. of 15-C-5 in THF at –30 °C.

^{1}H NMR (400.3 MHz, d_8-THF): δ_{H} = 2.68 (s, 3H; NCH_3), 7.13-7.31 (m, 9H; SC$H_{\mathrm{Ph,meta,para}}$ + PC$H_{\mathrm{Ph,meta,para}}$), 7.85-7.89 (m, 2H, $^{3}J_{\mathrm{HP}}$ = 12.9 Hz; PC$H_{\mathrm{Ph,ortho}}$), 7.98-8.00 (m, 2H; SC$H_{\mathrm{Ph,ortho}}$), 8.05-8.10 (m, 2H; PC$H_{\mathrm{Ph,ortho}}$)
^{13}C{^{1}H} NMR (100.7 MHz, d_8-THF): δ_{C} = 29.6 (s, NCH_3), 49.8 (d, $^{1}J_{\mathrm{CP}}$ = 86.3 Hz; *C*Cl), 127.6 + 127.7 (d + d, $^{3}J_{\mathrm{CP}}$ = 13.9 Hz; P$C_{\mathrm{Ph,meta}}$), 128.2 (S$C_{\mathrm{Ph,ortho}}$), 128.5 (s, S$C_{\mathrm{Ph,meta}}$), 129.9 (dd, $^{4}J_{\mathrm{CP}}$ = 4.13 Hz; P$C_{\mathrm{Ph,para}}$ + S$C_{\mathrm{Ph,para}}$), 133.1 + 133.2 (d + d, $^{2}J_{\mathrm{CP}}$ = 10.2 Hz + 9.7 Hz; P$C_{\mathrm{Ph,ortho}}$), 139.5 (d, $^{1}J_{\mathrm{CP}}$ = 85.9 Hz; P$C_{\mathrm{Ph,ipso}}$), 140.4 (d, $^{1}J_{\mathrm{CP}}$ = 90.0 Hz; P$C_{\mathrm{Ph,ipso}}$), 146.5 (s, S$C_{\mathrm{Ph,ipso}}$)
^{31}P{^{1}H} NMR (162.1 MHz, d_8-THF): δ_{P} = 44.1 (s)

Synthesis of *S*-84

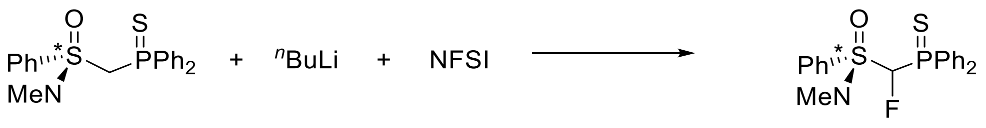

S-**82** *S*-**84**

385.48 g/mol 64.04 g/mol 315.34 g/mol 403.47 g/mol

377.4 mg (0.979 mmol) of *S*-**82** were dissolved in 7 mL THF and cooled to –80 °C. ^{n}BuLi (0.642 mL, 1.6 M in Hex, 1.028 mmol) was added dropwise. The reaction mixture was stirred for 15 min at –80 °C and then another hour at RT. NFSI (324.17 mg, 1.028 mmol) was dissolved in 7 mL THF. The reaction mixture of *S*-**82** and ^{n}BuLi was again cooled to –80 °C and then transferred to the NFSI solution *via* temperature gradient. The resulting light yellow solution was warm to RT slowy and stirred at RT for 4 h. 10 mL aqua dest. were added and the phases were separated. The aqueous phase was extracted three times with 30 mL DCM. The combined organic phases were dried over Na_2SO_4 and filtered. The solvent was evaporated to give the crude product as a sticky orange oil. The product was obtained as white sticky solid after purification by an automated flash column (119 mg, 0.295 mmol, 31 %).

^{1}H NMR (400.33Hz, d$_8$-THF): δ_H = 2.81 (s, 3H, NCH_3); 2.85 (s, 1.77H, NCH_3); 6.58 (d,$^1J_{P\text{-}H}$ = 44.6 Hz; 0.54H CF*H*); 6.66 (d,$^1J_{P\text{-}H}$ = 44.11 Hz; 1H, CF*H*), 7.29 – 7.39 (m, 7H); 7.43 – 7.52 (m, 8H); 7.75 – 7.86 (m, 6H); 7.88 – 7.97 (m, 4H)

^{13}C{^{1}H}{^{31}P} NMR (100.7 MHz, d$_8$-THF): 29.3 + 30.6 (s, N*C*H$_3$), 99.5 (d, $^1J_{CF}$ = 263.9 Hz, *C*F) + 103.8 (d, $^1J_{CF}$ = 271.0 Hz, *C*F), 129.1 (bs,P$C_{Ph,\ ortho/meta}$ + S$C_{Ph,\ meta}$), 129.2 (s, P$C_{Ph,\ ortho/meta}$), 129.3 (s, P$C_{Ph,\ ortho/meta}$), 129.3 (s, P$C_{Ph,\ ortho/meta}$), 129.4 (s, S$C_{Ph,\ meta}$), 130.1 (s, P$C_{Ph,\ ipso}$), 130.5 (s, S$C_{Ph,\ ortho}$), 130.9 (s, P$C_{Ph,\ ipso}$), 131.4 (s, S$C_{Ph,\ ortho}$), 132.4 (s, P$C_{Ph,\ ipso}$), 132.7 (s, P$C_{Ph,\ ortho/meta}$), 132.8 (s, P$C_{Ph,\ para}$), 133.0 (s, P$C_{Ph,\ ortho/meta}$), 133.1 (s, P$C_{Ph,\ ortho/meta}$), 133.5 (s, P$C_{Ph,\ ortho/meta}$), 133.5 (s, P$C_{Ph,\ ortho/meta}$), 133.5 (s, P$C_{Ph,\ ortho/meta}$), 133.5 (s, P$C_{Ph,\ ortho/meta}$), 134.0 (s, S$C_{Ph,\ para}$), 134.3 (s, S$C_{Ph,\ para}$), 137.5 (s, S$C_{Ph,\ ipso}$), 140.0 (s, S$C_{Ph,\ ipso}$)

^{31}P{^{1}H} NMR (162.06 Hz, d$_8$-THF): δ_P = 36.1 (d, $^2J_{PF}$ = 55.8 Hz), 36.9 (d, $^2J_{PF}$= 55.7 Hz)

^{19}F{^{1}H} NMR (235.33 Hz, d$_8$-THF): δ_F = -177.1 (d, $^2J_{FP}$ = 55.6 Hz); -175.6 (d, $^2J_{FP}$ = 55.8 Hz)

Elemental analysis for $C_{20}H_{19}FNOPS_2$

	C [%]	H [%]	N [%]	S [%]
calculated	59.54	4.75	3.47	15.89
measured	59.64	4.74	3.36	15.95

Synthesis of *S*-84-Li

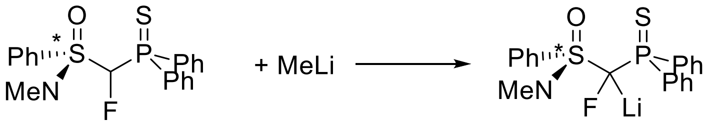

S-**84** *S*-**84-Li**

403.47 g/mol 21.98 g/mol 409.40 g/mol

In a Schlenk tube 14.4 mg (0.0357 mmol) of *S*-**84** were dissolved in 1 mL THF and cooled to –50 °C and 0.04 mL (0.0357 mmol, 0.92M in Et$_2$O) MeLi were added. The reaction mixture was allowed to react for 30 min. at –50 °C and subsequently, the solvent was removed *in vacuo* and the product was obtained as a yellow solid in 86 % yield (12.6 mg, 0.031 mmol). The product was NMR spectroscopically characterized at –30 °C.

^{1}H NMR (400.3 MHz, d_8-THF): δ_H = 2.72 (s, 3H; NC*H*$_3$), 6.84 – 6.88 (m, 2H, $C_{arom.}$); 6.91 – 7.02 (m, 4H; $C_{arom.}$), 7.09 – 7.14 (m, 3H, $C_{arom.}$), 7.26 – 7.31 (m, 2H, $C_{arom.}$), 7.60 – 7.62 (d, 2H, $C_{arom.}$), 7.65 – 7.70 (m, 2H, $C_{arom.}$)

^{13}C{^{1}H} NMR (100.7 MHz, d_8-THF): δ_C = 30.0 (s, N*C*H$_3$), 128.0 (d, $^3J_{CP}$ = 38.1 Hz; *PC*$_{Ph, meta}$), 127.9 (s, S*C*$_{Ph}$), 128.2 (d, $^3J_{CP}$ = 36.5 Hz; *PC*$_{Ph, meta}$), 128.3 (s, S*C*$_{Ph}$), 129.8 (s, S*C*$_{Ph, para}$), 130.2 (d, $^4J_{CP}$ = 3.3 Hz; *PC*$_{Ph, para}$), 130.6 (d, $^4J_{CP}$ = 2.6 Hz; *PC*$_{Ph, para}$), 132.6 (d, $^2J_{CP}$ = 8.4 Hz; *PC*$_{Ph, ortho}$), 132.7 (d , $^2J_{CP}$ = 9.6 Hz; *PC*$_{Ph, ortho}$), 136.7 (d, $^1J_{CP}$ = 77.9 Hz; *PC*$_{Ph, ipso}$), 139.55 (d, $^1J_{CP}$ = 95.7 Hz; *PC*$_{Ph, ipso}$), 146.3 (s, S*C*$_{Ph, ipso}$)

^{31}P{^{1}H} NMR (162.1 MHz, d_8-THF): δ_P = 33.4 (d, $^2J_{PF}$ = 43.8 Hz)

^{19}F{^{1}H} NMR (376.3 MHz, d_8-THF): δ_F = -210.4 (d, $^2J_{FP}$ = 44.0 Hz)

^{7}Li NMR (155.5 MHz, d_8-THF): δ_{Li} = 0.24 (s)

Synthesis of *S*-84-Na

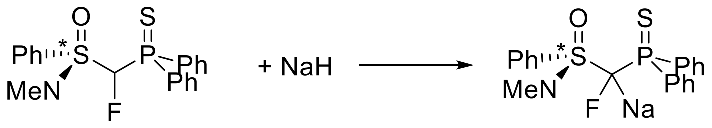

S-**84** *S*-**84-Na**

403.47 g/mol 23.99 g/mol 425.45 g/mol

24.3 mg (0.060 mmol) of *S*-**84** were dissolved in 1 mL THF and cooled to 0 °C. Subsquently, the solution of *S*-**84** was added to 4.3 mg (0.180 mmol) of NaH. The resulting yellowish solution was stirred at 0 °C for 1 h and then cannula filtered to remove the excess of NaH. The solvent was removed *in vacuo* and the product was obtained as a yellow solid in 87 % yield (22.2 mg, 0.052 mmol). The product was NMR spectroscopically characterized at –30 °C.

^{1}H NMR (400.3 MHz, d_8-THF): δ_H = 2.85 (s, 3H; NC*H*$_3$), 7.01 – 7.06 (m, 3H, $C_{ortho/meta}$); 7.11– 7.15 (m, 2H; $C_{para.}$), 7.26 – 7.30 (m, 4H, $C_{ortho/meta.}$), 7.42 – 7.47 (m, 2H, $C_{meta.}$), 7.69 – 7.71 (d, 2H, $C_{ortho/meta.}$), 7.78 – 7.83(m, 2H, $C_{meta.}$)

^{13}C{^{1}H} NMR (100.7 MHz, d_8-THF): δ_C = 30.1 (s, N*C*H$_3$), 127.8 (d, $^2J_{CP}$ = 12.0 Hz; *PC*$_{Ph, ortho}$), 127.8 (s, S*C*$_{Ph, ortho/meta}$), 128.0 (s, S*C*$_{Ph, ortho/meta}$), 128.2 (d, $^3J_{CP}$ = 12.4 Hz; *PC*$_{Ph, ortho}$), 129.4 (s, S*C*$_{Ph, para}$), 129.8 (s, P*C*$_{Ph, para}$), 130.4 8 (s, P*C*$_{Ph, para}$), 132.4 (d, $^3J_{CP}$ = 10.2 Hz; *PC*$_{Ph, meta}$), 132.6 (d, $^3J_{CP}$ = 12.4 Hz; *PC*$_{Ph, meta}$), 136.5 (d, $^1J_{CP}$ = 73.7 Hz; *PC*$_{Ph, ipso}$), 140.40 (d, $^1J_{CP}$ = 94.8 Hz; *PC*$_{Ph, ipso}$), 145.8 (s, SC$_{Ph, ipso}$)

^{31}P{^{1}H} NMR (162.1 MHz, d$_8$-THF): δ_P = 33.6 (d, $^2J_{PF}$ = 42.5 Hz)

^{19}F{^{1}H} NMR (376.3 MHz, d$_8$-THF): δ_F = -207.7 (d, $^2J_{FP}$ = 43.1 Hz)

Synthesis of *S*-84-K

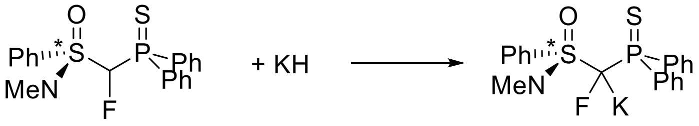

S-**84** *S*-**84-K**

403.47 g/mol 40.11 g/mol 441.56 g/mol

23.1 mg (0.0572 mmol) of *S*-**84** were dissolved in 1 mL THF and cooled to 0 °C. Subsequently, *S*-**84** was cannula transferred to 7 mg (0.172 mmol) of KH and the reaction mixture was stirred at 0 °C for 2 h. The residual amount of KH was filtered off and the filtrate was dried at 0 °C. The product was obtained as a slightly yellow solid in 92 % (23.3 mg, 0.053 mmol). The product was NMR spectroscopically characterized at –30 °C.

^{1}H NMR (400.3 MHz, d$_8$-THF): δ_H = 2.71 (s, 3H; NCH_3), 7.04 – 7.07 (m, 2H, C$_{arom.}$); 7.11 – 7.19 (m, 4H; C$_{arom.}$), 7.25 – 7.27 (m, 3H, C$_{arom.}$), 7.58 – 7.63 (m, 2H, C$_{arom.}$), 7.72 – 7.72 (d, 2H, C$_{arom.}$), 7.87 – 7.92 m, 2H, C$_{arom.}$)

^{13}C{^{1}H} NMR (100.7 MHz, d$_8$-THF): δ_C = 30.5 (s, N*C*H$_3$), 111.6 (dd, $^1J_{CP}$ = 53.9 Hz; $^1J_{CF}$ = 190.3 Hz *C*F), 127.9 (d, $^3J_{CP}$ = 11.7 Hz; *PC*$_{Ph,\ meta}$), 128.2 (s, S*C*$_{Ph}$), 128.3 (d, $^4J_{CP}$ = 5.8 Hz; *PC*$_{Ph,para}$), 128.3 (s, S*C*$_{Ph}$), 129.8 (s, S*C*$_{Ph,\ para}$), 129.8 (d, $^3J_{CP}$ = 19.2 Hz; *PC*$_{Ph,\ meta}$), 130.3 (s, *SC*$_{Ph,\ para}$), 132.8 (d, $^2J_{CP}$ = 8.1 Hz; *PC*$_{Ph,\ ortho}$), 132.7 (d , $^2J_{CP}$ = 9.1 Hz; *PC*$_{Ph,\ ortho}$), 137.30 (d, $^1J_{CP}$ = 80.5Hz; *PC*$_{Ph,\ ipso}$), 140.0 (d, $^1J_{CP}$ = 94.2 Hz; *PC*$_{Ph,\ ipso}$), 145.7 (s, S*C*$_{Ph,\ ipso}$)

^{31}P{^{1}H} NMR (162.1 MHz, d$_8$-THF): δ_P = 34.4 (d, $^2J_{PF}$ = 44.3 Hz)

^{19}F{^{1}H} NMR (235.31 MHz, d$_8$-THF): δ_F = -210.4 (dd, $^2J_{FP}$ = 44.7 Hz, J = 13.3Hz)

DOSY NMR Spectroscopy

General procedure of the sample preparation for DOSY NMR spectroscopic measurements.

All carbenoids were prepared according to the synthesis stated above.

Measurements in toluene:
4 mg (0.03 mmol) adamantane were added to a J. Young NMR tube and the NMR tube was evaporated and flushed with Ar three times. 0.6 mL cooled (–40 °C) d_8-Tol was added to the cooled (–40 °C) Schlenk flask containing the respective carbenoid. The carbenoid was dissolved in d_8-Tol and subsequently transferred to the J. Young NMR tube *via* a syringe under Ar. The J. Young NMR tube is cooled to –40 °C and the sample is kept at that temperature while transferring it to the NMR instrument.

Measurements in THF:
A J. Young NMR tube is evaporated and flushed with Ar three times. The d_8-THF is cooled to –40 °C and then 0.6 mL d_8-THF are added to the cooled (–40 °C) Schlenk flask containing the carbenoid. The J. Young NMR tube is placed in a cooling bath at –40 °C and the d_8-THF solution is transferred to the J. Young NMR tube. Then 4 µL TMS (0.03 mmol) are added to the J. Young tube under Ar. The sample is kept at –40 °C while transferring it to the NMR instrument.

NMR instrument:
The NMR instrument is cooled to –30 °C previous to the injection of the sample to prevent sample decomposition. The DOSY NMR spectra are recorded at -30 °C -10 °C and 27 °C, respectively. The instrument is warmed up to the respective temperature manually.

DOSY NMR data of *rac*-83-Li in d$_8$-THF

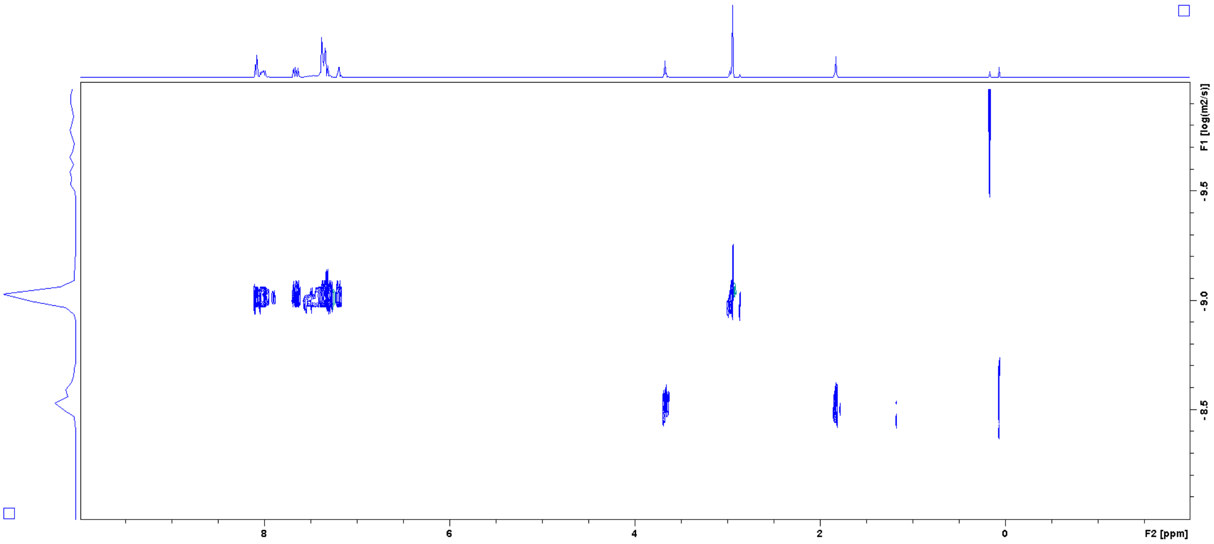

Figure 50. ^{1}H DOSY NMR spectrum for *rac*-**83-Li** in d$_8$-THF at 27 °C.

Table 13. ^{1}H DOSY NMR data for *rac*-**83-Li** at 27 °C in d$_8$THF.

Solvent	Int. reference	D_{ref} [m^2s^{-1}]	$logD_{ref}$	Ø $logD_{Carb}$	MW_{DOSY} [g/mol]	MW_{calc} [g/mol]	Species	Error [%]
THF	TMS	2.21E-9	-8.67	-9.05	464	497.96	Monomer +1THF	-8

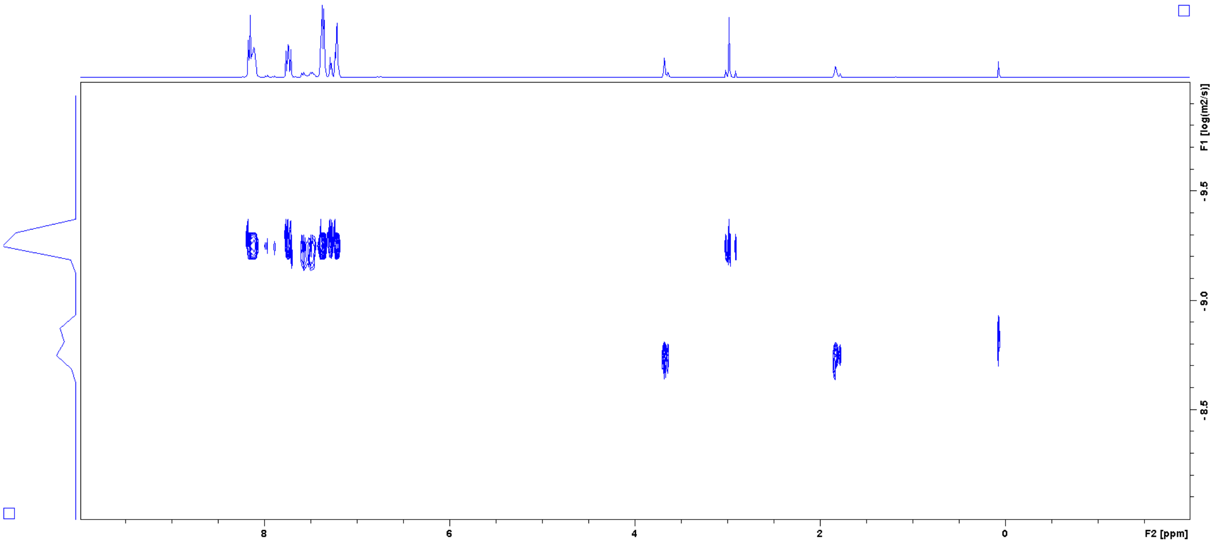

Figure 51. ^{1}H DOSY NMR spectrum for *rac*-**83-Li** in d$_8$-THF at –10 °C.

Table 14. ^{1}H DOSY NMR data for *rac*-**83-Li** at –10 °C in d$_8$THF.

Solvent	Int. reference	D_{ref} [m^2s^{-1}]	$logD_{ref}$	Ø $logD_{Carb}$	MW_{DOSY} [g/mol]	MW_{calc} [g/mol]	Species	Error [%]
THF	TMS	1.28E-9	-8.89	-9.33	554	570.07	Monomer + 2 THF	-3

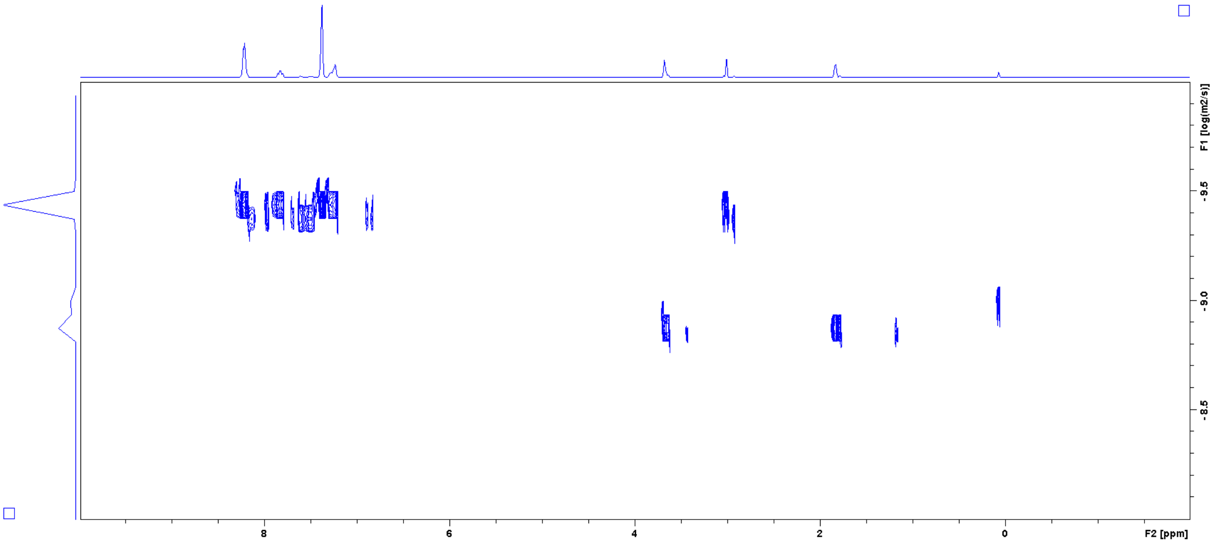

Figure 52. ^{1}H DOSY NMR spectrum for *rac*-**83-Li** in d$_8$-THF at –10 °C.

Table 15. ^{1}H DOSY NMR data for *rac*-**83-Li** at –30 °C in d$_8$THF.

Solvent	Int. reference	D_{ref} [m^2s^{-1}]	$logD_{ref}$	Ø $logD_{Carb}$	MW_{DOSY} [g/mol]	MW_{calc} [g/mol]	Species	Error [%]
THF	TMS	8.75E-10	-9.06	-9.51	600	606.13	Monomer + 2/3 THF	-1

DOSY NMR data of *rac*-83-Li in d_8-Tol

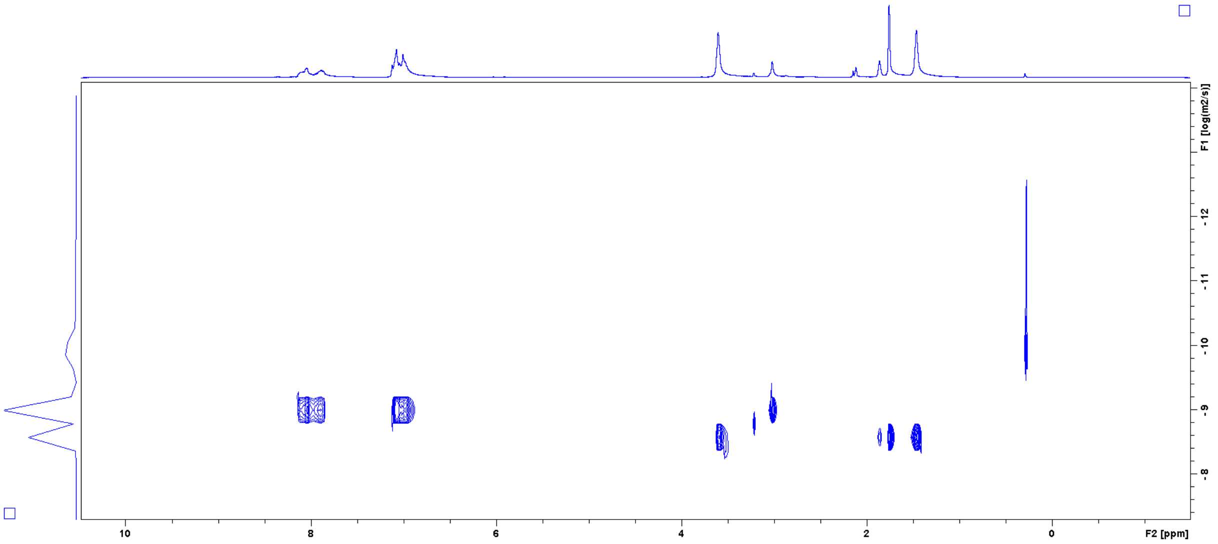

Figure 53. ^{1}H DOSY NMR spectrum for *rac*-**83-Li** in d_8-Tol at 27 °C.

Table 16. ^{1}H DOSY NMR data for *rac*-**83-Li** at 27 °C in d_8Tol.

Solvent	Int. reference	ØD$_{ref}$ [m^{2}s^{-1}]	ØlogD$_{ref}$	Ø logD$_{Carb}$	MW$_{DOSY}$ [g/mol]	MW$_{calc}$ [g/mol]	Species	Error [%]
Tol	Adam	1.69E-9	-8.77	-9.25	904	887.76	Dimer + 0/1 THF	+2

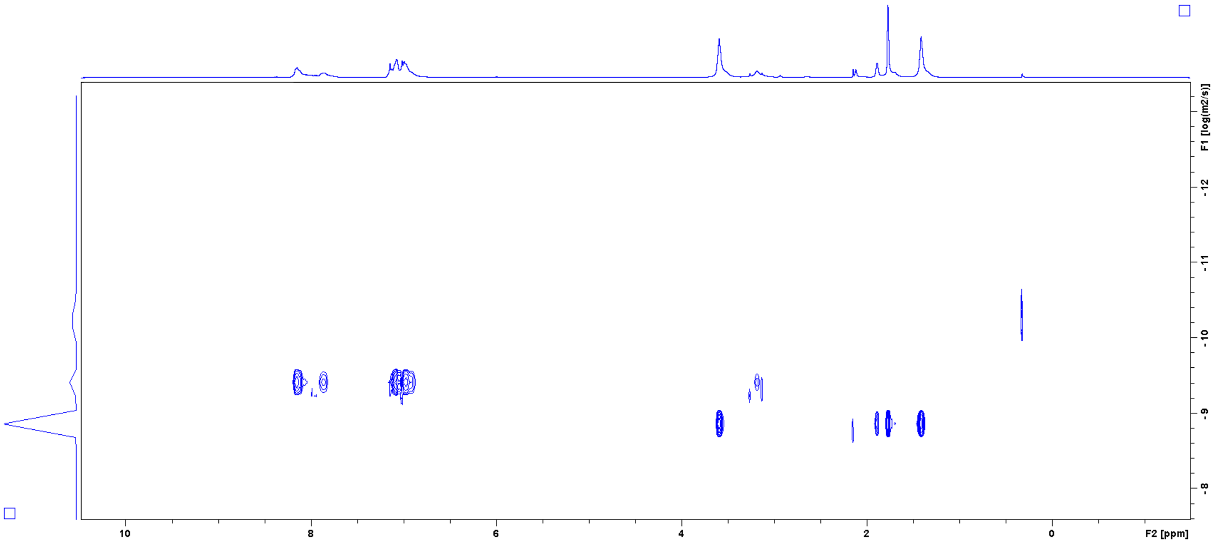

Figure 54. ^{1}H DOSY NMR spectrum for *rac*-**83-Li** in d_8-Tol at –10 °C.

Table 17. ^{1}H DOSY NMR data for *rac*-**83-Li** at –10 °C in d$_8$Tol.

Solvent	Int. reference	ØD$_{ref}$ [m^{2}s^{-1}]	ØlogD$_{ref}$	Ø logD$_{Carb}$	MW$_{DOSY}$ [g/mol]	MW$_{calc}$ [g/mol]	Species	Error [%]
Tol	Adam	8.62E-10	-9.06	-9.58	1051	1031.98	Dimer + 2/3 THF	+2

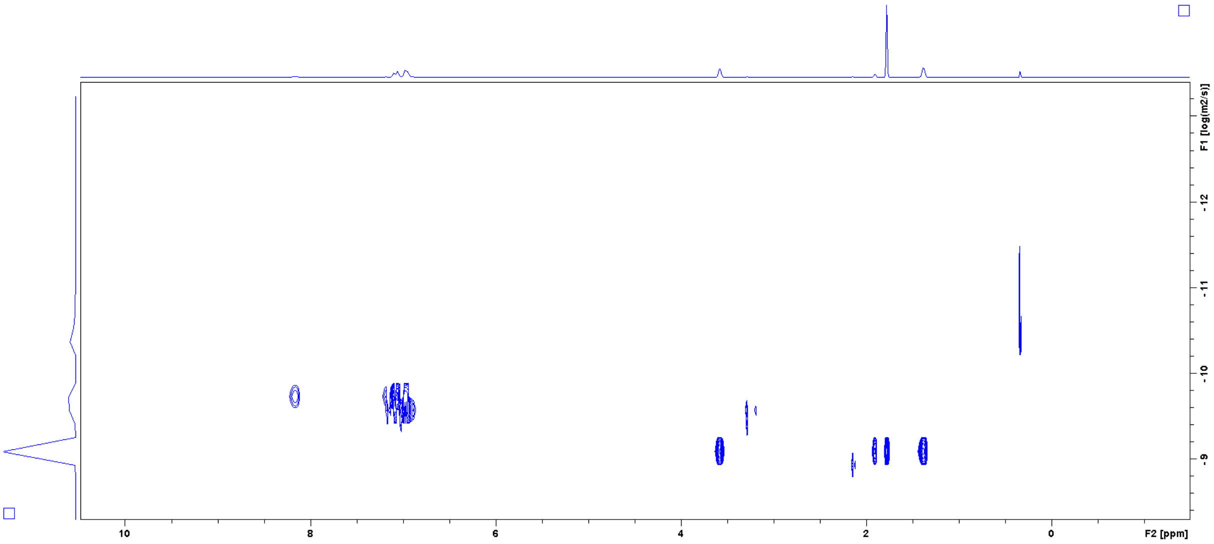

Figure 55. ^{1}H DOSY NMR spectrum for *rac*-**83-Li** in d$_8$-Tol at –30 °C.

Table 18. ^{1}H DOSY NMR data for *rac*-**83-Li** at –30 °C in d$_8$Tol.

Solvent	Int. reference	ØD$_{ref}$ [m^{2}s^{-1}]	ØlogD$_{ref}$	Ø logD$_{Carb}$	MW$_{DOSY}$ [g/mol]	MW$_{calc}$ [g/mol]	Species	Error [%]
Tol	Adam	5.36E-10	-9.27	-9.78	1025	1031.98	Dimer + 2/3 THF	-1

DOSY NMR Data of *rac*-83-Na in d_8-THF

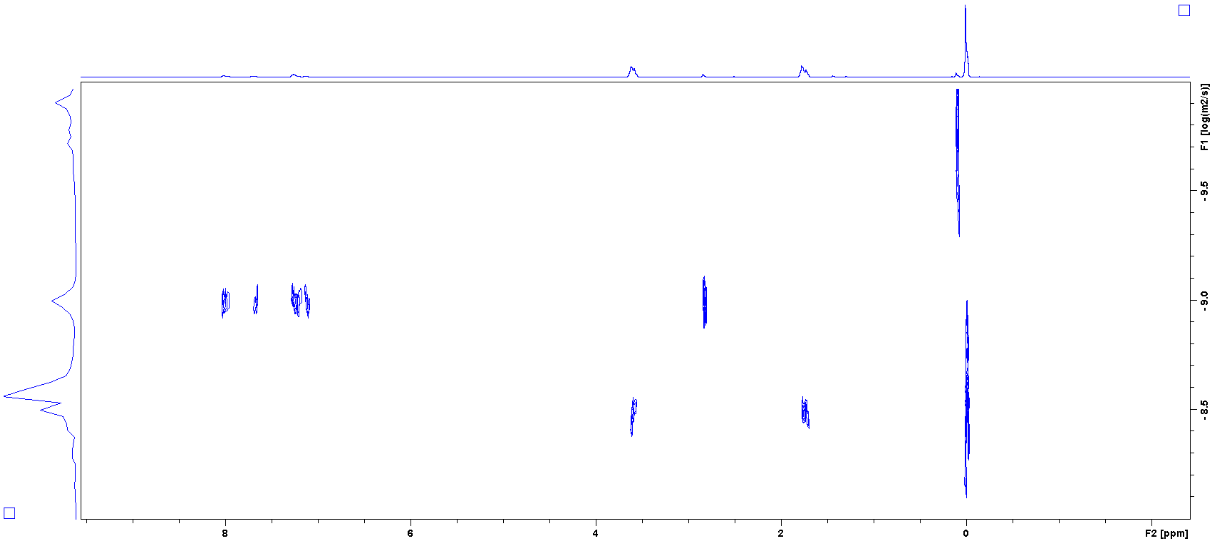

Figure 56. ^{1}H DOSY NMR spectrum for *rac*-**83-Na** in d_8-THF at 27 °C.

Table 19. 1H DOSY NMR data for *rac*-**83-Na** at 27 °C in d_8THF.

Solvent	Int. reference	D_{ref} [m^2s^{-1}]	$logD_{ref}$	Ø $logD_{Carb}$	MW_{DOSY} [g/mol]	MW_{calc} [g/mol]	Species	Error [%]
THF	TMS	2.33E-9	-8.63	-9.03	471	477.96	Monomer + 0/1 THF	-2

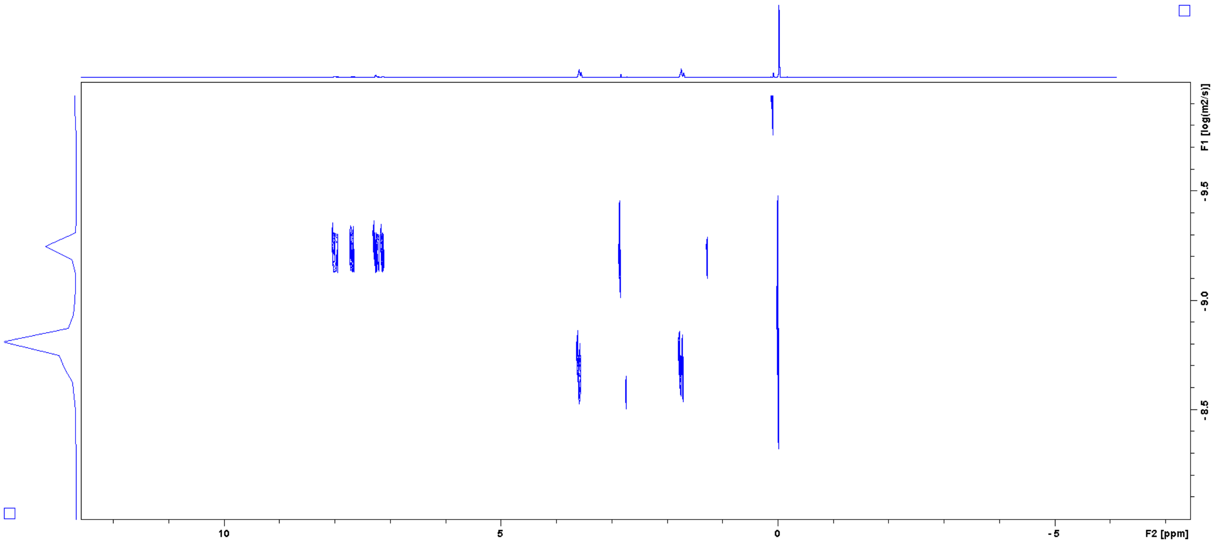

Figure 57. ^{1}H DOSY NMR spectrum for *rac*-**83-Na** in d_8-THF at –10 °C.

Table 20. 1H DOSY NMR data for *rac*-**83-Na** at –10 °C in d$_8$THF.

Solvent	Int. reference	D$_{ref}$ [m^{2}s^{-1}]	logD$_{ref}$	Ø logD$_{Carb}$	MW$_{DOSY}$ [g/mol]	MW$_{calc}$ [g/mol]	Species	Error [%]
THF	TMS	1.44E-9	-8.84	-9.30	595	586.12	Monomer + 2THF	+2

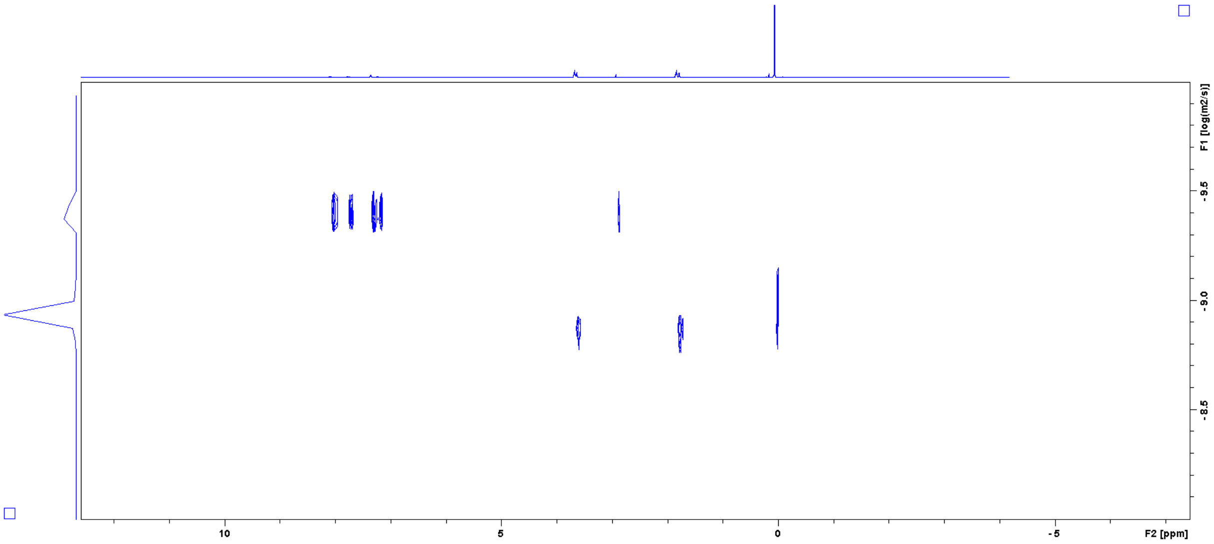

Figure 58. ^{1}H DOSY NMR spectrum for *rac*-**83-Na** in d$_8$-THF at –30 °C.

Table 21. ^{1}H DOSY NMR data for *rac*-**83-Na** at –30 °C in d$_8$THF.

Solvent	Int. reference	D$_{ref}$ [m^{2}s^{-1}]	logD$_{ref}$	Ø logD$_{Carb}$	MW$_{DOSY}$ [g/mol]	MW$_{calc}$ [g/mol]	Species	Error [%]
THF	TMS	1.01E-9	-8.99	-9.41	683	658.23	Monomer + 3THF	+4

DOSY NMR data of *rac*-83-Na in d_8-Tol

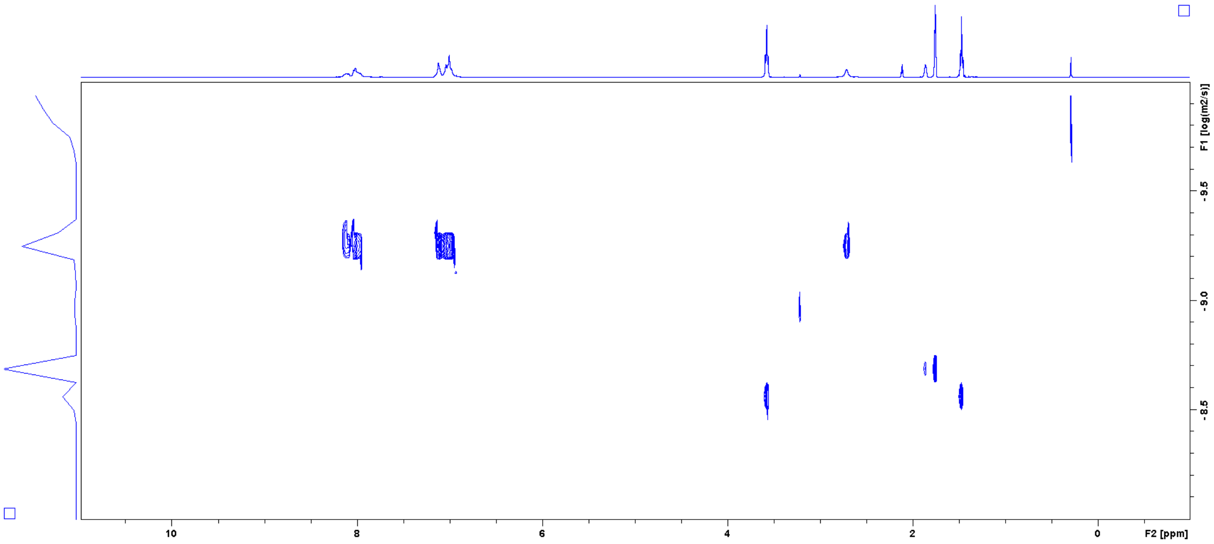

Figure 59. ^{1}H DOSY NMR spectrum for *rac*-**83-Na** in d_8-Tol at 27 °C.

Table 22. ^{1}H DOSY NMR data for *rac*-**83-Na** at 27 °C in d_8Tol.

Solvent	Int. reference	$\varnothing D_{ref}$ [m^2s^{-1}]	$\varnothing logD_{ref}$	$\varnothing$ $logD_{Carb}$	MW_{DOSY} [g/mol]	MW_{calc} [g/mol]	Species	Error [%]
Tol	Adam	1.80E-9	-8.75	-9.33	1330	1316.46	Dimer + 6THF	+2
						1325.70	Trimer	+1

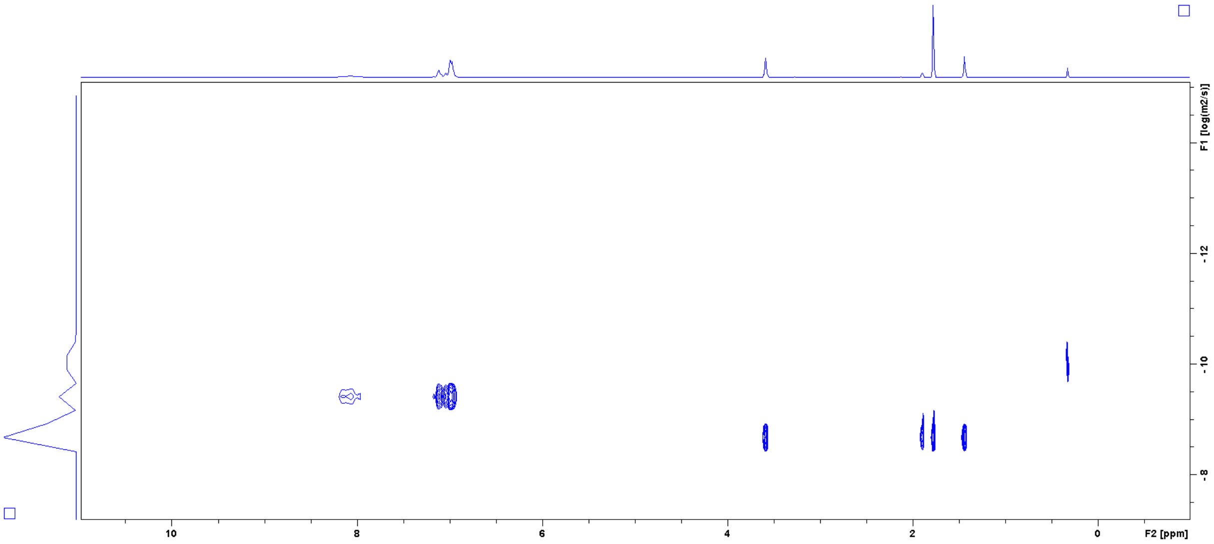

Figure 60. ^{1}H DOSY NMR spectrum for *rac*-**83-Na** in d_8-Tol at –10 °C.

Table 23. ^{1}H DOSY NMR data for *rac*-**83-Na** at –10 °C in d$_8$Tol.

Solvent	Int. reference	ØD$_{\mathrm{ref}}$ [m^{2}s^{-1}]	ØlogD$_{\mathrm{ref}}$	Ø logD$_{\mathrm{Carb}}$	MW$_{\mathrm{DOSY}}$ [g/mol]	MW$_{\mathrm{calc}}$ [g/mol]	Species	Error [%]
Tol	Adam	9.14E-10	-9.04	-9.62	1312	1316.46	Dimer + 6THF	-1
						1325.70	Trimer	-2

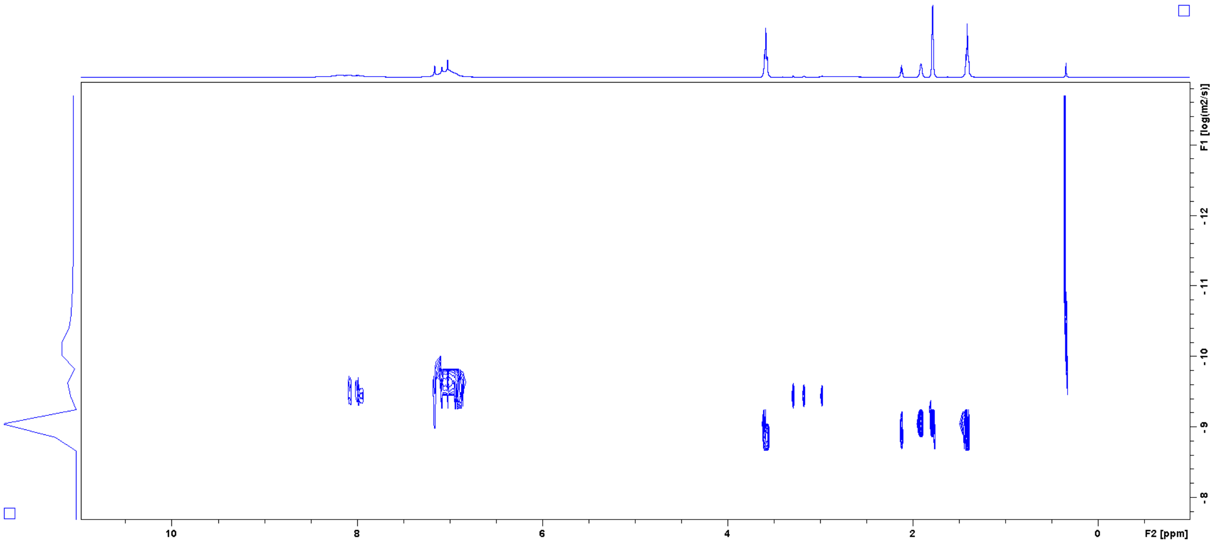

Figure 61. ^{1}H DOSY NMR spectrum for *rac*-**83-Na** in d$_8$-Tol at –30 °C.

Table 24. ^{1}H DOSY NMR data for *rac*-**83-Na** at –30 °C in d$_8$Tol.

Solvent	Int. reference	ØD$_{\mathrm{ref}}$ [m^{2}s^{-1}]	ØlogD$_{\mathrm{ref}}$	Ø logD$_{\mathrm{Carb}}$	MW$_{\mathrm{DOSY}}$ [g/mol]	MW$_{\mathrm{calc}}$ [g/mol]	Species	Error [%]
Tol	Adam	9.53E-10	-9.26	-9.81	1195	1172.24	Dimer + 4THF	+2

DOSY NMR data of *rac*-83-K in d$_8$-THF

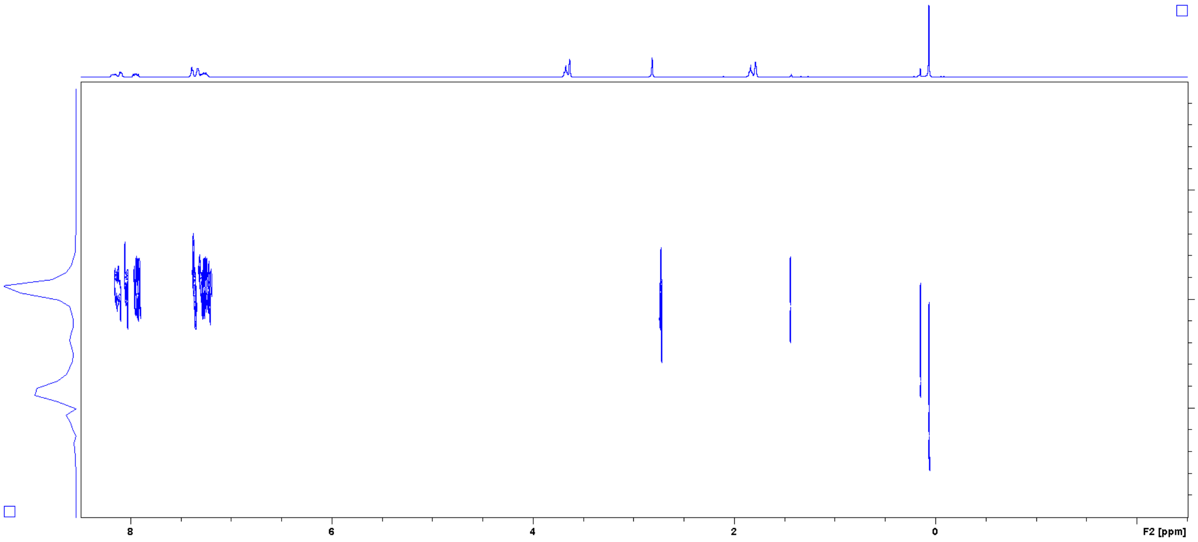

Figure 62. ^{1}H DOSY NMR spectrum for *rac*-**83-K** in d$_8$-THF at 27 °C.

Table 25. ^{1}H DOSY NMR data for *rac*-**83-K** at 27 °C in d$_8$THF.

Solvent	Int. reference	D$_{ref}$ [m^{2}s^{-1}]	logD$_{ref}$	Ø logD$_{Carb}$	MW$_{DOSY}$ [g/mol]	MW$_{calc}$ [g/mol]	Species	Error [%]
THF	TMS	2.17E-9	-8.66	-9.083	521	530.12	Monomer + 1THF	-2

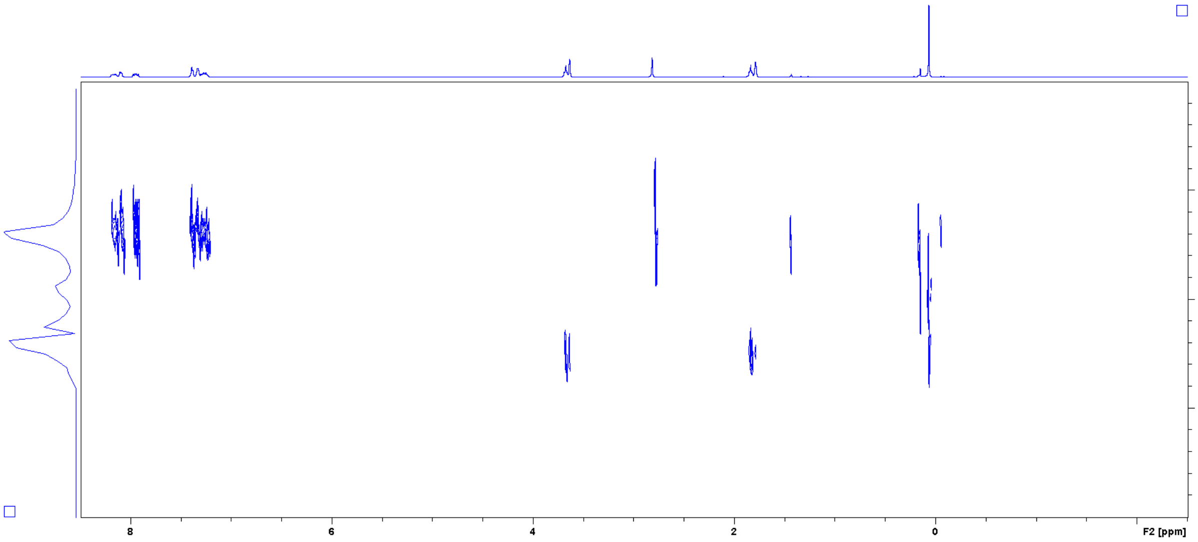

Figure 63. ^{1}H DOSY NMR spectrum for *rac*-**83-K** in d$_8$-THF at –10 °C.

Table 26. ^{1}H DOSY NMR data for *rac*-**83-K** at –10 °C in d$_8$THF.

Solvent	Int. reference	D_{ref} [m^{2}s^{-1}]	$\log D_{ref}$	Ø $\log D_{Carb}$	MW_{DOSY} [g/mol]	MW_{calc} [g/mol]	Species	Error [%]
THF	TMS	1.24E-9	-8.91	-9.34	555	566.18	Monomer + 1/2THF	-2

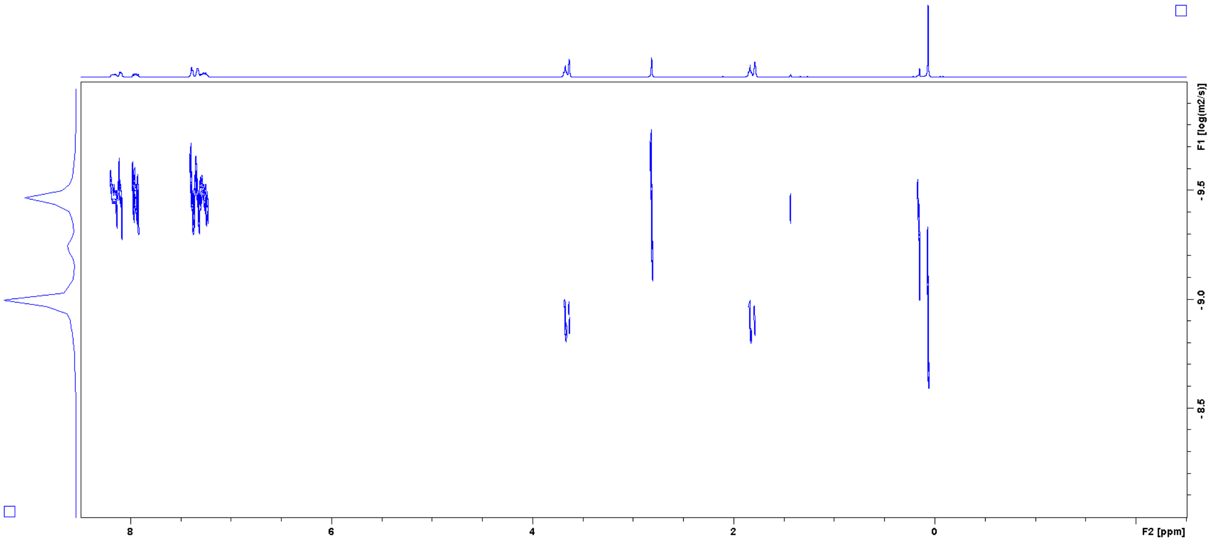

Figure 64. ^{1}H DOSY NMR spectrum for *rac*-**83-K** in d$_8$-THF at –30 °C.

Table 27. ^{1}H DOSY NMR data for *rac*-**83-K** at –30 °C in d$_8$THF.

Solvent	Int. reference	D_{ref} [m^{2}s^{-1}]	$\log D_{ref}$	Ø $\log D_{Carb}$	MW_{DOSY} [g/mol]	MW_{calc} [g/mol]	Species	Error [%]
THF	TMS	9.16E-10	-9.04	-9.51	633	638.29	Monomer + 2/3THF	-1

DOSY NMR data of *rac*-83-K in d_8-Tol

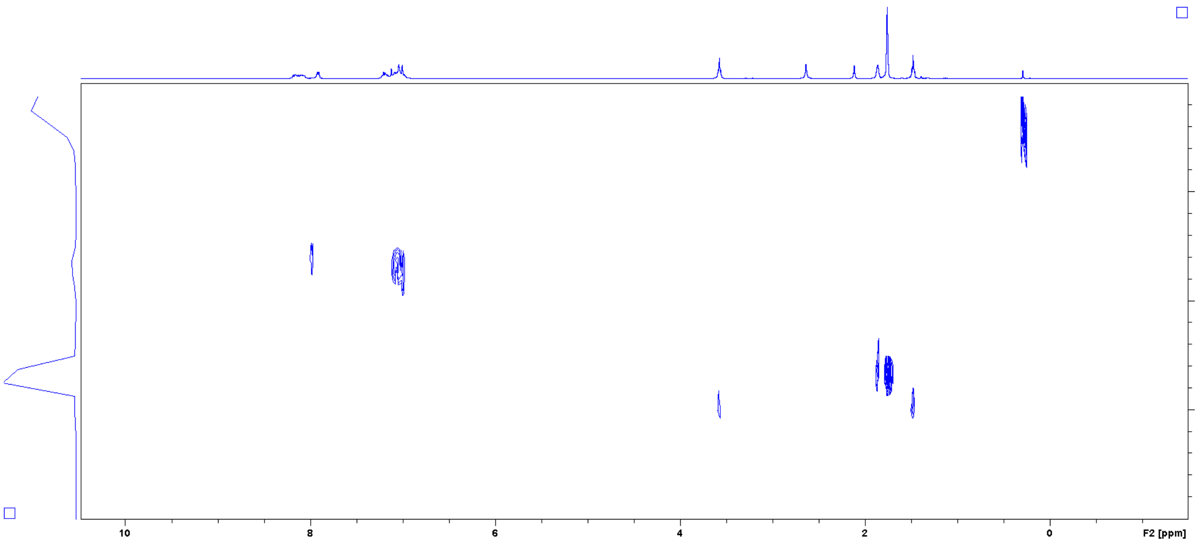

Figure 65. ^{1}H DOSY NMR spectrum for *rac*-**83-K** in d_8-Tol at 27 °C.

Table 28. ^{1}H DOSY NMR data for *rac*-**83-K** at 27 °C in d_8Tol.

Solvent	Int. reference	ØD$_{ref}$ [m^{2}s^{-1}]	ØlogD$_{ref}$	Ø logD$_{Carb}$	MW$_{DOSY}$ [g/mol]	MW$_{calc}$ [g/mol]	Species	Error [%]
Tol	Adam	1.71E-9	-8.77	-9.31	1135	1132.35	Dimer + 3THF	+1

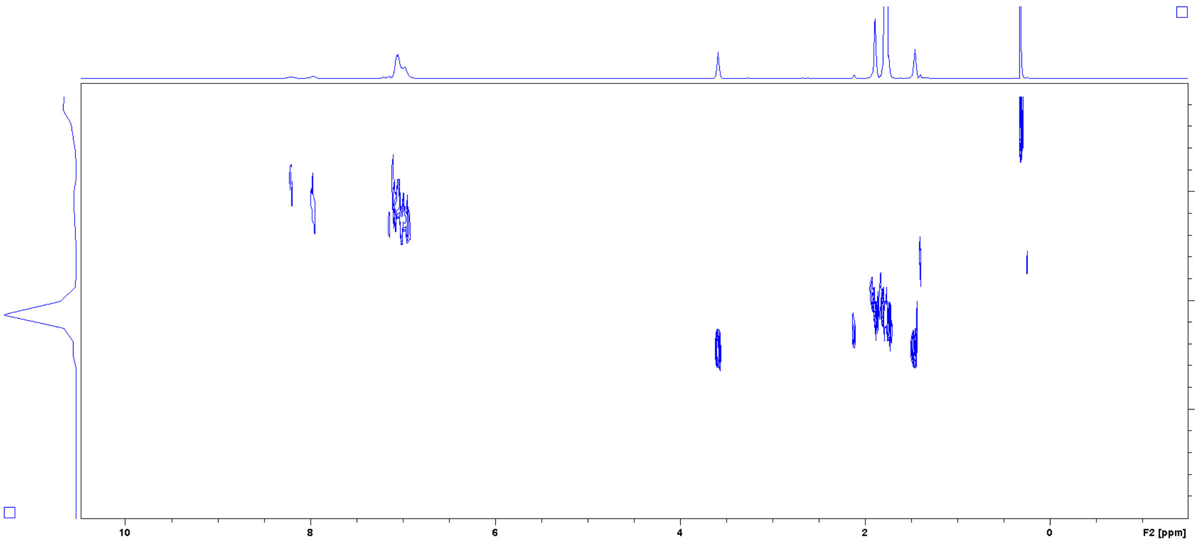

Figure 66. ^{1}H DOSY NMR spectrum for *rac*-**83-K** in d_8-Tol at –10 °C.

Table 29. ^{1}H DOSY NMR data for *rac*-**83-K** at –10 °C in d$_8$Tol.

Solvent	Int. reference	ØD$_{ref}$ [m^{2}s^{-1}]	ØlogD$_{ref}$	Ø logD$_{Carb}$	MW$_{DOSY}$ [g/mol]	MW$_{calc}$ [g/mol]	Species	Error [%]
Tol	Adam	9.51E-9	-9.02	-9.53	1012	1060.24	Dimer + 2THF	-5

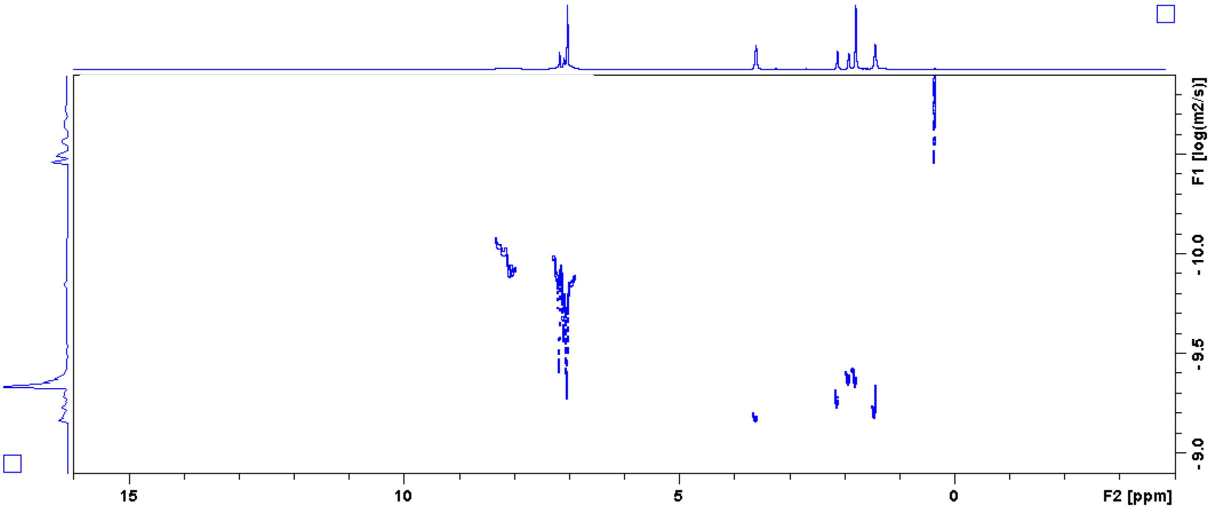

Figure 67. ^{1}H DOSY NMR spectrum for *rac*-**83-K** in d$_8$-Tol at –30 °C.

Table 30. ^{1}H DOSY NMR data for *rac*-**83-K** at –30 °C in d$_8$Tol.

Solvent	Int. reference	ØD$_{ref}$ [m^{2}s^{-1}]	ØlogD$_{ref}$	Ø logD$_{Carb}$	MW$_{DOSY}$ [g/mol]	MW$_{calc}$ [g/mol]	Species	Error [%]
Tol	Adam	4.70E-10	-9.33	-9.89	1252	1251.46	Dimer + 6THF	-1

DOSY NMR Data of *rac*-84-Li in d_8-THF

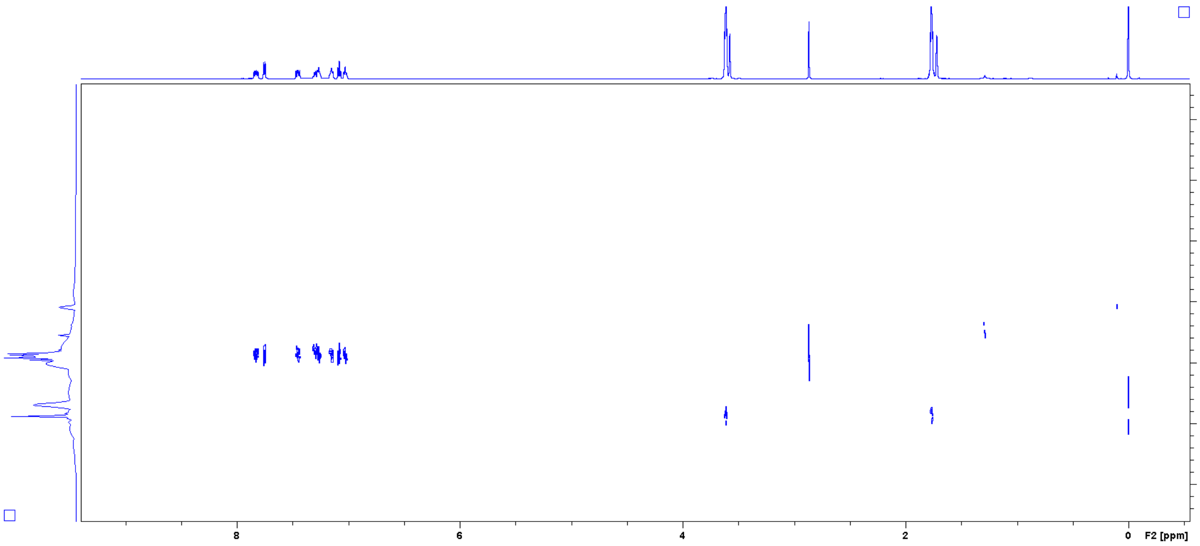

Figure 68. ^{1}H DOSY NMR spectrum for *rac*-**84-Li** in d_8-THF at 27 °C.

Table 31. ^{1}H DOSY NMR data for *rac*-**84-Li** at 27 °C in d_8THF.

Solvent	Int. reference	D_{ref} [m^2s^{-1}]	$\log D_{ref}$	Ø $\log D_{Carb}$	MW_{DOSY} [g/mol]	MW_{calc} [g/mol]	Species	Error [%]
THF	TMS	2.30E-9	-8.64	-9.07	554	553.62	Monomer + 2THF	+ 1

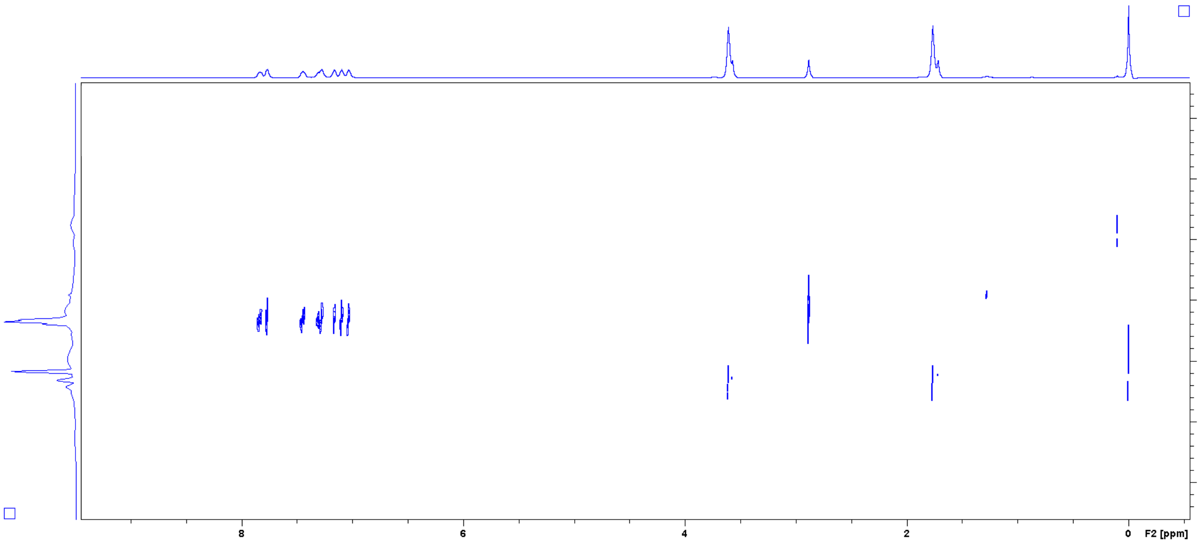

Figure 69. ^{1}H DOSY NMR spectrum for *rac*-**84-Li** in d_8-THF at –20 °C.

Table 32. ^{1}H DOSY NMR data for *rac*-**84-Li** at –10 °C in d_8THF.

Solvent	Int. reference	D_{ref} [m^2s^{-1}]	logD_{ref}	Ø logD_{Carb}	MW_{DOSY} [g/mol]	MW_{calc} [g/mol]	Species	Error [%]
THF	TMS	1.25E-10	-8.90	-9.34	550	553.62	Monomer + 2THF	- 1

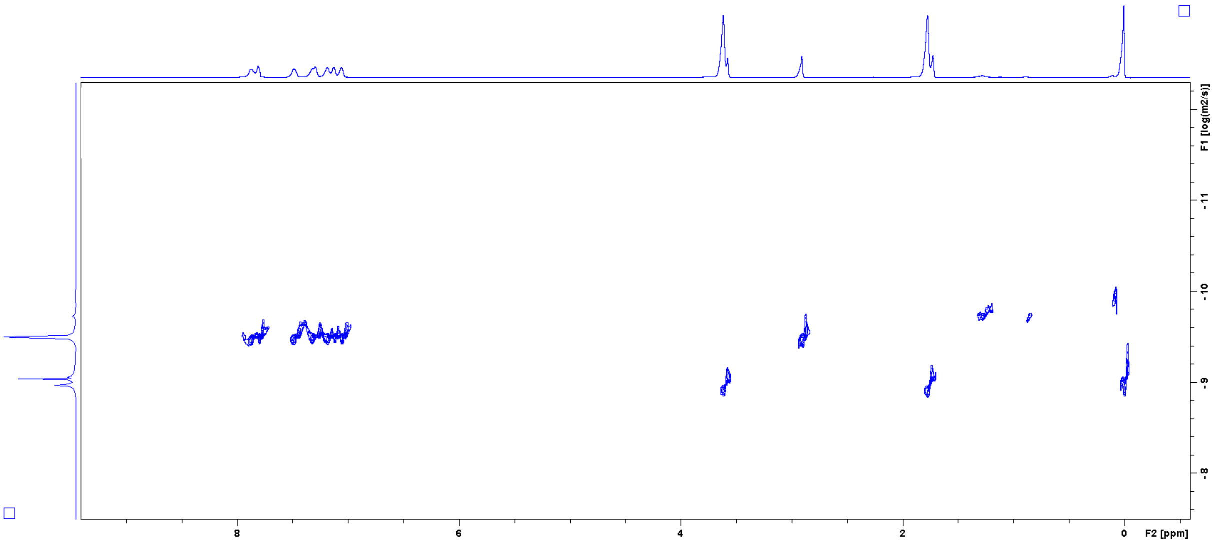

Figure 70. ^{1}H DOSY NMR spectrum for *rac*-**84-Li** in d_8-THF at –30 °C.

Table 33. ^{1}H DOSY NMR data for *rac*-**84-Li** at –30 °C in d_8THF.

Solvent	Int. reference	D_{ref} [m^2s^{-1}]	logD_{ref}	Ø logD_{Carb}	MW_{DOSY} [g/mol]	MW_{calc} [g/mol]	Species	Error [%]
THF	TMS	8.57E-10	-9.07	-9.52	588	589.68	Monomer + 2/3THF	- 1

DOSY NMR Data of *rac*-84-Li in d_8-Tol

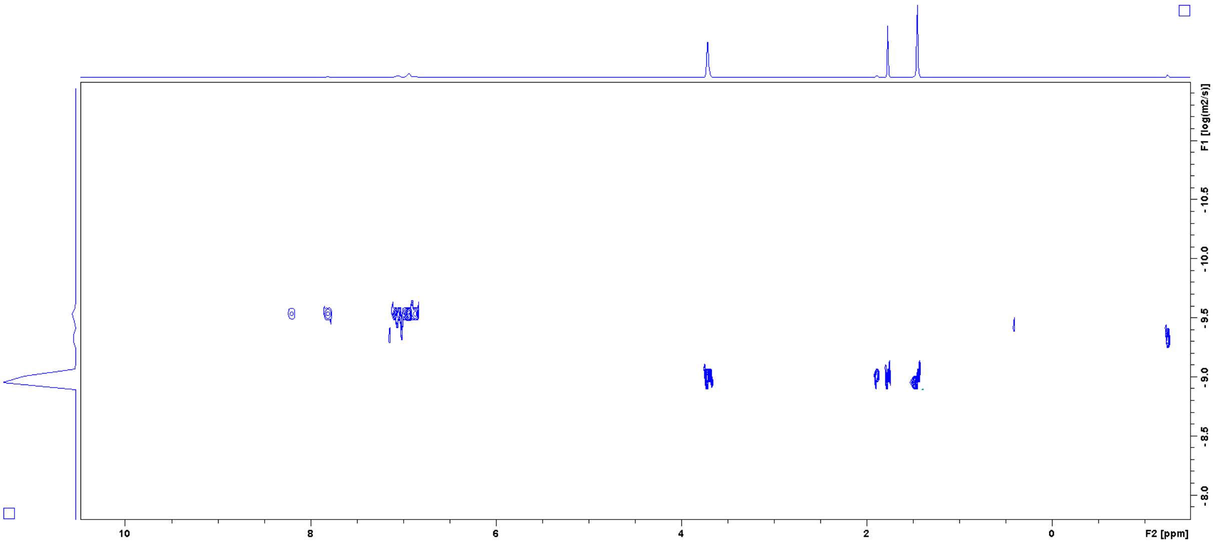

Figure 71. ^{1}H DOSY NMR spectrum for *rac*-**84-Li** in d_8-Tol at –10 °C.

Table 34. ^{1}H DOSY NMR data for *rac*-**84-Li** at –10 °C in d_8Tol.

Solvent	Int. reference	ØD_{ref} [m^2s^{-1}]	Ø$\log D_{ref}$	Ø $\log D_{Carb}$	MW_{DOSY} [g/mol]	MW_{calc} [g/mol]	Species	Error [%]
Tol	Adam	8.67E-10	-9.05	-9.55	991	999.08	Dimer + 2/3THF	- 1

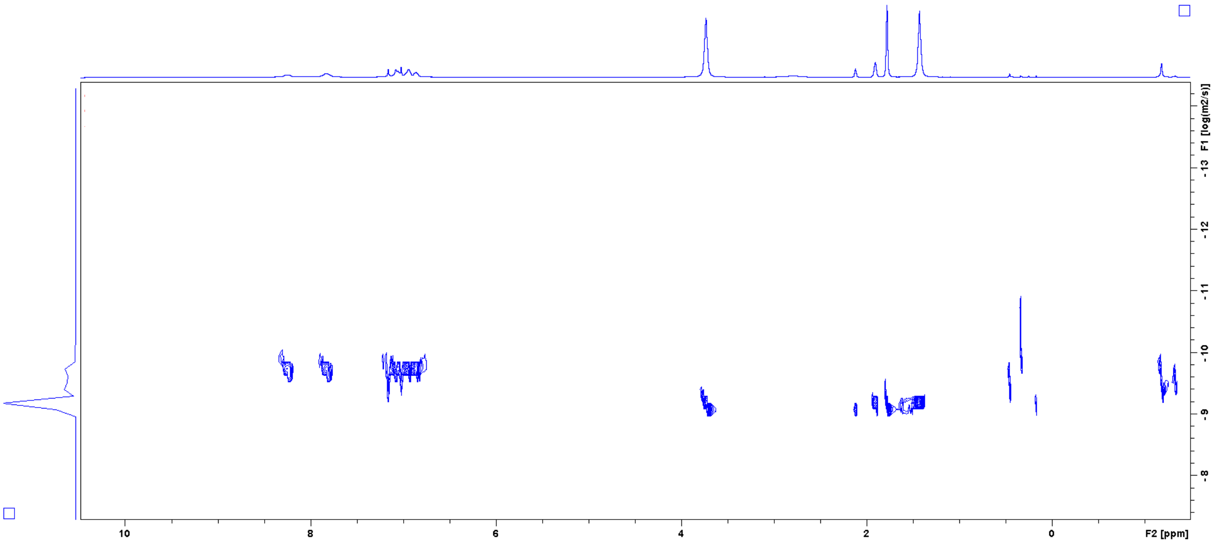

Figure 72. ^{1}H DOSY NMR spectrum for *rac*-**84-Li** in d_8-Tol at –30 °C.

Table 35. ^{1}H DOSY NMR data for *rac*-**84-Li** at –30 °C in d_8Tol.

Solvent	Int. reference	ØD$_{ref}$ [m^{2}s^{-1}]	ØlogD$_{ref}$	Ø logD$_{Carb}$	MW$_{DOSY}$ [g/mol]	MW$_{calc}$ [g/mol]	Species	Error [%]
Tol	Adam	5.19E-10	-9.26	-9.81	1193	1179.35	Dimer + 5THF	+ 2

DOSY NMR Data of *rac*-84-Na in d$_8$- THF

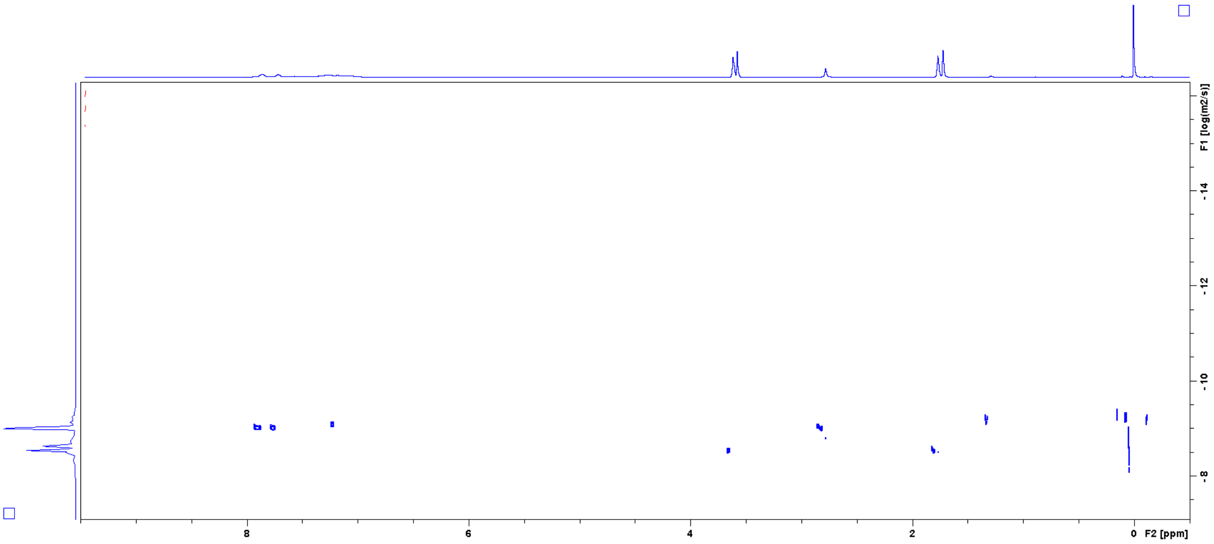

Figure 73. ^{1}H DOSY NMR spectrum for *rac*-**84-Na** in d$_8$-THF at 27 °C.

Table 36. ^{1}H DOSY NMR data for *rac*-**84-Na** at 27 °C in d$_8$THF.

Solvent	Int. reference	D_{ref} [m^{2}s^{-1}]	$\log D_{ref}$	Ø $\log D_{Carb}$	MW_{DOSY} [g/mol]	MW_{calc} [g/mol]	Species	Error [%]
THF	TMS	2.57E-9	-8.59	-9.05	611	605.73	Monomer + 2/3 THF	+ 1

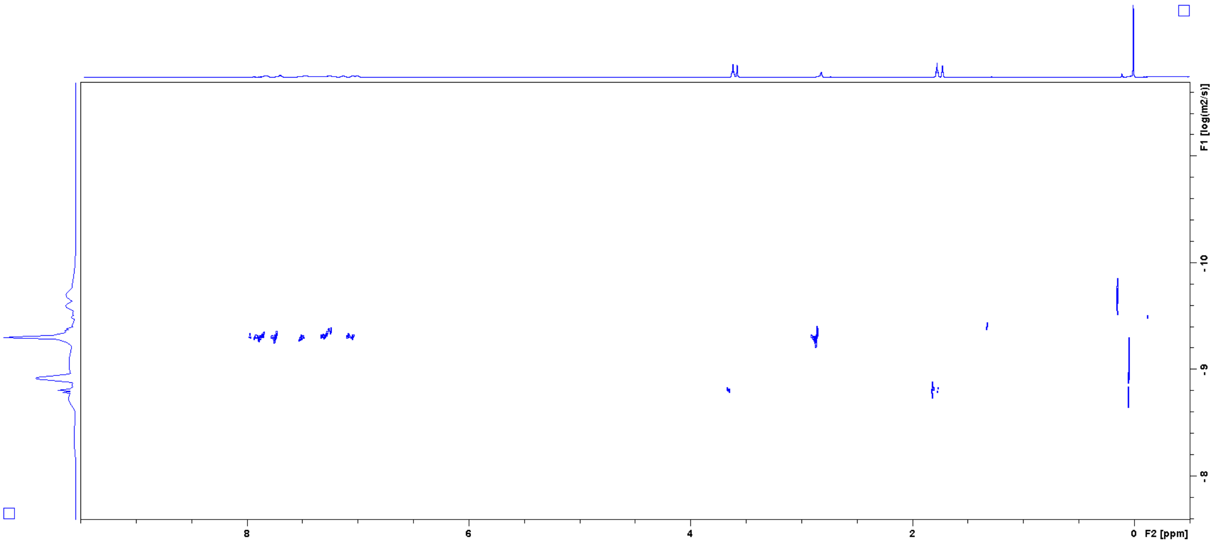

Figure 74. ^{1}H DOSY NMR spectrum for *rac*-**84-Na** in d$_8$-THF at –10 °C.

Table 37. ^{1}H DOSY NMR data for *rac*-**84-Na** at –10 °C in d_8THF.

Solvent	Int. reference	D_{ref} [m^2s^{-1}]	$\log D_{ref}$	Ø $\log D_{Carb}$	MW_{DOSY} [g/mol]	MW_{calc} [g/mol]	Species	Error [%]
THF	TMS	1.37E-9	-8.86	-9.32	606	605.73	Monomer + 2/3 THF	+ 1

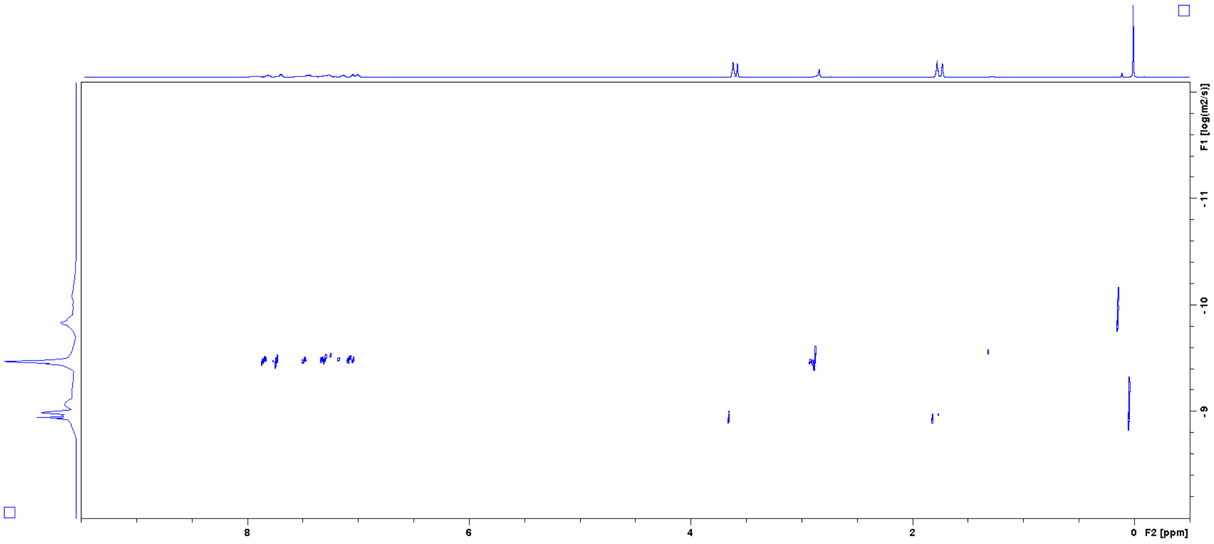

Figure 75. ^{1}H DOSY NMR spectrum for *rac*-**84-Na** in d_8-THF at –30 °C.

Table 38. ^{1}H DOSY NMR data for *rac*-**84-Na** at –30 °C in d_8THF.

Solvent	Int. reference	D_{ref} [m^2s^{-1}]	$\log D_{ref}$	Ø $\log D_{Carb}$	MW_{DOSY} [g/mol]	MW_{calc} [g/mol]	Species	Error [%]
THF	TMS	8.61E-10	-9.07	-9.50	545	533.62	Monomer + 1/2 THF	+3

DOSY NMR Data of *rac*-84-K in d_8- THF

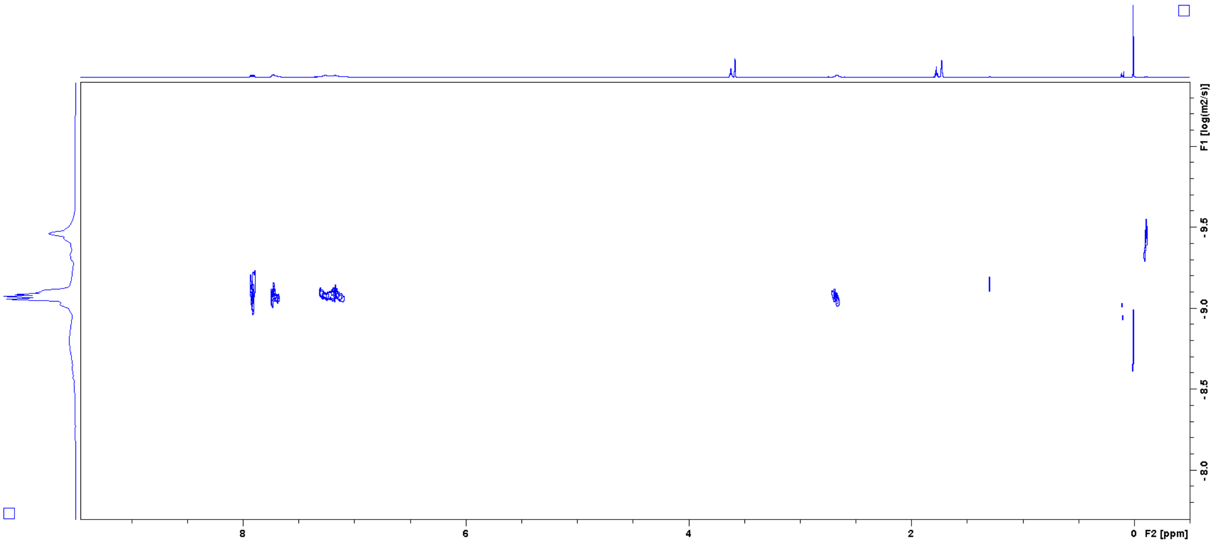

Figure 76. ^{1}H DOSY NMR spectrum for *rac*-**84-K** in d_8-THF at 27 °C.

Table 39. ^{1}H DOSY NMR data for *rac*-**84-K** at 27 °C in d_8THF.

Solvent	Int. reference	D_{ref} [m^2s^{-1}]	$logD_{ref}$	Ø $logD_{Carb}$	MW_{DOSY} [g/mol]	MW_{calc} [g/mol]	Species	Error [%]
THF	TMS	2.38E-9	-8.62	-9.07	590	585.78	Monomer + 2 THF	+ 1

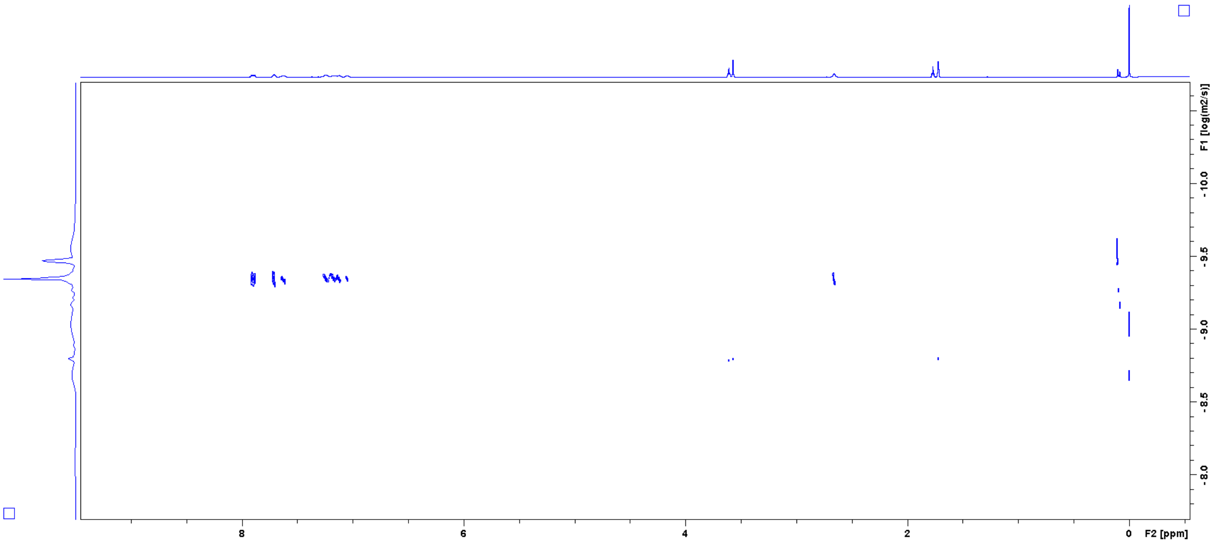

Figure 77. ^{1}H DOSY NMR spectrum for *rac*-**84-K** in d_8-THF at –10 °C.

Table 40. ^{1}H DOSY NMR data for *rac*-**84-K** at –10 °C in d_8THF.

Solvent	Int. reference	D_{ref} [m^2s^{-1}]	$logD_{ref}$	Ø $logD_{Carb}$	MW_{DOSY} [g/mol]	MW_{calc} [g/mol]	Species	Error [%]
THF	TMS	1.26E-9	-8.90	-9.35	592	585.78	Monomer + 2THF	+ 2

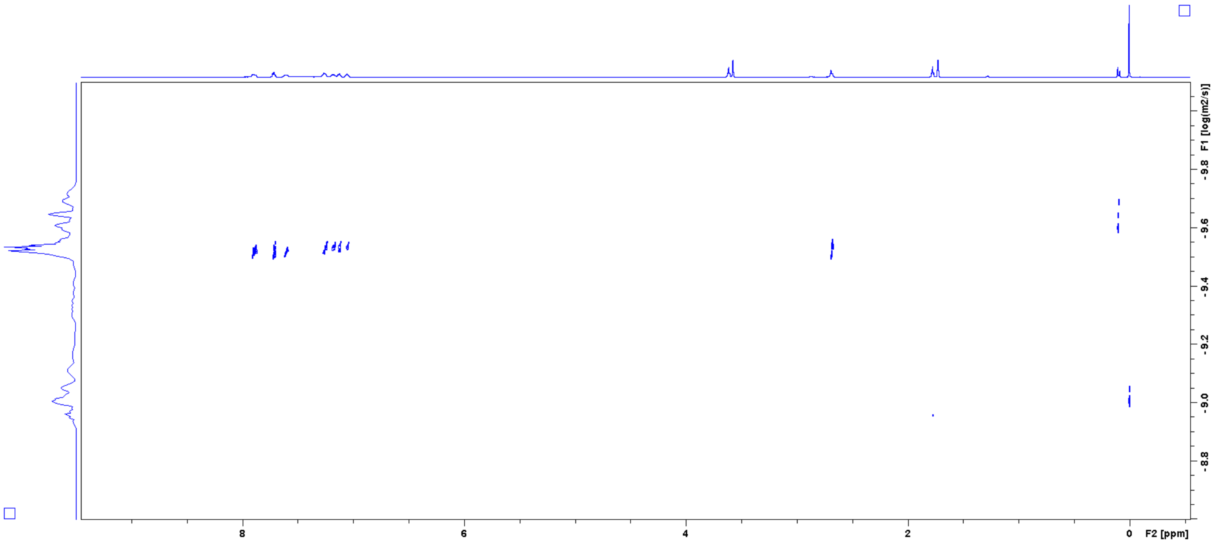

Figure 78. ^{1}H DOSY NMR spectrum for *rac*-**84-K** in d_8-THF at –30 °C.

Table 41. ^{1}H DOSY NMR data for *rac*-**84-K** at –30 °C in d_8THF.

Solvent	Int. reference	D_{ref} [m^2s^{-1}]	$logD_{ref}$	Ø $logD_{Carb}$	MW_{DOSY} [g/mol]	MW_{calc} [g/mol]	Species	Error [%]
THF	TMS	8.59E-10	-9.07	-9.53	612	621.84	Monomer + 2/3 THF	- 2

VT NMR Spectroscopy

The carbenoids were prepared according to the synthesis stated above. A J. Young NMR tube is evaporated and flushed with Ar three times and cooled to –40 °C.

For all samples exept *rac*-**84-K** in Tol: The deuterated solvent (d_8-THF or d_8-Tol) is cooled to –40 °C. 0.6 mL of cooled deuterated solvent is added to the Schlenk flask which is also cooled to –40 °C and the carbenoids were dissolved and subsequently, transferred *via* a syringe to the J. Young NMR tube.

For **84-K**: The reaction solution in THF is filtered *via* cannula to the cooled (0 °C) NMR tube and dried in vacuum at that temperature.

After removal of the protonated solvent cooled (–80 °C) d_8-Tol was added to the J. Young NMR tube which is also cooled to –80 °C. The sample is kept at this temperature while transferring it to the NMR instrument.

NMR instrument:

The NMR instrument is cooled to –30 °C previous to the injection of the sample to prevent sample decomposition. The VT NMR studies are performed in automation starting at –30 °C and incrementing the temperature by 10 °C steps with a start delay of 3515 sec. until a temperature of 50 °C is reached.

Palladium Catalyzed Cross-Coupling Reactions

General procedure using alkyllithium reagents

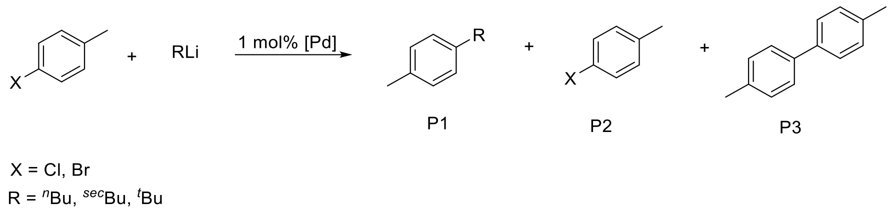

10.23 mg (0.015 mmol, 0.01eq.) of $Pd_2(dba)_3$ and 7.57 mg (0.015mmol, 0.01eq.) of **L1** were dissolved in 2 mL of toluene and stirred for 30 min at RT. 0.18 mL (1.5mmol, 1eq.) of the arylhalide were added and the reaction mixture were stirred for 10 min. 5 mL (1.8 mmol, 0.36 M in Hex/Tol, 1.2 eq.) of alkyllithium reagent were added slowly *via* a syringe pump (speed: 2.5 mL/h, d = 8mm) at RT. 3 mL of saturated NH_4Cl solution were added to the purple solution. The phases were separated and the aqueous phase was extracted with 7 mL of Et_2O four times. The organic phases were combined and dried in vacuum. The residue was dissolved in pentane and filtered through silica gel ($r_f = 0.5$). The solvent was removed to yield a colorless liquid. The NMR data of the products were in accordance with literature.[170]

Results

Table 42. Overview of the reaction conditions of the Pd catalyzed cross-coupling reactions using YPhos ligands and obtained yields determined by ^1H NMR spectroscopic data.

Pd source	Ligand	Cat. [%]	Temp [°C]	X	R	P1 [%]	P2 [%]	P3 [%]
$Pd_2(dba)_3$	L1	1	RT	Br	^{n}Bu	90	8	2
$Pd_2(dba)_3$	L1	1	RT	Cl	^{n}Bu	73	1	3
$Pd_2(dba)_3$	L1	1	RT	Cl	^{sec}Bu	70		1
$Pd_2(dba)_3$	L1	1	RT	Cl	^{t}Bu	24[a]	26	11
$Pd_2(dba)_3$	L1	1	0	Cl	^{t}Bu	-	78	-

[a] Instead of 1,1-dimethylethyl)benzene the isomerization product 4-(1-methylpropyl)toluene was observed.

Pd Catalyzed Cross-Coupling Reactions Using Carbenoids

10.23 mg (0.015 mmol, 0.01eq.) of $Pd_2(dba)_3$ and 7.57 mg (0.015mmol, 0.01eq.) of **L1** were dissolved in 2 mL of toluene and stirred for 15 min at RT. The reaction mixture was cooled to -80 °C and stirred for another 15 min. 0.18 mL (1.5mmol, 1eq.) of chlorotoluene were added and the solution was stirred for 10min at –80 °C. 0.11 mL (1.5 mmol, 1eq.) of choroiodomethane were dissolved in 7 mL of toluene and cooled to –80 °C. 1.34 mL (1.34M in Et_2O, 1.2eq.) of methyllithium were added and the yellow solution was stirred for 10 min at low temperatures. The yellow reaction solution were added to the toluene solution containing the Pd catalyst and the chlorotoluene to yield a red-brown solution. The reaction solution was allowed to warm up to RT overnight. 3 mL of a saturated NH_4Cl solution were added. The phases were separated and the aqueous phase was extracted with 6 mL Et_2O three times. The organic phases were combined and the solvent was evaporated. Pentane/EtOAc (20:1) was added to the brown residue and filtered through silica gel. No product formation was observed by NMR spectroscopy.

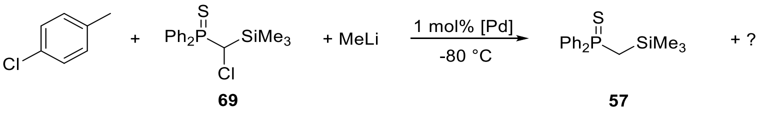

5.12 mg (0.0075mmol, 0.01eq.) of $Pd_2(dba)_3$ and 3.79 mg (0.0075 mmol, 0.01 eq.) of **L1** were dissolved in 2 mL of toluene and stirred at RT for 30 min. 304.6 mg (0.9 mmol, 1.2 eq.) of **69** were dissolved in 5 mL of toluene and cooled to –80 °C. 0.67 mL (0.9 mmol, 1.34M in Et_2O, 1.2 eq.) of MeLi were added slowly to **69**. The resulting yellow solution was stirred at low temperatures (< –55 °C) for 30 min. 0.09 mL (0.75mmol, 1eq.) of chlorotoluene were added to the catalyst containing solution. The reaction mixture was stirred for 10 min at RT. The yellow reaction solution of **69** and MeLi was added over 15 min. The reaction mixture was stirred overnight at RT. 2 mL of a saturated NH_4Cl solution was added to the reaction suspension. The phases were separated and the aqueous phase was extracted with Et_2O three times. The solvent of the combined organic phases were evaporated. The resulting residue was dissolved in pentane/ethylacetate and filtered through silica gel. The solvent was evaporated. The only product that was identified by NMR spectroscopy was **57**.

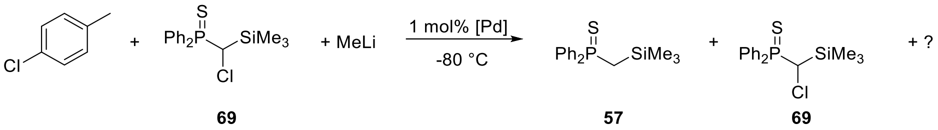

5.03 mg (0.00738 mmol, 0.01 eq)) of $Pd_2(dba)_3$ and 3.72 mg (0.00738 mmol, 0.01eq.) of **L1** were dissolved in 2 mL of toluene in a schlenk tube and stirred at RT for 30 min. 0.087 mL (0.738 mmol, 1eq.) of chlorotoluene were added to the reaction solution and stirred for another 10 min at RT. 300 mg of **69** (0.886 1.2eq.) were dissolved in 5 mL of toluene and cooled to –80 °C. 0.66 mL (1.34M in Et_2O, 1.2 eq.) of MeLi were added to **69**. This reaction mixture was added to the catalyst containing reaction solution at –80 °C. The red reaction solution was allowed to warm up to RT slowly overnight. 2 mL of a saturated NH_4Cl solution was added to the reaction solution. The phases were separated and the aqueous phase was extracted with 5 mL Et_2O three times. The combined organic phases were dried over Na_2SO_4 and the solvent was evaporated in vacuum. The reaction mixture was purified by column chromatography (pentane:ethylacetate 1:0.2). The species **57** and **69** were identified by NMR spectroscopy.

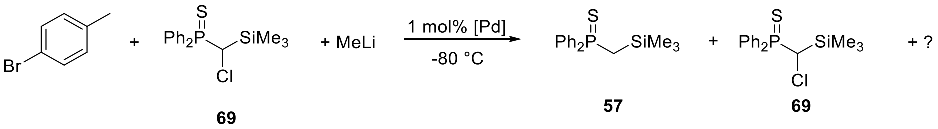

5.08 mg (0.00746 mmol, 0.01 eq) of $Pd_2(dba)_3$ and 3.76 mg (0.00746 mmol, 0.01eq.) of **L1** were dissolved in 5 mL toluene in a schlenk tube and stirred at RT for 30 min. 0.09 mL (0.74 mmol, 1eq.) of bromotoluene were added to the reaction solution and stirred for another 10 min at RT. 303 mg of **69** (0.895 1.2eq.) were dissolved in 5 mL of toluene and cooled to –80 °C. 0.67 mL (1.34M in Et_2O, 1.2 eq.) of MeLi were added to **69**. This mixture was stirred at –80 °C for 30 min. The reaction mixture containing the catalyst and the bromotoluene was added to the mixture of **69** and MeLi at -80 °C *via* a syringe pump (speed 2.1 mL/h, d = 8 mm). The red-brown solution was allowed to warm up to RT overnight. 3 mL of saturated NH_4Cl were added and the phases were separated. The aqueous phase was extracted with 3 mL of Et_2O three times. The combined organic phases were dried in vacuum and the reaction mixture was purified by column chromatography (Solvent gradient pentane : ethylacetate 100:1 → pentane: ethylacetate 0:1). The species **57** and **69** were identified by NMR spectroscopy.

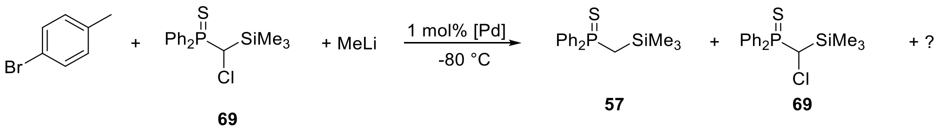

5.08 mg (0.00746 mmol, 0.01 eq) of $Pd_2(dba)_3$ and 3.76 mg (0.00746 mmol, 0.01eq.) of **L1** were dissolved in 5 mL toluene in a Schlenk tube and stirred at RT for 30 min. 303 mg of **69** (0.895 mmol, 1.2eq.) were dissolved in 5 mL of toluene and cooled to –80 °C. 0.67 mL (1.34M in Et_2O, 1.2 eq.) of MeLi were added to **69**. This mixture was stirred at –80 °C for 15 min. 0.09 mL (0.74 mmol, 1eq.) of bromotoluene were added to the reaction solution of **69** and MeLi and stirred for another 10 min at –80 °C. The catalyst containing solution was added to the other reaction solution at –80 °C *via* a syringe pump (speed 2.1 ml/h, d = 8mm). The red-brown solution was allowed to warm up slowly overnight and was quenched by addition of 3 mL of a saturated NH_4Cl solution. The phases were separated and the aqueous phase was extracted with 3 mL Et_2O three times. The solvent of the combined organic phases was evaporated. The product mixture was obtained as a brown oil. The species **57** and **69** were identified by NMR spectroscopy

References

[1] H. E. Simmons, R. D. Smith, *J. Am. Chem. Soc.* **1958**, *80*, 5323-5324.

[2] G. L. Closs, L. E. Closs, *Angew. Chem.* **1962**, *74*, 431-431.

[3] G. L. Closs, R. A. Moss, *J. Am. Chem. Soc.* **1964**, *86*, 4042-4053.

[4] a) M. Pasco, N. Gilboa, T. Mejuch, I. Marek, *Organometallics* **2013**, *32*, 942-950; b) V. Capriati, S. Florio, *Chem. Eur. J.* **2010**, *16*, 4152-4162; c) H. Lebel, J.-F. Marcoux, C. Molinaro, A. B. Charette, *Chem. Rev.* **2003**, *103*, 977-1050.

[5] A. Igau, H. Grutzmacher, A. Baceiredo, G. Bertrand, *J. Am. Chem. Soc.* **1988**, *110*, 6463-6466.

[6] A. J. Arduengo, III, R. L. Harlow, M. Kline, *J. Am. Chem. Soc.* **1991**, *113*, 361-363.

[7] V. Lavallo, Y. Canac, C. Präsang, B. Donnadieu, G. Bertrand, *Angew. Chem. Int. Ed.* **2005**, *44*, 5705-5709.

[8] S. Bellemin-Laponnaz, *Eur. J. Inorg. Chem.* **2020**, 10-20.

[9] a) J. Lee, H. Hahm, J. Kwak, M. Kim, *Adv. Synth. Catal.* **2019**, *361*, 1479-1499; b) E. Peris, *Chem. Rev.* **2018**, *118*, 9988-10031; c) D. Janssen-Müller, C. Schlepphorst, F. Glorius, *Chem. Soc. Rev.* **2017**, *46*, 4845-4854; d) J. L. Farmer, M. Pompeo, M. G. Organ, Wiley-Blackwell, **2016**, pp. 134-175.

[10] D. Enders, O. Niemeier, A. Henseler, *Chem. Rev.* **2007**, *107*, 5606-5655.

[11] a) M. Soleilhavoup, G. Bertrand, *Acc. Chem. Res.* **2015**, *48*, 256-266; b) H. Song, Y. Kim, J. Park, K. Kim, E. Lee, *Synlett* **2016**, *27*, 477-485.

[12] V. Lavallo, Y. Canac, B. Donnadieu, W. W. Schoeller, G. Bertrand, *Angew. Chem. Int. Ed.* **2006**, *45*, 3488-3491.

[13] G. D. Frey, V. Lavallo, B. Donnadieu, W. W. Schoeller, G. Bertrand, *Science* **2007**, *316*, 439-441.

[14] O. Back, G. Kuchenbeiser, B. Donnadieu, G. Bertrand, *Angew. Chem. Int. Ed.* **2009**, *48*, 5530-5533.

[15] V. Pace, W. Holzer, N. De Kimpe, *Chem. Rec.* **2016**, *16*, 2061-2076.

[16] T. Kimura, *Synthesis* **2017**, *49*, 5105-5119.

[17] D. Seyferth, D. E. Welch, G. Raab, *J. Am. Chem. Soc.* **1962**, *84*, 4266-4269.

[18] a) G. Boche, J. C. W. Lohrenz, *Chem. Rev.* **2001**, *101*, 697-756; b) M. Braun, *Angew. Chem. Int. Ed.* **1998**, *37*.

[19] a) C. Kupper, S. Molitor, V. H. Gessner, *Organometallics* **2014**, *33*, 347-353; b) S. Molitor, J. Becker, V. H. Gessner, *J. Am. Chem. Soc.* **2014**, *136*, 15517-15520; c) S. Molitor, K.-S. Feichtner, C. Kupper, V. H. Gessner, *Chem. Eur. J.* **2014**, *20*, 10752-10762.

[20] V. H. Gessner, *Chem. Commun.* **2016**, *52*, 12011-12023.

[21] a) G. Boche, K. Harms, M. Marsch, A. Mueller, *J. Chem. Soc., Chem. Commun.* **1994**, 1393-1394; b) G. Boche, M. Marsch, A. Müller, K. Harms, *Angew. Chem. Int. Ed.* **1993**, *32*, 1032-1033; c) G. Boche, M. Marsch, A. Mueller, K. Harms, *Angew. Chem.* **1993**, *105*, 1081-1082

[22] D. Seebach, R. Haessig, J. Gabriel, *Helv. Chim. Acta* **1983**, *66*, 308-337.

[23] G. Boche, F. Bosold, H. Hermann, M. Marsch, K. Harms, J. C. W. Lohrenz, *Chem. Eur. J.* **1998**, *4*, 814-817.

[24] G. Köbrich, A. Akhtar, F. Ansari, W. E. Breckoff, H. Büttner, W. Drischel, R. H. Fischer, K. Flory, H. Fröhlich, W. Goyert, H. Heinemann, I. Hornke, H. R. Merkle, H. Trapp, W. Zündorf, *Angew. Chem. Int. Ed.* **1967**, *6*, 41-52.

[25] a) A. Mueller, M. Marsch, K. Harms, J. C. W. Lohrenz, G. Boche, *Angew. Chem. Int. Ed.* **1996**, *35*, 1518-1520; b) G. Köbrich, H. R. Merkle, *Chem. Ber.* **1966**, *99*, 1782-1792; c) D. S. Matteson, D. Majumdar, *Organometallics* **1983**, *2*, 1529-1535; d) D. C. Kapeller, F. Hammerschmidt, *J. Am. Chem. Soc.* **2008**, *130*, 2329-2335.

[26] S. Molitor, V. H. Gessner, *Angew. Chem. Int. Ed.* **2016**, *55*, 7712-7716.

[27] a) G. Köbrich, R. H. Fischer, *Chem. Ber.* **1968**, *101*, 3208-3218; b) G. Köbrich, H. Trapp, *Z. Naturforsch.* **1963**, *186*, 1125-1126; c) G. Köbrich, H. Trapp, I. Hornke, *Tetrahedron Lett.* **1964**, 1131-1136; d) G. Köbrich, H. Trapp, I. Hornke, *Chem. Ber.* **1967**, *100*, 961-973.

[28] H. Hermann, J. C. W. Lohrenz, A. Kühn, G. Boche, *Tetrahedron* **2000**, *56*, 4109-4115.

[29] B. Waerder, S. Steinhauer, B. Neumann, H.-G. Stammler, A. Mix, Y. V. Vishnevskiy, B. Hoge, N. W. Mitzel, *Angew. Chem. Int. Ed.* **2014**, *53*, 11640-11644.

[30] D. M. Roddick, *Chem. Eng. News* **1997**, *75*, 6.

[31] a) C. Strohmann, V. H. Gessner, *Angew. Chem. Int. Ed.* **2007**, *46*, 4566-4569; b) V. H. Gessner, C. Strohmann, *J. Am. Chem. Soc.* **2008**, *130*, 14412-14413; c) C. Strohmann, V. H. Gessner, *Chem. Asian J.* **2008**, *3*, 1929-1934; d) H. Ahlbrecht, J. Harbach, T. Hauck, H. O. Kalinowski, *Chem. Ber.* **1992**, *125*, 1753-1762; e) I. Kamps, D. Bojer, S. A. Hayes, R. J. F. Berger, B. Neumann, N. W. Mitzel, *Chem. Eur. J.* **2009**, *15*, 11123-11127.

[32] a) P. O'Brien, C. M. Rosser, D. Caine, *Tetrahedron* **2003**, *59*, 9779-9791; b) P. Müller, D. Riegert, G. Bernardinelli, *Helv. Chim. Acta* **2004**, *87*, 227-239; c) J. Huang, P. O'Brien, *Chem. Commun.* **2005**, 5696-5698; d) D. M. Hodgson, S. M. Miles, *Angew. Chem. Int. Ed.* **2006**, *45*, 935-938.

[33] a) D. Seebach, *Chem. Ber.* **1972**, *105*, 487-510; b) M. Nitsche, D. Seebach, A. K. Beck, *Chem. Ber.* **1978**, *111*, 3644-3664.

[34] T. Rüffer, C. Bruhn, A. H. Maulitz, D. Stroehl, D. Steinborn, *Organometallics* **2000**, *19*, 2829-2831.

[35] T. Wagner, J. Lange, D. Grote, W. Sander, E. Schaumann, G. Adiwidjaja, A. Adam, J. Kopf, *Eur. J. Org. Chem.* **2009**, 5198-5207.

[36] a) G. Ludwig, D. Ströhl, H. Schmidt, D. Steinborn, *Inorg. Chim. Acta* **2015**, *429*, 30-33; b) G. Ludwig, T. Rüffer, A. Hoppe, T. Walther, H. Lang, S. G. Ebbinghaus, D. Steinborn, *Dalton Trans.* **2015**, *44*, 5323-5330.

[37] E. Niecke, P. Becker, M. Nieger, D. Stalke, W. W. Schoeller, *Angew. Chem.* **1995**, *107*, 2012-2015.

[38] T. Cantat, X. Jacques, L. Ricard, X. F. Le Goff, N. Mézailles, P. Le Floch, *Angew. Chem. Int. Ed.* **2007**, *46*, 5947-5950.

[39] a) J. Becker, V. H. Gessner, *Dalton Trans.* **2014**, *43*, 4320-4325; b) K.-S. Feichtner, V. H. Gessner, *Dalton Trans.* **2014**, *43*, 14399-14408.

[40] a) H. Heuclin, S. Y. F. Ho, X. F. Le Goff, C.-W. So, N. Mezailles, *J. Am. Chem. Soc.* **2013**, *135*, 8774-8777; b) S. Y. F. Ho, C.-W. So, N. Saffon-Merceron, N. Mezailles, *Chem. Commun.* **2015**, *51*, 2107-2110.

[41] J. Konu, T. Chivers, *Chem. Commun.* **2008**, 4995-4997.

[42] S. Molitor, V. H. Gessner, *Inorg. Chim. Acta* **2017**, *457*, 29-33.

[43] G. Köbrich, K. Flory, H. R. Merkle, *Tetrahedron Lett.* **1965**, 973-978.

[44] F. M. Perna, A. Salomone, M. Dammacco, S. Florio, V. Capriati, *Chem. Eur. J.* **2011**, *17*, 8216-8225.

[45] a) G. L. Closs, J. J. Coyle, *J. Org. Chem.* **1966**, *31*, 2759-2765; b) R. M. Magid, J. G. Welch, *Tetrahedron Lett.* **1967**, *8*, 2619-2624; c) E. T. Marquis, P. D. Gardner, *Chem. Commun.* **1966**, 726-727.

[46] R. Tarhouni, B. Kirschleger, M. Rambaud, J. Villieras, *Tetrahedron Lett.* **1984**, *25*, 835-838.

[47] T. J. Michnick, D. S. Matteson, *Synlett* **1991**, 631-632.

[48] V. Pace, L. Castoldi, W. Holzer, *J. Org. Chem.* **2013**, *78*, 7764-7770.

[49] a) D. Seyferth, R. L. Lambert, Jr., E. M. Hanson, *J. Organometal. Chem.* **1970**, *24*, 647-661; b) A. G. Brook, J. M. Duff, D. G. Anderson, *Can. J. Chem.* **1970**, *48*, 561-569; c) S. Touqeer, L. Castoldi, T. Langer, W. Holzer, V. Pace, *Chem. Commun.* **2018**, *54*, 10112-10115; d) K. M. Sadhu, D. S. Matteson, *Tetrahedron Lett.* **1986**, *27*, 795-798.

[50] a) S. Monticelli, E. Urban, T. Langer, W. Holzer, V. Pace, *Adv. Synth. Catal.* **2019**, *361*, 1001-1006; b) M. Zhu, L. Liu, H.-T. Yu, W.-X. Zhang, Z. Xi, *Chem. Eur. J.* **2018**, *24*, 19122-19135; c) A. Nomoto, A. Ogawa, in *Encyclopedia of Reagents for Organic Synthesis*, John Wiley & Sons, Ltd., Chichester, UK, **2007**; d) T. Satoh, *Chem. Soc. Rev.* **2007**, *36*, 1561-1572.

[51] C. Blomberg, *The Barbier Reaction and Related One-Step Processes. Reactivity and Structure: Concepts in Organic Chemistry, Vol. 31*, Springer-Verlag, **1993**.

[52] a) V. Pace, *Aust. J. Chem.* **2014**, *67*, 311-313; b) J. M. Concellon, H. Rodriguez-Solla, C. Simal, *Org. Lett.* **2008**, *10*, 4457-4460; c) J. M. Concellon, H. Rodriguez-Solla, P. L. Bernad, C. Simal, *J. Org. Chem.* **2009**, *74*, 2452-2459; d) V. Pace, L. Castoldi, W. Holzer, *Chem. Commun.* **2013**, *49*, 8383-8385; e) J. Barluenga, B. Baragana, J. M. Concellon, *J. Org. Chem.* **1995**, *60*, 6696-6699; f) V. Pace, W. Holzer, G. Verniest, A. R. Alcantara, N. De Kimpe, *Adv. Synth. Catal.* **2013**, *355*, 919-926; g) P. R. Blakemore, S. P. Marsden, H. D. Vater, *Org. Lett.* **2006**, *8*, 773-776.

[53] S. Dixon, S. M. Fillery, A. Kasatkin, D. Norton, E. Thomas, R. J. Whitby, *Tetrahedron* **2004**, *60*, 1401-1416.

[54] a) S. Molitor, V. H. Gessner, *Chem. Eur. J.* **2013**, *19*, 11858-11862; b) S. Molitor, K.-S. Feichtner, V. H. Gessner, *Chem. Eur. J.* **2017**, *23*, 2527-2531.

[55] a) T. Satoh, K. Takano, *Tetrahedron* **1996**, *52*, 2349-2358; b) T. Satoh, K. Takano, H. Ota, H. Someya, K. Matsuda, M. Koyama, *Tetrahedron* **1998**, *54*, 5557-5574.

[56] a) A. L. Barsamian, P. R. Blakemore, *Organometallics* **2012**, *31*, 19-22; b) C. R. Emerson, L. N. Zakharov, P. R. Blakemore, *Chem. Eur. J.* **2013**, *19*, 16342-16356; c) X. Sun, P. R. Blakemore, *Org. Lett.* **2013**, *15*, 4500-4503.

[57] a) D. Seebach, H. Siegel, K. Muellen, K. Hiltbrunner, *Angew. Chem.* **1979**, *91*, 844-845; b) H. Siegel, K. Hiltbrunner, D. Seebach, *Angew. Chem.* **1979**, *91*, 845-846; c) D. Seebach, H. Siegel, J. Gabriel, R. Hassig, *Helv. Chim. Acta* **1980**, *63*, 2046-2053; d) D. Seebach, J. Gabriel, R. Haessig, *Helv. Chim. Acta* **1984**, *67*, 1083-1099.

[58] G. Boche, F. Bosold, J. C. W. Lohrenz, A. Opel, P. Zulauf, *Chem. Ber.* **1993**, *126*, 1873-1885.

[59] H. Günther, D. Moskau, P. Bast, D. Schmalz, *Angew. Chem. Int. Ed.* **1987**, *26*, 1212-1220.

[60] G. Cainelli, N. Tangari, R. A. Umani, *Tetrahedron* **1972**, *28*, 3009-3013.

[61] A. Salomone, F. M. Perna, A. Falcicchio, S. O. Nilsson Lill, A. Moliterni, R. Michel, S. Florio, D. Stalke, V. Capriati, *Chem. Sci.* **2014**, *5*, 528-538.

[62] V. Schulze, R. Löwe, S. Fau, R. W. Hoffmann, *J. Chem. Soc., Perkin Trans. 2* **1998**, 463-466.

[63] a) S. E. Denmark, J. P. Edwards, S. R. Wilson, *J. Am. Chem. Soc.* **1991**, *113*, 723-725; b) A. B. Charette, J.-F. Marcoux, C. Molinaro, A. Beauchemin, C. Brochu, E. Isabel, *J. Am. Chem. Soc.* **2000**, *122*, 4508-4509.

[64] a) A. Voituriez, L. E. Zimmer, A. B. Charette, *J. Org. Chem.* **2010**, *75*, 1244-1250; b) A. B. Charette, C. Molinaro, C. Brochu, *J. Am. Chem. Soc.* **2001**, *123*, 12160-12167.

[65] a) D. Seebach, H. Siegel, K. Müllen, K. Hiltbrunner, *Angew. Chem. Int. Ed.* **1979**, *18*, 784-785; b) H. Siegel, K. Hiltbrunner, D. Seebach, *Angew. Chem. Int. Ed.* **1979**, *18*, 785-786.

[66] S. Molitor, Julius-Maximilians-Universität Würzburg (Würzburg, Germany), **2016**.

[67] P. V. R. Schleyer, T. Clark, A. J. Kos, G. W. Spitznagel, C. Rohde, D. Arad, K. N. Houk, N. G. Rondan, *J. Am. Chem. Soc.* **1984**, *106*, 6467-6475.

[68] B. T. Luke, J. A. Pople, P. v. R. Schleyer, T. Clark, *Chem. Phys. Lett.* **1983**, *102*, 148-154.

[69] a) V. H. Gessner, C. Daeschlein, C. Strohmann, *Chem. Eur. J.* **2009**, *15*, 3320-3334; b) T. Stey, D. Stalke, in *The Chemistry of Organolithium Compounds* (Eds.: Z. Rappoport, I. Marek), Wiley, Chichester, UK, **2004**, pp. 47-120.

[70] C. Rohde, T. Clark, E. Kaufmann, P. v. R. Schleyer, *J. Chem. Soc., Chem. Commun.* **1982**, 882-884.

[71] T. Clark, P. v. R. Schleyer, K. N. Houk, N. G. Rondan, *J. Chem. Soc., Chem. Commun.* **1981**, 579-581.

[72] D. M. Hodgson, C. D. Bray, N. D. Kindon, *Org. Lett.* **2005**, *7*, 2305-2308.

[73] E. Niecke, M. Nieger, O. Schmidt, D. Gudat, W. W. Schoeller, *J. Am. Chem. Soc.* **1999**, *121*, 519-522.

[74] a) T. Kimura, T. Satoh, *J. Organomet. Chem.* **2012**, *715*, 1-4; b) T. Kimura, T. Satoh, *Tetrahedron* **2013**, *69*, 6371-6374.

[75] S. Harder, J. Boersma, L. Brandsma, *Organometallics* **1989**, *8*, 1688-1696.

[76] a) F. Bosold, P. Zulauf, M. Marsch, K. Harms, J. Lohrenz, G. Boche, *Angew. Chem.* **1991**, *103*, 1497-1499; b) F. Bosold, P. Zulauf, M. Marsch, K. Harms, J. Lohrenz, G. Boche, *Angew. Chem. Int. Ed.* **1991**, *30*, 1455-1457.

[77] a) C. Strohmann, V. H. Gessner, *Angew. Chem. Int. Ed.* **2007**, *46*, 8281-8283; b) D. Bojer, I. Kamps, X. Tian, A. Hepp, T. Pape, R. Froehlich, N. W. Mitzel, *Angew. Chem. Int. Ed.* **2007**, *46*, 4176-4179.

[78] K. Sorger, W. Bauer, P. v. R. Schleyer, D. Stalke, *Angew. Chem. Int. Ed.* **1995**, *34*, 1594-1596.

[79] G. Boche, A. Opel, M. Marsch, K. Harms, F. Haller, J. C. W. Lohrenz, C. Thuemmler, W. Koch, *Chem. Ber.* **1992**, *125*, 2265-2273.

[80] T. Baumgartner, D. Gudat, M. Nieger, E. Niecke, T. J. Schiffer, *J. Am. Chem. Soc.* **1999**, *121*, 5953 - 5960.

[81] S. Molitor, V. H. Gessner, *Chem. Eur. J.* **2017**, *23*, 12372-12379.

[82] a) R. Tarhouni, B. Kirschleger, J. Villieras, *J. Organomet. Chem.* **1984**, *272*, C1-C4; b) G. Köbrich, J. Grosser, *Tetrahedron Lett.* **1972**, *13*, 4117-4120.

[83] J. Villieras, C. Bacquet, D. Masure, J. F. Normant, *J. Organomet. Chem.* **1973**, *50*, C7-C11.

[84] a) L.-P. B. Beaulieu, J. F. Schneider, A. B. Charette, *J. Am. Chem. Soc.* **2013**, *135*, 7819-7822; b) A. B. Charette, H. Juteau, *J. Am. Chem. Soc.* **1994**, *116*, 2651-2652; c) A. B. Charette, H. Juteau, H. Lebel, C. Molinaro, *J. Am. Chem. Soc.* **1998**, *120*, 11943-11952.

[85] a) A. Hirai, M. Nakamura, E. Nakamura, *Chem. Lett.* **1998**, 927-928; b) M. Nakamura, A. Hirai, E. Nakamura, *J. Am. Chem. Soc.* **2003**, *125*, 2341-2350; c) H. C. Stiasny, R. W. Hoffmann, *Chem. Eur. J.* **1995**, *1*, 619-624; d) U. Burger, R. Huisgen, *Tetrahedron Lett.* **1970**, *11*, 3049-3051.

[86] Z. Ke, C. Zhao, D. L. Phillips, *J. Org. Chem.* **2007**, *72*, 848-860.

[87] U. Schöllkopf, M. Eisert, *Liebigs Ann. Chem.* **1963**, *664*, 76-88.

[88] a) P. Fritsch, *Liebigs Ann. Chem.* **1894**, *279*, 319-323; b) H. Wiechell, *Liebigs Ann. Chem.* **1894**, *279*, 337-344; c) W. P. Buttenberg, *Liebigs Ann. Chem.* **1894**, *279*, 324-337.

[89] a) G. Bertrand, *Carbene Chemistry: From Fleeting Intermediates to Powerful Reagents*, Frontis Media, Lausanne, Switzerland u.a., **2002**; b) R. A. Moss, M. S. Platz, J. J. Maitland, *Reactive Intermediate Chemistry*, John Wiley & Sons, Inc., Hoboken, New Jersey, **2004**; c) D. C. Graham, K. J. Cavell, B. F. Yates, *J. Phys. Org. Chem.* **2005**, *18*,

298-309; d) M. K. Denk, A. Hezarkhani, F.-L. Zheng, *Eur. J. Inorg. Chem.* **2007**, 3527-3534.

[90] W. Kirmse, P. P. Gaspar, *Carbene Chemistry*, Academic Press, **1971**.

[91] P. A. Morken, P. C. Bachand, D. C. Swenson, D. J. Burton, *J. Am. Chem. Soc.* **1993**, *115*, 5430-5439.

[92] M. J. Goldstein, W. R. Dolbier, Jr., *J. Am. Chem. Soc.* **1965**, *87*, 2293-2295.

[93] W. Kirmse, G. Wächtershäuser, *Tetrahedron* **1966**, *22*, 73-80.

[94] a) V. Pace, A. Pelosi, D. Antermite, O. Rosati, M. Curini, W. Holzer, *Chem. Commun.* **2016**, *52*, 2639-2642; b) S. Monticelli, M. Rui, L. Castoldi, G. Missere, V. Pace, *Monatsh. Chem.* **2018**, *149*, 1285-1291; c) L. Castoldi, S. Monticelli, R. Senatore, L. Ielo, V. Pace, *Chem. Commun.* **2018**, *54*, 6692-6704; d) V. Pace, L. Castoldi, S. Monticelli, M. Rui, S. Collina, *Synlett* **2017**, *28*, 879-888.

[95] a) V. Pace, L. Castoldi, A. D. Mamuye, W. Holzer, *Synthesis* **2014**, *46*, 2897-2909, 2813 pp; b) A. D. Mamuye, L. Castoldi, U. Azzena, W. Holzer, V. Pace, *Org. Biomol. Chem.* **2015**, *13*, 1969-1973.

[96] a) S. Balieu, G. E. Hallett, M. Burns, T. Bootwicha, J. Studley, V. K. Aggarwal, *J. Am. Chem. Soc.* **2015**, *137*, 4398-4403; b) R. P. Sonawane, V. Jheengut, C. Rabalakos, R. Larouche-Gauthier, H. K. Scott, V. K. Aggarwal, *Angew. Chem. Int. Ed.* **2011**, *50*, 3760-3763.

[97] T. Boddaert, C. Francois, L. Mistico, O. Querolle, L. Meerpoel, P. Angibaud, M. Durandetti, J. Maddaluno, *Chem. Eur. J.* **2014**, *20*, 10131-10139.

[98] L. Field, C. H. Banks, *J. Org. Chem.* **1975**, *40*, 2774-2779.

[99] a) G. Köbrich, H. R. Merkle, *Chem. Ber.* **1967**, *100*, 3371-3384; b) G. Köbrich, H. R. Merkle, *Angew. Chem. Int. Ed.* **1967**, *6*, 74.

[100] a) T. Hata, H. Kitagawa, H. Masai, T. Kurahashi, M. Shimizu, T. Hiyama, *Angew. Chem.* **2001**, *113*, 812-814; b) T. Kurahashi, T. Hata, H. Masai, H. Kitagawa, M. Shimizu, T. Hiyama, *Tetrahedron* **2002**, *58*, 6381-6395.

[101] a) E. Negishi, K. Akiyoshi, B. O'Connor, K. Takagi, G. Wu, *J. Am. Chem. Soc.* **1989**, *111*, 3089-3091; b) A. N. Kasatkin, R. J. Whitby, *Tetrahedron Lett.* **1999**, *40*, 9353-9357; c) E. Thomas, A. N. Kasatkin, R. J. Whitby, *Tetrahedron Lett.* **2006**, *47*, 9181-9185.

[102] E. Thomas, S. Dixon, R. J. Whitby, *Tetrahedron* **2007**, *63*, 11686-11701.

[103] F. J. Feher, D. D. Gergens, J. W. Ziller, *Organometallics* **1993**, *12*, 2810-2813.

[104] E. Poverenov, D. Milstein, *Chem. Commun.* **2007**, 3189-3191.

[105] S. Molitor, V. H. Gessner, *Synlett* **2015**, *26*, 861-865.

[106] P. P. Power, *Nature* **2010**, *463*, 171-177.

[107] a) T. Hata, H. Kitagawa, H. Masai, T. Kurahashi, M. Shimizu, T. Hiyama, *Angew. Chem. Int. Ed.* **2001**, *40*, 790-792; b) M. Shimizu, M. Schelper, I. Nagao, K. Shimono, T. Kurahashi, T. Hiyama, *Chem. Lett.* **2006**, *35*, 1222-1223.

[108] K. V. Zaitsev, A. A. Kapranov, Y. F. Oprunenko, A. V. Churakov, J. A. K. Howard, B. N. Tarasevich, S. S. Karlov, G. S. Zaitseva, *J. Organomet. Chem.* **2012**, *700*, 207-213.

[109] M. Dräger, L. Ross, *Z. anorg. allg. Chem.* **1980**, *460*, 207-216.

[110] H. Schneider, M. J. Krahfuss, U. Radius, *Z. Anorg. Allg. Chem.* **2016**, *642*, 1282-1286.

[111] H. Preut, H. J. Haupt, F. Huber, *Z. Anorg. Allg. Chem.* **1973**, *396*, 81-89.

[112] A. Khan, R. A. Gossage, D. A. Foucher, *Can. J. Chem.* **2010**, *88*, 1046-1052.

[113] M.-L. Dumartin, H. El Hamzaoui, B. Jousseaume, M.-C. Rascle, T. Toupance, H. Allouchi, *Organometallics* **2007**, *26*, 5576-5580.

[114] a) H. Puff, C. Bach, H. Reuter, W. Schuh, *J. Organomet. Chem.* **1984**, *277*, 17-28; b) M. Dräger, B. Mathiasch, L. Ross, M. Ross, *Z. Anorg. Allg. Chem.* **1983**, *506*, 99-109.

[115] a) E. M. Leitao, T. Jurca, I. Manners, *Nat. Chem.* **2013**, *5*, 817-829; b) R. J. Less, R. L. Melen, V. Naseri, D. S. Wright, *Chem. Commun.* **2009**, 4929-4937; c) N. T. Coles, R. L. Webster, *Isr. J. Chem.* **2017**, *57*, 1070-1081; d) T. J. Clark, I. Manners, *J. Organomet. Chem.* **2007**, *692*, 2849-2853.

[116] a) R. L. Melen, *Chem. Soc. Rev.* **2016**, *45*, 775-788; b) R. J. Less, R. L. Melen, D. S. Wright, *RSC Adv.* **2012**, *2*, 2191-2199.

[117] a) X. Wang, J. Liu, J. Yu, L. Hou, W. Sun, Y. Wang, S. Chen, A. Li, W. Wang, *Inorg. Chem.* **2018**, *57*, 2969-2972; b) C. A. Kraus, W. V. Sessions, *J. Am. Chem. Soc.* **1925**, *47*, 2361-2368.

[118] H. Schneider, D. Schmidt, U. Radius, *Chem. Commun.* **2015**, *51*, 10138-10141.

[119] W. P. Neumann, B. Schneider, R. Sommer, *Liebigs Ann. Chem.* **1966**, *692*, 1-11.

[120] S. J. Geier, C. M. Vogels, N. R. Mellonie, E. N. Daley, A. Decken, S. Doherty, S. A. Westcott, *Chem. Eur. J.* **2017**, *23*, 14485-14499.

[121] P. Ramírez-López, A. Ros, B. Estepa, R. Fernández, B. Fiser, E. Gómez-Bengoa, J. M. Lassaletta, *ACS Catal.* **2016**, *6*, 3955-3964.

[122] M. Bluhm, A. Maderna, H. Pritzkow, S. Bethke, R. Gleiter, W. Siebert, *Eur. J. Inorg. Chem.* **1999**, *1999*, 1693-1700.

[123] C. Sun, B. Potter, J. P. Morken, *J. Am. Chem. Soc.* **2014**, *136*, 6534-6537.

[124] a) K. Hong, X. Liu, J. P. Morken, *J. Am. Chem. Soc.* **2014**, *136*, 10581-10584; b) B. Potter, A. A. Szymaniak, E. K. Edelstein, J. P. Morken, *J. Am. Chem. Soc.* **2014**, *136*, 17918-17921; c) M. V. Joannou, B. S. Moyer, M. J. Goldfogel, S. J. Meek, *Angew. Chem. Int. Ed.* **2015**, *54*, 14141-14145; d) M. V. Joannou, B. S. Moyer, S. J. Meek, *J. Am. Chem. Soc.* **2015**, *137*, 6176-6179.

[125] a) J. R. Coombs, L. Zhang, J. P. Morken, *Org. Lett.* **2015**, *17*, 1708-1711; b) D. S. Matteson, R. J. Moody, *Organometallics* **1982**, *1*, 20-28; c) K. Endo, M. Hirokami, T. Shibata, *J. Org. Chem.* **2010**, *75*, 3469-3472.

[126] a) C. R. Johnson, J. E. Keiser, *Org. Synth.* **1966**, *46*; b) C. R. Johnson, J. E. Keiser, *Org. Synth. Coll.* **1973**, *5*, 791.

[127] C. R. Johnson, M. Haake, C. W. Schroeck, *J. Am. Chem. Soc.* **1970**, *92*, 6594-6598.

[128] a) J. Brandt, H.-J. Gais, *Tetrahedron: Asymmetry* **1997**, *8*, 909 - 912; b) C. S. Shiner, A. H. Berks, *J. Org. Chem.* **1988**, *53*, 5542-5545.

[129] K.-S. Feichtner, S. Englert, V. H. Gessner, *Chem. - Eur. J.* **2016**, *22*, 506-510.

[130] E. L. Hahn, *Phys. Rev.* **1950**, *80*, 580-594.

[131] P. S. Pregosin, in *Spectroscopic Properties of Inorganic and Organometallic Compounds: Techniques, Materials and Applications, Vol. 42*, The Royal Society of Chemistry, **2012**, pp. 248-268.

[132] G. Pagès, V. Gilard, R. Martino, M. Malet-Martino, *Analyst* **2017**, *142*, 3771-3796.

[133] K. F. Morris, C. S. Johnson, Jr., *J. Am. Chem. Soc.* **1992**, *114*, 3139-3141.

[134] R. Neufeld, D. Stalke, *Chem. Sci.* **2015**, *6*, 3354-3364.

[135] S. Auge, P.-O. Schmit, C. A. Crutchfield, M. T. Islam, D. J. Harris, E. Durand, M. Clemancey, A.-A. Quoineaud, J.-M. Lancelin, Y. Prigent, F. Taulelle, M.-A. Delsuc, *J. Phys. Chem. B* **2009**, *113*, 1914-1918.

[136] S. Viel, D. Capitani, L. Mannina, A. Segre, *Biomacromolecules* **2003**, *4*, 1843-1847.

[137] A. Chen, D. Wu, C. S. Johnson, Jr., *J. Am. Chem. Soc.* **1995**, *117*, 7965-7970.

[138] D. K. Wilkins, S. B. Grimshaw, V. Receveur, C. M. Dobson, J. A. Jones, L. J. Smith, *Biochemistry* **1999**, *38*, 16424-16431.

[139] a) C. A. Crutchfield, D. J. Harris, *J. Magn. Reson.* **2007**, *185*, 179-182; b) D. Li, I. Keresztes, R. Hopson, P. G. Williard, *Acc. Chem. Res.* **2009**, *42*, 270-280.

[140] D. R. Armstrong, E. Crosbie, E. Hevia, R. E. Mulvey, D. L. Ramsay, S. D. Robertson, *Chem. Sci.* **2014**, *5*, 3031-3045.

[141] D. R. Armstrong, P. Garcia-Alvarez, A. R. Kennedy, R. E. Mulvey, J. A. Parkinson, *Angew. Chem. Int. Ed.* **2010**, *49*, 3185-3188.

[142] a) E. J. Cabrita, S. Berger, *Magn. Reson. Chem.* **2001**, *39*, S142-S148; b) S. Yao, G. J. Howlett, R. S. Norton, *J. Biomol. NMR* **2000**, *16*, 109-119; c) E. Durand, M. Clemancey, J.-M. Lancelin, J. Verstraete, D. Espinat, A.-A. Quoineaud, *J. Phys. Chem. C* **2009**, *113*, 16266-16276.

[143] S. Bachmann, B. Gernert, D. Stalke, *Chem. Commun.* **2016**, *52*, 12861-12864.

[144] a) R. Neufeld, D. Stalke, *Chem. - Eur. J.* **2016**, *22*, 12624-12628; b) C. Schnegelsberg, S. Bachmann, M. Kolter, T. Auth, M. John, D. Stalke, K. Koszinowski, *Chem. Eur. J.* **2016**, *22*, 7752-7762.

[145] O. Tai, R. Hopson, P. G. Williard, *Org. Lett.* **2017**, *19*, 3966-3969.

[146] O. Tai, R. Hopson, P. G. Williard, *J. Org. Chem.* **2017**, *82*, 6223-6231.

[147] Y.-R. Luo, *Comprehensive Handbook of Chemical Bond Energies*, CRC Press, Boca Raton, FL, **2007**.

[148] a) G. Binnig, H. Rohrer, C. Gerber, E. Weibel, *Appl. Phys. Lett.* **1982**, *40*, 178-180; b) G. Binnig, H. Rohrer, C. Gerber, E. Weibel, *Phys. Rev. Lett.* **1982**, *49*, 57-61; c) G. Binnig, H. Rohrer, *Rev. Mod. Phys.* **1987**, *59*, 615-625.

[149] L. E. C. van de Leemput, H. van Kempen, *Rep. Prog. Phys.* **1992**, *55*, 1165 - 1240.

[150] a) M. Casarin, D. Forrer, T. Orzali, M. Petukhov, M. Sambi, E. Tondello, A. Vittadini, *J. Phys. Chem. C* **2007**, *111*, 9365-9373; b) L. C. Teague, J. J. Boland, *J. Phys. Chem. B* **2003**, *107*, 3820-3823; c) K. Kaiser, L. Gross, F. Schulz, *ACS Nano* **2019**, *13*, 6947-6954.

[151] a) X. H. Chen, Q. Kong, J. C. Polanyi, D. Rogers, S. So, *Surf. Sci.* **1995**, *340*, 224-230; b) S. Robert, S. Gauthier, F. Bocquet, S. Rousset, J. L. Duvault, J. Klein, *Surf. Sci.* **1996**, *350*, 136-144.

[152] a) Y. Hasegawa, Y. Ling, S. Yamazaki, T. Hashizume, H. Shinohara, T. Sakurai, *Mater. Sci. Eng. A* **1996**, *217-218*, 23-26; b) Y. Hasegawa, Y. Ling, T. Hashizume, H. Shinohara, A. Sakai, H. W. Pickering, T. Sakurai, *Phys. Rev. B* **1997**, *56*, 6470.

[153] a) F. Song, J. W. Wells, Z. Jiang, M. Saxegaard, E. Wahlström, *ACS Appl. Mater. Interfaces* **2015**, *7*, 8525 - 8532; b) R. Q. Hwang, C. Günther, J. Schröder, S. Günther, E. Kopatzki, R. J. Behm, *J. Vac. Sci. Technol. A* **1992**, *10*, 1970-1980; c) U. Köhler, V. Dorna, C. Jensen, M. Kneppe, G. Piaszenski, K. Reshöft, C. Wolf, in *Crystal Growth - From Fundamentals to Technology* (Eds.: G. Müller, J.-J. Métois, P. Rudolph), Elsevier Science B.V., Amsterdam, Netherlands, **2004**, pp. 391-412.

[154] A. Biffis, P. Centomo, A. Del Zotto, M. Zecca, *Chem. Rev.* **2018**, *118*, 2249-2295.

[155] a) T. Mizoroki, K. Mori, A. Ozaki, *Bull. Chem. Soc. Jap.* **1971**, *44*, 581; b) K. Mori, T. Mizoroki, A. Ozaki, *Bull. Chem. Soc. Jap.* **1973**, *46*, 1505-1508.

[156] R. F. Heck, J. P. Nolley, Jr., *J. Org. Chem.* **1972**, *37*, 2320-2322.

[157] M. Julia, M. Duteil, *Bull. Soc. Chim. Fr.* **1973**, 2790.

[158] A. F. P. Biajoli, C. S. Schwalm, J. Limberger, T. S. Claudino, A. L. Monteiro, *J. Braz. Chem. Soc.* **2014**, *25*, 2186-2214.

[159] C. C. C. Johansson Seechurn, M. O. Kitching, T. J. Colacot, V. Snieckus, *Angew. Chem., Int. Ed.* **2012**, *51*, 5062-5085.

[160] a) J. K. Stille, *Angew. Chem. Int. Ed.* **1986**, *25*, 508-524; b) P. Espinet, A. M. Echavarren, *Angew. Chem. Int. Ed.* **2004**, *43*, 4704-4734.

[161] a) A. Suzuki, *Angew. Chem. Int. Ed.* **2011**, *50*, 6722-6737; b) N. Miyaura, *Metal Catalyzed Cross-Coupling Reactions, Vol. 1*, Wiley-VCH, **2004**.

[162] a) E.-I. Negishi, *Angew. Chem. Int. Ed.* **2011**, *50*, 6738-6764; b) P. Knochel, R. D. Singer, *Chem. Rev.* **1993**, *93*, 2117-2188; c) V. B. Phapale, D. J. Cardenas, *Chem. Soc. Rev.* **2009**, *38*, 1598-1607.

[163] C. E. I. Knappke, A. J. von Wangelin, *Chem. Soc. Rev.* **2011**, *40*, 4948-4962.

[164] S. Murahashi, M. Yamamura, K. Yanagisawa, N. Mita, K. Kondo, *J. Org. Chem.* **1979**, *44*, 2408-2417.

[165] M. Giannerini, M. Fananas-Mastral, B. L. Feringa, *Nat. Chem.* **2013**, *5*, 667-672.

[166] a) T. Scherpf, C. Schwarz, L. T. Scharf, J.-A. Zur, A. Helbig, V. H. Gessner, *Angew. Chem. Int. Ed.* **2018**, *57*, 12859-12864; b) K. Issleib, R. Lindner, *Liebigs Ann. Chem.* **1966**, *699*, 40-52.

[167] P. Weber, T. Scherpf, I. Rodstein, D. Lichte, L. T. Scharf, L. J. Goossen, V. H. Gessner, *Angew. Chem. Int. Ed.* **2019**, *58*, 3203-3207.

[168] X.-Q. Hu, D. Lichte, I. Rodstein, P. Weber, A.-K. Seitz, T. Scherpf, V. H. Gessner, L. J. Goossen, *Org. Lett.* **2019**, *21*, 7558-7562.

[169] W. B. Reid, J. J. Spillane, S. B. Krause, D. A. Watson, *J. Am. Chem. Soc.* **2016**, *138*, 5539-5542.

[170] a) I. Cepanec, M. Litvić, J. Udiković, I. Pogorelić, M. Lovrić, *Tetrahedron* **2007**, *63*, 5614-5621; b) W. M. Czaplik, M. Mayer, A. Jacobi von Wangelin, *Angew. Chem. Int. Ed.* **2009**, *48*, 607-610; c) C.-T. Yang, Z.-Q. Zhang, Y.-C. Liu, L. Liu, *Angew. Chem. Int. Ed.* **2011**, *50*, 3904-3907; d) F. Mohanazadeh, H. Amini, *Bull. Korean Chem. Soc.* **2010**, *31*, 3038-3040.

Katharina Dilchert

PhD Candidate Chemistry

Personal Details

Date of Birth	
Nationality	Geman

Education

Since 10|2016	**Doctoral studies** at the chair of inorganic chemistry II, Ruhr-University Bochum, Germany
02|2018 – 04|2018 02|2019 – 04|2019	**Visiting Scholar** at the chair of pure and applied chemistry, University of Strathclyde, Scotland, UK
08|2016 – 09|2016	**Research assistant** at the chair of inorganic and metal organic chemistry, Technical University of Munich, Germany
06|2015 – 07|2016	**Research assistant** at the chair of inorganic chemistry II, Ruhr-University Bochum, Germany
10|2013 – 05|2015	**M.Sc. Chemistry**, Ruhr-University Bochum, Germany, 1.1 (very good)
10|2010 – 09|2013	**B.Sc. Chemistry**, Ruhr-University Bochum, Germany, 1.8 (good)
06|2010	**Abitur** Gymnasium Wanne, Herne, 1.0

Teaching Activities

06|2015 – 07|2018	Supervision of basic practical laboratory courses as well as several Bachelor, Master and Erasmus students

Workshops

10|2017	"How to publish in peer-review journals", Ruhr-University Bochum, Germany
06|2017	Summer School of Solvation Science of the Cluster of Excellence RESOLV, Ruhr-University Bochum, Germany
02|2015	DFG – Priority Program SSP 1708 – Materials Synthesis near room temperature, Rostock, Germany

Awards & Scholarships

10|2018	**Funding "Project International"** by Research School PLUS for an international research stay and attendance of an international conference
04|2017	Poster award at the 19th JCF Frühjahrsymposium

Since 03|2017	**Doctoral Scholarship** of the *Graduate School of Solvation Science* of the Cluster of Excellence RESOLV
07|2016 – 07|2019	Several **GdCh – Travelling Scholarships** for attendance of scientific conferences
12|2014 – 05|2015	**Qualification Scholarship** of the *Graduate School of Solvation Science* of the Cluster of Excellence RESOLV

Voluntary Work

Since 07|2017	Fire protection assistant
Since 03|2017	First Aider
Since 10|2016	Young Chemists Forum Bochum ♦ Organization of scientific guest lectures, field trips & symposia
Since 01|2018	**Deputy speaker** of the Young Chemists Forum Bochum

Language Skills

German	Mother tongue
English	fluent

Computer Skills

Office	Word, Excel, PowerPoint
Mathematics	Origin
Graphic Design Software	CorelDraw

Publications

S. Wannapaiboon, K. Sumida, **K. Dilchert**, M. Tu, S. Kitagawa, S. Furukawa, R. A. Fischer, *J. Mater. Chem. A Mater. Energy Sustain.* **2017**, *5*, 13665-13673.

S. Wegner, C. Rutz, K. Schuette, J. Barthel, A. Bushmelev, A. Schmidt, **K. Dilchert**, R. A. Fischer, C. Janiak, *Chem. Eur. J.* **2017**, *23*, 6330-6340.

K. Freitag, M. Molon, P. Jerabek, **K. Dilchert**, C. Roesler, R. W. Seidel, C. Gemel, G. Frenking, R. A. Fischer, *Chem. Sci.* **2016**, *7*, 6413-6421.

H. Banh, **K. Dilchert**, C. Schulz, C. Gemel. R. W. Seidel, R. Gautier, S. Kahlal, J. Saillard, R. A. Fischer*, Angew. Chem. Int. Ed.* **2016**, *55,* 3285-3289.

K. Freitag, C. Gemel, P. Jerabek, M. I. Oppel, R. W. Seidel, G. Frenking, H. Banh, **K. Dilchert**, *Angew. Chem. Int. Ed.* **2015**, *54*, 4370-4374.

M. Molon, **K. Dilchert**, C. Gemel, R. W. Seidel, J. Schaumann, R. A. Fischer, *Inorg. Chem.* **2013**, *52*, 14275-14283.

Posters & Talks

K. Dilchert, V. H. Däschlein-Gessner "(Stereo-)selective Dehydrocoupling of Main Group Element Hydride Species by Li/Cl Carbenoids", Gordon Research Seminar & Conference, Rhode Island, USA, July 2019 (Poster)

K. Dilchert, V. H. Däschlein-Gessner "Synthesis and Characterization of Chiral Carbenoids and their Use in Stereoselective Dehydrocoupling of Phosphines", Young Chemist Symposium, Bochum, Germany, October 2018 (Talk)

K. Dilchert, V. H. Däschlein-Gessner "Synthesis of a Chiral Carbenoid and its Use in Stereoselective Dehydrocoupling of Phosphines", International Conference on Organometallic Chemistry, Florence, Italy, July 2018 (Poster)

K. Dilchert, K.-S. Feichtner, V. H. Däschlein-Gessner „Synthesis of a Chiral Carbenoid and its Use in Stereoselective Dehydrocoupling of Phosphines", Agichem 2017, Göttingen, Germany, August 2017 (Poster)

K. Dilchert, S. Molitor, V. H. Däschlein-Gessner „Carbenoids in Homologation Reactions", 19. JCF Frühjahrsymposium, Mainz, Germany, April 2017 (Poster)

K. Dilchert, M. Molon, C. Gemel, R. A. Fischer „Post-Functionalization of Zinc-Rich Transition Metal Complexes", 27. International Conference on Organometallic Chemistry, Melbourne, Australia, July 2016 (Poster)

K. Dilchert, C. Gemel, S. Wegner, C. Janiak, M. Cokoja, R. A. Fischer „Solvent Controlled Synthesis and Semi-Hydrogenation Catalysis with Hume-Rothery Intermetallic Clusters and Nanoparticles", 49. Jahrestreffen Deutscher Katalytiker, Weimar, Germany, March 2016 (Poster)

K. Dilchert, J. Weßing, C. Gemel, R. A. Fischer „Bottom-Up! Intermetallic Nickel Gallium molecular Clusters and Complexes as potential Precursors for Intermetallic Nanoparticles", 14. International Symposium on Inorganic Ring Systems, Regensburg, Germany, July 2015 (Poster)

Declaration of Originality

I hereby declare

- that the submitted dissertation

  Structure and Reactivity Studies of Stabilized Carbenoids

  is entirely my own work and has been composed without having received unpermitted assistance, and that no sources have been used otherwise indicated, including entirely or partially included text excerpts as well as graphs, tables and the use of analysis software.

- that the submitted electronic version corresponds to the printed version of the dissertation and that it, in this or similar form, has not yet been submitted and assessed as a component of doctoral performance.

- that digital images only contain the original data.

- that no commercial brokerage or consultancy services were used.

- that I have read, understood and have complied with the DFG-Memorandum ‘Safeguarding Good Scientific Practice’

Bochum, 03. April 2020

Katharina Dilchert

Crystal Structure Determination

Crystal Structure Determination of 71

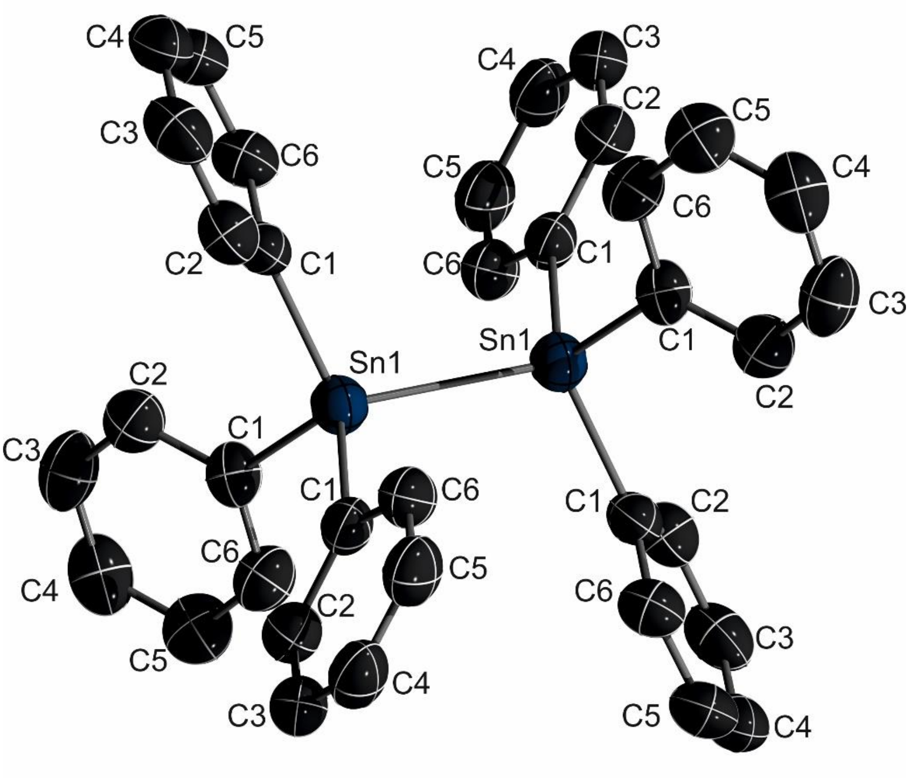

Figure 1. ORTEP of compound **71**. Ellipsoids are drawn at the 50% probability level.

Table 1. Atomic coordinates (x 10^4) and equivalent isotropic displacement parameters ($Å^2$x 10^3) for **71**. U(eq) is defined as one third of the trace of the orthogonalized U^{ij} tensor.

	x	y	z	U(eq)
Sn(1)	0	0	6620(1)	50(1)
C(1)	1328(3)	819(3)	7474(5)	48(1)
C(2)	1761(3)	494(3)	8406(6)	56(1)
C(3)	2610(4)	1056(4)	8941(6)	65(1)
C(4)	3034(3)	1944(4)	8579(6)	65(1)
C(5)	2629(3)	2280(4)	7670(6)	64(1)
C(6)	1779(3)	1716(3)	7113(5)	56(1)
C(7A)	5962(5)	1992(4)	-1705(9)	47(1)
C(8A)	6316(5)	1664(5)	-2788(10)	54(1)
C(9A)	5835(7)	763(6)	-3235(12)	55(1)
C(10A)	5013(7)	208(6)	-2610(12)	57(2)

C(11A)	4659(6)	513(5)	-1484(10)	55(1)
C(12A)	5151(5)	1399(5)	-1028(10)	54(1)
Sn(2A)	6667	3333	-917(1)	49(1)
Sn(3A)	6667	3333	2289(1)	47(1)
C(13A)	7304(5)	4660(4)	3186(9)	47(1)
C(14A)	6896(6)	4861(6)	4381(11)	65(2)
C(15A)	7318(7)	5723(6)	5017(12)	68(2)
C(16A)	8136(7)	6353(6)	4560(10)	57(2)
C(17A)	8529(7)	6193(6)	3308(13)	68(2)
C(18A)	8095(6)	5335(6)	2616(11)	65(2)
Sn(2B)	6240(1)	2512(1)	1373(2)	39(1)
Sn(3B)	7105(1)	4220(1)	270(2)	39(1)
C(7B)	5704(14)	1576(15)	-480(20)	47(1)
C(8B)	4846(15)	865(15)	-480(30)	54(1)
C(9B)	4545(19)	228(18)	-1710(40)	55(1)
C(10B)	5090(20)	320(20)	-2910(40)	57(2)
C(11B)	5950(20)	1000(20)	-2950(40)	55(1)
C(12B)	6237(17)	1625(18)	-1740(30)	54(1)
C(13B)	7533(16)	5114(16)	2200(20)	47(1)
C(14B)	8357(18)	5869(18)	2330(40)	65(2)
C(15B)	8530(30)	6420(20)	3660(50)	68(2)
C(16B)	7920(40)	6230(30)	4800(60)	57(2)
C(17B)	7100(30)	5490(30)	4710(40)	68(2)
C(18B)	6930(20)	4950(20)	3410(30)	65(2)
C(7C)	7165(17)	2320(18)	2700(30)	47(1)
C(8C)	7260(20)	1574(19)	2650(40)	54(1)
C(9C)	7870(30)	1510(30)	3640(50)	55(1)
C(10C)	8380(30)	2160(30)	4680(60)	57(2)
C(11C)	8330(30)	2910(30)	4740(50)	55(1)
C(12C)	7721(18)	2970(20)	3760(30)	54(1)
C(13C)	6225(18)	4429(18)	-1150(30)	47(1)
C(14C)	6140(20)	5178(19)	-1070(40)	65(2)
C(15C)	5480(20)	5200(20)	-1990(40)	68(2)
C(16C)	4920(20)	4530(20)	-2950(40)	57(2)
C(17C)	4990(20)	3780(20)	-3060(40)	68(2)
C(18C)	5640(20)	3760(20)	-2150(40)	65(2)
C(7D)	5127(15)	2310(20)	2710(30)	47(1)
C(8D)	4806(19)	1770(20)	4010(30)	54(1)
C(9D)	4000(20)	1650(20)	4700(40)	55(1)

C(10D)	3560(20)	2040(20)	4110(40)	57(2)
C(11D)	3866(18)	2590(20)	2840(40)	55(1)
C(12D)	4641(17)	2700(20)	2190(40)	54(1)
C(13D)	8232(14)	4432(19)	-1050(30)	47(1)
C(14D)	8460(20)	4890(20)	-2450(30)	65(2)
C(15D)	9280(30)	5140(30)	-3180(50)	68(2)
C(16D)	9880(20)	4970(30)	-2480(50)	57(2)
C(17D)	9669(16)	4500(20)	-1120(50)	68(2)
C(18D)	8847(15)	4230(20)	-420(40)	65(2)

Table 2. Anisotropic displacement parameters (Å^{2}x 10^3) for **71**. The anisotropic displacement factor exponent takes the form: -2p^2[h^2 a*^{2}U^{11} + ... + 2 h k a* b* U^{12}]

	U^{11}	U^{22}	U^{33}	U^{23}	U^{13}	U^{12}
Sn(1)	52(1)	52(1)	45(1)	0	0	26(1)
C(1)	41(2)	56(2)	42(2)	3(2)	5(2)	22(2)
C(2)	58(3)	62(3)	53(2)	3(2)	6(2)	33(2)
C(3)	61(3)	91(4)	54(3)	16(3)	9(2)	45(3)
C(4)	45(2)	84(4)	54(3)	1(3)	4(2)	23(2)
C(5)	53(3)	62(3)	63(3)	9(2)	13(2)	19(2)
C(6)	51(2)	59(3)	57(2)	10(2)	6(2)	28(2)
C(7A)	50(3)	44(2)	54(3)	-5(2)	-11(2)	29(2)
C(8A)	47(3)	44(3)	64(3)	-4(2)	5(2)	16(2)
C(9A)	56(3)	49(3)	60(3)	-6(3)	-1(3)	26(3)
C(10A)	66(4)	43(3)	54(3)	-3(2)	-4(3)	21(3)
C(11A)	56(3)	49(3)	60(3)	-6(3)	-1(3)	26(3)
C(12A)	47(3)	44(3)	64(3)	-4(2)	5(2)	16(2)
Sn(2A)	44(1)	44(1)	57(1)	0	0	22(1)
Sn(3A)	42(1)	42(1)	57(1)	0	0	21(1)
C(13A)	50(3)	44(2)	54(3)	-5(2)	-11(2)	29(2)
C(14A)	61(4)	53(3)	73(4)	-4(3)	3(3)	23(3)
C(15A)	75(4)	48(4)	79(5)	-1(3)	5(3)	28(3)
C(16A)	66(4)	43(3)	54(3)	-3(2)	-4(3)	21(3)
C(17A)	75(4)	48(4)	79(5)	-1(3)	5(3)	28(3)
C(18A)	61(4)	53(3)	73(4)	-4(3)	3(3)	23(3)
Sn(2B)	36(1)	45(1)	37(1)	0(1)	-2(1)	21(1)
Sn(3B)	35(1)	41(1)	38(1)	1(1)	-1(1)	17(1)
C(7B)	50(3)	44(2)	54(3)	-5(2)	-11(2)	29(2)

C(8B)	47(3)	44(3)	64(3)	-4(2)	5(2)	16(2)
C(9B)	56(3)	49(3)	60(3)	-6(3)	-1(3)	26(3)
C(10B)	66(4)	43(3)	54(3)	-3(2)	-4(3)	21(3)
C(11B)	56(3)	49(3)	60(3)	-6(3)	-1(3)	26(3)
C(12B)	47(3)	44(3)	64(3)	-4(2)	5(2)	16(2)
C(13B)	50(3)	44(2)	54(3)	-5(2)	-11(2)	29(2)
C(14B)	61(4)	53(3)	73(4)	-4(3)	3(3)	23(3)
C(15B)	75(4)	48(4)	79(5)	-1(3)	5(3)	28(3)
C(16B)	66(4)	43(3)	54(3)	-3(2)	-4(3)	21(3)
C(17B)	75(4)	48(4)	79(5)	-1(3)	5(3)	28(3)
C(18B)	61(4)	53(3)	73(4)	-4(3)	3(3)	23(3)
C(7C)	50(3)	44(2)	54(3)	-5(2)	-11(2)	29(2)
C(8C)	47(3)	44(3)	64(3)	-4(2)	5(2)	16(2)
C(9C)	56(3)	49(3)	60(3)	-6(3)	-1(3)	26(3)
C(10C)	66(4)	43(3)	54(3)	-3(2)	-4(3)	21(3)
C(11C)	56(3)	49(3)	60(3)	-6(3)	-1(3)	26(3)
C(12C)	47(3)	44(3)	64(3)	-4(2)	5(2)	16(2)
C(13C)	50(3)	44(2)	54(3)	-5(2)	-11(2)	29(2)
C(14C)	61(4)	53(3)	73(4)	-4(3)	3(3)	23(3)
C(15C)	75(4)	48(4)	79(5)	-1(3)	5(3)	28(3)
C(16C)	66(4)	43(3)	54(3)	-3(2)	-4(3)	21(3)
C(17C)	75(4)	48(4)	79(5)	-1(3)	5(3)	28(3)
C(18C)	61(4)	53(3)	73(4)	-4(3)	3(3)	23(3)
C(7D)	50(3)	44(2)	54(3)	-5(2)	-11(2)	29(2)
C(8D)	47(3)	44(3)	64(3)	-4(2)	5(2)	16(2)
C(9D)	56(3)	49(3)	60(3)	-6(3)	-1(3)	26(3)
C(10D)	66(4)	43(3)	54(3)	-3(2)	-4(3)	21(3)
C(11D)	56(3)	49(3)	60(3)	-6(3)	-1(3)	26(3)
C(12D)	47(3)	44(3)	64(3)	-4(2)	5(2)	16(2)
C(13D)	50(3)	44(2)	54(3)	-5(2)	-11(2)	29(2)
C(14D)	61(4)	53(3)	73(4)	-4(3)	3(3)	23(3)
C(15D)	75(4)	48(4)	79(5)	-1(3)	5(3)	28(3)
C(16D)	66(4)	43(3)	54(3)	-3(2)	-4(3)	21(3)
C(17D)	75(4)	48(4)	79(5)	-1(3)	5(3)	28(3)
C(18D)	61(4)	53(3)	73(4)	-4(3)	3(3)	23(3)

Crystal Structure Determination of 72

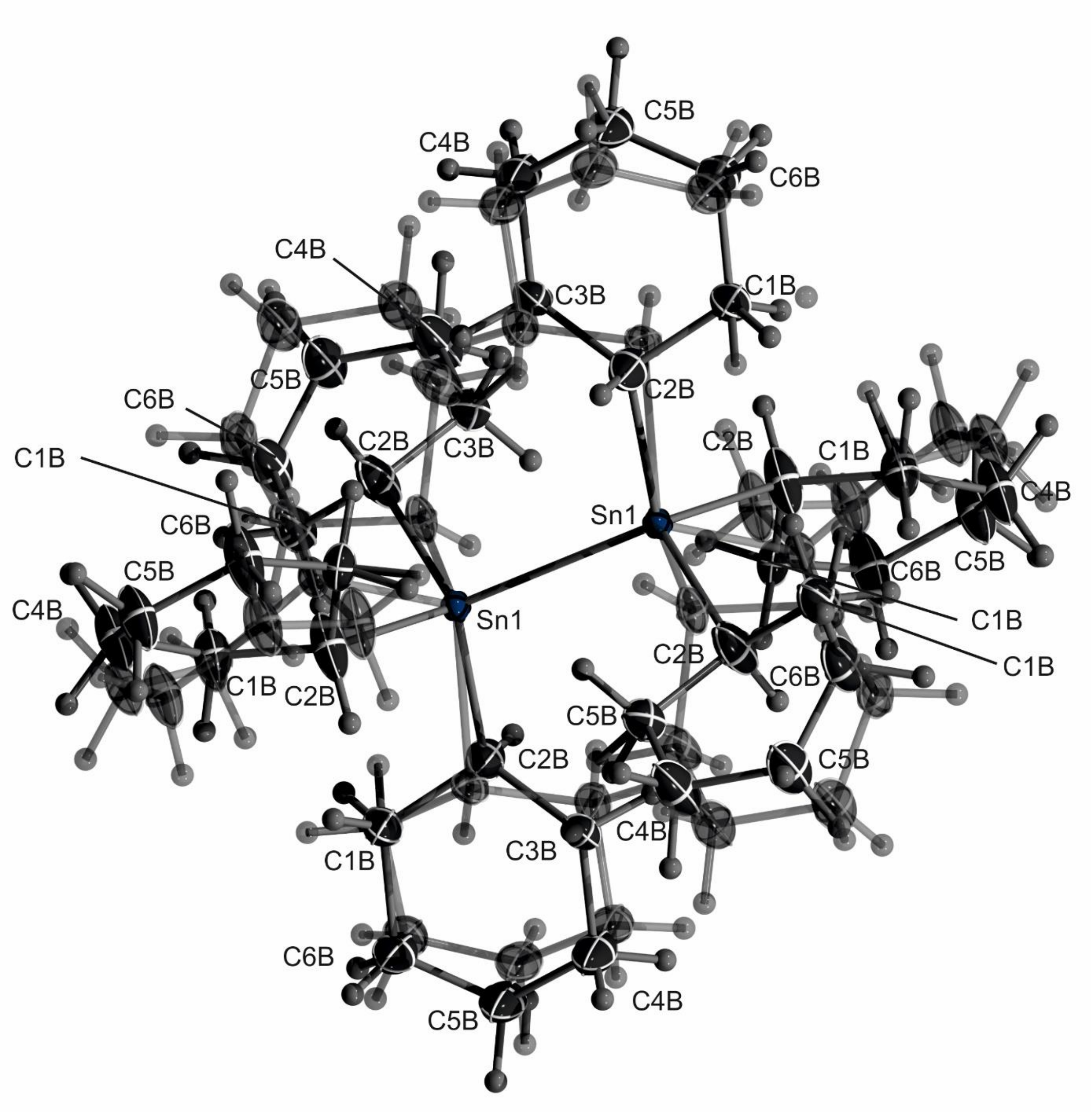

Figure 2. ORTEP of compound **72**. Ellipsoids are drawn at the 50% probability level

Table 3. Atomic coordinates (x 10^4) and equivalent isotropic displacement parameters (Å^{2}x 10^3) for **72**. U(eq) is defined as one third of the trace of the orthogonalized U^{ij} tensor.

	x	y	z	U(eq)
Sn(1)	3333	6667	1235(1)	13(1)
C(1A)	1110(40)	4400(40)	541(7)	26(1)
C(2A)	989(8)	4958(9)	1004(2)	22(1)

C(3A)	462(12)	3307(11)	1264(2)	36(1)
C(4A)	-256(11)	2842(12)	381(3)	31(1)
C(5A)	-978(11)	1555(11)	658(2)	36(1)
C(6A)	-1081(11)	1876(11)	1104(3)	33(1)
C(1B)	1060(40)	4490(30)	558(7)	28(2)
C(2B)	1467(10)	4414(10)	987(2)	36(1)
C(3B)	-3(8)	3675(8)	1268(2)	23(1)
C(4B)	-572(11)	3259(11)	401(2)	37(1)
C(5B)	-1626(10)	2060(10)	662(2)	36(1)
C(6B)	-1548(11)	2379(11)	1105(2)	43(1)

Table 4. Anisotropic displacement parameters (Å^{2}x 10^3) for **72**. The anisotropic displacement factor exponent takes the form: -2p^2[h^2 a*^{2}U^{11} + ... + 2 h k a* b* U^{12}]

	U^{11}	U^{22}	U^{33}	U^{23}	U^{13}	U^{12}
Sn(1)	14(1)	14(1)	10(1)	0	0	7(1)
C(1A)	25(2)	31(2)	13(1)	-5(1)	-1(2)	7(2)
C(2A)	17(2)	29(1)	14(1)	-4(1)	-2(2)	8(1)
C(3A)	35(2)	31(2)	17(1)	2(1)	-5(2)	-2(2)
C(4A)	30(2)	32(2)	19(1)	-9(1)	-2(2)	7(2)
C(5A)	30(2)	34(1)	23(1)	-6(1)	-2(1)	0(1)
C(6A)	28(2)	32(2)	22(1)	-4(1)	-1(2)	2(2)
C(1B)	25(2)	28(2)	20(1)	-1(2)	-3(1)	7(2)
C(2B)	32(2)	36(2)	16(1)	-3(2)	-1(1)	-2(2)
C(3B)	23(2)	25(2)	19(1)	0(1)	-6(1)	11(1)
C(4B)	30(2)	38(2)	19(1)	-7(1)	-2(1)	1(2)
C(5B)	30(2)	34(1)	23(1)	-6(1)	-2(1)	0(1)
C(6B)	33(2)	41(2)	21(1)	-3(2)	-1(2)	-6(2)

Crystal Structure Determination of 74

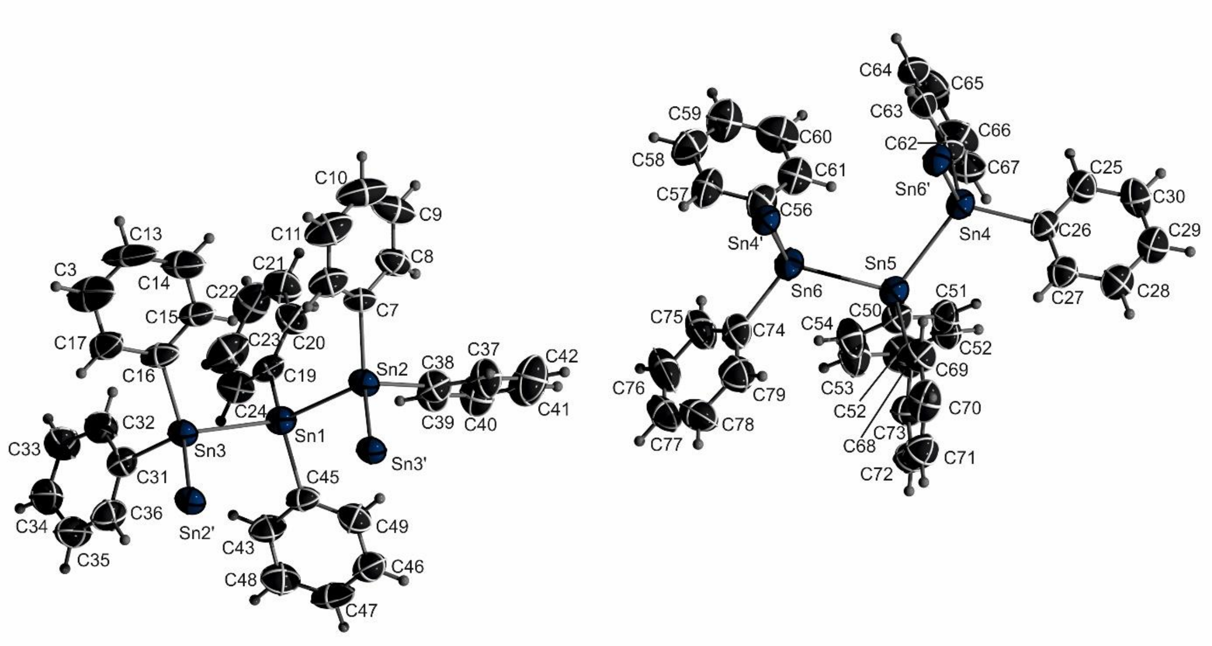

Figure 3. ORTEP of compound **74**. Ellipsoids of carbon atoms are drawn at the 50% probability level, the ellipsoids of tin atoms are drawn at the 30% probability level.

Table 5. Atomic coordinates (x 10^4) and equivalent isotropic displacement parameters (Å^{2}x 10^3) for **74**. U(eq) is defined as one third of the trace of the orthogonalized U^{ij} tensor.

	x	y	z	U(eq)
Sn(1)	-5683(1)	4806(1)	-1047(1)	46(1)
Sn(2)	-4456(1)	5254(1)	-1140(1)	47(1)
Sn(3)	-3818(1)	4552(1)	-53(1)	46(1)
C(3)	-3594(14)	1396(13)	-457(8)	132(10)
C(7)	-4233(5)	6760(7)	-1309(5)	46(2)
C(8)	-4106(5)	7039(10)	-1936(6)	61(3)
C(9)	-3950(6)	7983(11)	-2061(8)	78(4)
C(10)	-3919(7)	8652(11)	-1606(9)	92(5)
C(11)	-4032(8)	8401(11)	-966(9)	93(5)
C(12)	-4186(6)	7456(10)	-829(7)	69(3)
C(13)	-3991(14)	983(10)	-67(8)	137(10)
C(14)	-4375(9)	1507(11)	295(7)	88(5)
C(15)	-4311(6)	2499(8)	299(6)	62(3)
C(16)	-3906(6)	2983(8)	-68(5)	60(3)
C(17)	-3553(9)	2427(10)	-467(6)	84(5)

C(19)	-6233(5)	5378(7)	-1850(5)	49(2)
C(20)	-6005(6)	6041(10)	-2258(6)	63(3)
C(21)	-6393(8)	6392(13)	-2787(6)	80(4)
C(22)	-6958(8)	6103(13)	-2877(7)	84(5)
C(23)	-7200(8)	5436(13)	-2467(8)	88(5)
C(24)	-6838(6)	5055(10)	-1945(6)	68(3)
C(31)	-2856(5)	4953(8)	-39(5)	52(2)
C(32)	-2440(5)	4440(10)	332(6)	62(3)
C(33)	-1819(6)	4664(12)	363(7)	72(3)
C(34)	-1616(6)	5450(11)	18(7)	70(3)
C(35)	-2069(7)	6008(11)	-324(8)	79(4)
C(36)	-2659(6)	5761(10)	-351(7)	67(3)
C(37)	-3563(7)	4464(11)	-2098(6)	71(3)
C(38)	-4191(5)	4524(9)	-1973(5)	56(2)
C(39)	-4613(6)	4107(10)	-2417(6)	63(3)
C(40)	-4456(7)	3678(12)	-2953(6)	76(4)
C(41)	-3838(8)	3647(12)	-3071(7)	84(4)
C(42)	-3402(8)	4033(14)	-2655(8)	90(5)
C(43)	-6328(6)	2808(9)	-962(6)	64(3)
C(45)	-5785(5)	3225(7)	-1063(5)	53(2)
C(46)	-5375(7)	1633(10)	-1245(6)	69(3)
C(47)	-5941(9)	1228(10)	-1161(7)	81(4)
C(48)	-6422(6)	1793(10)	-984(7)	72(3)
C(49)	-5305(6)	2627(10)	-1210(6)	64(3)
Sn(4)	-480(1)	5721(1)	-3921(1)	50(1)
Sn(5)	320(1)	6852(1)	-4570(1)	51(1)
Sn(6)	-1044(1)	4347(1)	-4740(1)	55(1)
C(25)	-1439(6)	6247(10)	-2977(6)	62(3)
C(26)	-1199(4)	6573(8)	-3531(5)	52(2)
C(27)	-1473(6)	7334(9)	-3863(6)	60(3)
C(28)	-1968(6)	7806(11)	-3621(6)	67(3)
C(29)	-2193(6)	7509(11)	-3071(7)	70(3)
C(30)	-1919(6)	6743(11)	-2731(6)	68(3)
C(50)	911(5)	7724(9)	-3947(5)	55(2)
C(51)	705(6)	8133(9)	-3395(6)	61(3)
C(52)	1086(6)	8682(10)	-2994(6)	67(3)
C(53)	1675(6)	8889(11)	-3131(7)	72(3)
C(54)	1892(6)	8488(12)	-3668(8)	83(4)
C(55)	1513(6)	7910(11)	-4091(6)	69(3)

C(56)	-1628(5)	5248(10)	-5386(7)	66(3)
C(57)	-2082(6)	5804(11)	-5134(8)	76(4)
C(58)	-2437(6)	6420(12)	-5533(8)	81(4)
C(59)	-2343(6)	6482(14)	-6158(8)	85(4)
C(60)	-1892(7)	5933(13)	-6409(8)	84(4)
C(61)	-1550(6)	5302(11)	-6016(7)	69(3)
C(62)	57(5)	5141(9)	-3110(6)	59(3)
C(63)	217(6)	4156(11)	-3070(6)	67(3)
C(64)	615(7)	3833(14)	-2522(9)	92(6)
C(65)	819(8)	4489(17)	-2086(9)	94(5)
C(66)	664(8)	5454(15)	-2138(8)	91(5)
C(67)	281(6)	5755(11)	-2635(6)	71(3)
C(68)	-116(5)	7833(10)	-5260(6)	60(3)
C(69)	-603(6)	7526(10)	-5679(6)	62(3)
C(70)	-836(7)	8140(12)	-6162(6)	77(4)
C(71)	-578(7)	9068(12)	-6230(7)	80(4)
C(72)	-116(8)	9372(12)	-5830(7)	82(4)
C(73)	123(6)	8757(9)	-5329(6)	63(3)
C(74)	-1649(6)	3491(10)	-4200(6)	62(3)
C(75)	-2263(7)	3530(13)	-4379(8)	88(5)
C(76)	-2668(9)	3047(14)	-4026(9)	101(6)
C(77)	-2465(8)	2516(12)	-3498(7)	79(4)
C(78)	-1878(9)	2480(13)	-3336(8)	90(5)
C(79)	-1445(8)	2967(13)	-3696(8)	84(4)

Table 6. Anisotropic displacement parameters (Å^{2}x 10^3) for **74.** The anisotropic displacement factor exponent takes the form: -2p^2[h^2 a*^{2}U^{11} + ... + 2 h k a* b* U^{12}]

	U^{11}	U^{22}	U^{33}	U^{23}	U^{13}	U^{12}
Sn(1)	53(1)	44(1)	40(1)	-2(1)	-3(1)	-3(1)
Sn(2)	54(1)	46(1)	39(1)	1(1)	-1(1)	-6(1)
Sn(3)	54(1)	44(1)	41(1)	0(1)	0(1)	-3(1)
C(3)	280(30)	61(9)	63(9)	-19(7)	56(14)	16(13)
C(7)	53(5)	40(5)	46(5)	7(4)	-6(4)	-3(4)
C(8)	60(6)	67(7)	55(6)	20(5)	-3(5)	-1(5)
C(9)	55(6)	86(10)	89(10)	42(8)	-22(6)	-25(6)
C(10)	95(10)	54(8)	121(14)	23(8)	-45(10)	-10(7)
C(11)	108(12)	58(8)	107(13)	-13(8)	-33(10)	-11(8)

C(12)	79(8)	55(7)	70(8)	2(6)	-16(6)	-1(6)
C(13)	330(30)	30(7)	60(9)	7(6)	41(13)	10(11)
C(14)	156(15)	50(7)	59(8)	2(6)	10(8)	-9(8)
C(15)	93(8)	35(5)	56(6)	6(4)	1(6)	1(5)
C(16)	99(9)	34(5)	44(5)	-4(4)	-7(5)	-3(5)
C(17)	144(14)	55(7)	57(7)	8(6)	32(8)	29(8)
C(19)	59(6)	36(5)	49(5)	-2(4)	-9(4)	6(4)
C(20)	66(7)	69(8)	54(6)	2(5)	1(5)	-1(6)
C(21)	96(10)	94(11)	50(7)	20(7)	3(6)	13(8)
C(22)	98(11)	100(12)	52(7)	-6(7)	-19(7)	32(9)
C(23)	78(9)	88(10)	91(11)	-6(9)	-35(8)	8(8)
C(24)	68(7)	70(8)	63(7)	6(6)	-8(6)	-10(6)
C(31)	57(6)	49(6)	50(6)	-2(4)	-3(4)	0(4)
C(32)	53(6)	70(8)	61(7)	9(6)	-6(5)	-3(5)
C(33)	65(7)	88(10)	62(8)	13(7)	-6(6)	2(6)
C(34)	59(7)	74(8)	75(8)	0(7)	0(6)	-3(6)
C(35)	71(8)	70(9)	96(11)	23(8)	2(7)	-2(6)
C(36)	62(7)	63(8)	73(8)	4(6)	-9(6)	1(5)
C(37)	81(8)	81(9)	51(7)	-17(6)	5(6)	-2(7)
C(38)	61(6)	58(6)	46(6)	-4(5)	-5(4)	-1(5)
C(39)	77(7)	62(7)	50(6)	-4(5)	2(5)	-2(6)
C(40)	82(9)	98(11)	48(6)	-12(6)	-4(6)	10(7)
C(41)	113(12)	81(10)	58(8)	-14(7)	3(7)	3(8)
C(42)	80(9)	104(12)	86(10)	-27(9)	-3(8)	10(8)
C(43)	70(7)	45(6)	76(8)	-1(5)	-3(6)	-9(5)
C(45)	74(7)	34(5)	49(6)	-2(4)	0(5)	-3(4)
C(46)	91(9)	54(7)	63(7)	3(5)	4(6)	12(6)
C(47)	131(13)	37(6)	72(8)	0(6)	-3(8)	-1(7)
C(48)	71(8)	66(8)	80(9)	0(6)	-5(6)	-16(6)
C(49)	68(7)	67(8)	56(6)	4(5)	2(5)	-5(6)
Sn(4)	52(1)	49(1)	48(1)	-3(1)	0(1)	1(1)
Sn(5)	53(1)	50(1)	49(1)	-3(1)	1(1)	0(1)
Sn(6)	52(1)	55(1)	58(1)	-8(1)	3(1)	-1(1)
C(25)	67(7)	67(7)	52(6)	-2(5)	3(5)	9(6)
C(26)	41(5)	55(6)	59(6)	-1(5)	-4(4)	3(4)
C(27)	70(7)	53(6)	58(6)	-8(5)	6(5)	0(5)
C(28)	61(7)	71(8)	69(8)	-2(6)	-6(5)	2(6)
C(29)	66(7)	75(9)	68(8)	-6(6)	2(6)	9(6)
C(30)	63(7)	95(10)	47(6)	-3(6)	1(5)	3(6)

C(50)	62(6)	54(6)	48(6)	-3(4)	-1(4)	3(5)
C(51)	73(7)	56(7)	55(6)	-11(5)	18(5)	-2(5)
C(52)	87(8)	62(7)	52(6)	-5(5)	18(6)	2(6)
C(53)	73(8)	75(9)	67(8)	-13(6)	-12(6)	-5(6)
C(54)	58(7)	94(11)	99(11)	-33(9)	12(7)	-17(7)
C(55)	54(6)	87(9)	66(7)	-15(6)	9(5)	-12(6)
C(56)	47(6)	71(8)	78(8)	-5(6)	-6(5)	4(5)
C(57)	60(7)	79(9)	90(10)	-21(7)	1(6)	7(6)
C(58)	60(7)	80(10)	99(11)	2(8)	-14(7)	13(6)
C(59)	61(7)	105(12)	85(10)	-9(9)	-16(7)	6(7)
C(60)	77(9)	99(11)	70(9)	11(8)	-23(7)	-8(8)
C(61)	62(7)	76(9)	66(8)	-12(6)	-7(6)	-1(6)
C(62)	55(6)	65(7)	56(6)	8(5)	7(5)	6(5)
C(63)	68(7)	77(8)	59(7)	7(6)	22(6)	6(6)
C(64)	81(9)	88(11)	112(13)	53(10)	35(9)	35(8)
C(65)	88(11)	123(16)	72(10)	13(10)	8(8)	8(10)
C(66)	86(10)	116(14)	69(9)	20(9)	-13(7)	-10(9)
C(67)	80(8)	75(9)	56(7)	8(6)	-6(6)	-1(6)
C(68)	53(6)	72(8)	54(6)	-5(5)	7(5)	7(5)
C(69)	67(7)	67(7)	52(6)	-2(5)	-3(5)	1(6)
C(70)	77(8)	96(11)	57(7)	-17(7)	-8(6)	12(7)
C(71)	91(10)	79(10)	68(8)	2(7)	-2(7)	16(8)
C(72)	105(11)	73(9)	69(9)	16(7)	11(8)	18(8)
C(73)	73(7)	54(7)	62(7)	2(5)	5(5)	-4(5)
C(74)	72(7)	66(7)	49(6)	-16(5)	7(5)	-3(6)
C(75)	75(9)	98(12)	95(11)	-15(9)	35(8)	-28(8)
C(76)	98(11)	110(13)	102(13)	-42(11)	54(10)	-44(10)
C(77)	96(10)	81(9)	64(8)	-18(7)	32(7)	-26(8)
C(78)	119(13)	80(10)	75(9)	5(8)	28(9)	-24(9)
C(79)	87(10)	85(11)	81(10)	-4(8)	11(8)	-4(8)

Crystal Structure Determination of 76

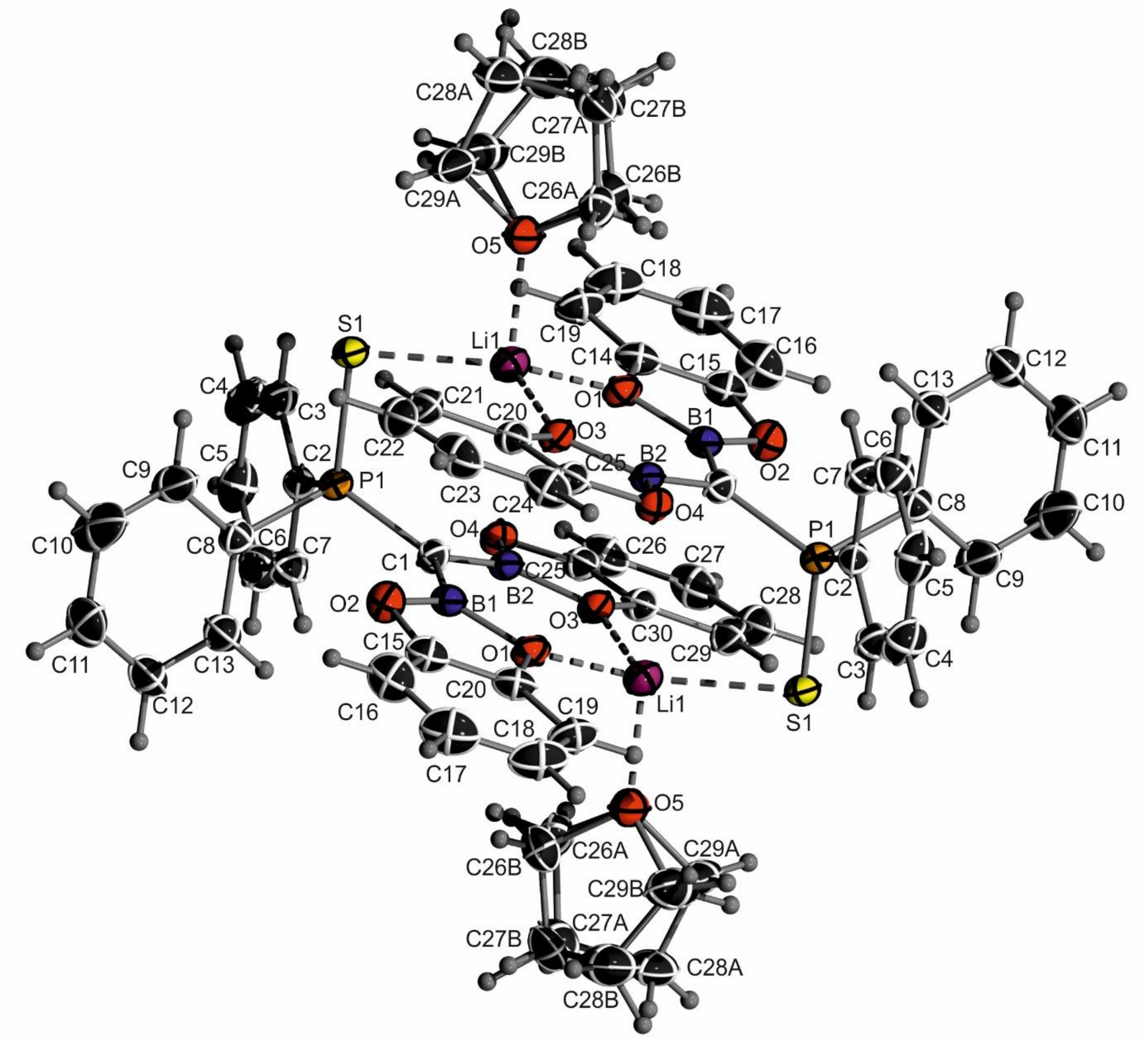

Figure 4. ORTEP of compound **76**. Ellipsoids are drawn at the 50% probability level.

Table 7. Atomic coordinates (x 10^4) and equivalent isotropic displacement parameters ($Å^2$x 10^3) for **76**. U(eq) is defined as one third of the trace of the orthogonalized U^{ij} tensor.

	x	y	z	U(eq)
S(1)	4989(1)	-3566(1)	2955(1)	29(1)
P(1)	6737(1)	-2235(1)	3670(1)	21(1)
O(1)	6834(1)	888(1)	6662(1)	24(1)
O(2)	7404(1)	-904(1)	6594(1)	28(1)
O(3)	6036(1)	1263(1)	4528(1)	24(1)
O(4)	6227(1)	-72(1)	2752(1)	25(1)
B(1)	6974(2)	-279(2)	5885(2)	23(1)
B(2)	6335(2)	110(2)	3936(2)	22(1)

Li(1)	6308(3)	2215(3)	6267(3)	30(1)
C(1)	6731(2)	-706(2)	4540(2)	22(1)
C(2)	7231(2)	-2342(2)	2404(2)	24(1)
C(3)	6490(2)	-3303(2)	1190(2)	31(1)
C(4)	6915(2)	-3386(2)	256(2)	39(1)
C(5)	8063(2)	-2517(2)	521(2)	40(1)
C(6)	8796(2)	-1552(2)	1728(2)	37(1)
C(7)	8377(2)	-1471(2)	2662(2)	32(1)
C(8)	8114(2)	-2601(2)	4650(2)	25(1)
C(9)	7934(2)	-3753(2)	4643(2)	45(1)
C(10)	9003(3)	-3994(2)	5408(3)	64(1)
C(11)	10247(3)	-3100(2)	6175(2)	48(1)
C(12)	10433(2)	-1955(2)	6187(2)	36(1)
C(13)	9366(2)	-1712(2)	5426(2)	34(1)
C(14)	7207(2)	943(2)	7838(2)	26(1)
C(15)	7555(2)	-134(2)	7785(2)	28(1)
C(16)	7995(2)	-327(2)	8823(2)	40(1)
C(17)	8045(2)	615(2)	9923(2)	45(1)
C(18)	7668(2)	1682(2)	9964(2)	42(1)
C(19)	7236(2)	1872(2)	8908(2)	34(1)
C(20)	5772(2)	1753(2)	3686(2)	24(1)
C(21)	5428(2)	2844(2)	3812(2)	32(1)
C(22)	5228(2)	3106(2)	2806(2)	37(1)
C(23)	5390(2)	2317(2)	1759(2)	39(1)
C(24)	5740(2)	1216(2)	1652(2)	35(1)
C(25)	5898(2)	949(2)	2631(2)	26(1)
O(5)	8007(1)	3518(1)	7015(1)	38(1)
C(26A)	9059(5)	3305(4)	6588(4)	31(1)
C(27A)	10271(7)	4416(7)	7518(7)	42(2)
C(28A)	9724(4)	5429(4)	8199(5)	49(1)
C(29A)	8246(6)	4819(5)	7704(9)	85(3)
C(26B)	9274(7)	3249(7)	7126(10)	55(2)
C(27B)	10416(10)	4376(11)	7822(10)	50(3)
C(28B)	9975(7)	4926(8)	8775(7)	67(2)
C(29B)	8528(8)	4649(8)	8189(8)	61(2)

Table 8. Anisotropic displacement parameters (Å^{2}x 10^3) for **76**. The anisotropic displacement factor exponent takes the form: -2p^2[h^2 a*^{2}U^{11} + ... + 2 h k a* b* U^{12}]

	U^{11}	U^{22}	U^{33}	U^{23}	U^{13}	U^{12}
S(1)	23(1)	19(1)	34(1)	5(1)	10(1)	2(1)
P(1)	20(1)	17(1)	22(1)	6(1)	7(1)	4(1)
O(1)	27(1)	23(1)	17(1)	6(1)	7(1)	5(1)
O(2)	33(1)	28(1)	25(1)	13(1)	12(1)	10(1)
O(3)	29(1)	20(1)	23(1)	10(1)	9(1)	7(1)
O(4)	28(1)	25(1)	21(1)	10(1)	10(1)	9(1)
B(1)	20(1)	21(1)	22(1)	8(1)	6(1)	2(1)
B(2)	19(1)	19(1)	20(1)	5(1)	6(1)	2(1)
Li(1)	31(2)	27(2)	28(2)	9(1)	11(1)	9(1)
C(1)	23(1)	20(1)	21(1)	7(1)	8(1)	5(1)
C(2)	26(1)	23(1)	24(1)	9(1)	9(1)	11(1)
C(3)	34(1)	26(1)	25(1)	9(1)	8(1)	8(1)
C(4)	53(1)	36(1)	24(1)	10(1)	14(1)	15(1)
C(5)	54(1)	42(1)	36(1)	21(1)	27(1)	23(1)
C(6)	37(1)	38(1)	43(1)	18(1)	24(1)	13(1)
C(7)	30(1)	30(1)	30(1)	9(1)	12(1)	7(1)
C(8)	25(1)	24(1)	24(1)	9(1)	10(1)	9(1)
C(9)	44(1)	27(1)	41(1)	15(1)	-4(1)	2(1)
C(10)	71(2)	35(1)	61(2)	29(1)	-6(1)	10(1)
C(11)	49(1)	46(1)	41(1)	22(1)	2(1)	21(1)
C(12)	26(1)	44(1)	36(1)	18(1)	9(1)	11(1)
C(13)	26(1)	33(1)	41(1)	20(1)	10(1)	8(1)
C(14)	23(1)	30(1)	20(1)	10(1)	6(1)	0(1)
C(15)	25(1)	32(1)	25(1)	12(1)	9(1)	3(1)
C(16)	42(1)	49(1)	35(1)	27(1)	15(1)	12(1)
C(17)	48(1)	57(1)	26(1)	23(1)	11(1)	5(1)
C(18)	46(1)	45(1)	22(1)	8(1)	14(1)	-2(1)
C(19)	37(1)	30(1)	24(1)	6(1)	12(1)	1(1)
C(20)	21(1)	25(1)	24(1)	13(1)	5(1)	3(1)
C(21)	32(1)	24(1)	33(1)	13(1)	8(1)	6(1)
C(22)	32(1)	32(1)	47(1)	26(1)	7(1)	6(1)
C(23)	34(1)	47(1)	39(1)	30(1)	9(1)	8(1)
C(24)	32(1)	43(1)	30(1)	21(1)	10(1)	9(1)
C(25)	21(1)	27(1)	26(1)	13(1)	5(1)	4(1)
O(5)	29(1)	31(1)	43(1)	5(1)	16(1)	4(1)
C(26A)	32(2)	32(2)	38(2)	17(2)	19(2)	13(1)

C(27A)	25(2)	51(2)	53(3)	30(2)	11(2)	10(2)
C(28A)	31(2)	38(2)	59(3)	10(2)	16(2)	-4(2)
C(29A)	36(2)	29(2)	133(6)	-13(3)	37(3)	-4(2)
C(26B)	29(2)	46(3)	75(4)	13(3)	19(3)	15(2)
C(27B)	28(3)	48(3)	62(5)	26(3)	2(3)	14(2)
C(28B)	45(3)	55(4)	66(3)	10(3)	12(2)	-7(2)
C(29B)	45(3)	48(3)	56(3)	-5(3)	23(2)	-2(2)

Crystal Structure Determination of *S*, *S*-82

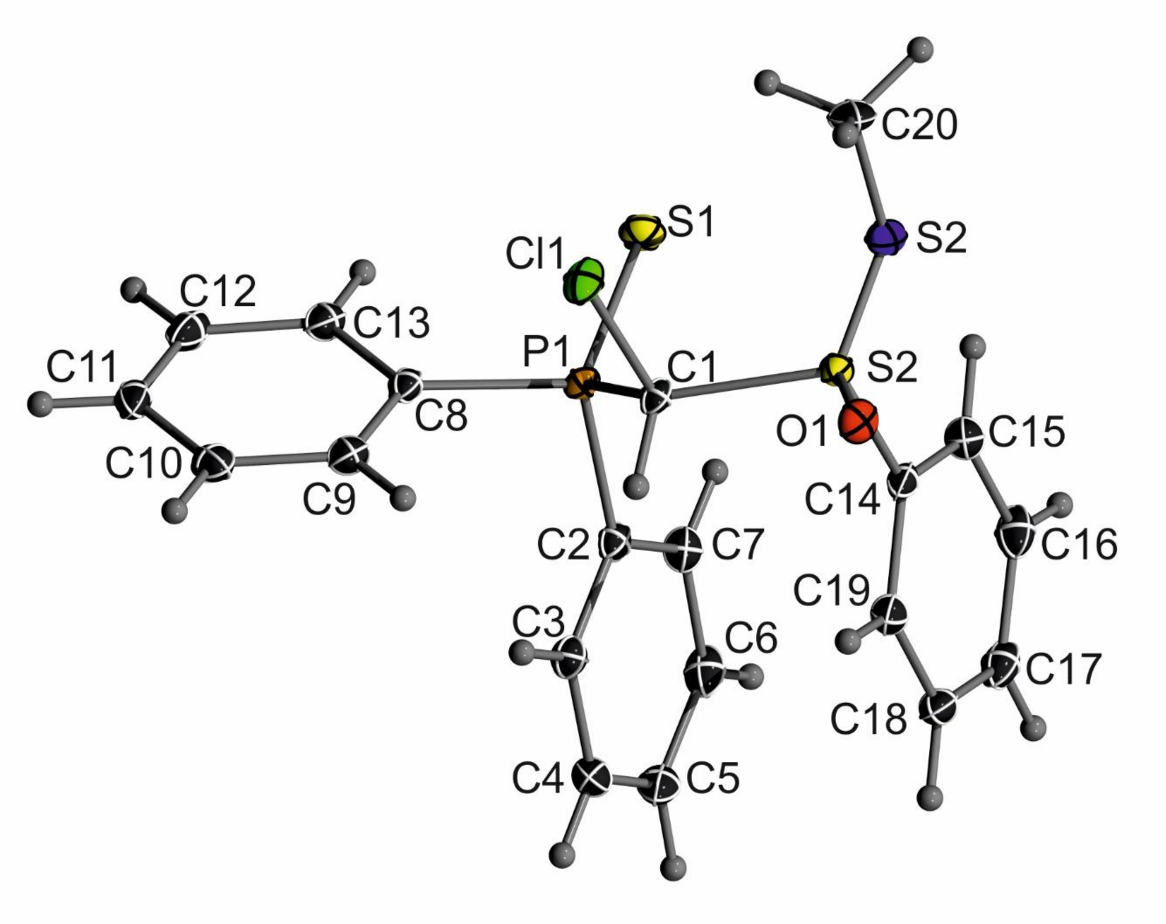

Figure 5. ORTEP of compound *S,S*-**82**. Ellipsoids are drawn at the 50% probability level.

Table 9. Atomic coordinates (x 10^4) and equivalent isotropic displacement parameters (Å^{2}x 10^3) for *S,S*-**82**. U(eq) is defined as one third of the trace of the orthogonalized U^{ij} tensor.

	x	y	z	U(eq)
Cl(1)	8242(1)	11120(1)	5139(1)	18(1)
S(1)	8417(1)	9172(1)	1976(1)	18(1)
S(2)	6077(1)	8978(1)	4718(1)	13(1)
P(1)	7297(1)	10780(1)	2498(1)	11(1)
O(1)	5466(1)	9451(1)	5862(1)	17(1)
N(1)	7085(1)	7744(1)	4670(1)	17(1)
C(1)	6767(1)	10695(2)	4131(1)	12(1)
C(2)	5613(1)	11040(2)	1648(1)	13(1)
C(3)	4751(2)	12213(2)	1896(1)	16(1)
C(4)	3489(2)	12413(2)	1225(1)	19(1)

C(5)	3072(2)	11476(2)	295(1)	20(1)
C(6)	3918(2)	10310(2)	44(1)	20(1)
C(7)	5188(2)	10086(2)	724(1)	16(1)
C(8)	8193(1)	12485(2)	2376(1)	14(1)
C(9)	7820(2)	13670(2)	3063(1)	16(1)
C(10)	8456(2)	14971(2)	2860(1)	19(1)
C(11)	9481(2)	15091(2)	1965(1)	21(1)
C(12)	9853(2)	13930(2)	1278(1)	21(1)
C(13)	9229(2)	12614(2)	1488(1)	17(1)
C(14)	4674(1)	8571(2)	3646(1)	15(1)
C(15)	4767(2)	7442(2)	2839(1)	18(1)
C(16)	3614(2)	7182(2)	2027(1)	21(1)
C(17)	2423(2)	8058(2)	2018(1)	21(1)
C(18)	2342(2)	9184(2)	2840(1)	20(1)
C(19)	3472(2)	9445(2)	3671(1)	17(1)
C(20)	8416(2)	7676(2)	5438(2)	23(1)

Table 10. Anisotropic displacement parameters (Å^{2}x 10^3) for *S*, *S*-**82**. The anisotropic displacement factor exponent takes the form: -2p^2[h^2 a*^{2}U^{11} + ... + 2 h k a* b* U^{12}]

	U^{11}	U^{22}	U^{33}	U^{23}	U^{13}	U^{12}
Cl(1)	18(1)	22(1)	15(1)	0(1)	-4(1)	-5(1)
S(1)	16(1)	17(1)	20(1)	-4(1)	3(1)	3(1)
S(2)	11(1)	13(1)	13(1)	2(1)	-1(1)	-1(1)
P(1)	10(1)	13(1)	11(1)	-1(1)	1(1)	0(1)
O(1)	18(1)	20(1)	13(1)	1(1)	2(1)	-1(1)
N(1)	14(1)	17(1)	20(1)	0(1)	-3(1)	1(1)
C(1)	11(1)	14(1)	11(1)	-1(1)	-1(1)	-2(1)
C(2)	13(1)	15(1)	11(1)	2(1)	0(1)	-2(1)
C(3)	16(1)	16(1)	15(1)	-1(1)	0(1)	-2(1)
C(4)	17(1)	16(1)	24(1)	4(1)	1(1)	1(1)
C(5)	17(1)	23(1)	20(1)	7(1)	-6(1)	-2(1)
C(6)	25(1)	20(1)	16(1)	1(1)	-4(1)	-6(1)
C(7)	18(1)	17(1)	14(1)	-1(1)	1(1)	-2(1)
C(8)	11(1)	16(1)	15(1)	2(1)	-2(1)	-2(1)
C(9)	14(1)	18(1)	16(1)	0(1)	1(1)	0(1)
C(10)	17(1)	17(1)	23(1)	-1(1)	-5(1)	0(1)
C(11)	16(1)	20(1)	28(1)	9(1)	-6(1)	-5(1)

C(12)	14(1)	30(1)	20(1)	9(1)	1(1)	-2(1)
C(13)	14(1)	21(1)	16(1)	2(1)	1(1)	1(1)
C(14)	12(1)	16(1)	16(1)	4(1)	-1(1)	-4(1)
C(15)	17(1)	16(1)	20(1)	2(1)	1(1)	-1(1)
C(16)	24(1)	20(1)	20(1)	-1(1)	-2(1)	-6(1)
C(17)	19(1)	25(1)	19(1)	5(1)	-4(1)	-7(1)
C(18)	13(1)	22(1)	24(1)	6(1)	-1(1)	-1(1)
C(19)	16(1)	16(1)	18(1)	2(1)	1(1)	-2(1)
C(20)	14(1)	22(1)	31(1)	3(1)	-7(1)	3(1)

Crystal Structure Determination of *rac*-83-Li

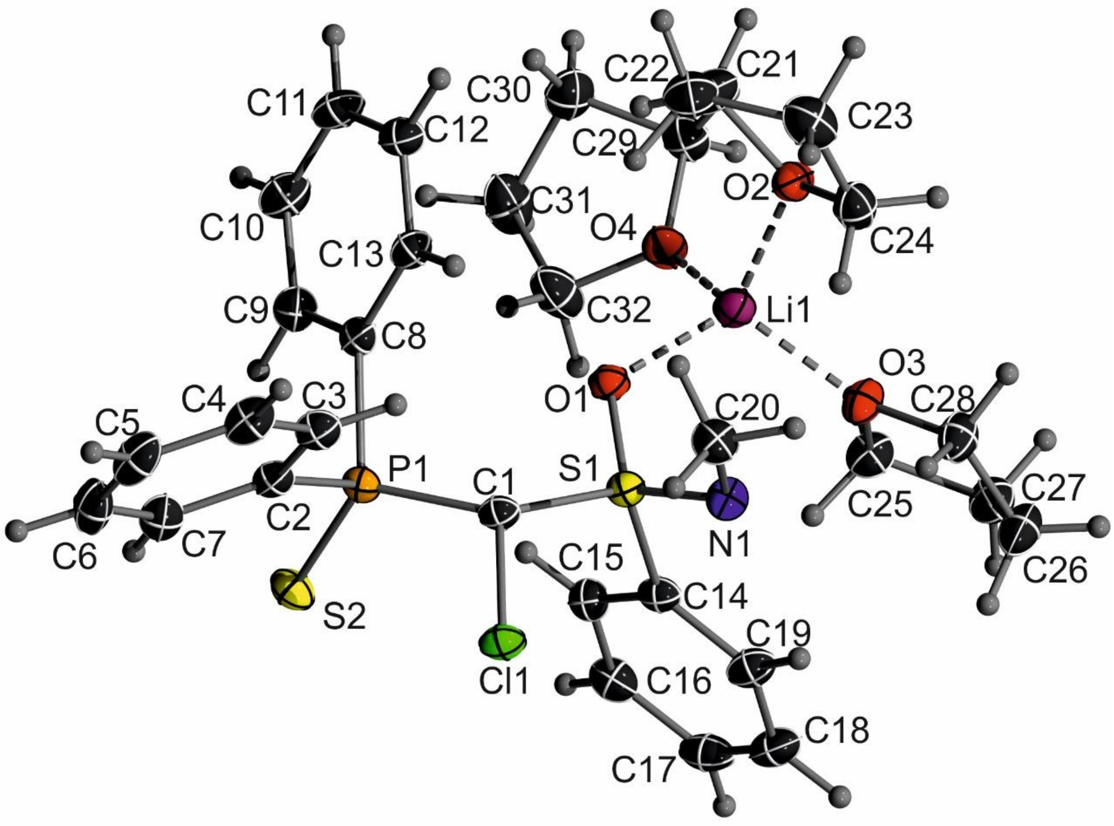

Figure 6. ORTEP of compound *rac*-**83-Li**. Ellipsoids are drawn at the 50% probability level.

Table 11. Atomic coordinates (x 10^4) and equivalent isotropic displacement parameters (Å^{2}x 10^3) for *rac*-**83-Li**. U(eq) is defined as one third of the trace of the orthogonalized U^{ij} tensor.

	x	y	z	U(eq)
Li(1)	3025(3)	5815(1)	2182(1)	24(1)
Cl(1)	7063(1)	6836(1)	4726(1)	23(1)
S(1)	5020(1)	6278(1)	3538(1)	18(1)
S(2)	4178(1)	8238(1)	4248(1)	25(1)
P(1)	5592(1)	7799(1)	3658(1)	18(1)
N(1)	5930(1)	5632(1)	3632(1)	22(1)
O(1)	4221(1)	6458(1)	2803(1)	21(1)
O(2)	4174(1)	5459(1)	1439(1)	26(1)
O(3)	2257(1)	5067(1)	2676(1)	25(1)
O(4)	1346(1)	6334(1)	1695(1)	28(1)
C(1)	6080(2)	6955(1)	3822(1)	19(1)
C(2)	7437(2)	8218(1)	3797(1)	21(1)
C(3)	8700(2)	7909(1)	3563(1)	25(1)

C(4)	10076(2)	8240(1)	3634(1)	30(1)
C(5)	10206(2)	8880(1)	3932(1)	33(1)
C(6)	8963(2)	9187(1)	4161(1)	32(1)
C(7)	7577(2)	8854(1)	4099(1)	27(1)
C(8)	5005(2)	7904(1)	2667(1)	19(1)
C(9)	3838(2)	8345(1)	2424(1)	24(1)
C(10)	3452(2)	8468(1)	1671(1)	31(1)
C(11)	4214(2)	8148(1)	1157(1)	29(1)
C(12)	5372(2)	7704(1)	1397(1)	26(1)
C(13)	5773(2)	7585(1)	2146(1)	22(1)
C(14)	3547(2)	6118(1)	4088(1)	20(1)
C(15)	2388(2)	6588(1)	4062(1)	23(1)
C(16)	1206(2)	6475(1)	4473(1)	26(1)
C(17)	1186(2)	5904(1)	4902(1)	29(1)
C(18)	2356(2)	5444(1)	4931(1)	31(1)
C(19)	3547(2)	5552(1)	4523(1)	26(1)
C(20)	7429(2)	5645(1)	3382(1)	26(1)
C(21)	4621(2)	5950(1)	928(1)	32(1)
C(22)	6331(2)	5978(1)	1085(1)	34(1)
C(23)	6709(2)	5247(1)	1247(1)	38(1)
C(24)	5443(2)	5019(1)	1666(1)	31(1)
C(25)	770(2)	5080(1)	2898(1)	27(1)
C(26)	449(2)	4369(1)	3118(1)	31(1)
C(27)	2012(2)	4109(1)	3416(1)	35(1)
C(28)	3023(2)	4455(1)	2924(1)	29(1)
C(29)	656(2)	6284(1)	936(1)	28(1)
C(30)	416(2)	6997(1)	677(1)	35(1)
C(31)	2(2)	7338(1)	1368(1)	39(1)
C(32)	946(2)	6968(1)	1994(1)	39(1)

Table 12. Anisotropic displacement parameters (Å^{2}x 10^3) for *rac*-**83-Li**. The anisotropic displacement factor exponent takes the form: $-2p^2[h^2 a^{*2}U^{11} + ... + 2 h k a^* b^* U^{12}]$

	U^{11}	U^{22}	U^{33}	U^{23}	U^{13}	U^{12}
Li(1)	23(1)	24(1)	23(1)	1(1)	1(1)	-1(1)
Cl(1)	21(1)	29(1)	17(1)	2(1)	-2(1)	-1(1)
S(1)	16(1)	20(1)	17(1)	1(1)	1(1)	-1(1)
S(2)	22(1)	28(1)	25(1)	-6(1)	6(1)	1(1)

P(1)	15(1)	20(1)	17(1)	-1(1)	1(1)	-1(1)
N(1)	19(1)	23(1)	25(1)	1(1)	4(1)	1(1)
O(1)	21(1)	24(1)	18(1)	1(1)	0(1)	-3(1)
O(2)	28(1)	26(1)	23(1)	2(1)	5(1)	1(1)
O(3)	22(1)	24(1)	32(1)	4(1)	9(1)	0(1)
O(4)	29(1)	26(1)	25(1)	-1(1)	-4(1)	5(1)
C(1)	18(1)	23(1)	16(1)	1(1)	-1(1)	0(1)
C(2)	18(1)	24(1)	20(1)	4(1)	-1(1)	-3(1)
C(3)	22(1)	29(1)	23(1)	2(1)	0(1)	-2(1)
C(4)	20(1)	36(1)	32(1)	8(1)	2(1)	-2(1)
C(5)	24(1)	36(1)	38(1)	11(1)	-5(1)	-11(1)
C(6)	31(1)	24(1)	39(1)	3(1)	-8(1)	-8(1)
C(7)	24(1)	26(1)	29(1)	2(1)	-4(1)	0(1)
C(8)	16(1)	21(1)	20(1)	2(1)	-1(1)	-3(1)
C(9)	21(1)	25(1)	27(1)	1(1)	0(1)	1(1)
C(10)	25(1)	35(1)	30(1)	7(1)	-3(1)	5(1)
C(11)	28(1)	37(1)	21(1)	8(1)	-2(1)	-2(1)
C(12)	27(1)	30(1)	22(1)	2(1)	5(1)	-2(1)
C(13)	20(1)	24(1)	23(1)	3(1)	2(1)	0(1)
C(14)	17(1)	26(1)	17(1)	0(1)	0(1)	-2(1)
C(15)	21(1)	25(1)	24(1)	0(1)	2(1)	-2(1)
C(16)	20(1)	34(1)	26(1)	-6(1)	3(1)	-1(1)
C(17)	23(1)	45(1)	21(1)	-3(1)	5(1)	-8(1)
C(18)	30(1)	40(1)	22(1)	8(1)	2(1)	-6(1)
C(19)	22(1)	32(1)	23(1)	5(1)	0(1)	-1(1)
C(20)	20(1)	29(1)	29(1)	0(1)	4(1)	2(1)
C(21)	28(1)	40(1)	29(1)	11(1)	4(1)	1(1)
C(22)	29(1)	40(1)	32(1)	2(1)	8(1)	0(1)
C(23)	31(1)	43(1)	39(1)	-5(1)	4(1)	8(1)
C(24)	33(1)	26(1)	31(1)	-1(1)	-2(1)	2(1)
C(25)	20(1)	31(1)	30(1)	3(1)	5(1)	1(1)
C(26)	29(1)	31(1)	34(1)	-1(1)	10(1)	-6(1)
C(27)	37(1)	25(1)	45(1)	8(1)	13(1)	2(1)
C(28)	29(1)	22(1)	38(1)	2(1)	10(1)	4(1)
C(29)	24(1)	30(1)	27(1)	-2(1)	-5(1)	1(1)
C(30)	34(1)	33(1)	34(1)	6(1)	-6(1)	2(1)
C(31)	34(1)	34(1)	47(1)	-6(1)	-8(1)	10(1)
C(32)	42(1)	37(1)	36(1)	-9(1)	-5(1)	12(1)

Crystal Structure Determination of *rac*-83-Na

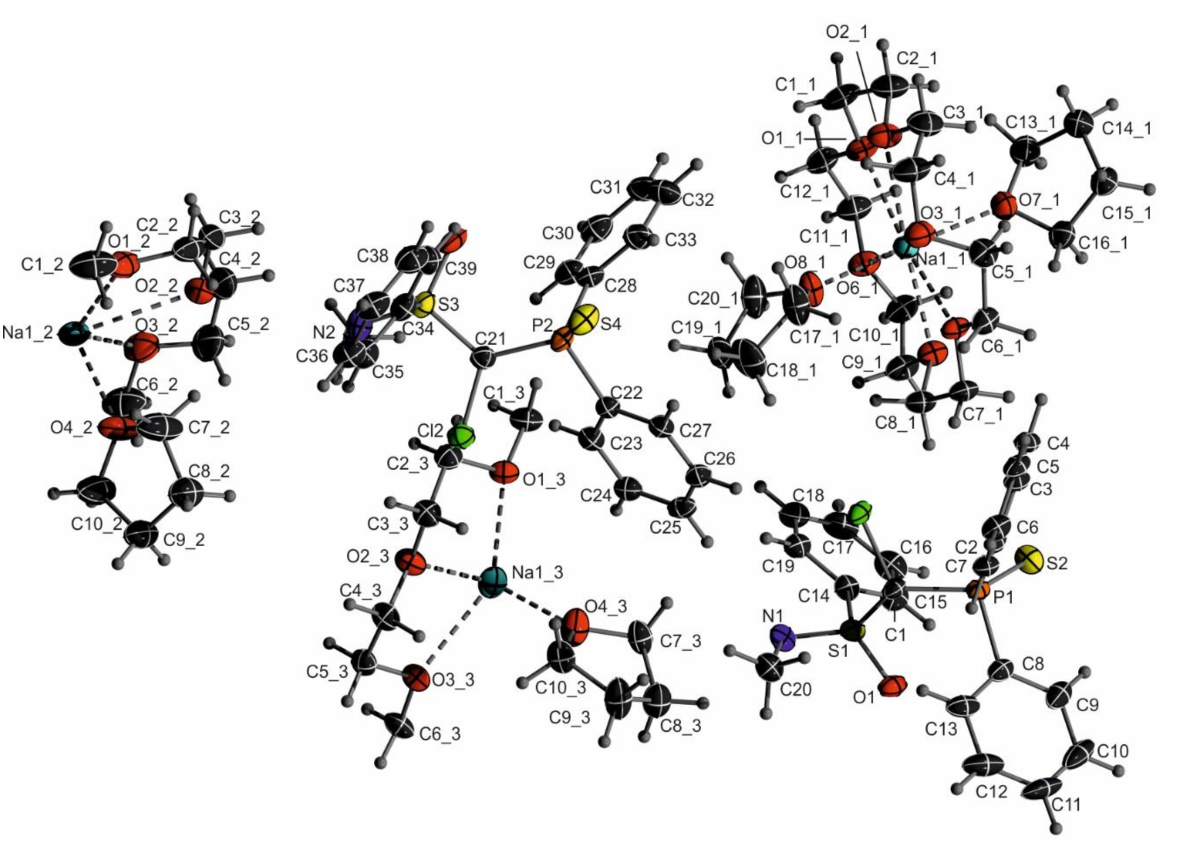

Figure 7. ORTEP of compound *rac*-**83-Na**. Ellipsoids are drawn at the 50% probability level.

Table 13. Atomic coordinates (x 10^4) and equivalent isotropic displacement parameters (Å^2 x 10^3) for *rac*-**83-Na**. U(eq) is defined as one third of the trace of the orthogonalized U^{ij} tensor.

	x	y	z	U(eq)
Cl(1)	5297(1)	1768(1)	3051(1)	27(1)
S(1)	6898(1)	1295(1)	2077(1)	24(1)
P(1)	5741(1)	280(1)	3199(1)	21(1)
O(1)	7226(2)	655(1)	1907(1)	29(1)
N(1)	6416(3)	1916(1)	1645(1)	28(1)
C(1)	5676(3)	1081(1)	2710(1)	23(1)
Cl(2)	3175(1)	5885(1)	1360(1)	30(1)
S(2)	7494(1)	-31(1)	3571(1)	33(1)
P(2)	3322(1)	5396(1)	2621(1)	25(1)
O(2)	3629(3)	6907(1)	2614(1)	37(1)
N(2)	3800(3)	7396(1)	1467(1)	35(1)
C(2)	4145(3)	312(1)	3762(1)	23(1)
S(3)	3242(1)	6876(1)	2032(1)	29(1)

C(3)	4340(3)	413(2)	4297(1)	26(1)
S(4)	1287(1)	5249(1)	3047(1)	34(1)
C(4)	3134(4)	479(2)	4716(1)	27(1)
C(5)	1711(4)	436(2)	4605(1)	29(1)
C(6)	1503(4)	329(2)	4077(2)	31(1)
C(7)	2714(3)	270(2)	3656(1)	26(1)
C(8)	5213(3)	-332(2)	2826(1)	28(1)
C(9)	5733(4)	-993(2)	2961(2)	39(1)
C(10)	5215(5)	-1474(2)	2716(2)	52(1)
C(11)	4209(5)	-1306(2)	2340(2)	54(1)
C(12)	3724(4)	-646(2)	2192(2)	48(1)
C(13)	4231(4)	-163(2)	2432(2)	34(1)
C(14)	8590(3)	1584(2)	2198(1)	26(1)
C(15)	9674(4)	1103(2)	2333(2)	34(1)
C(16)	11020(4)	1309(2)	2417(2)	39(1)
C(17)	11268(4)	1983(2)	2373(2)	40(1)
C(18)	10172(4)	2459(2)	2255(2)	35(1)
C(19)	8816(3)	2257(2)	2172(1)	28(1)
C(20)	4964(4)	1873(2)	1482(2)	34(1)
C(21)	3724(4)	6062(2)	1986(1)	28(1)
C(22)	4017(3)	4643(2)	2373(1)	23(1)
C(23)	5285(3)	4670(2)	1957(1)	28(1)
C(24)	5833(4)	4091(2)	1789(1)	30(1)
C(25)	5127(4)	3476(2)	2039(1)	30(1)
C(26)	3870(4)	3449(2)	2456(1)	29(1)
C(27)	3306(3)	4030(2)	2620(1)	25(1)
C(28)	4620(3)	5446(2)	3112(1)	26(1)
C(29)	6042(4)	5693(2)	2904(2)	33(1)
C(30)	7045(4)	5657(2)	3283(2)	41(1)
C(31)	6599(5)	5393(2)	3877(2)	47(1)
C(32)	5182(5)	5158(2)	4090(2)	51(1)
C(33)	4200(4)	5176(2)	3707(2)	39(1)
C(34)	1292(4)	7024(2)	2050(2)	33(1)
C(35)	674(4)	7154(2)	1545(2)	37(1)
C(36)	-848(4)	7273(2)	1583(2)	39(1)
C(37)	-1694(4)	7264(2)	2120(2)	40(1)
C(38)	-1058(4)	7132(2)	2617(2)	41(1)
C(39)	443(4)	7005(2)	2585(2)	37(1)
C(40)	5367(4)	7393(2)	1235(2)	40(1)

Na11	9080(1)	2667(1)	4848(1)	28(1)
O11	10339(3)	3581(1)	5159(1)	34(1)
C11	9450(4)	4011(2)	5459(2)	43(1)
O21	7260(3)	3377(1)	5628(1)	38(1)
C21	8316(4)	3579(2)	5915(2)	45(1)
O31	5283(3)	2539(1)	5321(1)	40(1)
C31	6073(4)	3029(2)	6053(2)	45(1)
O41	7332(2)	1781(1)	4727(1)	27(1)
C41	4874(5)	2920(2)	5748(2)	48(1)
O51	10202(2)	1923(1)	4188(1)	29(1)
C51	5533(4)	1843(2)	5555(2)	37(1)
O61	11677(2)	3028(1)	4275(1)	31(1)
C61	5989(4)	1508(2)	5067(2)	31(1)
O71	9979(3)	1952(1)	5645(1)	39(1)
C71	7883(4)	1406(2)	4304(1)	30(1)
O81	8176(2)	3351(1)	4064(1)	33(1)
C81	9102(4)	1782(2)	3873(2)	32(1)
C91	11518(4)	2160(2)	3804(2)	37(1)
C101	12463(4)	2459(2)	4132(2)	34(1)
C111	12505(4)	3404(2)	4533(2)	38(1)
C121	11505(4)	3921(2)	4747(2)	37(1)
C131	10812(5)	2026(2)	6080(2)	45(1)
C141	9953(5)	1633(2)	6660(2)	46(1)
C151	9144(4)	1100(2)	6482(2)	35(1)
C161	9603(4)	1252(2)	5821(2)	36(1)
C171	6665(4)	3390(2)	3988(2)	44(1)
C181	6689(6)	3586(3)	3335(2)	66(1)
C191	8181(5)	3904(2)	3085(2)	50(1)
C201	8915(4)	3870(2)	3610(2)	48(1)
Na12	0	10000	0	37(1)
O12	-2102(3)	9835(1)	934(1)	46(1)
C12	-3541(5)	10087(3)	871(2)	58(1)
O22	281(4)	9020(1)	1022(1)	50(1)
C22	-2099(6)	9288(2)	1432(2)	56(1)
O32	2663(3)	9340(2)	98(1)	51(1)
C32	-588(6)	9146(2)	1534(2)	56(1)
O42	-845(3)	9106(2)	-314(1)	52(1)
C42	1768(6)	8864(2)	1091(2)	62(1)
C52	2580(6)	8726(2)	535(2)	63(1)

C62	3416(5)	9253(3)	-446(2)	59(1)
C72	-2056(6)	8707(3)	37(2)	70(2)
C82	-2222(5)	8133(2)	-243(2)	52(1)
C92	-1432(5)	8376(2)	-860(2)	48(1)
C102	-757(7)	9025(3)	-879(2)	68(2)
Na13	10000	5000	0	34(1)
O13	8359(2)	5391(1)	956(1)	28(1)
C13	9216(4)	5444(2)	1384(2)	34(1)
O23	7590(2)	5836(1)	-159(1)	30(1)
C23	7503(4)	5978(2)	798(2)	32(1)
O33	8914(2)	5249(1)	-1025(1)	28(1)
C33	6603(4)	5891(2)	353(1)	32(1)
O43	8725(3)	3979(1)	286(1)	43(1)
C43	6827(4)	5796(2)	-620(2)	32(1)
C53	7936(4)	5801(2)	-1153(2)	31(1)
C63	9919(3)	5195(2)	-1536(1)	32(1)
C73	9138(4)	3316(2)	576(2)	38(1)
C83	8435(4)	2844(2)	302(2)	44(1)
C93	6981(4)	3196(2)	200(2)	50(1)
C103	7310(4)	3941(2)	119(2)	38(1)

Table 14. Anisotropic displacement parameters (Å^2 x 10^3) for *rac*-**83-Na**. The anisotropic displacement factor exponent takes the form: $-2\square^2[h^2 a^{*2}U^{11} + ... + 2 h k a^* b^* U^{12}]$

	U^{11}	U^{22}	U^{33}	U^{23}	U^{13}	U^{12}
Cl(1)	29(1)	21(1)	29(1)	-10(1)	4(1)	-1(1)
S(1)	21(1)	26(1)	23(1)	-8(1)	2(1)	-3(1)
P(1)	20(1)	22(1)	21(1)	-7(1)	2(1)	-2(1)
O(1)	30(1)	30(1)	28(1)	-14(1)	6(1)	-4(1)
N(1)	24(1)	34(1)	26(1)	-5(1)	-1(1)	-6(1)
C(1)	25(2)	19(1)	26(1)	-10(1)	1(1)	0(1)
Cl(2)	29(1)	32(1)	32(1)	-10(1)	-8(1)	0(1)
S(2)	24(1)	42(1)	29(1)	-8(1)	-3(1)	7(1)
P(2)	20(1)	21(1)	32(1)	-7(1)	0(1)	-3(1)
O(2)	45(1)	21(1)	47(1)	-17(1)	0(1)	-3(1)
N(2)	25(1)	32(2)	47(2)	-3(1)	-9(1)	1(1)
C(2)	25(2)	16(1)	25(1)	-5(1)	2(1)	-3(1)
S(3)	30(1)	24(1)	37(1)	-10(1)	-9(1)	-1(1)

C(3)	24(2)	26(2)	29(2)	-11(1)	-2(1)	-4(1)
S(4)	23(1)	31(1)	47(1)	-12(1)	6(1)	-5(1)
C(4)	31(2)	29(2)	23(1)	-12(1)	3(1)	-4(1)
C(5)	28(2)	24(2)	32(2)	-12(1)	9(1)	-4(1)
C(6)	23(2)	31(2)	39(2)	-14(1)	1(1)	-3(1)
C(7)	25(2)	28(2)	27(2)	-12(1)	-2(1)	-1(1)
C(8)	28(2)	25(2)	29(2)	-11(1)	8(1)	-6(1)
C(9)	49(2)	26(2)	34(2)	-8(1)	19(2)	-5(1)
C(10)	70(3)	26(2)	49(2)	-18(2)	33(2)	-13(2)
C(11)	64(3)	50(2)	53(2)	-38(2)	24(2)	-30(2)
C(12)	42(2)	66(3)	45(2)	-35(2)	10(2)	-23(2)
C(13)	29(2)	44(2)	33(2)	-21(2)	8(1)	-12(1)
C(14)	19(2)	30(2)	24(1)	-5(1)	5(1)	-5(1)
C(15)	27(2)	36(2)	36(2)	-8(1)	4(1)	0(1)
C(16)	24(2)	55(2)	36(2)	-11(2)	-1(1)	5(2)
C(17)	26(2)	60(2)	34(2)	-18(2)	3(1)	-11(2)
C(18)	31(2)	42(2)	31(2)	-12(1)	3(1)	-16(2)
C(19)	23(2)	32(2)	29(2)	-10(1)	3(1)	-4(1)
C(20)	27(2)	40(2)	32(2)	-6(1)	-3(1)	-2(1)
C(21)	28(2)	29(2)	29(2)	-9(1)	-6(1)	-2(1)
C(22)	18(1)	25(2)	26(1)	-7(1)	-6(1)	-1(1)
C(23)	24(2)	33(2)	28(2)	-6(1)	-5(1)	-4(1)
C(24)	26(2)	36(2)	30(2)	-13(1)	-6(1)	3(1)
C(25)	29(2)	34(2)	35(2)	-17(1)	-14(1)	5(1)
C(26)	32(2)	29(2)	31(2)	-9(1)	-10(1)	-7(1)
C(27)	22(2)	29(2)	26(2)	-7(1)	-6(1)	-3(1)
C(28)	26(2)	27(2)	30(2)	-13(1)	-5(1)	-1(1)
C(29)	29(2)	31(2)	41(2)	-14(1)	-4(1)	1(1)
C(30)	36(2)	37(2)	57(2)	-20(2)	-13(2)	0(2)
C(31)	59(3)	47(2)	50(2)	-23(2)	-30(2)	3(2)
C(32)	65(3)	57(3)	37(2)	-17(2)	-18(2)	-6(2)
C(33)	43(2)	41(2)	34(2)	-12(2)	-5(2)	-9(2)
C(34)	30(2)	27(2)	43(2)	-10(1)	-6(1)	4(1)
C(35)	32(2)	36(2)	41(2)	-11(2)	-3(2)	0(1)
C(36)	31(2)	42(2)	50(2)	-17(2)	-10(2)	-1(2)
C(37)	27(2)	40(2)	56(2)	-23(2)	-3(2)	0(1)
C(38)	36(2)	42(2)	46(2)	-18(2)	2(2)	-1(2)
C(39)	37(2)	38(2)	38(2)	-10(2)	-9(2)	4(2)
C(40)	29(2)	33(2)	53(2)	-1(2)	-2(2)	-2(1)

Na11	30(1)	27(1)	31(1)	-8(1)	-10(1)	0(1)
O11	30(1)	34(1)	40(1)	-20(1)	1(1)	-3(1)
C11	35(2)	40(2)	63(2)	-34(2)	2(2)	-3(2)
O21	35(1)	44(1)	40(1)	-20(1)	-1(1)	-7(1)
C21	41(2)	56(2)	45(2)	-30(2)	-2(2)	0(2)
O31	44(2)	39(1)	39(1)	-17(1)	-2(1)	0(1)
C31	45(2)	57(2)	37(2)	-22(2)	4(2)	-6(2)
O41	23(1)	28(1)	30(1)	-13(1)	2(1)	-7(1)
C41	45(2)	55(2)	49(2)	-31(2)	5(2)	-9(2)
O51	20(1)	33(1)	34(1)	-14(1)	3(1)	-3(1)
C51	30(2)	41(2)	36(2)	-9(2)	7(1)	-5(1)
O61	22(1)	35(1)	41(1)	-18(1)	-4(1)	-1(1)
C61	24(2)	30(2)	39(2)	-9(1)	3(1)	-10(1)
O71	47(2)	33(1)	39(1)	-6(1)	-17(1)	1(1)
C71	29(2)	31(2)	33(2)	-17(1)	0(1)	-5(1)
O81	22(1)	37(1)	34(1)	6(1)	-7(1)	-5(1)
C81	30(2)	39(2)	32(2)	-18(1)	-1(1)	-4(1)
C91	29(2)	39(2)	43(2)	-19(2)	11(2)	-9(1)
C101	22(2)	37(2)	45(2)	-17(2)	5(1)	-1(1)
C111	24(2)	45(2)	50(2)	-24(2)	-5(2)	-7(1)
C121	27(2)	35(2)	52(2)	-19(2)	-1(2)	-12(1)
C131	47(2)	40(2)	50(2)	-9(2)	-19(2)	-4(2)
C141	60(3)	41(2)	39(2)	-10(2)	-13(2)	-2(2)
C151	32(2)	34(2)	40(2)	-9(2)	-2(1)	3(1)
C161	37(2)	31(2)	40(2)	-10(2)	-9(2)	6(1)
C171	24(2)	51(2)	50(2)	10(2)	-11(2)	-5(2)
C181	62(3)	79(3)	58(3)	-3(2)	-37(2)	-1(3)
C191	70(3)	43(2)	30(2)	-1(2)	1(2)	12(2)
C201	28(2)	44(2)	57(2)	13(2)	0(2)	-4(2)
Na12	41(1)	42(1)	33(1)	-18(1)	0(1)	-7(1)
O12	53(2)	45(2)	37(1)	-17(1)	12(1)	-12(1)
C12	33(2)	85(3)	66(3)	-46(3)	10(2)	-8(2)
O22	82(2)	39(1)	34(1)	-12(1)	-20(1)	2(1)
C22	91(4)	41(2)	32(2)	-14(2)	16(2)	-26(2)
O32	50(2)	52(2)	58(2)	-26(1)	-16(1)	16(1)
C32	107(4)	35(2)	27(2)	-5(2)	-9(2)	-16(2)
O42	52(2)	72(2)	38(1)	-31(1)	8(1)	-26(1)
C42	94(4)	44(2)	60(3)	-11(2)	-48(3)	14(2)
C52	74(3)	48(3)	73(3)	-15(2)	-33(3)	23(2)

C62	44(2)	74(3)	69(3)	-41(3)	-6(2)	17(2)
C72	73(3)	91(4)	50(3)	-37(3)	18(2)	-41(3)
C82	55(3)	54(2)	47(2)	-16(2)	4(2)	-15(2)
C92	51(2)	50(2)	44(2)	-19(2)	0(2)	-11(2)
C102	95(4)	63(3)	43(2)	-22(2)	18(2)	-35(3)
Na13	26(1)	34(1)	42(1)	-6(1)	-5(1)	-7(1)
O13	22(1)	35(1)	30(1)	-13(1)	-5(1)	-1(1)
C13	25(2)	46(2)	34(2)	-18(2)	-2(1)	-4(1)
O23	19(1)	44(1)	28(1)	-11(1)	-4(1)	-1(1)
C23	30(2)	34(2)	32(2)	-11(1)	1(1)	0(1)
O33	20(1)	36(1)	24(1)	-6(1)	-3(1)	-1(1)
C33	23(2)	39(2)	32(2)	-9(1)	-1(1)	5(1)
O43	28(1)	36(1)	62(2)	1(1)	-19(1)	-6(1)
C43	23(2)	41(2)	35(2)	-8(1)	-11(1)	2(1)
C53	29(2)	34(2)	32(2)	-5(1)	-12(1)	1(1)
C63	22(2)	50(2)	23(2)	-7(1)	-1(1)	-6(1)
C73	31(2)	39(2)	38(2)	4(2)	-8(2)	-5(1)
C83	37(2)	40(2)	53(2)	-3(2)	-12(2)	-6(2)
C93	35(2)	44(2)	64(3)	10(2)	-19(2)	-14(2)
C103	26(2)	43(2)	43(2)	-3(2)	-12(2)	-3(1)

Crystal Structure Determination of *rac*-83-K

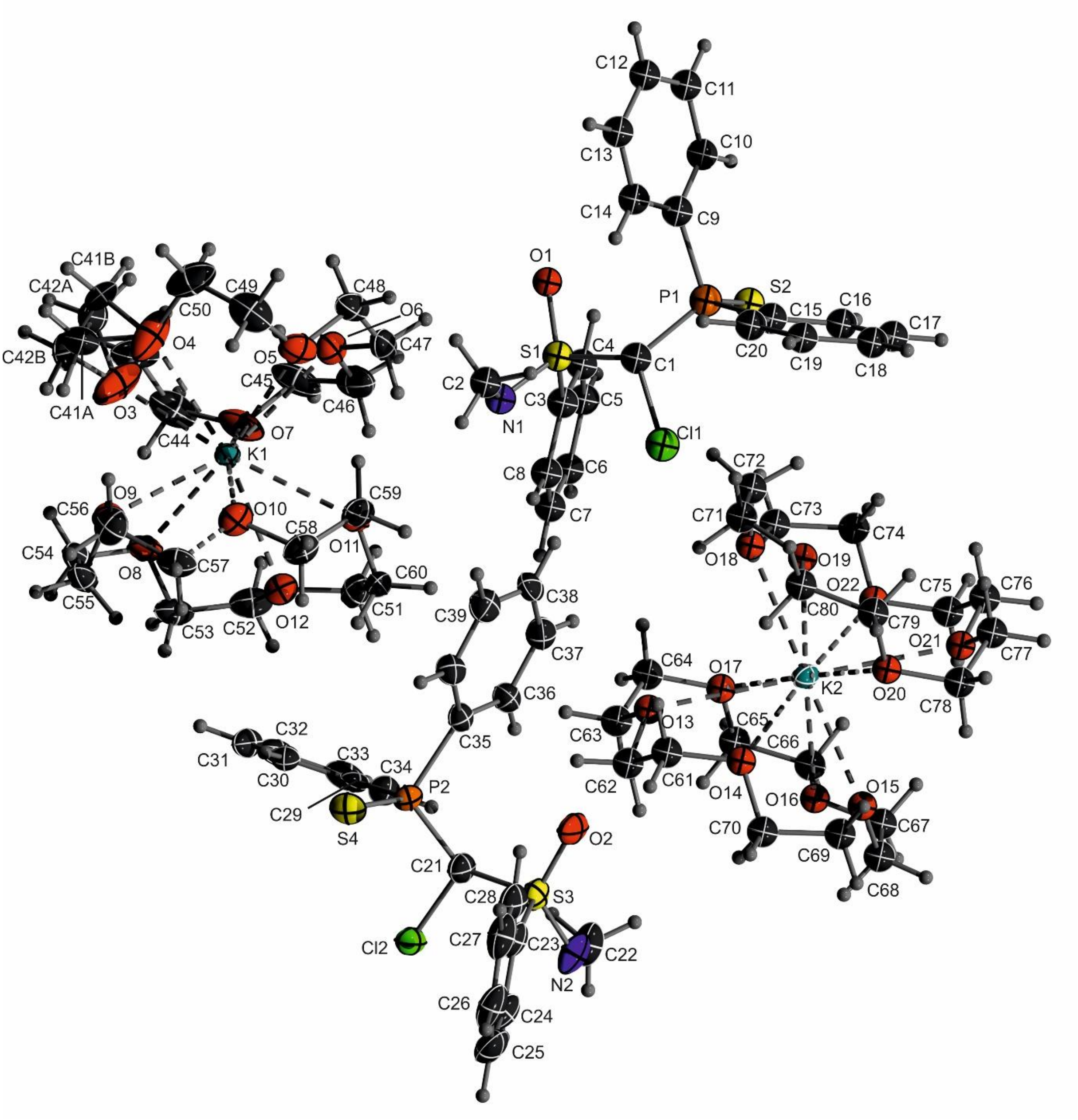

Figure 8. ORTEP of compound ***rac***-83-K. Ellipsoids are drawn at the 50% probability level.

Table 15. Atomic coordinates (x 10^4) and equivalent isotropic displacement parameters ($Å^2$x 10^3) for *rac*-**83-K** U(eq) is defined as one third of the trace of the orthogonalized U^{ij} tensor.

	x	y	z	U(eq)
K(1)	611(1)	2885(1)	5268(1)	23(1)
K(2)	844(1)	2086(1)	240(1)	26(1)
Cl(1)	5143(1)	3909(1)	1892(1)	29(1)
Cl(2)	4361(2)	-1071(1)	2976(1)	33(1)

S(1)	3370(2)	4472(1)	2859(1)	29(1)
S(2)	2343(2)	5332(1)	1408(1)	38(1)
S(3)	6150(2)	-379(1)	2092(1)	31(1)
S(4)	6968(2)	15(1)	3768(1)	36(1)
P(1)	4159(1)	5281(1)	1794(1)	23(1)
P(2)	5394(1)	220(1)	3279(1)	24(1)
O(1)	2901(5)	5113(2)	3072(2)	42(1)
O(2)	6544(5)	290(2)	1925(2)	42(1)
O(3)	-1213(6)	3280(3)	6248(3)	68(2)
O(4)	1613(6)	3800(4)	6123(2)	63(2)
O(5)	2488(5)	3998(2)	4935(2)	42(1)
O(6)	-402(4)	4046(2)	4615(2)	36(1)
O(7)	-2420(5)	3151(2)	5156(3)	50(1)
O(8)	-1317(5)	1859(2)	5720(2)	36(1)
O(9)	1523(5)	2086(2)	6121(2)	39(1)
O(10)	3516(4)	2348(2)	5138(2)	35(1)
O(11)	1994(4)	2592(2)	4149(2)	32(1)
O(12)	-222(4)	1780(2)	4577(2)	32(1)
O(13)	613(6)	1464(3)	1431(2)	61(2)
O(14)	3140(6)	1213(3)	641(2)	57(1)
O(15)	1944(5)	1046(3)	-433(2)	47(1)
O(16)	-1043(5)	991(3)	-94(2)	45(1)
O(17)	-1938(5)	1777(2)	843(2)	44(1)
O(18)	-365(5)	3139(2)	901(2)	41(1)
O(19)	2635(5)	3160(3)	515(2)	43(1)
O(20)	3745(5)	2341(2)	-343(2)	40(1)
O(21)	1229(5)	2683(2)	-936(2)	38(1)
O(22)	-1430(4)	2885(2)	-207(2)	36(1)
N(1)	4016(5)	3978(3)	3251(2)	34(1)
N(2)	5509(5)	-837(3)	1667(2)	42(1)
C(1)	4483(6)	4627(3)	2249(2)	27(1)
C(2)	5475(7)	4109(4)	3425(3)	46(2)
C(3)	1754(6)	4051(3)	2703(2)	30(1)
C(4)	540(7)	4423(4)	2598(3)	37(1)
C(5)	-758(7)	4101(4)	2493(3)	44(2)
C(6)	-821(7)	3447(4)	2486(3)	45(2)
C(7)	395(8)	3081(4)	2586(3)	46(2)
C(8)	1684(6)	3385(3)	2701(3)	35(1)
C(9)	4458(6)	6029(3)	2189(2)	26(1)

C(10)	3709(7)	6584(3)	2082(3)	37(1)
C(11)	4059(9)	7175(3)	2345(3)	46(2)
C(12)	5121(9)	7190(3)	2712(3)	47(2)
C(13)	5875(8)	6633(3)	2836(3)	43(2)
C(14)	5534(6)	6058(3)	2578(3)	36(1)
C(15)	5763(5)	5272(3)	1263(2)	25(1)
C(16)	5583(7)	5363(3)	689(2)	35(1)
C(17)	6802(8)	5369(3)	280(3)	47(2)
C(18)	8152(7)	5283(3)	456(3)	44(2)
C(19)	8349(7)	5185(3)	1029(4)	49(2)
C(20)	7143(6)	5182(3)	1442(3)	35(1)
C(21)	5052(6)	-305(3)	2714(2)	32(1)
C(22)	3991(7)	-737(4)	1540(3)	47(2)
C(23)	7800(6)	-814(3)	2205(2)	34(1)
C(24)	7856(7)	-1482(4)	2171(3)	41(2)
C(25)	9164(9)	-1806(4)	2225(3)	49(2)
C(26)	10410(7)	-1438(4)	2315(3)	48(2)
C(27)	10308(7)	-789(4)	2367(3)	48(2)
C(28)	8999(7)	-463(4)	2313(3)	38(1)
C(29)	3621(5)	242(3)	3707(2)	25(1)
C(30)	3539(6)	308(3)	4297(2)	30(1)
C(31)	2149(7)	352(3)	4606(3)	40(2)
C(32)	900(6)	317(3)	4325(3)	37(1)
C(33)	994(6)	248(3)	3738(3)	40(2)
C(34)	2341(6)	209(3)	3425(3)	33(1)
C(35)	5545(6)	1051(3)	3009(2)	26(1)
C(36)	4554(6)	1313(3)	2660(2)	31(1)
C(37)	4615(7)	1962(3)	2504(3)	37(1)
C(38)	5653(7)	2365(3)	2693(3)	36(1)
C(39)	6663(7)	2111(4)	3043(3)	39(1)
C(40)	6609(6)	1466(3)	3193(3)	32(1)
C(43)	-2547(9)	3569(4)	6134(4)	66(3)
C(44)	-3218(7)	3149(4)	5717(4)	56(2)
C(45)	-2815(8)	3666(4)	4790(4)	56(2)
C(46)	-1565(9)	3783(4)	4339(3)	53(2)
C(47)	844(8)	4194(3)	4230(3)	40(2)
C(48)	1966(7)	4479(3)	4568(3)	38(1)
C(49)	3226(8)	4234(4)	5389(4)	54(2)
C(50)	2233(9)	4396(4)	5912(4)	61(2)

C(51)	18(7)	1921(3)	3980(3)	38(1)
C(52)	-1688(7)	1585(3)	4760(3)	42(2)
C(53)	-1701(7)	1344(3)	5361(3)	39(2)
C(54)	-818(7)	1642(3)	6255(3)	40(2)
C(55)	772(7)	1485(3)	6201(3)	40(2)
C(56)	3080(7)	2026(4)	6111(3)	44(2)
C(57)	3786(7)	1842(3)	5531(3)	41(2)
C(58)	4177(6)	2221(3)	4571(3)	38(1)
C(59)	3514(7)	2665(3)	4162(3)	34(1)
C(60)	1599(7)	2040(3)	3838(2)	34(1)
C(61)	3120(8)	1139(5)	1249(3)	53(2)
C(62)	1649(9)	949(4)	1511(4)	57(2)
C(63)	-855(8)	1282(4)	1636(3)	49(2)
C(64)	-1893(9)	1754(4)	1455(3)	55(2)
C(65)	-2854(8)	1318(4)	617(4)	51(2)
C(66)	-2472(7)	1270(4)	-23(3)	40(1)
C(67)	-486(7)	906(4)	-666(3)	39(2)
C(68)	990(7)	621(4)	-681(3)	38(1)
C(69)	3266(7)	764(4)	-285(3)	44(2)
C(70)	3267(9)	624(4)	340(3)	52(2)
C(71)	2056(7)	3393(3)	1067(3)	38(1)
C(72)	584(7)	3659(4)	1015(3)	39(1)
C(73)	-1730(7)	3362(3)	717(3)	42(2)
C(74)	-1683(7)	3492(3)	78(3)	38(1)
C(75)	-1305(8)	2940(4)	-822(3)	45(2)
C(76)	194(8)	3151(3)	-1062(3)	42(2)
C(77)	2668(8)	2876(4)	-1139(3)	42(2)
C(78)	3715(8)	2373(4)	-951(3)	45(2)
C(79)	4627(7)	2826(4)	-117(3)	46(2)
C(80)	4109(7)	2926(4)	503(3)	50(2)
C(41A)	680(30)	3606(11)	6655(8)	56(7)
C(42A)	-800(30)	3838(12)	6574(9)	66(8)
C(41B)	504(11)	4050(7)	6569(5)	31(4)
C(42B)	-372(13)	3463(8)	6739(5)	34(4)

Table 16. Anisotropic displacement parameters ($Å^2 x\ 10^3$) for *rac*-**83-K**. The anisotropic displacement factor exponent takes the form: $-2\pi^2[\ h^2\ a^{*2}U^{11} + ... + 2\ h\ k\ a^*\ b^*\ U^{12}\ ]$

	U^{11}	U^{22}	U^{33}	U^{23}	U^{13}	U^{12}
K(1)	23(1)	20(1)	24(1)	1(1)	4(1)	5(1)
K(2)	26(1)	24(1)	26(1)	-4(1)	3(1)	-1(1)
Cl(1)	31(1)	24(1)	31(1)	0(1)	1(1)	2(1)
Cl(2)	35(1)	27(1)	37(1)	-3(1)	5(1)	-2(1)
S(1)	33(1)	29(1)	23(1)	2(1)	2(1)	-2(1)
S(2)	26(1)	48(1)	41(1)	12(1)	-9(1)	-6(1)
S(3)	30(1)	36(1)	26(1)	0(1)	6(1)	2(1)
S(4)	27(1)	36(1)	46(1)	-1(1)	-9(1)	7(1)
P(1)	21(1)	23(1)	24(1)	3(1)	0(1)	-1(1)
P(2)	18(1)	26(1)	28(1)	-3(1)	0(1)	3(1)
O(1)	54(3)	36(3)	32(2)	4(2)	16(2)	0(2)
O(2)	50(3)	38(2)	34(2)	-7(2)	20(2)	-8(2)
O(3)	45(3)	82(4)	69(4)	-39(3)	27(3)	-19(3)
O(4)	38(3)	102(5)	46(3)	-26(3)	5(2)	-18(3)
O(5)	35(2)	35(2)	54(3)	-1(2)	5(2)	6(2)
O(6)	32(2)	38(2)	37(2)	2(2)	1(2)	3(2)
O(7)	39(2)	34(3)	79(4)	11(2)	-11(2)	4(2)
O(8)	36(2)	24(2)	46(2)	-1(2)	11(2)	2(2)
O(9)	43(2)	36(2)	37(2)	1(2)	1(2)	11(2)
O(10)	26(2)	41(2)	39(2)	-3(2)	-1(2)	4(2)
O(11)	33(2)	27(2)	34(2)	-1(2)	9(2)	4(2)
O(12)	25(2)	35(2)	36(2)	-4(2)	-6(2)	1(2)
O(13)	44(3)	90(5)	47(3)	11(3)	5(2)	-18(3)
O(14)	62(3)	62(4)	48(3)	-1(3)	-13(2)	16(3)
O(15)	36(2)	48(3)	57(3)	-13(2)	-8(2)	10(2)
O(16)	33(2)	53(3)	49(3)	-9(2)	3(2)	3(2)
O(17)	42(2)	41(3)	45(3)	-6(2)	19(2)	-10(2)
O(18)	44(2)	36(2)	43(2)	-3(2)	6(2)	-2(2)
O(19)	33(2)	54(3)	43(2)	-9(2)	-1(2)	-1(2)
O(20)	35(2)	35(2)	50(3)	-3(2)	5(2)	-5(2)
O(21)	47(2)	30(2)	37(2)	0(2)	1(2)	-1(2)
O(22)	30(2)	25(2)	51(3)	0(2)	-8(2)	1(2)
N(1)	33(2)	41(3)	28(2)	4(2)	-9(2)	-2(2)
N(2)	26(2)	67(4)	32(3)	-13(3)	-2(2)	4(2)
C(1)	40(3)	21(3)	19(2)	2(2)	1(2)	2(2)
C(2)	39(3)	64(5)	36(3)	1(3)	-13(3)	-3(3)

C(3)	23(2)	47(4)	19(2)	6(2)	8(2)	2(2)
C(4)	38(3)	41(4)	29(3)	7(3)	6(2)	13(3)
C(5)	26(3)	67(5)	36(3)	24(3)	10(2)	7(3)
C(6)	28(3)	67(5)	41(4)	24(3)	-3(2)	-13(3)
C(7)	44(4)	44(4)	48(4)	10(3)	1(3)	-6(3)
C(8)	30(3)	36(3)	39(3)	9(3)	-3(2)	2(2)
C(9)	27(2)	21(3)	28(3)	-4(2)	11(2)	-1(2)
C(10)	44(3)	35(3)	30(3)	3(3)	7(2)	11(3)
C(11)	66(4)	21(3)	48(4)	3(3)	5(3)	22(3)
C(12)	63(4)	29(4)	46(4)	-7(3)	10(3)	-5(3)
C(13)	44(4)	39(4)	45(4)	-7(3)	1(3)	-1(3)
C(14)	28(3)	35(3)	45(3)	-9(3)	-4(2)	2(2)
C(15)	21(2)	21(3)	33(3)	-3(2)	1(2)	-5(2)
C(16)	38(3)	41(4)	24(3)	-1(2)	7(2)	-12(3)
C(17)	61(4)	40(4)	35(3)	-4(3)	20(3)	-17(3)
C(18)	47(4)	27(3)	52(4)	-9(3)	31(3)	-5(3)
C(19)	27(3)	26(3)	91(6)	3(3)	9(3)	3(2)
C(20)	25(3)	28(3)	51(4)	4(3)	2(2)	0(2)
C(21)	30(3)	34(3)	30(3)	-2(2)	6(2)	-3(2)
C(22)	37(3)	71(5)	34(3)	-2(3)	-2(3)	1(3)
C(23)	27(3)	49(4)	22(3)	-6(2)	7(2)	4(2)
C(24)	30(3)	56(4)	37(3)	-14(3)	0(2)	-2(3)
C(25)	58(4)	52(4)	37(3)	-15(3)	0(3)	14(3)
C(26)	33(3)	80(6)	31(3)	-12(3)	1(2)	19(3)
C(27)	33(3)	81(6)	29(3)	-2(3)	0(2)	-3(3)
C(28)	33(3)	49(4)	30(3)	-1(3)	10(2)	3(3)
C(29)	23(2)	17(3)	34(3)	2(2)	5(2)	-2(2)
C(30)	35(3)	25(3)	30(3)	-2(2)	-3(2)	-5(2)
C(31)	47(4)	31(3)	38(3)	-2(3)	21(3)	-8(3)
C(32)	29(3)	25(3)	55(4)	4(3)	16(3)	-3(2)
C(33)	23(3)	28(3)	67(4)	8(3)	4(3)	1(2)
C(34)	26(3)	33(3)	38(3)	0(3)	1(2)	1(2)
C(35)	22(2)	30(3)	26(3)	2(2)	2(2)	1(2)
C(36)	29(3)	31(3)	33(3)	3(2)	-1(2)	1(2)
C(37)	34(3)	41(4)	34(3)	2(3)	-1(2)	6(3)
C(38)	45(3)	29(3)	32(3)	8(2)	9(3)	0(3)
C(39)	34(3)	44(4)	39(3)	1(3)	2(2)	-10(3)
C(40)	27(3)	35(3)	35(3)	2(2)	-2(2)	-6(2)
C(43)	56(5)	36(4)	94(6)	-10(4)	51(5)	1(3)

C(44)	27(3)	43(4)	94(6)	17(4)	12(3)	6(3)
C(45)	37(3)	33(4)	101(6)	18(4)	-27(4)	-1(3)
C(46)	69(5)	38(4)	58(4)	0(3)	-34(4)	6(3)
C(47)	50(4)	35(3)	32(3)	6(3)	13(3)	11(3)
C(48)	34(3)	30(3)	48(4)	3(3)	14(3)	7(2)
C(49)	34(3)	52(5)	76(5)	11(4)	-16(3)	-7(3)
C(50)	51(4)	62(5)	73(5)	-31(4)	-25(4)	11(4)
C(51)	41(3)	45(4)	30(3)	-4(3)	-12(2)	9(3)
C(52)	24(3)	37(4)	67(4)	-11(3)	-6(3)	-4(3)
C(53)	28(3)	26(3)	61(4)	-4(3)	13(3)	-3(2)
C(54)	46(3)	30(3)	39(3)	8(3)	18(3)	8(3)
C(55)	49(4)	29(3)	38(3)	7(3)	14(3)	14(3)
C(56)	37(3)	53(4)	43(4)	-1(3)	-13(3)	4(3)
C(57)	32(3)	33(3)	59(4)	-1(3)	-12(3)	7(3)
C(58)	27(3)	42(4)	44(3)	-9(3)	4(2)	4(3)
C(59)	32(3)	31(3)	37(3)	-2(2)	9(2)	2(2)
C(60)	49(3)	27(3)	25(3)	-1(2)	3(2)	6(3)
C(61)	49(4)	70(5)	42(4)	3(4)	-7(3)	2(4)
C(62)	51(4)	63(5)	60(5)	23(4)	-19(3)	-8(4)
C(63)	51(4)	57(5)	37(4)	1(3)	10(3)	-21(3)
C(64)	63(5)	53(5)	42(4)	-10(3)	20(3)	-13(4)
C(65)	35(3)	41(4)	73(5)	5(4)	12(3)	-8(3)
C(66)	26(3)	41(4)	53(4)	-3(3)	-1(3)	0(3)
C(67)	39(3)	50(4)	26(3)	-8(3)	1(2)	10(3)
C(68)	33(3)	51(4)	28(3)	-9(3)	6(2)	-3(3)
C(69)	37(3)	52(4)	44(4)	-4(3)	-4(3)	12(3)
C(70)	57(4)	40(4)	59(5)	7(3)	-4(3)	15(3)
C(71)	39(3)	39(4)	35(3)	-11(3)	-4(2)	-4(3)
C(72)	38(3)	45(4)	33(3)	-18(3)	0(2)	-5(3)
C(73)	31(3)	30(3)	64(4)	-11(3)	-3(3)	-1(2)
C(74)	27(3)	29(3)	56(4)	-1(3)	-1(3)	0(2)
C(75)	54(4)	37(4)	46(4)	8(3)	-19(3)	-1(3)
C(76)	58(4)	28(3)	40(3)	1(3)	-10(3)	2(3)
C(77)	51(4)	39(4)	35(3)	2(3)	8(3)	-13(3)
C(78)	46(4)	41(4)	44(4)	-9(3)	16(3)	-4(3)
C(79)	33(3)	38(4)	69(5)	-9(3)	-5(3)	0(3)
C(80)	25(3)	63(5)	64(4)	-18(4)	-7(3)	2(3)
C(41A)	86(18)	29(12)	52(10)	0(8)	-6(10)	4(10)
C(42A)	110(20)	45(12)	38(10)	0(9)	33(11)	0(12)

C(41B)	26(5)	37(10)	31(6)	-15(5)	-1(4)	1(5)
C(42B)	25(6)	46(9)	29(6)	9(5)	6(4)	-4(5)